S L I P P E R L U B R I C A T I O N I N A X I A L P I S T O N P U M P S

by

Y.P. Kakoullis, B.Sc.
University of Birmingham

A thesis submitted for the degree of Ph.D.
under special regulations

Department of Mechanical Engineering
University of Birmingham

February 1979

S Y N O P S I S

The performance of hydrostatic type slippers in axial piston pumps has been studied both experimentally and theoretically.

The experimental work covers measurements of slipper clearance, slipper pocket pressure and piston spin. These measurements were taken from typical axial piston pumps running under normal operating conditions using a data logging system. The effect of operating conditions was also investigated and the resulting trends are described and discussed.

In the theoretical work the behaviour of an idealised slipper was studied under steady state conditions. It was established that a flat slipper of this type does not work on a purely hydrostatic basis. Additional lift can be generated hydrodynamically if the slipper is suitably tilted; however, if the slipper is flat it cannot satisfy moment equilibrium. One mechanism which was found to satisfy load, flow as well as moment equilibrium was the presence of suitable amounts of non-flatness on the slipper loads. A parabolic type of non-flatness was simulated and the relationships between tilt, pocket pressure central clearance and minimum clearance were derived with respect to non-flatness.

In conclusion, the theory is applied to the design procedure and a method is presented which enables the optimum non-flatness and minimum clearance to be estimated at particular operating conditions.

ACKNOWLEDGEMENTS

The author wishes to thank Dr. C.J. Hooke for supervising the project and offering much help and encouragement, Mr. D.F. Hadley for providing technical assistance and advice and Messrs J. Currie, P.J. Cleife and Dr. R. Dunlop for valuable guidance and advice offered during progress meetings. Thanks are also due to Misses E. Bale and K. Burrow for typing this thesis.

Finally the author wishes to thank the National Engineering Laboratory, Commercial Shearing Inc. and Commercial Hydraulics Limited for financing the project and providing manufacturing and testing facilities.

CONTENTS

ABBREVIATIONS

A.D.C.	Analogue to Digital Converter.
B.D.C.	Bottom dead centre.
C.H.L.	Commercial Hydraulics (U.K.) Limited.
H.P.	High (Delivery) pressure.
L.P.	Low (Inlet) pressure.
N.E.L.	National Engineering Laboratory.
P.C.D.	Pitch circle diameter.
P.C.R.	Pitch circle radius.
T.D.C.	Top dead centre.

NOTATION

All symbols marked with a $^{-}$ e.g. $\bar{P}$ denote a dimensionless quantity. As a general rule variables related to radius have been made dimensionless by dividing by $\bar{R}_4$ whereas variables related to clearance are divided by h_c.

Symbol	Description	Defined on page
A_{d1}, A_{d2}	Hydrodynamic pressure coefficient (inner and outer land)	2.19
A_s	Hydrostatic pressure coefficient (inner land only)	2.20
b	Non-flatness ($b = f \times h_c$)	2.10
$\bar{b}$	Pseudo-dimensional non-flatness ($\bar{b} = b \times Z$)	3.4
C_1, C_2, C_p	Auxiliary constants	2.29
C_f	Capacitance of fixed capacitor	4.6
C_t	Capacitance between transducer and slippper	4.5
d	Clearance of test surface (experimental)	4.5
d_o	Offset of transducer	4.5
d_1, d_2	Offset at mid-radius of inner and outer land	2.11
$\bar{d}_1, \bar{d}_2$	Dimensionless offset ($\bar{d}_1 = d_1/h_c$, $\bar{d}_2 = d_2/h_c$)	2.12
e_1, e_2	Auxiliary constants	2.29
E	e.m.f. induced in coil transducer	6.2
f	Dimensionless non-flatness	2.10
F_p	Dimensionless load due to piston pressure	2.41
F	Total external load on slipper	3.20

Symbol	Description	Defined on page
F	Flux linkage	6.2
g	Auxiliary variable	2.24
h, $\bar{h}$	Slipper clearance (general) ($\bar{h} = h/h_c$)	2.14
h_c	Central clearance	2.9
h_{m1}, h_{m2}	Clearance at mid-radius (inner and outer land)	2.21
h_{min}	True minimum clearance	2.51
h_n, h_x	Minimum and maximum clearance (at radius R_4)	2.10
$\bar{H}_c$	Pseudo-dimensional central clearance ($\bar{H}_c = h_c \times Z$)	2.17
$\bar{H}_{min}$	Pseudo-dimensional minimum clearance ($\bar{H}_{min} = h_{min} \times Z$)	2.51
I_1 to I_{13}	Frequenctly used integrals	Appendix A
K_1, K_2	Transducer constants	4.5
l	Effective orifice length	2.42
$\bar{L}_{d1}, \bar{L}_{d2}$	Hydrodynamic lift (inner and outer land)	2.33
$\bar{L}_s$	Hydrostatic lift	2.29
$\bar{M}_{dx1}, \bar{M}_{dx2}$	Hydrodynamic moment about the x-axis	2.34
$\bar{M}_{dy1}, \bar{M}_{dy2}$	Hydrodynamic moment about the y-axis	2.33
M_s	Maximum hydrostatic moment	2.31
$\bar{M}_{sx}, \bar{M}_{sy}$	Hydrostatic moment about x and y-axes	2.30
M_x, M_y	Total external moment about x and y-axes	3.20
N	Number of turns of the coil	6.2
$P, \bar{P}$	Pressure (general) ($\bar{P} = P/P_s$)	2.17

Symbol	Description	Defined on page
x_c, y_c	Co-ordinates of pressure centre	
$\bar{x}_c, \bar{y}_c$	Dimensionless co-ordinates ($\bar{x}_c = x_c/R_4$, $\bar{y}_c = y_c/R_4$)	2.45
$\bar{x}_d, \bar{y}_d$	Co-ordinates of hydrodynamic pressure centre	
x_ℓ, y_ℓ	Co-ordinates of external load	3.21
$\bar{x}_s, \bar{y}_s$	Co-ordinates of hydrostatic pressure centre	2.31
Z	Variable incorporating operating conditions	2.17
Z	Auxiliary variable (experiment)	4.10
α	Swashplate angle	2.31
β	Auxiliary variable	2.24
γ	Derived variable of ϕ	A-1
η	Viscosity of fluid	2.17
θ	Angle (Polar co-ordinate)	2.9
θ_1, θ_2	Angular boundaries of cavitating region	2.33
θ_m	Angular position of maximum tilt	2.10
θ	Angle of rotation of piston (experimental)	6.2
π	Constant (3.1416)	
ϕ	Derived variable of θ ($\phi = \theta - \theta_m$)	2.21
ϕ	Angle of rotation of cylinder block (experimental)	6.2
$\omega, \bar{\omega}$	Spin of slipper/slipper plate ($\bar{\omega} = \omega R_4/U$)	2.8

Symbol	Description	Defined on page
P_p	Piston pressure	2.17
$P_s, \bar{P}_s$	Slipper pressure ($\bar{P}_s = P_s/P_p$)	2.17
Q_1	Flow due to pressure	2.43
Q_2	Flow due to velocity	2.43
Q_f	Orifice coefficient	2.44
Q_{in}	Flow through orifice	2.42
Q_p	Term related to flow due to pressure	2.44
Q_v	Term related to flow due to velocity	2.44
$R, \bar{R}$	Radius (general) ($\bar{R} = R/R_4$)	2.9
R_1, R_1	Inner land, inner radius	2.9
R_2, R_2	Inner land, outer radius	2.9
R_3, R_3	Outer land, inner radius	2.9
R_4, R_4	Outer land, outer radius	2.9
R_{m1}, R_{m2}	Mean land radius (inner and outer land)	2.9
R_o	Effective radius of orifice	2.42
R_p	Piston radius	2.9
S_1, S_2	Slope of inner and outer land	2.12
t	Dimensionless tilt of slipper	2.10
u	Auxiliary variable	2.24
U	Velocity of slipper plate	2.7
v	Auxiliary variable	2.24
V_o	Output voltage (experiment)	4.5
V_m	Maximum output voltage (experiment)	4.7
w	Auxiliary variable	2.24

1.0. GENERAL BACKGROUND

1.1. Introduction

Hydraulic systems and units are to be found in a large variety of engineering applications. Such applications include power transmissions, hydraulic presses, servo-mechanisms etc. A fundamental element of most hydraulic systems is the hydraulic pump which when coupled to a mechanical drive unit converts mechanical energy into pressure energy. Many different types of hydraulic pumps have been devised each with its own advantages, disadvantages and range of applications. One of the most important is the axial piston pump.

The advantages of axial piston pumps include high efficiency (typically 90%), operating pressures of up to 700 bar and variable displacement. The disadvantages are mainly cost, in view of the number of precision machined components required, and vulnerability to contamination of the hydraulic fluid. For this reason one of the most significant applications of axial piston units is high performance power transmissions, especially in the medium to high power range.

There are two main varieties of axial piston pumps: the swash plate type and the bent axis type. This thesis is concerned with the swash plate pump. A typical such unit is shown in Fig. 1.1 and it consists of a cylinder block (1) which is coupled to the driving shaft and has an odd number of bores (in this case 9) with an equal number of pistons (2) in them. The slippers (3) rest on the slipper plate (4) which is attached to the swashplate (5). When the pump is running the slippers slide on the slipper plate, which is at an angle to the shaft, thus, forcing the pistons into reciprocating motion within the bores. When a piston is moving out of the bore, oil is sucked through

the inlet port of the portplate (6), through the cylinder slot (7) into the bore. Conversely when the piston is moving into the bore, oil is pushed out through the cylinder slot and the outlet port of the portplate. Thus, the combined effect of all the pistons results in the continuous pumping action of the oil which when obstructed by the load gives rise to hydraulic pressure. More detailed description of axial piston pumps is given by Holzbock[1] and Ernst[2].

When in normal operation, heavy loads are exerted onto the pistons by the pressurised oil. This load is transmitted to the slipper plate via the slipper. If the slipper was allowed to sit hard on the slipper plate while in motion, the two surfaces would wear rapidly with consequences that would be catastrophic for the whole unit. Therefore, what is required for a successful slipper design is a mechanism which enables the slipper to slide on the slipper plate with the minimum of friction and wear whilst supporting the piston load. This must be consistently achieved over the range of operating pressures, speeds and temperatures.

Some commercial units have overcome this problem by the use of an auxiliary slipper plate which rotates with the slippers on roller bearings. However, the majority of units employ a self-lubricating mechanism which generates enough pressure under the slipper so as to keep the latter floating on a film of hydraulic fluid. This pressure can be generated in one of two ways:-

a) Purely hydrodynamically.

b) Largely hydrostatically.

The first one, as the name implies, generates pressure in view of the slippers motion. Such a design is used in the Vickers Dynapad pump[3]. In this case the material and dimensions of the slipper are chosen so that when loaded the slipper distorts

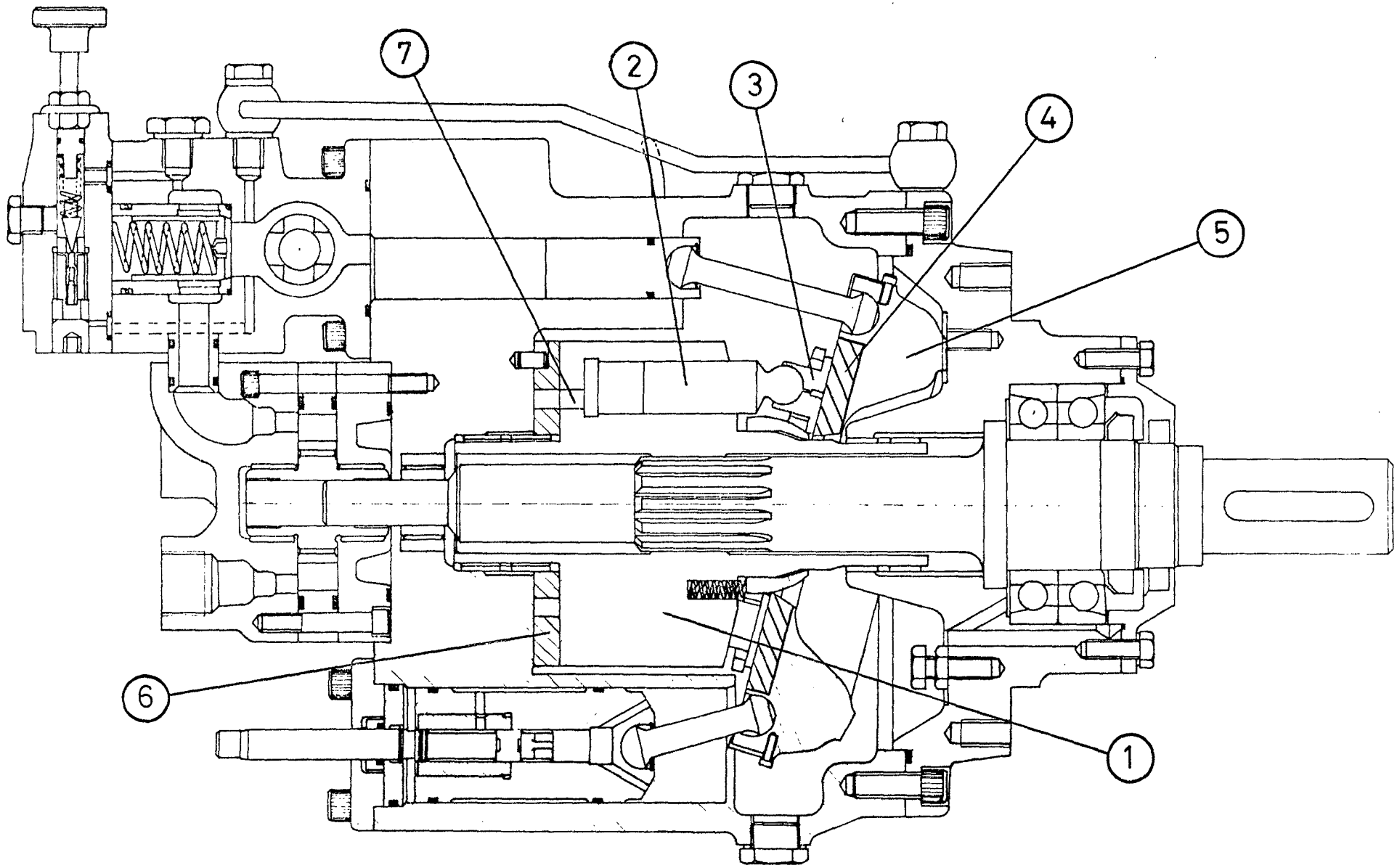

FIGURE 1.1 CROSS SECTION OF A TYPICAL AXIAL PISTON PUMP

to form a converging wedge. It is this wedge that generates hydrodynamic lift but only while the slipper is in motion. Units of this type are commercially available as pumps with operating speeds and pressures of up to 3000 rev/min and 350 bar, respectivel with excellent efficiency specifications. What is less certain with these units are their characteristics at start-up. Also, their performance at low speeds - high pressures or when the pump is run as a motor. These are situations in which there is load on the pistons but not enough speed to generate hydrodynamic lift under the slipper.

Most slippers operating on hydrostatic principles have a circular recess or pocket (1) which is surrounded by a land (2) as shown in Fig. 1.2. The orifice (3) connects the slipper pocket to the piston bore which feeds it with oil thus establishing a pressure in the slipper pocket which is approximately equal to piston pressure. It has been widely acknowledged that the force du to this pressure plus the force due to the hydrostatic pressure distribution on the land provides the necessary lift to support the load on the slipper. (This view is discussed further in the following section). A variation of this design has been the addition of an outer land (4) to enhance the stability of the slipper. Invariably the slot between the two lands communicates with the fluid outside the slipper by means of slots machined across the outer land or holes drilled from the top and breaking into the slot. Another variation of hydrostatic slippers concerns the spherical ball. On most designs it is part of the piston mating with a spherical cavity on the slipper. However, designs with the ball on the slipper have been successfully developed. This has the effect of bringing the centre of mass of the slipper nearer to the centre of the sphere thus reducing centrifugal

couples.

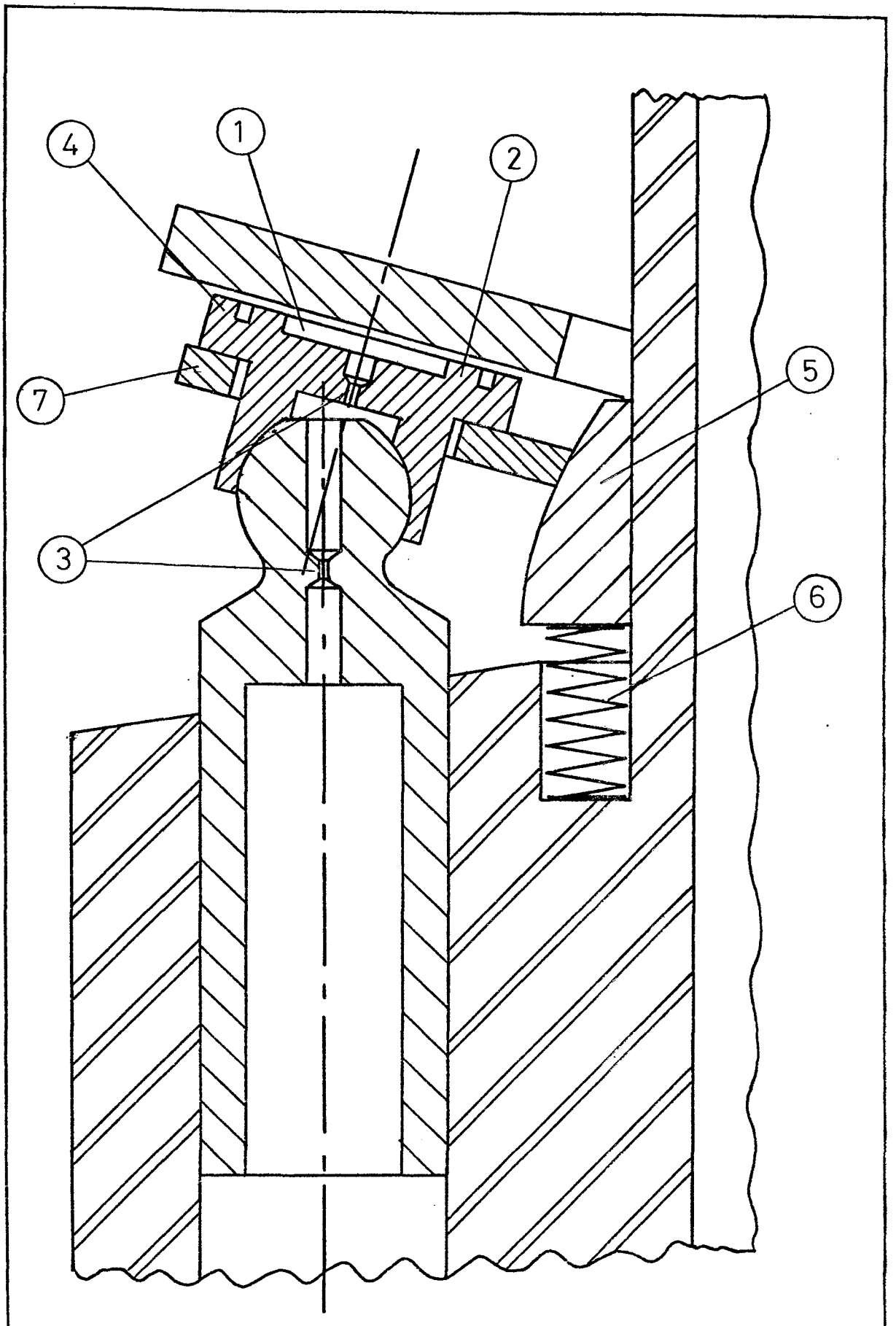

PISTON-SLIPPER ASSEMBLY

FIGURE 1.2

Variation also exists in the area of retention of the slippers. Retention is necessary if the pump is to be run at low boost pressures otherwise slippers tend to lift off at the high to low pressure transition and they tend to mark the slipper plate where they land. In some designs a spring was inserted inside each cylinder thus constantly pressing the pistons and slippers outwards. In other units (Fig. 1.2) this was modified to a swivel bush (5) pressing against one or more springs (6). The swivel bush has a spherical surface and supports a swivel plate (7) which in turn presses the slippers against the slipper plate.

As far as material is concerned early units employed phosphor bronze in either the slippers or slipper plate. However, a more satisfactory performance has been obtained by using steel slippers and slipper plate after they have been tufftrided. This has significantly improved resistance to wear and fatigue strength and is widely practiced at present.

1.2. Forces acting on the slippers

Before discussing the problems it is important to understand the forces and couples that can be exerted on the slipper while in normal operation. These are the following:-

a) Force on the piston due to pressure in the cylinder. The component acting on the slipper is $P_p \pi R_p^2/\cos\alpha$. This can be calculated from a knowledge of P_p which is normally close to inlet or outlet pressure depending on the postion of the piston bore.

b) Viscous and frictional drag on the piston due to its motion within the piston bore. This motion consists of reciprocation which provides the pumping action and rotation relative

to the cylinder block. The drag due to reciprocation is related to the attitude and clearance between the piston and bore. Little is known about the magnitude of this drag except that it can increase or decrease the load exerted on the slipper depending on whether the piston is moving in or out of the bore. However, because it is acting in the same direction as the pressure loads which are generally much larger, drag along the axis of the piston is considered to have a second order effect on slipper lubrication.

Ample evidence that pistons rotate within the bores can be found from markings on the pistons. Piston spin was measured experimentally using a typical axial piston pump running at normal operating conditions (see Chapter 6). Correlation between piston spin and slipper clearance results (Chapter 5) shows that the drag due to piston rotation in conjunction with pressure and friction in the ball joint plays a major role in determining the tilt of slippers.

c) Spring forces can be exterted on the slippers through a swivel plate or with individual springs in the piston bores depending on the design of the unit. The purpose of the springs is to provide a hold down load on the slippers to stop them moving off the slipper plate when the pressure in the piston bore is inadequate. Spring loads are particularly important in the high to low pressure transition where the pressure load is suddenly removed and the inertia forces tend to lift the slipper away from the plate; they are essentia in applications where the pump is required to operate on open circuit or with low inlet pressure.

d) Centrifugal force which is caused by the rotation of the slipper about the pump shaft. This tends to swing the slipper outwards in the radial direction and can be calculated from a knowledge of the pump speed and slipper geometry.

e) Inertia force due to the reciprocating motion of the piston and slipper. This is normally a simple sinusoidal function of the angular position of the cylinder block and it is maximum at the transition regions and zero at the middle of the L.P. and H.P. regions. In the case of a pump it acts towards the cylinder block at the high to low pressure transition. The direction is reversed at the transition from low to high pressure.

f) Friction in the piston/slipper joint in conjunction with pressure and drag on the piston has been shown to have a considerable effect on the angle of tilt of the slippers (see Chapters 5 and 6). Little is known about its magnitude, however, and at present it appears to be a difficult parameter to measure especially during operation.

g) Pressure force on the undersurface of the slipper. This force presents the largest contribution in supporting the heavy loads imposed by the piston, springs, inertia etc. on the slipper. The design procedure for the majority of units assumes this lift to be due to hydrostatic pressure. This is generated in the slipper pocket by oil fed in from the piston through the orifice. However, an elementary calculation of the ratio of hydrostatic lift to piston load at zero tilt shows that this lift is insufficient in the best of circumstances. The ratio can be obtained using[5].

$$\frac{\frac{1}{2}\,(R_2^{\,2} - R_1^{\,2})\,\cos\alpha\; P_s}{R_p^{\,2}\,\ln\,(R_2/R_1)\; P_p}$$

This ratio has the maximum value of 0.968 at zero stroke ($\alpha = 0$) assuming zero pressure drop across the orifice ($P_s = P_p$). At more realistic conditions, say 15^o swashplate angle and 2% pressure drop across the orifice, the ratio drops even further to 0.916 (see also section on analysis of hydrostatic components).

The insufficiency of the hydrostatic lift to support the load was also shown experimentally. With the boost pressure on but not the main motor, the pump was turned manually. When any slipper land passed over a displacement transducer, the clearance shown was consistently zero. (See section on experiment). The fact that slippers do work when in motion leaves no option but to assume that the remainder of the necessary lift is generated hydrodynamically.

h) Drag force on the slipper due to sliding on the oil film. This is inversely proportional to the oil film thickness. From similar cases it is known that this force force has a second order effect and consequently it is ignored in this stage of the work.

1.3. Defining the problem.

Axial piston pumps with hydrostatic type slippers have been operating successfully for some time. Typical of the design methods for the slippers is that developed at the National Engineering Laboratory in East Kilbride. This was supported on simple hydrostatic theory which assumed the piston pressure and slipper pocket pressure to be equal. Using empirical factors to relate the inner and outer radius of the inner land of the slipper

and also to account for the pressure distribution across the land, the theory went on to equate piston and slipper load at zero stroke. This produced relationships between piston bore and the radii of the slipper lands while all other less significant dimensions were established according to space, material strength etc.

Despite its simplicity, this method proved to be remarkably effective and units with progressively increasing operating pressures were developed. However, as pressures rose above 350 bar and operating temperatures exceeded 80°C, the number of problems that could not be solved using the conventional approach multiplied.

Evidence for problems has come from markings on the slipper track of the slipper plate and also on the slippers themselves. These can take a number of different forms.

The easiest to explain is the polishing predominantly on the high pressure side of the pump spread over the full width of the track. This is a result of too low clearance occuring when the overclamp ratio is too high. Polishing is more severe at high pressures and temperatures.

The other type of marking appears in the low pressure or boost side of the pump and takes the form of a sequence of crescent type markings starting at the transition from high to low pressure and they are most severe towards the centre of the unit. This has been explained as an unbalanced situation in which the slipper is pushed off when the load is removed by the still high pressure in the slipper pocket and the inertia loads. As the slipper is lifted, the pressure underneath is discharged and the slipper is forced down, thus, marking the slipper plate. The force due to the squeeze effect over-comes the load and the slipper is lifted again. The process is thus repeated until

the load and the lift balance each other.

A final type of marking can appear on the transition from low to high pressure. Here the slipper is subjected to a suddenly increased load and forced to sit momentarily on the slipper plate.

It appears, therefore, that design of hydrostatic slippers is limited by the onset of instability on the low clamp side and by too low clearance in the high pressure region on the high clamp side.

Most slipper designs have been based on an empirical choice of clamping ratio. It is the purpose of this work to establish a more complete understanding of the operation of the slipper and a more satisfactory design method.

1.4. Previous work

Although there is a substantial amount of literature related to slippers in axial piston machines it appears that most of the work done is based on purely hydrostatic grounds the dynamic aspects being largely ignored.

One of the earliest theoretical analyses on hydrostatic bearings was produced by Lord Rayleigh[5] in 1917. In this work he relates the load carried by a thrust shaft bearing to bearing pressure and geometry.

Ernst[2] applies hydrostatic theory to slippers but confines his investigation to the flow in and out of the slipper pocket

The operation of slippers in hydrostatic motors is analysed more fully by Cunningham and McGillivray[6]. This work is backed by an experimental investigation and includes design procedures and recommendations.

An experimental study of the friction characteristics of

pistons and slippers is presented by Boinghoff[7]. Although some dynamic considerations are included, they are confined to very low speeds (typically 1 rev/min).

Howarth[8] introduces the effect of tilt on the performance of slippers under static conditions. Balancing considerations include load and flow equilibrium but not moment equilibrium.

A substantial amount of literature has also been published by the British Hydromechanics Research Association between 1958 and 1969 following an extensive research programme ([9] to[20]). The various aspects of the slipper studied included lift, axial and tilting stiffness and leakage under a range of operating conditions. The theory to support the investigation was developed by Fisher[14] and considers a stationary hydrostatic slipper against a rotating slipper plate. The pocket pressure is expressed as a power series and the load, moment and flow are derived as functions of tilt. In the calculation of equilibrium conditions Fisher acknowledged that a slipper is unstable under the conditions imposed by normal lubrication theory and the assumptions regarding the flatness of the bearing surface. He concluded by suggesting that the fact that slippers do work can be explained by the non-flatness of the surfaces or the non-linearity of the fluid properties.

The effects of tilt, sliding and squeeze action on externally pressurized bearings were analysed by Royle and Raizada[21] using the finite difference method. The work concentrates on flat bearings and although tilting moments are considered, no mention is made of possible mechanisms to counterbalance them.

Extensive research also appears to have preceded the design of the Vickers Dynapad Pump[3]. Unfortunately, very little of it appears to have been released.

1.5. Scope of work

As an initial approach to the subject this work concentrates both theoretically and experimentally on the study of hydrostatic slippers with two loads. The aim of the theoretical study is to explore fundamental aspects of slipper behaviour and hence provide information and guidelines to assist in the design procedure. Due to the complexity of the subject, the problem is considered in an idealised form. One of the most important idealisations is the restriction of the analysis to steady state conditions; i.e. time related effects such as inertia, squeeze film, step loads etc. are not included. Although such dynamic effects are undoubtedly present in real pumps at normal operating conditions it is not possible to incorporate them in the analysis at this stage until the basic aspects of the lubrication mechanism are exposed and understood. The study of the problem in its idealised form is considered an essential preliminary to a full dynamic analysis, if the latter becomes necessary.

The analysis is first applied on a flat slipper, such as the one used in the C.H.L. 92 ml/rev unit, and it is shown that the hydrostatic lift of this design cannot support the exerted loads under any circumstances. Additional lift can be generated hydrodynamically when the slippers are suitably tilted and in motion. The pressure distribution on the loads, however, is such that it produces a couple tending to restore the slippers to the zero tilt position. The effects of non-flatness on the loads are then considered and it is shown that suitable amounts of non-flatness in conjunction with tilt produce a mechanism which on one hand generates adequate total lift and on the other hand it is self balancing. The basic theory as well as the relationships between clearance, tilt and pressure at equilibrium are included in Chapter 2.

The above theory is applied to the design process in Chapter 3. It is shown that the required non-flatness can vary over a large range of physical values without affecting significantly the minimum clearance. Some typical non-flat profiles are compared and it is shown that best performance can be obtained using slippers with a flat inner load and a chamferred outer load. This Chapter also includes a method for the calculation of optimum non-flatness and the prediction of minimum clearance at particular operating conditions.

The experimental study includes measurements of slipper land clearance and slipper pocket pressure. The measurements were stored and processed using a data logging system based on a PDP11/10 processor. Two pumps were used in the tests: the first was a 330 ml/rev variable displacement supplied by N.E.L. and the second was a 92 ml/rev fixed displacement pump supplied by C.H.L. Despite the large difference in size the two units were based on a similar design philosophy. The instrumentation for clearance measurements consisted of purpose built capacitance transducers which were installed inthe slipper plate and they were used in conjunction with a Wayne Kerr displacement measuring unit. Pressure measurements were obtained using a strain gauge type pressure transducer which was also installed in the slipper plate. The instrumentation and results related to these measuremen are discussed in Chapters 4 and 5 respectively.

Another experimental investigation involved the measurement of piston spin. A C.H.L. 92 ml/rev variable displacement pump was used for this purpose. The motion of a piston was monitored on-line using a coil type transducer which was embedded in the cylinder block in conjunction with a magnet which was attached to the piston. The instrumentation and results are outlined in Chapter 6.

2. THEORY

2.1. Introduction

The function and problems of the slipper were outlined in chapter 1. It was clearly shown that there is a need for a more fundamental understanding of its operation and behaviour so that its further development and improvement in performance can be made possible.

This chapter describes how this can be done following a theoretical approach.

The primary purpose of the analysis that follows is to provide insight into how slippers work in their conventional form under conventional operating conditions. This in turn should provide the additional information required to assist the development and refinement of the subject. The necessity and advantage of this type of theoretical analysis are well known. The savings in time, money and effort can be quite substantial when something is designed and tested on paper before it is tried in the laboratory.

One cannot of course underestimate the importance of experimental and empirical evidence. After all, the final confirmation of a successful design will come when it is put into practice in a real pump. But empirical knowledge on its own is not enough when one is trying to modify a component such as the slipper without understanding its fundamental behaviour.

Experience has shown that when theoretical and empirical knowledge are coupled together they can provide a very powerful tool in further design and development.

On the other hand one must be prepared to accept the limitations of this approach. Obviously, it would be very

desirable to be able to simulate the slipper at different positions round its path, during transient loads, with all the viscous and frictional effects etc. and to be able to extract the clearances and pressures accurately. It must be said that an analysis of such detail at least at this stage is not possible. The nature of the subject is so complex that full simulation would probably make the problem incomprehensible in view of the vast number of variables and parameters which would be involved. But is full simulation really necessary? As stated above the object of this exercise is to provide insight and information which can have direct practical applications. With knowledge on the subject being so limited (see Chapter 1) there must certainly be a lot of information that can be gained by idealising the subject or neglecting certain aspects of it for the time being. This will have the obvious advantages of relative simplicity and being easier to use. Admittedly the accuracy and generality of the analysis will decrease by introducing idealisations. But if the assumptions are kept to a necessary minimum, then the analysis, despite its imperfections can become a fast and powerful tool in exploring the fundamental mechanisms which make the slipper work and at the moment little is known about them.

Having accepted that certain idealisations are inevitable, the next stage is to define these idealisations rigorously and apply them in such a way that their effect on the accuracy and generality of the analysis is minimal.

The most important of these idealisations is to assume steady state conditions throughout. This implies that the

element of time is excluded and parameters such as operating conditions, slipper pressures and flows as well as slipper attitude and geometry are considered as constant with respect to time. A further minor simplification in conjunction with steady state is to reverse the interaction between slipper and slipper plate by assuming that the latter moves in relation to the slipper. This does not alter the nature of the problem and it is usually applied to such cases in lubrication.

The problem is thus modified to a stationary slipper with the slipper plate sliding underneath it. The linear and rotational motion normally described by the slipper in a pump will be expressed mathematically in section 2.2. The essence of these assumptions is that the position, tilt and clearance of the slipper at any point on the co-ordinate axes does not change with time. As a result of this all pressures, lifts, moments, loads and flows are constant for a particular configuration.

The idealisation of the slippers behaviour into steady state is a major assumption but how justified is it, especially since dynamic conditions are known to exist in practice. The answer to that lies in the fact that including dynamic conditions will not reveal much about the fundamental mechanisms of slipper behaviour; especially when little is known about steady state. On the contrary the added complexity would tend to overshadow basic trends due to geometry, non-flatness etc. Slippers are known to work perfectly well at near steady state conditions. Such conditions exist when the pump is running at zero swash and no-load. They also work in experimental rigs such as the

one used at B.H.R.A.[10] and recently at Birmingham University where the piston/slipper is kept stationary and the slipper plate rotates in relation to it. Introducing dynamic conditions under such circumstances does not alter the basic lubrication mechanism but it makes the operation of the slipper more critical. Ample evidence of this can be found on most slipper plates where polishing or picking marks can be seen near the transition regions. This clearly implies that if the slipper cannot operate under steady state then it has very little chance of surviving under dynamic effects where conditions are much harsher. Since the object of this exercise is to seek information of a basic nature which can be found by studying steady state, it seems logical that the study and understanding of steady state must be the essential preliminary to a dynamic analysis.

A similar approach has prevailed in ignoring external couples such as friction in the ball joint. Its presence cannot be disputed as will be seen in the experimental part. The question is whether it plays an active part in the lubrication mechanism or if it is an additional factor which makes the operation of slippers more critical like dynamic effects. This distinction is important because it determines whether friction ought to be included in the analysis from the beginning or not. Experimental evidence up to date indicates that the effects of friction are of the second type. Such evidence comes from the experimental rigs mentioned above where the piston/slipper operated successfully while it remained stationary and the effectsof friction under such circumstances were clearly negligible. But even when friction

is present in a real pump under normal conditions its effect is variable and generally not in a desirable direction. Such an instance occurs in the middle of the high pressure region where friction in the ball joint makes the slipper tilt inwards in the radial direction (see Chapter on Experiment). This means that friction plays no part in the determination of tangential tilt which is a major factor in generating hydrodynamic pressure. Similarly in the middle of the low pressure region, the effect of friction is superimposed on the centrifugal effects thus giving rise to a high radial tilt outwards. But again it is not in the tangential direction. One area where friction does affect tangential tilt is the low to high pressure transition, but it is in the wrong sense because it forces the slipper to enter the high pressure region tilted forward (leading edge down). Clearly such an effect is most undesirable because it often causes problems in that area. The fact that slippers do generally survive such situations means that there must be some other mechanism which is built into the slipper, it generates adequate lift when in motion, it is self-stabilising and it has the capacity to withstand external detrimental effects such as friction, dynamic loading etc. when they occur. It is this basic mechanism which is investigated in the present analysis. The possibility of incorporating frictional effects will be discussed at a later stage in Chapter 3.

Another simplification is related to slipper geometry and in particular to the flatness of the slipper lands. It will be shown later that slippers such as the ones investigated in

this work cannot operate successfully if the lands are flat. Although there are many types of non-flatness that can make the slipper work, it is not possible to examine them all. The study of the effects of non-flatness is limited, therefore, to the simulation of a particular slipper land profile which was thought to be the most typical. This is discussed further in section 2.2.6.

There are also some further assumptions which will be briefly mentioned here as they are discussed more fully in the main body of the analysis. Some basic assumptions related to the properties of the operating fluid are outlined in section 2.3. These are generally applicable to a large number of similar lubrication problems. An assumption which can be applied to this particular problem in view of the slipper geometry is the 'short bearing approximation' and this is also discussed in section 2.3. Some idealisations regarding pressure distribution under the slipper were found to be very useful in solving Reynolds' equation. These are outlined and discussed in section 2.4. Finally, the occurrence of cavitation between the slipper and slipper plate is discussed in section 2.5. A method of predicting and accounting theoretically for some of the effects of cavitation is also included.

To summarise, the aim and usefulness of this analysis does not rely on a complete simulation but on an approximation of slipper behaviour. Although the problem is considered in an idealised form, it explores fundamental aspects which have not, to the author's knowledge, been investigated previously. Such an aspect is the effect of non-flatness which, as will

be shown, can play a major role in the lift generation and balancing mechanism of the slipper.

Because of the assumptions which had to be introduced at this stage, the analysis suffers a number of limitations. Once the steady state has been fully investigated and understood, the analysis could be extended to include dynamic effects, friction etc. However, as far as the present thesis is concerned these effects remain outside its scope.

2.1.1. Simulation of the analysis

The most convenient way of testing and using the analysis is by the use of a computer programme. The programme was written in FORTRAN IV as applied to a DEC PDP11/10 computer system and it was extensively used to produce the results and plots shown in this chapter.

The analysis and simulation is orientated towards a slipper design with two lands and an orifice such as the one shown in fig. 1.2. Such a design is used in the C.H.L. 92 ml/rev and the Hastie 330 ml/rev pump. The results and plots in this chapter have been obtained using the dimensions of the C.H.L. slipper. The results are very similar when the dimensions of the Hastie slipper are used instead. This is because the ratios of the land and piston radii in both slippers are very similar.

2.2. Geometric Definitions

2.2.1. Motion

With the theoretical investigation confined to steady state, the slipper can be considered as stationary with the slipper plate moving underneath with a linear velocity U. The second important parameter, which is required to complete

the description of the motion of the slipper is the rotational spin ω (fig. 2.1). Since U represents only the linear content of the slipper's motion, ω must include all types of rotational motion such as the spin of the slipper about its own axis as well as the rotation inflicted on the slipper by the motion of the cylinder block. It does not, however, include any other types of motion about the piston ball such as swinging or swashing. The inclusion of such motion into the analysis would obviously not conform to the assumptions about steady state.

The advantages of describing completely the slipper's motion with two simple variables are primarily its simplicity but also its versatility. Different types of spin are now simply additive and either can be easily incorporated or modified.

2.2.2. Co-ordinate Axes

The co-ordinate axes are defined by looking at the slipper from the piston end (fig. 2.1). The x-axis coincides with the positive linear velocity of the slipper plate. The y-axis is normal to the x-axis and points in the approximately opposite direction from the physical centre of the slipper plate. In a real situation the x-axis would be tangential to the slipper path whilst the y-axis would be normal and pointing away from the centre of the path. Since the slipper path is generally an ellipse, the y-axis will not always pass through the centre of the slipper plate. Both the x and y axes lie on the working surface of the slipper plate. As far as the z-axis is concerned it is defined as pointing away from the slipper plate towards the

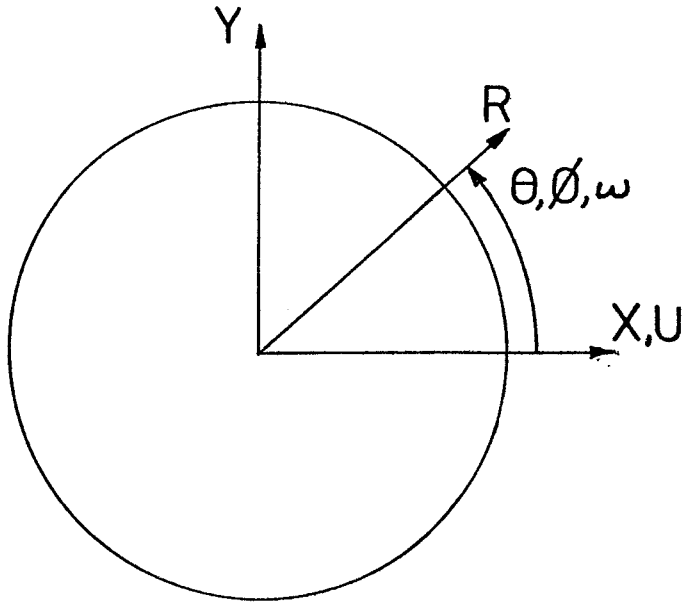

FIG. 2.1 DEFINITION OF COORDINATE AXES

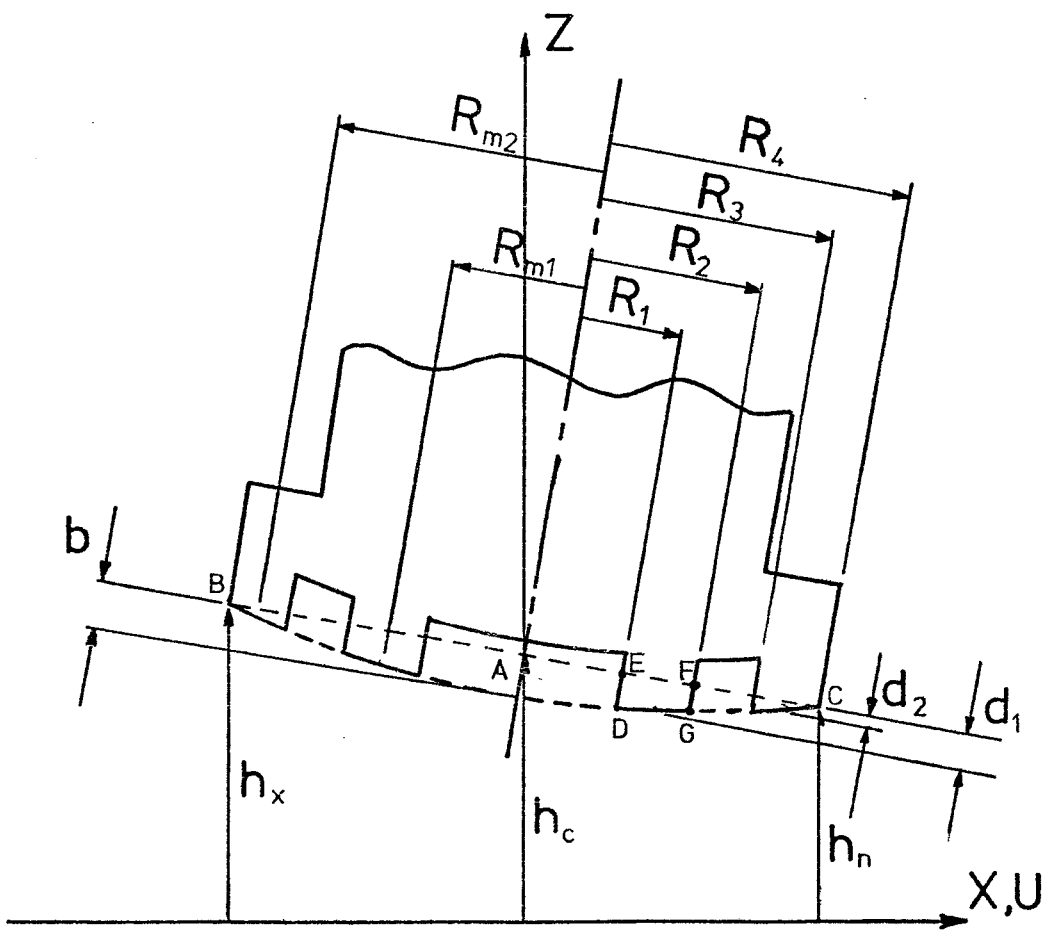

SLIPPER GEOMETRY (PARABOLIC PROFILE)

FIGURE 2.2

piston. Because the slipper will generally be tilted, the z-axis will not always coincide with the axis of the slipper. A convenient point which is chosen to lie always on the z-axis is point A on fig. 2.2. This is defined as the intersection of the axis of the slipper with the plane which passes through the undersurface of the slipper at radius R_4.

2.2.3. Angles

All angles and angular velocities are measured in the anticlockwise direction, x to y axis (fig. 2.1).

2.2.4. Radii

The most important geometric parameters of the slipper are the radii of the inner and outer land R_1, R_2, R_3 and R_4 which are defined as shown in fig. 2.2. Also R_{m1} and R_{m2} refer to the mean radius of the inner and outer land respectively. Piston radius is represented by R_p. Almost all radii are used in a dimensionless form. This is achieved by dividing by R_2 or R_4 depending on whether the slipper has one or two lands respectively. In this work, a two land slipper is used throughout, therefore the conversion takes the form:-

$$\bar{R} = R/R_4 \qquad 2.1$$

2.2.5. Attitude

As far as attitude is concerned the slipper can be completely specified in terms of central clearance, maximum tilt, angular position of maximum tilt and non-flatness. Central clearance h_c is defined as the distance of the slipper plate from point A (fig. 2.2). Tilt is used as a non-dimensional ratio defined as:-

$$t = \frac{h_x - h_n}{h_x + h_n} \qquad 2.2$$

where h_x and h_n are the distances of points B and C respectively from the slipper plate (fig. 2.2). The limiting values of tilt are zero and one. With tilt equal to zero the slipper is parallel to the slipper plate or more precisely, symmetrical about the z-axis. On the other hand when tilt is equal to one the slipper makes contact with the slipper plate at point C. Angular position of maximum tilt θ_m is the angle where h_x is encountered from the x-axis.

2.2.6. Non-flatness

Non-flatness in the analysis is represented by a single parameter f. It is used as a dimensionless quantity which is defined as:-

$$f = b/h_c \qquad 2.3$$

where b is the distance of the non-flat surface from point A. (Fig. 2.2). Obviously non-flatness can appear on a real slipper in a large variety of different forms. Although one wishes to incorporate as many types of non-flatness as possible in the interests of generality, it is also necessary to take appropriate measures so as to avoid making the analysis unduly complex. These two conflicting requirements cannot be satisfied completely and in trying to reach a compromise between the two, the following points were borne in mind:-

a) The types of non-flatness that can be incorporated into the analysis must relate to and respresent typical non-flat profiles as they occur in practice.

b) It must be possible to alter the type of profile without having to change the main body of the analysis.

In order to achieve these objectives certain simplifications have to be introduced which although they idealise the shape of the slipper, nonetheless they provide a sound basis for a first approach to the effect of non-flatness.

(i) Only axisymmetric configurations are considered. This means that wavy or saddle-shaped lands cannot be incorporated.

(ii) Only straight lands are considered. This means that rounded land edges or curved lands cannot be incorporated. Hence, all allowable profiles must have land surfaces which are part of a conical surface.

(iii) Non-flatness of a particular profile must be expressed through a single variable.

Although the last condition appears to limit severely the generality of the analysis, in fact there is a large number of profiles which can be represented in this way. Typical examples are conical profiles, spherical profiles or profiles with chamferred outer land and flat inner land. etc. In fact any profile can be represented provided it conforms to the three conditions above and as long as the slope of the lands S and the offset d (fig. 2.2) are functions of the non-flatness f and of the radii of the lands only. This is of primary importance because it enables the analysis to use land slopes and offsets rather than non-flatness. It also implies that the analysis does not

need to be altered when examining different profiles thus satisfying condition (b) above. The obvious practical advantages are found when simulating the analysis through a computer programme. The main body of the programme can then be written in terms of s and d with a small subroutine at the beginning defining them in terms of f and land radii. In the event of altering the profile one needs to make the appropriate modifications in this subroutine only.

Before exaimining how some typical profiles can be simulated in practice the parameters d and s must be defined. The offset d of a land is defined as the distance of the middle of the land (at radius R_m) from the plane BAC (fig. 2.2). In its non-dimensional form:-

$$\bar{d} = d/h_c \qquad 2.4$$

The slope of a land is defined as:-

$$S = \frac{GF - DE}{(\bar{R}_2 - \bar{R}_1)\, h_c} \qquad 2.5$$

and it is independent of $\bar{R}$, for a particular land since all lands are considered to be straight.

A number of profiles can now be examined in detail:-

(i) Conical profile (fig. 2.3). The slopes of the two lands S_1 and S_2 are the same. Assuming, for convenience, that the outer land intersects plane BAC at radius R_4 then:-

$$\bar{d}_1 = f\,(1 - \bar{R}_{m1}) \qquad 2.6$$

$$\bar{d}_2 = f\,(1 - \bar{R}_{m2}) \qquad 2.7$$

$$S_1 = S_2 = f \qquad 2.8$$

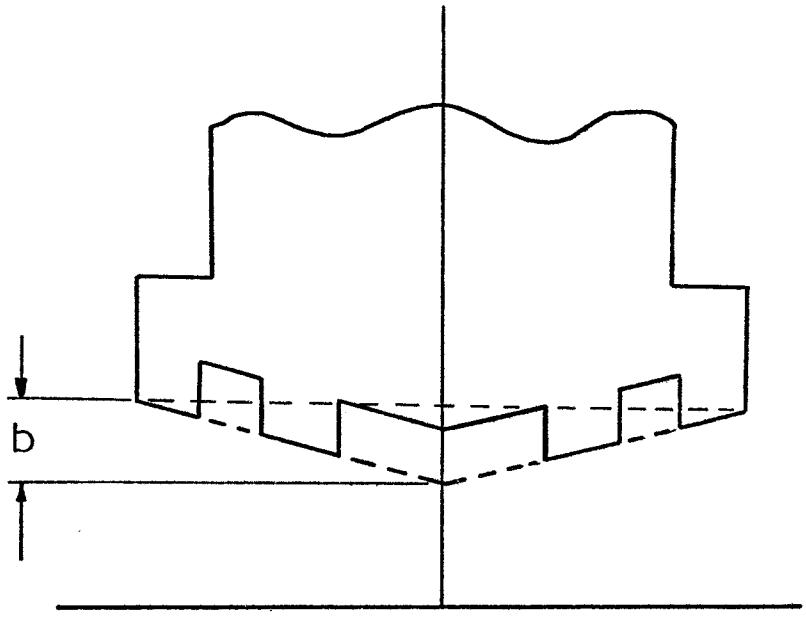

FIG. 2.3 CONICAL PROFILE

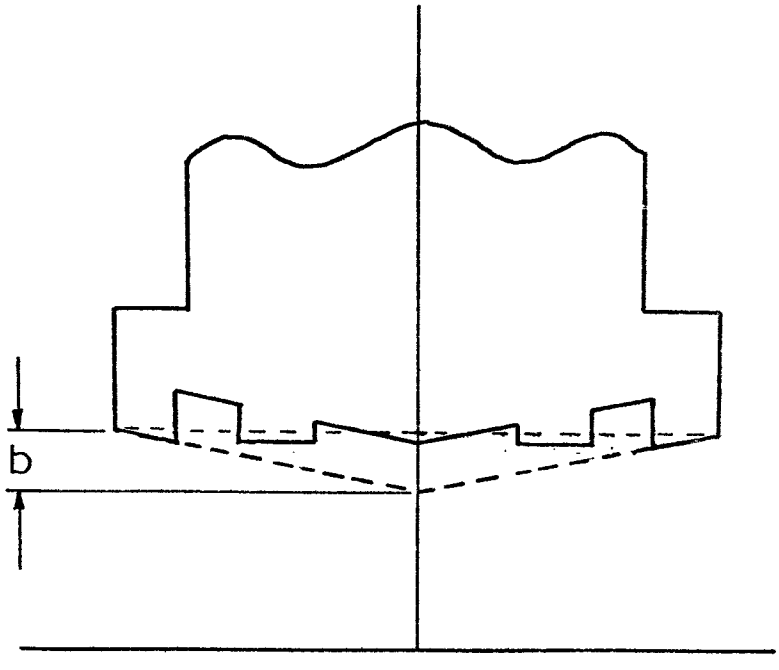

FIG. 2.4 CHAMFERRED PROFILE

(ii) Chamferred profile (fig. 2.4). The slope and offset of the outer land are the same as above. However for the inner land:-

$$S_1 = 0 \qquad 2.9$$

$$d_1 = f\ (1 - \bar{R}_3) \qquad 2.10$$

(iii) Parabolic profile (fig. 2.2). This profile is generated by the revolution of a parabola about the slipper axis and superimposed on plane BAC. Since all the lands must be straight, they are considered as being tangential to the parabola at radius R_m. It can be shown that in this case:-

$$\bar{d}_1 = f\ (1 - \bar{R}_{m1}^2) \qquad 2.11$$

$$\bar{d}_2 = f\ (1 - \bar{R}_{m2}^2) \qquad 2.12$$

$$S_1 = 2\ f\ \bar{R}_{m1} \qquad 2.13$$

$$S_2 = 2\ f\ \bar{R}_{m2} \qquad 2.14$$

Out of these three prototype profiles, it was considered that the most appropriate to analyse first was the parabolic one. This choice was the result of careful studies on a substantial number of slippers which indicated that the majority of slippers were to some degree convex. Fig. 2.5 shows a typical Talysurf trace taken across the slipper lands which shows small but definite amounts of convexity to be present. The parabolic profile was thus thought to be the most representative of the types of non-flatness as found in practice.

The choice of this profile is a further idealisation of the problem simply because it precludes the effects of other possible profiles. It is not practical at this stage to

examine more than one type of non-flatness at the same time. It is, however, worth noting the consequences of such an idealisation and the limitations that it imposes on the analysis. One such limitation results from the assumption that the lands are straight or rather part of a conical surface. This cannot obviously account for the effect of rounded land edges which are not uncommon in practice (fig. 2.5). Since working land clearances in a real pump can be of the same order of magnitude (about 1 micron or even less), the effect of rounded or chamferred land edges could be considerable. This assumption, however, was considered to be a reasonable first approximation which could be modified later if it was found necessary.

Another type of non-flatness which cannot be examined with the present analysis is a saddle-shape as shown in fig. 2.6. Its effects, however, are uncertain and it will not be considered.

2.2.7. Clearance

The clearance h is defined as the clearance of any general point with co-ordinates R, θ on either land. It is more useful in its non-dimensional form by dividing it by h_c:-

$$\bar{h} = h/h_c \qquad 2.15$$

It can be shown that in terms of geometry and attitude it can be expressed as:-

$$\bar{h} = 1 + t \cos(\theta - \theta_m)\,\bar{R} - \bar{d} + S\,(\bar{R} - \bar{R}_m) \qquad 2.16$$

assuming that the angle of tilt is sufficiently small to have a negligible effect on the projection of $\bar{d}$ on the z-axis. This expression can be applied to any of the three

TALYSURF TRACES SHOWING NON-FLATNESS OF TYPICAL SLIPPERS

FIGURE 2.5

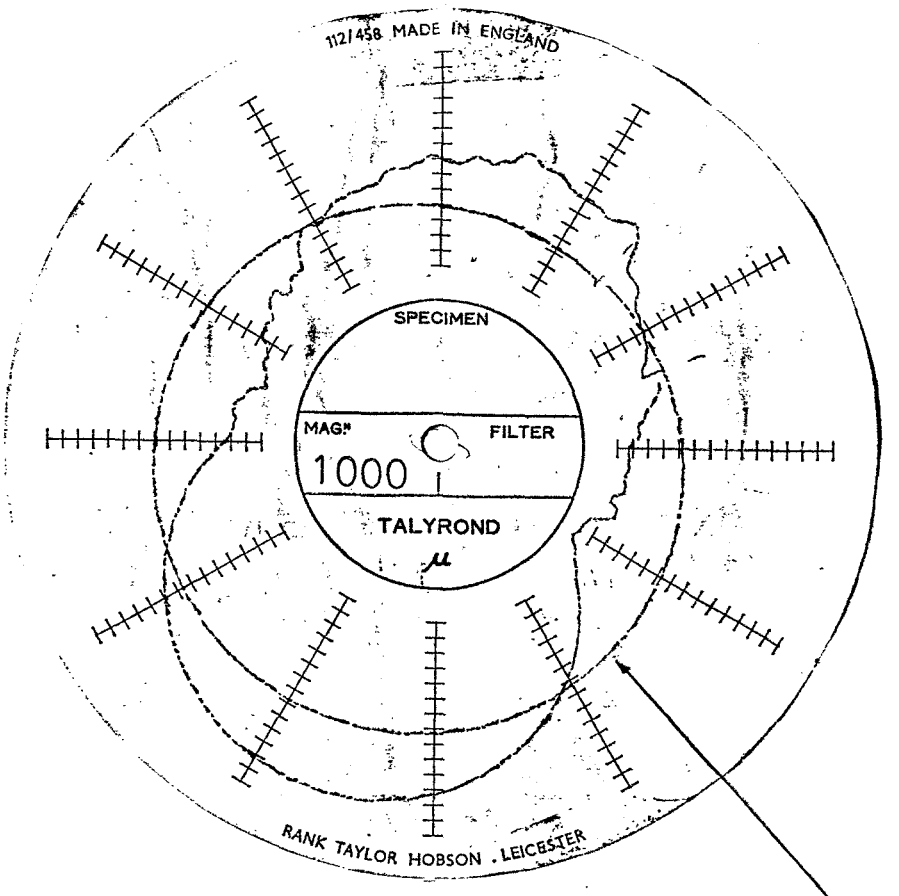

CIRCULAR NON-FLATNESS ON THE INNER LAND OF A TYPICAL SLIPPER

FIGURE 2.6

profiles mentioned in section 2.2.6.

The differentials with respect to $\bar{R}$ and θ are:-

$$\frac{\partial \bar{h}}{\partial \bar{R}} = t \cos (\theta - \theta_m) + S \qquad 2.17$$

$$\frac{\partial \bar{h}}{\partial \theta} = - t \sin (\theta - \theta_m) \bar{R} \qquad 2.18$$

Obviously the relations 2.16, 2.17 and 2.18 can be applied to either the inner or outer land by substituting the appropriate $\bar{d}$, S and $\bar{R}_m$.

2.3. Reynolds' equation and assumptions

The theoretical analysis of the behaviour of the slipper has its starting point at Reynolds' equation. In order to reduce the equation to a workable form, it is customary to introduce a number of assumptions which simplify the analysis considerably without altering the nature of the problem[22].

(i) Body forces acting on the lubricant such as gravitational, magnetic or electrical are neglected.

(ii) The inertia of the fluid is also neglected.

(iii) The pressure is assumed to be constant through the thickness of the lubricating fluid.

(iv) By assuming that the radius of curvature is large compared with the oil film thickness, surface velocities are considered to be constant in direction. Moreover it is assumed that the velocity of a surface is the same as the velocity of the adjacent layer of lubricant.

(v) The lubricant is Newtonian.

(vi) Viscosity is considered to be constant through the thickness of the lubricating film.

(vii) The flow is laminar.

A further assumption which was found to be of particular value when applied to this analysis is the "short bearing approximation". This approximation, as suggested by its name, can be applied to narrow bearings or rather more precisely to bearings in which the width is much smaller than the length. In this work it takes effect by eliminating the $dP/d\theta$ term in Reynolds' equation. This assumes that pressure gradients and therefore flows due to pressure in the tangential direction are considerably smaller than corresponding ones in the radial direction and, therefore, they can be ignored. However, tangential flows due to the relative motion between the slipper and slipper plate are included and they are discussed in greater detail in section 2.7.2.3. The application of this assumption to the analysis is justified by the fact that the ratio of land width to mean land length is around 0.04 (using the dimensions of the inner land of the C.H.L. slipper). Moreover the pressure difference across the inner land is relatively high (for most practical purposes it is equal to piston pressure minus case pressure).

Obviously the introduction of this assumption limits the accuracy of the analysis but on the other hand it has the advantage of increasing the speed of computation considerably. Caution must be exercised, however, when applying the analysis and related computer programs to other slipper designs. Although adequate for this type of design the accuracy of the computation will inevitably be reduced as the width to length ratio of the lands is

increased.

It is more convenient to use Reynolds' equation in its polar form[22]. Ignoring pressure gradients in the θ direction the equation can be expressed as:-

$$\frac{1}{R}\frac{\partial}{\partial R}\left(Rh^3\frac{\partial P}{\partial R}\right) = 6\eta\left(U\cos\theta\frac{\partial h}{\partial R} - \frac{U\sin\theta}{R}\frac{\partial h}{\partial\theta} + \omega\frac{\partial h}{\partial\theta}\right) \qquad 2.19$$

where P is the pressure at any point and ω is the spin.

The above equation can be made dimensionless by the use of 2.1, 2.15 and:-

$$\bar{P} = P/P_s \qquad 2.20$$

$$\bar{\omega} = \omega R_4/U \qquad 2.21$$

Thus, 2.10 can be modified to:-

$$\frac{1}{\bar{R}}\frac{\partial}{\partial\bar{R}}\left(\bar{R}\bar{h}^3\frac{\partial\bar{P}}{\partial\bar{R}}\right) = \frac{6\eta UR_4}{h_c^2 P_s}\left(\cos\theta\frac{\partial\bar{h}}{\partial\bar{R}} - \frac{\sin\theta}{\bar{R}}\frac{\partial\bar{h}}{\partial\theta} + \bar{\omega}\frac{\partial\bar{h}}{\partial\theta}\right) \qquad 2.22$$

The only part of this equation which still contains dimensional variables is the group outside the bracket on the R.H.S. It is convenient at this stage to split this group into appropriate variables in the following fashion:-

$$\bar{H}_c = \sqrt{\frac{h_c^2 P_p}{6\eta UR_4}} \qquad 2.23$$

$$\bar{P}_s = P_s/P_p \qquad 2.24$$

Additionally all operating conditions can be grouped in one single variable Z where:-

$$Z = \sqrt{\frac{P_p}{6\eta UR_4}} \qquad 2.25$$

In this way:-

$$\bar{H}_c = Z h_c \qquad 2.26$$

By expanding the L.H.S. and by substituting the differentials of $\bar{h}$ obtainable from 2.17 and 2.18 into the

R.H.S., equation 2.22 can be modified to:-

$$\bar{h}^3 \left[\frac{\partial \bar{P}}{\partial \bar{R}} \frac{1}{\bar{R}} + \frac{3}{\bar{h}} \frac{\partial \bar{h}}{\partial \bar{R}} + \frac{\partial^2 \bar{P}}{\partial \bar{R}^2} \right] =$$

$$\frac{1}{\bar{H}_c^2 \bar{P}_s} \left[S \cos\theta_m - t \cos\theta_m - \bar{\omega} t \bar{R} \sin(\theta - \theta_m) \right] \qquad 2.27$$

2.4. Pressure distribution under the slipper

In the previous section Reynolds' equation was adjusted to suit this particular problem by applying slipper geometry to the R.H.S. of the equation. Further adjustments can be made on the L.H.S. of 2.27 by introducing information related to pressure. Obviously the pressure distribution is not known completely but a number of facts are known about it and they can be of considerable use when applied into Reynolds' equation.

The first observation is related to the groove between the two slipper lands (fig. 1.2). Because of the two slots machined across the outer land, the pressure inside the groove will be for most practical purposes equal to case pressure. This leads to a second observation about the outer land. Because pressure on either side of the outer land will be equal to case pressure, the pressure distribution on the outer land itself will be purely hydrodynamic and it will be independent of pocket pressure. Thirdly the pressure variation inside the slipper pocket is expected to be negligible at steady state conditions. Although the pressure level is not yet known, it is reasonable to assume that it is uniform and equal to P_s. Finally the pressure distribution on the inner land occurs as a result of two factors which are superimposed on each other. In the first

instance there is a pressure drop from P_s at R_1 to O at R_2. This is the result of the pressure in the slipper pocket and it will be called the hydrostatic component. Secondly, some pressure will be generated hydrodynamically in exactly the same way as on the outer land. The overall pressure distribution on the inner land will be equal to the algebraic sum of the hydrostatic and hydrodynamic components.

The boundary conditions are thus determined as follows:-

At radius R_2, R_3 and R_4, pressure is zero.

In the region O to R_1 pressure is uniform and is equal to P_s.

The next stage is obviously to place the above observations and boundary conditions into mathematical form by relating pressure to geometry, where this is possible. The configuration used is shown in graphical form in fig. 2.7 and is as follows:-

1. Region $R_3 < R < R_4$ or outer land.

$$\bar{P} = \frac{A_{d2}}{\bar{H}_c^2 \bar{P}_s} (\bar{R} - \bar{R}_3) (\bar{R} - \bar{R}_4) \qquad 2.28$$

The expression is parabolic and it is symmetrical about the mid-radius $\bar{R}_{m2}$. It also satisfies the boundary conditions since $\bar{P} = O$ at $\bar{R} = \bar{R}_3$ and $\bar{R} = \bar{R}_4$. $\bar{P}$ is also proportional to A_{d2}. This is a hydrodynamic pressure coefficient and will be determined in the following section.

2. Region $\bar{R}_2 < \bar{R} < \bar{R}_3$. This is the groove between the lands and as it was mentioned above $\bar{P} = O$.

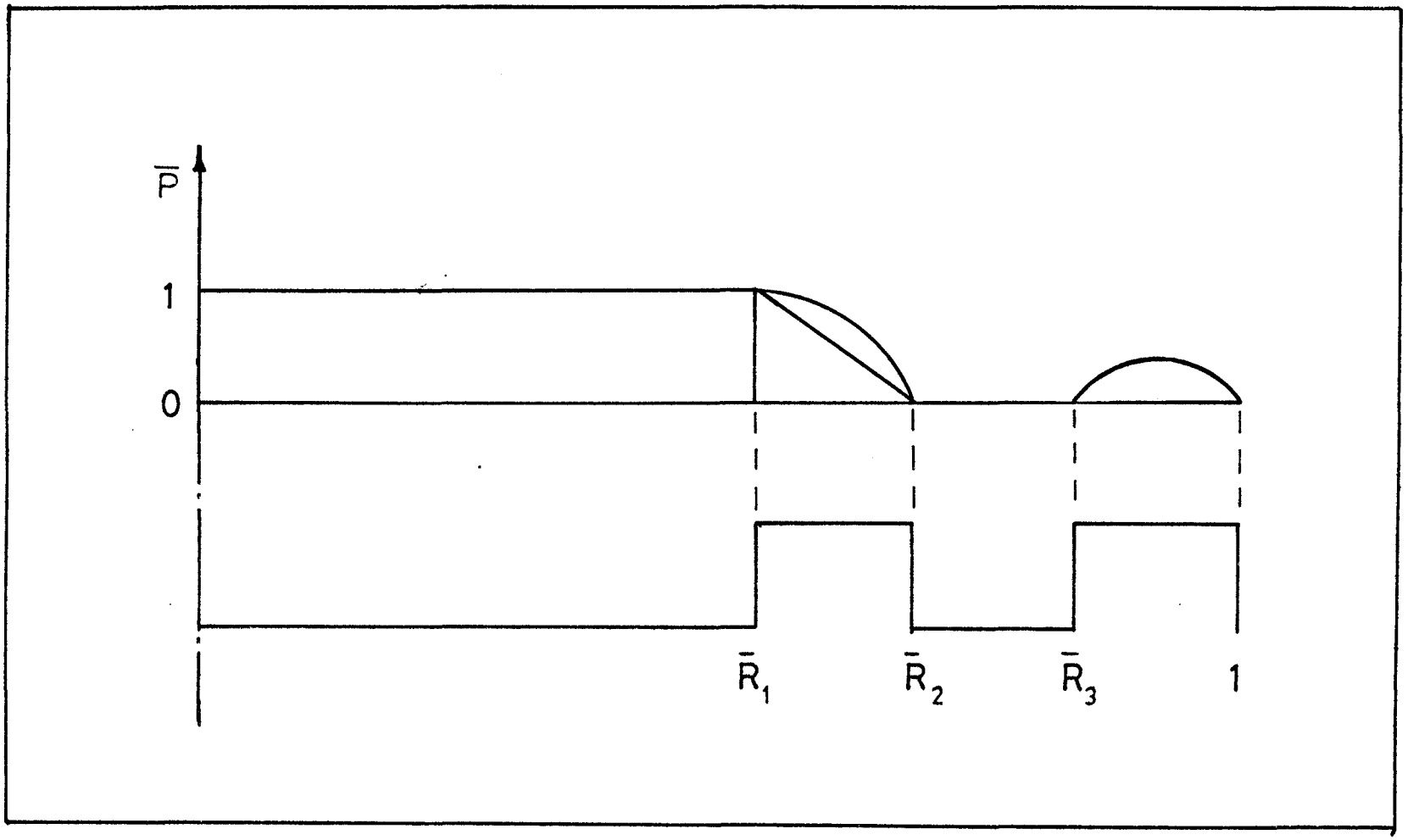

FIG. 2.7 ASSUMED PRESSURE DISTRIBUTION UNDER THE SLIPPER

3. Region $\bar{R}_1 < \bar{R} < \bar{R}_2$ or inner land. The overall pressure distribution is the result of hydrostatic and hydrodynamic effects which are superimposed on each other. Their interaction in the presence of cavitation is discussed in section 2.5.3 and their combined effect under load equilibrium in section 2.7.1. In this section they are considered individually and they are derived as functions of central clearance and pocket pressure. Firstly, the hydrodynamic pressure distribution can be expressed using an expression similar to 2.28. In this case:-

$$\bar{P} = \frac{A_{d1}}{\bar{H}_c^2 \bar{P}_s} (\bar{R} - \bar{R}_1) (\bar{R} - \bar{R}_2) \qquad 2.29$$

As before it is a parabolic function and it has no effect on either edge of the land, in this case at $\bar{R} = \bar{R}_1$ and $\bar{R} = \bar{R}_2$. The hydrostatic pressure is expressed as the summation of a linear and a parabolic term i.e.:-

$$\bar{P} = \frac{\bar{R}_2 - \bar{R}}{\bar{R}_2 - \bar{R}_1} + A_s (\bar{R} - \bar{R}_1) (\bar{R} - \bar{R}_2) \qquad 2.30$$

The parabolic term satisfies the boundary conditions as before whereas the linear term represents the linear pressure drop from 1 at $\bar{R} = \bar{R}_1$ to 0 at $\bar{R} = \bar{R}_2$. A_{d1} and A_s are hydrodynamic and hydrostatic pressure coefficients respectively and they will be determined in the following section.

4. Region $0 < \bar{R} < \bar{R}_1$ or slipper pocket. Pressure in this region is considered to be uniform and equal to P_s. In non-dimensional terms $\bar{P} = 1$.

Although the parabolic expression used in 2.28, 2.29 and 2.30 are approximations of the actual pressure distribution as it may be found in practice, they are considered to be adequate in this case in view of the narrow nature of the lands. Clearly errors will increase when either land width, tilt or local non-flatness are large. It also has the further limitation that it cannot account for partial cavitation across either land. However, the main reason for using this method is that it can provide rapid calculation of non-dimensional lifts and moments. As will be seen later, this calculation will form the nucleus of a number of iterative loops and if a more accurate and longer method was adopted, the computing costs would outweigh the merits of greater accuracy.

2.4.1. Determination of pressure coefficients

Having approximated the pressure distribution on the lands by a parabola the hydrodynamic and hydrostatic pressure coefficients can be determined by:-

a) Satisfying the boundary conditions.

b) Satisfying Reynolds' equation at mid-radius.

The first condition has already been incorporated in the expressions 2.28, 2.29 and 2.30 in the previous section. This section deals with the second condition.

Considering the inner land, as the most general case, the total pressure distribution will be the summation of expressions 2.29 and 2.30. The first and second

differentials at $\bar{R} = \bar{R}_{m1}$ will be:-

$$\frac{\partial \bar{P}}{\partial \bar{R}} = \frac{-1}{\bar{R}_2 - \bar{R}_1} \qquad 2.31$$

$$\frac{\partial^2 \bar{P}}{\partial \bar{R}^2} = 2 A_s + \frac{2 A_{d1}}{\bar{H}_c^2 \bar{P}_s} \qquad 2.32$$

Substituting these as well as 2.16 and 2.17 into the L.H.S. of 2.27 enables the pressure coefficients to be related as follows:-

$$A_{d1} = \frac{1}{2 \bar{h}_{m1}^3} \left[S_1 \cos\theta + t \cos\theta_m - \bar{\omega} t \bar{R}_{m1} \sin\phi \right] \qquad 2.33$$

$$A_s = \frac{1}{2 (\bar{R}_2 - \bar{R}_1)} \left[\frac{1}{\bar{R}_{m1}} + \frac{3 (t \cos\phi + S_1)}{1 + t \cos\phi \bar{R}_{m1} - \bar{d}_1} \right] \qquad 2.34$$

where $\bar{h}_{m1}$ is the clearance at mid-radius and ϕ is defined as:-

$$\phi = \theta - \theta_m \qquad 2.35$$

The expression for the hydrodynamic pressure coefficient on the outer land can be similarly expressed as:-

$$A_{d2} = \frac{1}{2 \bar{h}_{m2}^3} \left[S_2 \cos\theta + t \cos\theta_m - \bar{\omega} t \bar{R}_{m2} \sin\phi \right] \qquad 2.36$$

Relations 2.33, 2.34 and 2.36 show that the pressure coefficients and hence the pressure profile on either land at any angle θ are functions of slipper geometry, attitude and spin. The only unknowns are $\bar{H}_c$ and $\bar{P}_s$ which occur in all hydrodynamic terms.

2.5. Cavitation

Cavitation within the context of this work is interpreted as a "lack of pressure". It is usually caused by oil flowing through diverging surfaces as a result of

which pressure drops. In some cases it could theoretically become negative. However, once it reaches the level of the vapour pressure corresponding to the oil temperature, so called "void volumes" of vapourised oil are formed and oil pressure remains constant until the "void" is eliminated. Another possible cause of cavitation would be the sudden lifting off of the slipper in such a way that oil was unable to replenish the increased volume in time. However, the latter case would occur only under dynamic conditions and as such it falls outside the scope of this work.

Full interpretation of cavitation can be extremely involved but for the purpose of this work it is adequate to assume zero pressure whenever the latter is detected to become negative. Therefore, in order to include the effect of cavitation it is necessary to know the angular limits which mark the boundaries of the negative pressure region. These will be used to modify the limits of the integrals which estimate the lift and moments on the slipper so that the contribution from the negative pressure regions will be nil.

One limitation of this approach, which has already been mentioned in section 2.4.1, is that it cannot account for partial cavitation across any land because it assumes a predefined pressure profile. This is not an unlikely thing to happen in practice but its effect is considered to be very small. The limits of partial cavitation mentioned in this section refer to the θ direction and not the radial one.

2.5.1. Cavitation on the outer land (Purely hydrodynamic case)

The pressure on the outer land can be found by substituting 2.35 into 2.28 giving:-

$$\bar{P} = \frac{1}{\bar{H}_c^2 \bar{P}_s} \left[\bar{R}^2 - \bar{R} (\bar{R}_3 + \bar{R}_4) + \bar{R}_3 \bar{R}_4 \right] \frac{1}{2 \bar{h}_{m2}^3}$$

$$\left[S_2 \cos\theta + t \cos\theta_m - \bar{\omega} t \bar{R}_{m2} \sin\phi \right] \qquad 2.37$$

In order to find the sign of this expression it is necessary to examine each group separately. Firstly, assuming positive velocity, $\bar{H}_c^2$ will be positive. $\bar{P}_s$ must also be positive otherwise the operation of the slipper under steady state becomes impossible. The clearance at mid-radius must also be always positive and this leaves the sign of $\bar{P}$ to be determined by the two groups inside the brackets. Of these the parabolic expression is known to be negative for $\bar{R}_3 < \bar{R} < \bar{R}_4$, therefore, $\bar{P}$ will be positive when the remaining expression is negative.

Algebraic manipulation can be made easier by grouping together the $\sin\theta$ and $\cos\theta$ terms.

$$t \cos\theta_m + \cos\theta (S_2 + \bar{\omega} t \bar{R}_{m2} \sin\theta_m) + \sin\theta (-\bar{\omega} t \bar{R}_{m2} \cos\theta_m)$$

Let:-

$$u = t \cos\theta_m \qquad 2.38$$

$$v = S_2 + \bar{\omega} t \bar{R}_{m2} \sin\theta_m \qquad 2.39$$

$$w = \bar{\omega} t \bar{R}_{m2} \cos\theta_m \qquad 2.40$$

$$g = \sqrt{v^2 + w^2} \qquad 2.41$$

$$\tan\beta = w/v \qquad 2.42$$

so that the expression simplifies to:-

$$u + v \cos\theta + w \sin\theta$$

a) "Full cavitation" will occur when the pressure is theoretically negative everywhere on the outer land. This will be the case when:-

$$u + v\cos\theta + w\sin\theta > o$$

for all values of θ. The only way for this to happen is when $u > g$ or:-

$$\left[(S_2 + \bar{\omega}\, t\, \bar{R}_{m2}\sin\theta_m)^2 + (\bar{\omega}\, t\, \bar{R}_{m2}\cos\theta_m)^2\right]^{\frac{1}{2}} < t\cos\theta_m$$

This is theoretically possible when a flat slipper is travelling tilted forward in which case the outer land presents a diverging wedge to the oil flow. In this case the pressure everywhere on the outer land is set to zero and the limits of θ for the integration are $\theta_1 = o$ and $\theta_2 = o$.

b) "No cavitation" will occur when pressure is positive everywhere on the outer land. In this case:-

$$u + v\cos\theta + w\sin\theta < o$$

for all values of θ. This will be so when $u < -g$ or:-

$$\left[(S_2 + \bar{\omega}\, t\, \bar{R}_{m2}\sin\theta_m)^2 + (\bar{\omega}\, t\, \bar{R}_{m2}\cos\theta_m)^2\right]^{\frac{1}{2}} > -\, t\cos\theta_m$$

Such a case will occur when a flat slipper is travelling tilted backwards (trailing end down) when a converging wedge will be presented to the oil flow. In this case the hydrodynamic lift and moments will be calculated by integrating the pressure from o to 2π i.e. $\theta_1 = o$ and $\theta_2 = 2\pi$

c) "Partial cavitation" will occur when the pressure is positive only on some part of the outer land. This means that the value of $u + v\cos\theta + w\sin\theta$ could be

positive or negative depending on the value of θ.

The criterion for this case is:-

$$-g < u < g$$

The boundaries of positive pressure can be found by equating this expression to zero i.e.:-

$$v \cos\theta + w \sin\theta = - u \qquad 2.43$$

The solution of this equation can be found by dividing throughout by g. Since $\tan\beta = w/v$ it follows that $\cos\beta = v/g$ and $\sin\beta = w/g$. Therefore 2.43 can be rewritten as:-

$$\cos\beta \cos\theta + \sin\beta \sin\theta = -u/g \quad \text{or}$$

$$\cos(\beta - \theta) = -u/g \text{ hence}$$

$$\theta = \beta \pm \cos^{-1}(u/g) = \tan^{-1}(w/v) \pm \cos^{-1}(u/g)$$

The boundaries of positive pressure are given by:-

$$\theta_1 = \tan^{-1}(w/v) + \cos^{-1}(u/g) \qquad 2.44$$

$$\theta_2 = 2\pi + \tan^{-1}(w/v) - \cos^{-1}(u/g) \qquad 2.45$$

This situation will occur when the slipper is convex and not tilted. The front of the slipper will present a converging surface to the oil flow and positive pressure will be encountered. Conversely the back of the slipper will be divergent to the oil flow and will cavitate.

2.5.2. Cavitation in the slipper pocket (hydrostatic case)

As the slipper pocket can be continuously fed with oil through the orifice, cavitation is unlikely to occur there under normal circumstances in the steady state condition. The only remaining possibility is when the orifice is zero or very small and the slipper is heavily tilted forward. However, it is not possible to detect such a possibility at

this stage because slipper pocket pressure $\bar{P}_s$ is not known. In fact it is a primary variable which will be calculated later on. The only approach which can be adopted is to assume that there is no cavitation in the pocket and on the basis of that calculate $\bar{P}_s$. If that turns out to be positive the original assumption is in agreement with the result and the analysis proceeds. If $\bar{P}_s$ is found to be negative, then it must be reset to zero and the procedure for calculating the lift, moments etc. must be repeated (see also section 2.8).

2.5.3. Cavitation on the inner land (Mixed hydrostatic and hydrodynamic effects)

This case is even more difficult to assess than the previous one because the hydrodynamic and hydrostatic pressures are superimposed and neither is known in advance. Cavitation will occur when:-

a) Both are negative.

b) One is negative and greater in magnitude than the positive one.

Neither of these conditions can be anticipated at this stage because it is not possible to know the magnitude of either effect without prior knowledge of $\bar{H}_c$ and $\bar{P}_s$. Therefore an iterative approach needs to be applied as before. The logic in this case is to start by assuming that there is no cavitation at all. This in fact is the most common case since hydrodynamic pressure is superimposed on hydrostatic and provided that there is pressure in the pocket any "void volumes" generated hydrodynamically will be replenished by oil from the pocket. So the limits of integrating pressure hydrostatically and hydrodynamically will initially be zero

to 2π. The lift and moments can then be calculated and this will eventually produce the values of $\bar{P}_s$ and $\bar{H}_c$. If $\bar{P}_s$ is positive the analysis proceeds. If $\bar{P}_s$ is negative then it is necessary to go back, reset all hydrostatic contributions to zero and calculate the limits of positive hydrodynamic pressure using a method similar to the one applied for the outer land. The lift and moments can then be calculated between the appropriate limits which will produce an approximate value for $\bar{H}_c$ (see also section 2.8).

2.6. Forces and moments due to pressure under the slipper

Knowing the pressure coefficients, it is now possible to evaluate the forces and moments acting on the undersurface of the slipper. This is done by integrating the expressions for the pressure distribution in the $\bar{R}$ and θ fields within the appropriate boundaries.

All forces and moments in this section are calculated and presented in a non-dimensional form. Also all the hydrodynamic effects are calculated as multiples of $\bar{H}_c$ and $\bar{P}_s$ which are at the moment unknown.

In order to make the algebra easier to manipulate, some of the frequently encountered integrals have been put together in Appendix A. These integrals will be constantly referred to throughout this section. It is convenient in some cases to work with ϕ or γ rather than θ. The transformation of θ into ϕ is straightforward (relation 2.35). Transforming ϕ into γ is slightly more involved and the procedure is described in detail in Appendix B.

2.6.1. Hydrostatic effects

Within the region $O-\bar{R}_1$ (slipper pocket) the dimensionless pressure has been assumed constant and equal to 1. Therefore this area will produce a hydrostatic lift equal to $\pi \bar{R}_1^2$. The moment of this pressure distribution about any of the axes is zero.

The hydrostatic lift on the inner land is:-

$$\int_o^{2\pi} \int_{\bar{R}_1}^{\bar{R}_2} \bar{P}\ \bar{R}\ d\bar{R}\ d\theta$$

Substituting 2.30 and adding the slipper pocket lift gives the total hydrostatic lift:-

$$\bar{L}_s = \pi\ \bar{R}_1^2 + \int_o^{2\pi} \int_{\bar{R}_1}^{\bar{R}_2} \left[\frac{\bar{R}_2 - \bar{R}}{\bar{R}_2 + \bar{R}_1} + A_s \left(\bar{R}^2 - \bar{R}\ (\bar{R}_1 + \bar{R}_2) + \bar{R}_1\ \bar{R}_2 \right) \right] \bar{R}\ d\bar{R}\ d\theta$$

Since A_s is not a function of $\bar{R}$ the expression can be integrated with respect to $\bar{R}$ giving:-

$$\bar{L}_s = \pi\ \bar{R}_1^2 + \int_o^{2\pi} (C_p + C_1\ A_s)\ d\theta \qquad 2.46$$

where C_p and C_1 are constants equal to:-

$$C_p = \left(\bar{R}_2^2 + \bar{R}_1\ \bar{R}_2 - 2\ \bar{R}_1^2 \right) /6 \qquad 2.47$$

$$C_1 = (\bar{R}_1 - \bar{R}_2)^3\ (\bar{R}_1 + \bar{R}_2)\ /12 \qquad 2.48$$

We can now substitute into 2.46 the expression for A_s given in 2.34.

The expression can be put into standard form by the use of the substitution:-

$$e_1 = t\ \bar{R}_{m1}\ /(1 - \bar{d}_1) \qquad 2.49$$

and also by transforming all θ's to ϕ's. Integrating from o to 2π with respect to ϕ gives:-

$$\bar{L}_s = \pi \bar{R}_1^2 + 2\pi C_p + \frac{C_1}{2(\bar{R}_2 - \bar{R}_1)} \left[\frac{2\pi}{\bar{R}_{m1}} + \frac{3}{1 - \bar{d}_1} (t I_{10} + S_1 I_8) \right] \quad 2.50$$

where I_8 and I_{10} are integrals which are solved in Appendix A.

The moment about the y-axis is given by:-

$$\bar{M}_{sy} = \int_0^{2\pi} (C_p + C_1 A_s) \bar{R}_{m1} \cos\theta \, d\theta$$

Substituting for A_s, as before, discarding terms whose integral is zero and integrating from o to 2π gives:-

$$\bar{M}_{sy} = \frac{3 C_1 \bar{R}_{m1} \cos\theta_m}{2(\bar{R}_2 - \bar{R}_1)(1 - \bar{d}_1)} \left(t I_{11} + S_1 I_{10} \right) \quad 2.51$$

Similar considerations produce the moment about the x-axis:-

$$\bar{M}_{sx} = \frac{3 C_1 \bar{R}_{m1} \sin\theta_m}{2(\bar{R}_2 - \bar{R}_1)(1 - \bar{d}_1)} \left(t I_{11} + S_1 I_{10} \right) \quad 2.52$$

2.6.2. Analysis of hydrostatic effects

Referring to relation 2.50 it can be seen that the hydrostatic lift $\bar{L}_s$ is a function of tilt and non-flatness but not of θ_m. The relationship between $\bar{L}_s$ tilt and parabolic non-flatness is shown in fig. 2.8. The values that $\bar{L}_s$ can take range from about 1.52 up to 1.62. The effect of tilt is small compared to the effect of non-flatness especially for small or negative values of non-flatness.

Comparing the hydrostatic lift in the slipper pocket ($\pi \bar{R}_1^2$) which is equal to 1.337 to the range of $\bar{L}_s$ we can deduce that the inner land contributes between 13% to 18% of the total hydrostatic lift.

As far as the load exerted on the slipper by the piston ($\pi \bar{R}_p^2/\cos\alpha$) is concerned, its minimum value (at zero swash) is 1.648 which is about 2% above the maximum hydrostatic lift that can be provided by the slipper. At more realistic conditions of 15^o swashplate angle the piston load becomes 1.706 and the deficiency of the hydrostatic lift increases to 5.3%.

It is obvious therefore that the hydrostatic lift alone is not enough to support the load and additional lift must be generated hydrodynamically.

The equilibrium of the slipper also depends on the sum of the moments exerted on it being zero or, in the absence of external couples, when the pressure centre coincides with the origin.

Referring to relations 2.51 and 2.52 it can be seen that the hydrostatic moments $\bar{M}_{sx}$ and $\bar{M}_{sy}$ are functions of tilt, non-flatness and θ_m. However, their relation to θ_m is a simple sinusoidal function of the form $\bar{M}_{sx} = M_s \sin\theta_m$ and $\bar{M}_{sy} = M_s \cos\theta_m$ where M_s is the maximum moment and it has the same magnitude for both $\bar{M}_{sx}$ and $\bar{M}_{sy}$.

Plots of M_s against tilt for a range of values of non-flatness are shown in fig. 2.9.

The co-ordinates of the pressure centre for hydrostatic effects alone are given by:-

$$\bar{x}_s = M_s \cos\theta_m/\bar{L}_s \qquad 2.53$$

$$\bar{y}_s = M_s \sin\theta_m/\bar{L}_s \qquad 2.54$$

The locus of the pressure centre as θ_m varies is obviously a circle with radius $M_s/\bar{L}_s$. When the ratio $M_s/\bar{L}_s$ is negative as in the case of non-flatness up to 0.6

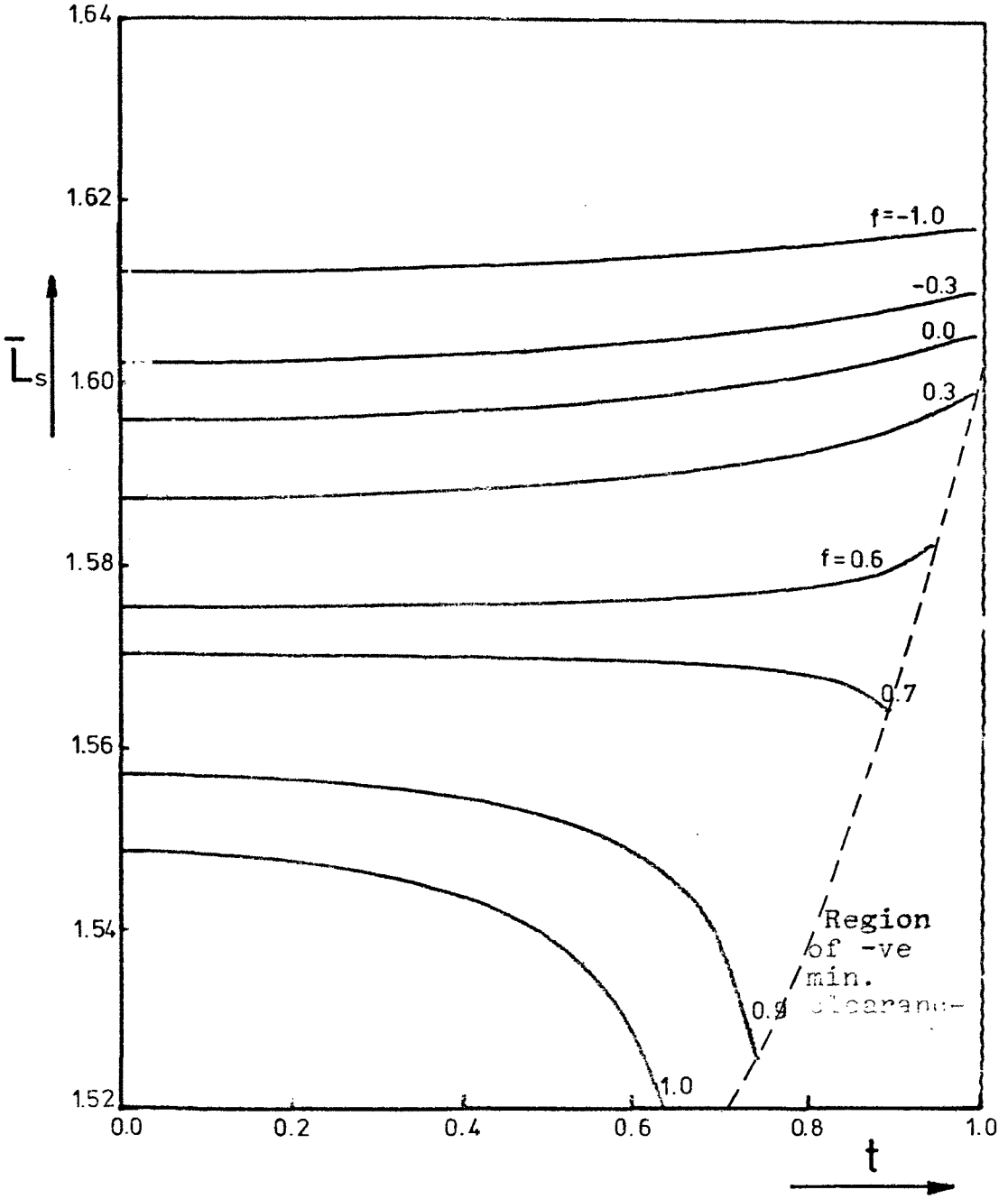

RELATIONSHIP BETWEEN HYDROSTATIC LIFT & TILT

FIGURE 2.8

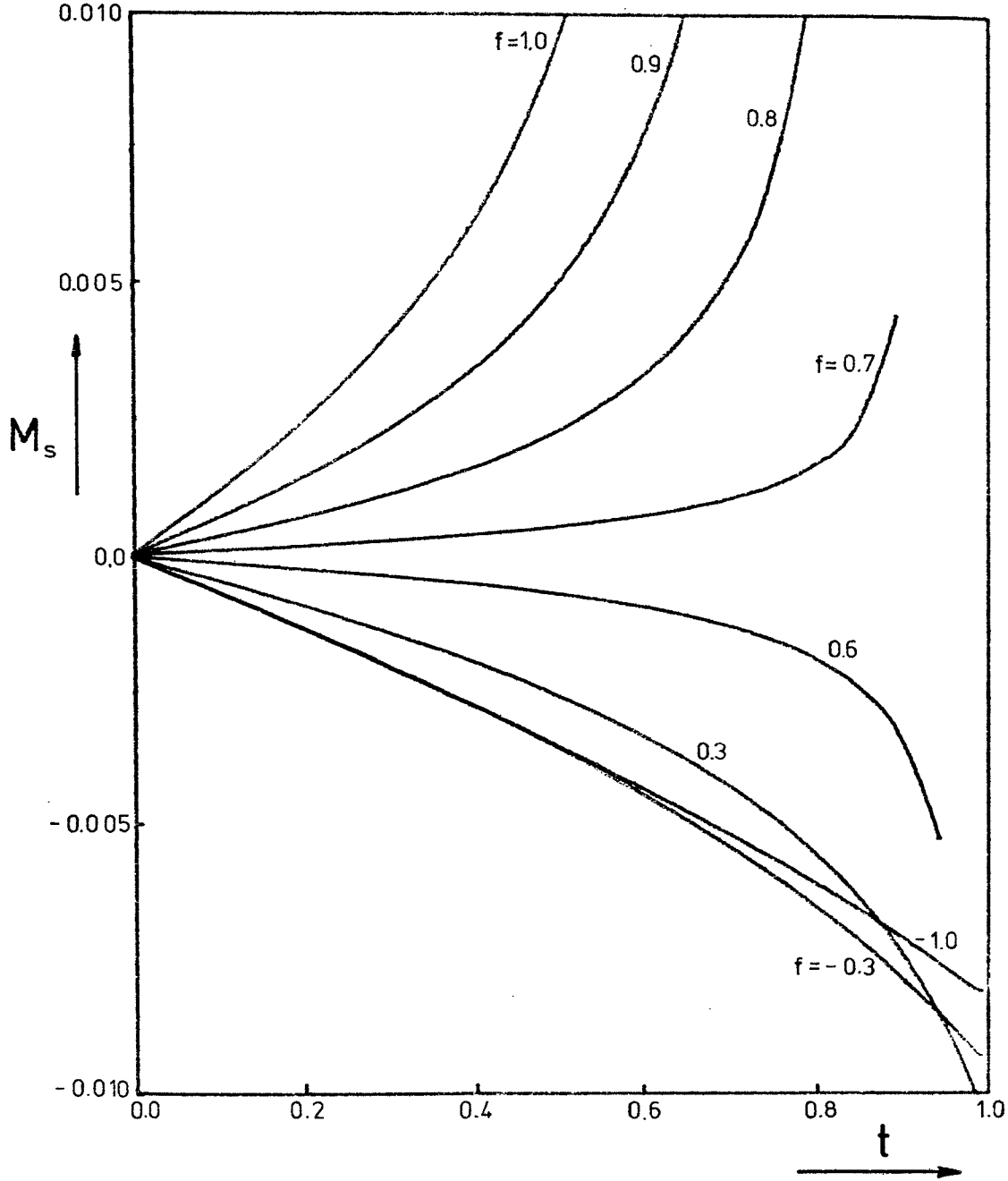

RELATIONSHIP BETWEEN HYDROSTATIC MOMENT & TILT

FIGURE 2.9

(fig. 2.9), the pressure centre follows the position of minimum clearance (at an angle $\theta_m + \pi$). When non-flatness is 0.7 or greater the pressure centre coincides with the angular position of maximum clearance (at an angle θ_m). The only possibility for the pressure centre to coincide with the origin is when the tilt is zero.

Although it has been shown that this slipper configuration cannot support the load exerted on it by the piston, there is nothing to suggest that a slipper with increased ratios ($\bar{R}_1/\bar{R}_p$ and $\bar{R}_2/\bar{R}_p$) would not be able to do so. The question is whether it would be in equilibrium and whether it would be able to return to the equilibrium position if for whatever reason it is tilted in any direction. From the graph on figure 2.9 it is obvious that moment equilibrium is only possible when the tilt is zero whatever the non-flatness. When the slipper is tilted a restoring moment will tend to bring it to its equilibrium position if parabolic non-flatness is 0.6 or less. In the event of non-flatness being greater than 0.7 the hydrostatic moments will be in the opposite sense tending to tilt the slipper further. Therefore, the possibility of a slipper operating on a largely hydrostatic basis, at least under steady state conditions, can only be a viable proposition if the hydrostatic areas on the slipper are suitably enlarged whilst parabolic non-flatness is maintained below 0.6.

2.6.3. Hydrodynamic effects

In this section the hydrodynamic lift and moments on the inner land are evaluated. In order to include every possible type of cavitation (of the ones outlined in section

2.5.1) the limits of integration have been left as θ_1 and θ_2. Conversion of θ to $\emptyset$ can easily be done using relation 2.35. The procedure for converting $\emptyset$ to γ is outlined in Appendix B.

All the calculations in this section will be referring to the inner land. Calculations referring to the outer land are not included because they are identical to the inner land with the appropriate symbols substituted.

The hydrodynamic pressure on the inner land is given by 2.29. The lift due to this pressure is given by:-

$$\bar{L}_{d1} = \int_{\theta_1}^{\theta_2} \int_{\bar{R}_1}^{\bar{R}_2} \bar{P}\ \bar{R}\ d\bar{R}\ d\theta$$

Substituting 2.29 for $\bar{P}$ and integrating with respect to $\bar{R}$, since A_{d1} is independent of $\bar{R}$, produces:-

$$\bar{L}_{d1} = \frac{C_1}{\bar{H}_c^2\ \bar{P}_s} \int_{\theta_1}^{\theta_2} A_{d1}\ d\theta \qquad 2.55$$

Substituting A_{d1} from 2.33 and integrating gives the general formulae for hydrodynamic lift:-

$$\bar{L}_{d1} = \frac{C_1}{\bar{H}_c^2\ \bar{P}_s\ 2\ (1 - d_1)^3} \Big(S_1\ (\cos\theta_m\ I_3 - \sin\theta_m\ I_2) + t\ \cos\theta_m\ I_1 - \bar{\omega}\ t\ \bar{R}_{m1}\ I_2 \Big) \qquad 2.56$$

The hydrodynamic moment about the y-axis is given by:-

$$\bar{M}_{dy1} = \frac{C_1}{\bar{H}_c^2\ \bar{P}_s} \int_{\theta_1}^{\theta_2} A_{d1}\ \bar{R}_{m1}\ \cos\theta\ d\theta$$

Substituting for A_{d1} and integrating as before gives:-

$$\bar{M}_{dy1} = \frac{C_1}{\bar{H}_c^2 \bar{P}_s 2 (1 - \bar{d}_1)^3} \Big[S_1 (I_6 \cos^2\theta_m + I_5 \sin^2\theta_m - I_4 \sin 2\theta_m) + t \cos\theta_m (I_3 \cos\theta_m - I_2 \sin\theta_m) - \bar{\omega} t \bar{R}_{m1} (I_4 \cos\theta_m - I_5 \sin\theta_m) \Big] \quad 2.57$$

The hydrodynamic moment about the x-axis is similarly given by:-

$$\bar{M}_{dx1} = \frac{C_1}{\bar{H}_c^2 \bar{P}_s} \int_{\theta_1}^{\theta_2} A_{d1} \bar{R}_{m1} \sin\theta \, d\theta$$

Substituting and integrating as before gives:-

$$\bar{M}_{dx1} = \frac{C_1 \bar{R}_{m1}}{\bar{H}_c^2 \bar{P}_s 2 (1 - \bar{d}_1)^3} \Big[S_1 (I_7 \sin\theta_m \cos\theta_m + I_4 \cos 2\theta_m) + t \cos\theta_m (I_3 \sin\theta_m + I_2 \cos\theta_m) - \bar{\omega} t \bar{R}_{m1} (I_4 \sin\theta_m + I_5 \cos\theta_m) \Big] \quad 2.58$$

The hydrodynamic lift and moments on the outer land can be evaluated using relations which are identical to 2.56, 2.57 and 2.58 except that C_1, $\bar{R}_{m1}$, $\bar{d}_1$ and S_1 need to be replaced by C_2, $\bar{R}_{m2}$, $\bar{d}_2$ and S_2 respectively.

Since all the variables in 2.56, 2.57 and 2.58 are known except for $\bar{H}_c$ and $\bar{P}_s$ it is convenient to isolate them by expressing the lift and moments as multiples of the unknown variables. Let:-

$$L_{d1} = \bar{L}_{d1} \bar{H}_c^2 \bar{P}_s$$

$$M_{yd1} = \bar{M}_{yd1} \bar{H}_c^2 \bar{P}_s$$

$$M_{xd1} = \bar{M}_{xd1} \bar{H}_c^2 \bar{P}_s$$

2.6.4. Analysis of hydrodynamic effects

Since all hydrodynamic components are multiples of $\bar{H}_c^2 \bar{P}_s$ which is still unknown, any quantitative comparison between hydrostatic and hydrodynamic lifts and moments is impossible. However, it is possible at this stage to investigate the hydrodynamic effects alone and examine how they could affect slipper equilibrium.

It was shown earlier that the hydrostatic lift alone cannot support the piston load for this slipper configuration, therefore, some lift must be generated hydrodynamically. Also, for moment equilibrium the hydrodynamic moment must be able to balance the hydrostatic moment. One of the requirements to satisfy this is that the hydrodynamic pressure centre must lie diametrically opposite the hydrostatic pressure centre.

The behaviour of the hydrostatic pressure centre was examined before (see section 2.6.2) and it was shown that it lies on a circle with radius $M_s/\bar{L}_s$. The hydrodynamic pressure centre can now be examined in a similar fashion in an attempt to find possibilities when the slipper can balance itself. Due to the complexity of the problem the effect of each one of the parameters that can cause hydrodynamic lift was investigated separately whilst θ_m, the position of maximum tilt, was varied between 0 and 2π. Curves consist either of solid or broken lines to distinguish between positive and negative hydrodynamic lift.

2.6.4.1. Effect of tilt

With non-flatness and spin equal to zero, θ_m was varied between 0 and 2π for values of tilt equal to 0.1, 0.5 and

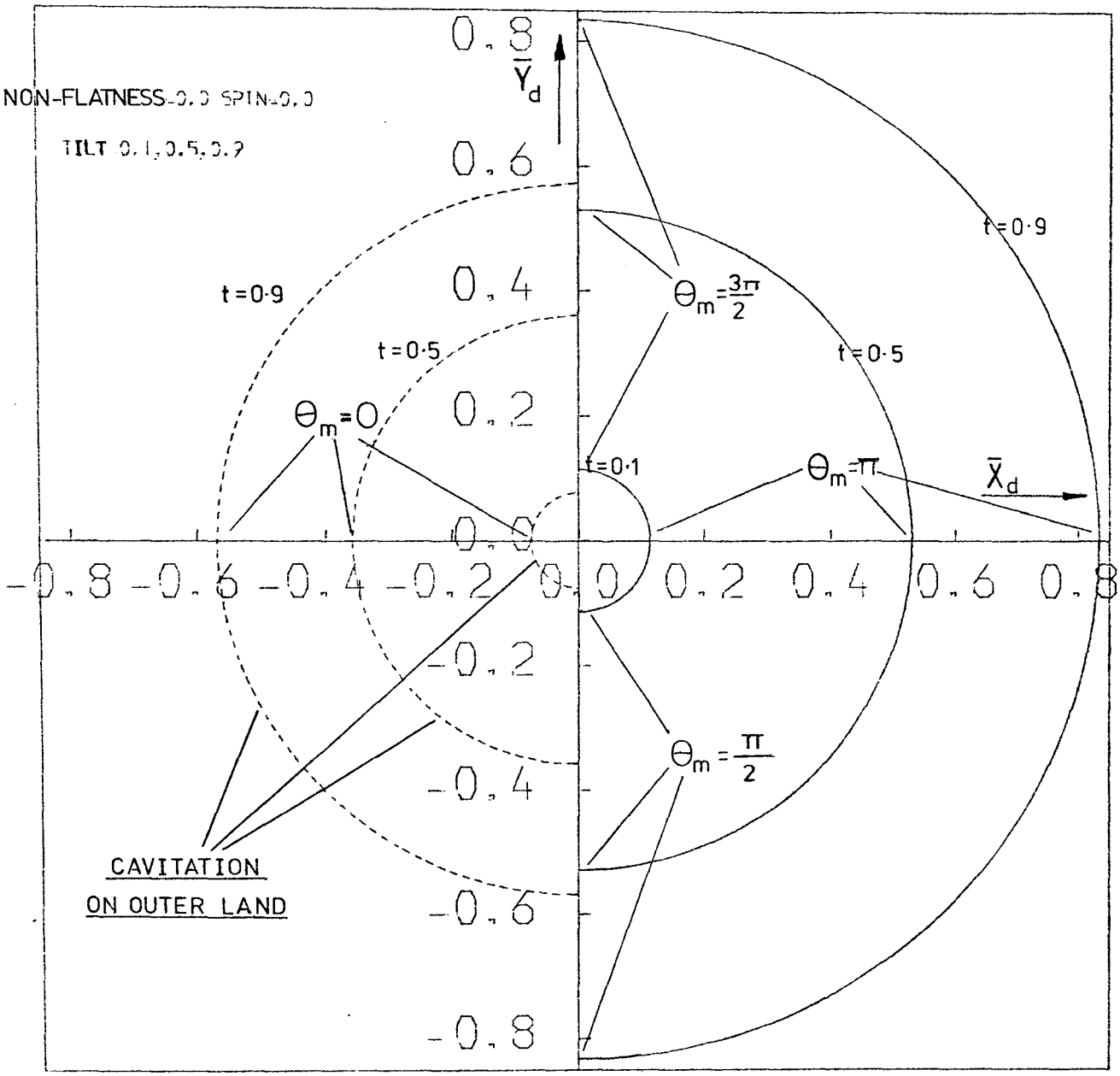

LOCUS OF HYDRODYNAMIC PRESSURE CENTRE

RELATIONSHIP WITH TILT

FIGURE 2.10

0.9. The results are shown in fig. 2.10. In all cases, the locus of pressure centre consists of two semicircles facing each other with the transition from one radius to the other occurring at $\theta_m = \pi/2$ and $\theta_m = {}^3\pi/2$. The reason for this is because for values of θ_m between $\pi/2 < \theta_m < \frac{3\pi}{2}$ the slipper lands offer a converging wedge to the oil flow and a positive hydrodynamic lift at all points. Conversely when $3\pi/2 < \theta_m < \pi/2$ a diverging wedge is formed at every point on the lands and a negative hydrodynamic lift is generated. In this case the effect of the outer land is discarded due to cavitation thus bringing the pressure centre nearer to the origin. The most significant fact, however, is that the pressure centre lies always at $\theta_m + \pi$ or at the position of minimum clearance in exactly the same fashion as the hydrostatic pressure centre. This implies that in this case the moments due to hydrostatic and hydrodynamic contributions add rather than cancel each other. Moreover, the sense of the resultant couple is such that it tends to restore the slipper to the zero tilt position where, of course, the hydrodynamic lift is zero and the hydrostatic lift is inadequate to support the piston load by itself. Therefore, the possibility of a flat, non-spinning slipper functioning under steady state conditions in the absence of external couples can be ruled out.

2.6.4.2. Effect of spin

Since spin alone cannot generate hydrodynamic components it was investigated in conjunction with tilt. With non-flatness equal to zero and tilt equal to 0.1, θ_m was varied between 0 and 2π for values of spin equal to

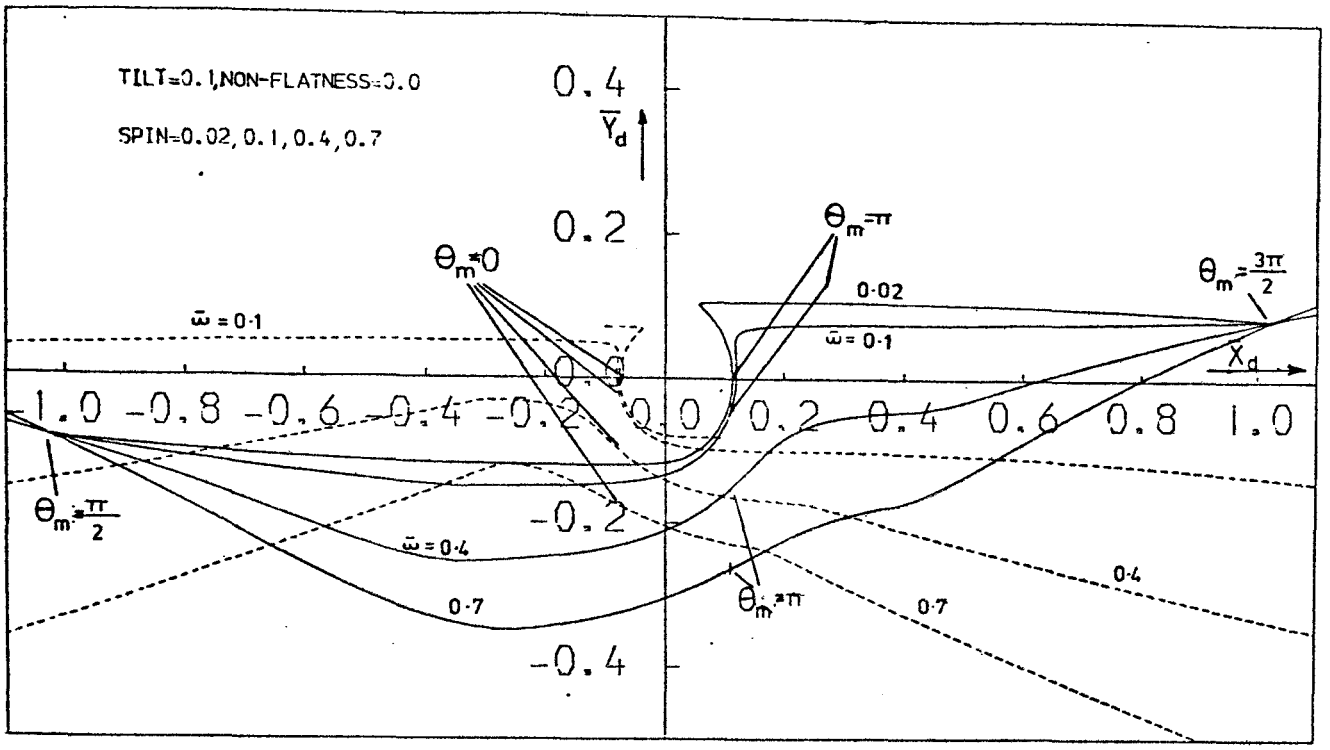

EFFECT OF SPIN ON HYDRODYNAMIC PRESSURE CENTRE

FIGURE 2.11

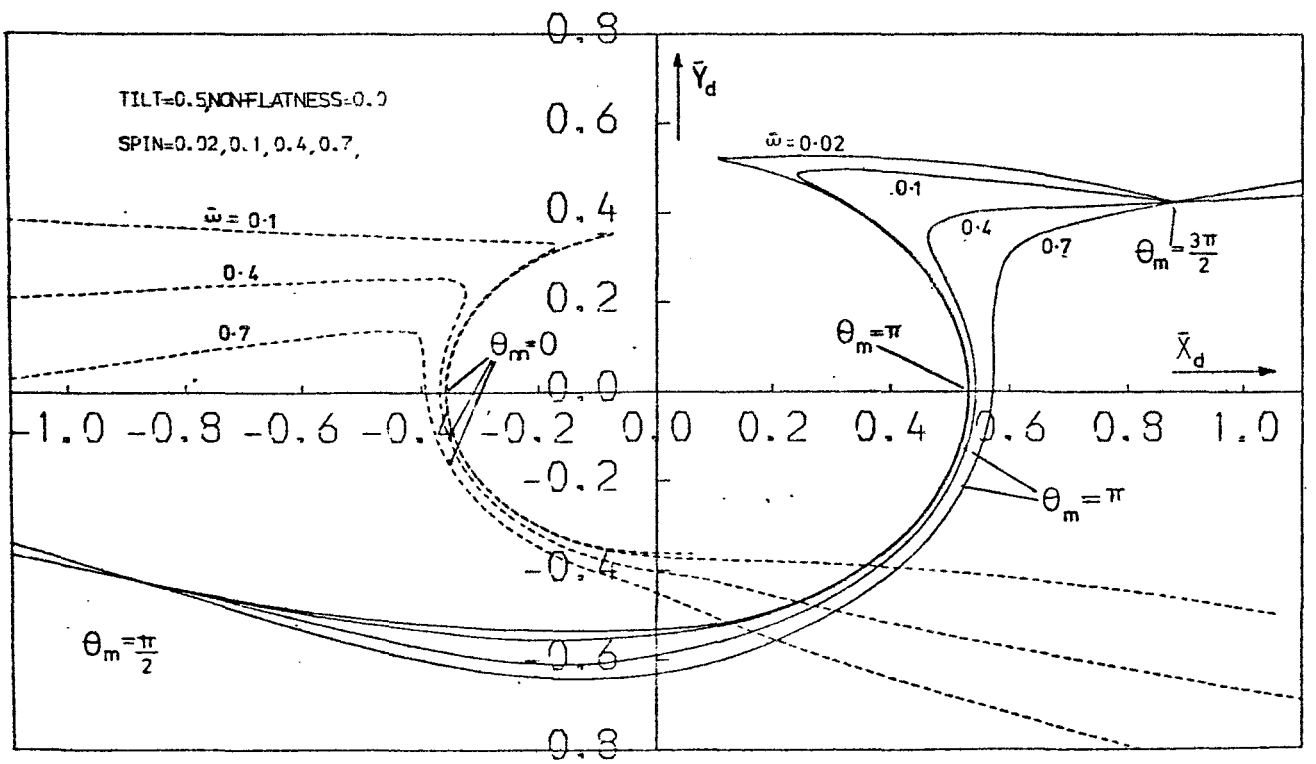

EFFECT OF SPIN ON HYDRODYNAMIC PRESSURE CENTRE

FIGURE 2.12

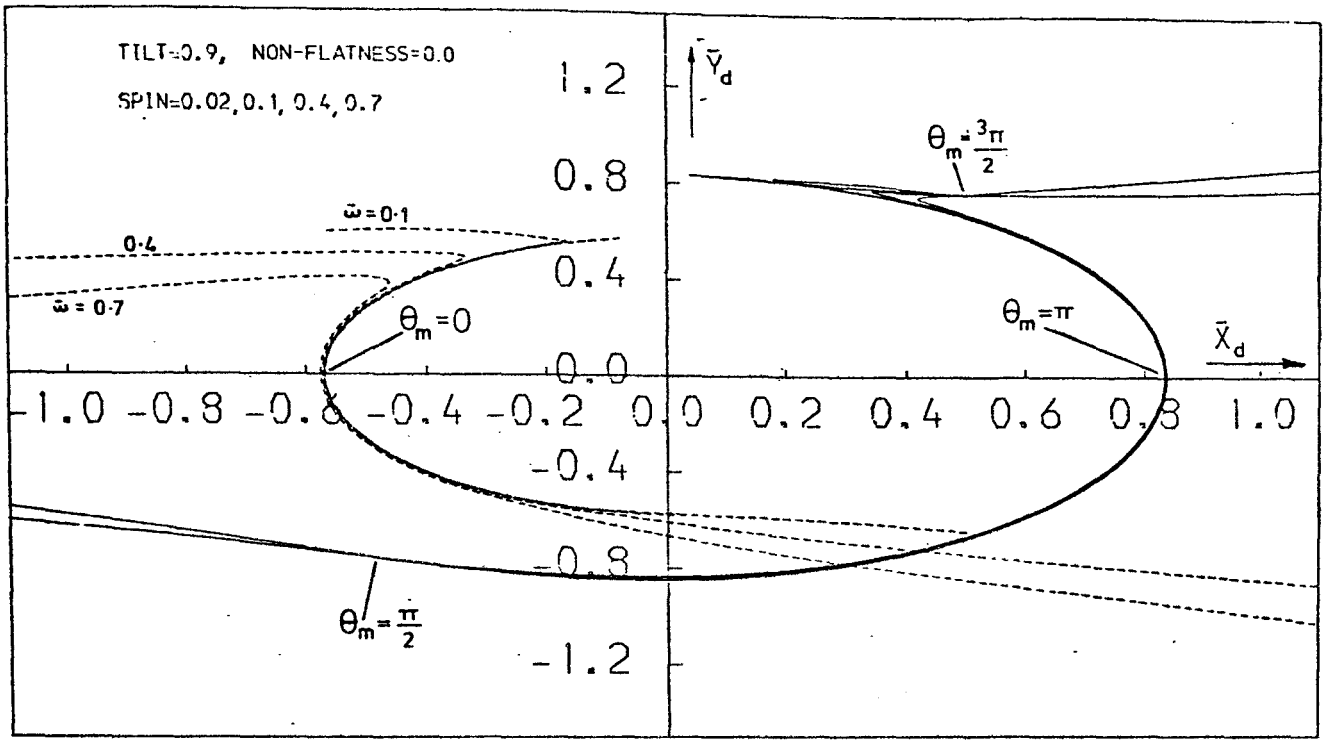

EFFECT OF SPIN ON HYDRODYNAMIC PRESSURE CENTRE

FIGURE 2.13

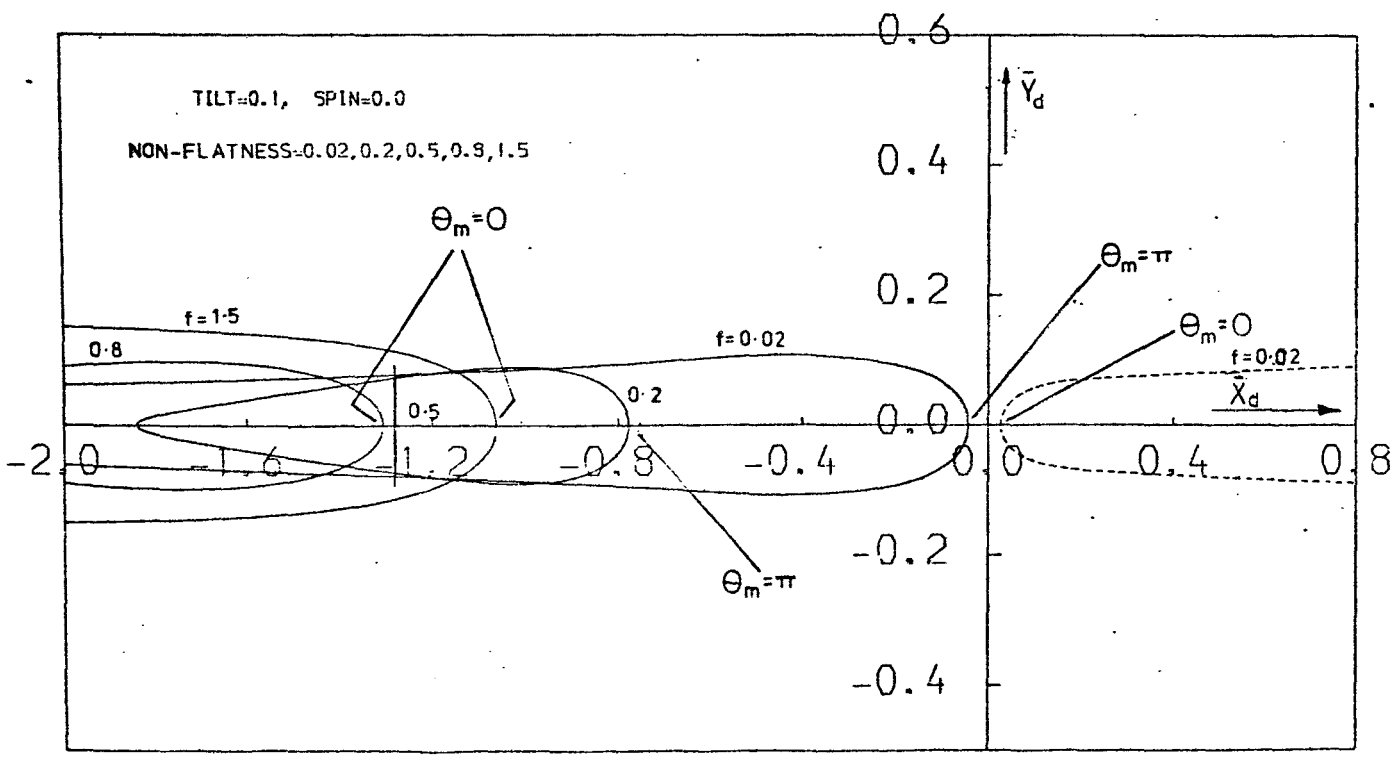

EFFECT OF NON-FLATNESS ON HYDRODYNAMIC PRESSURE CENTRE

FIGURE 2.14

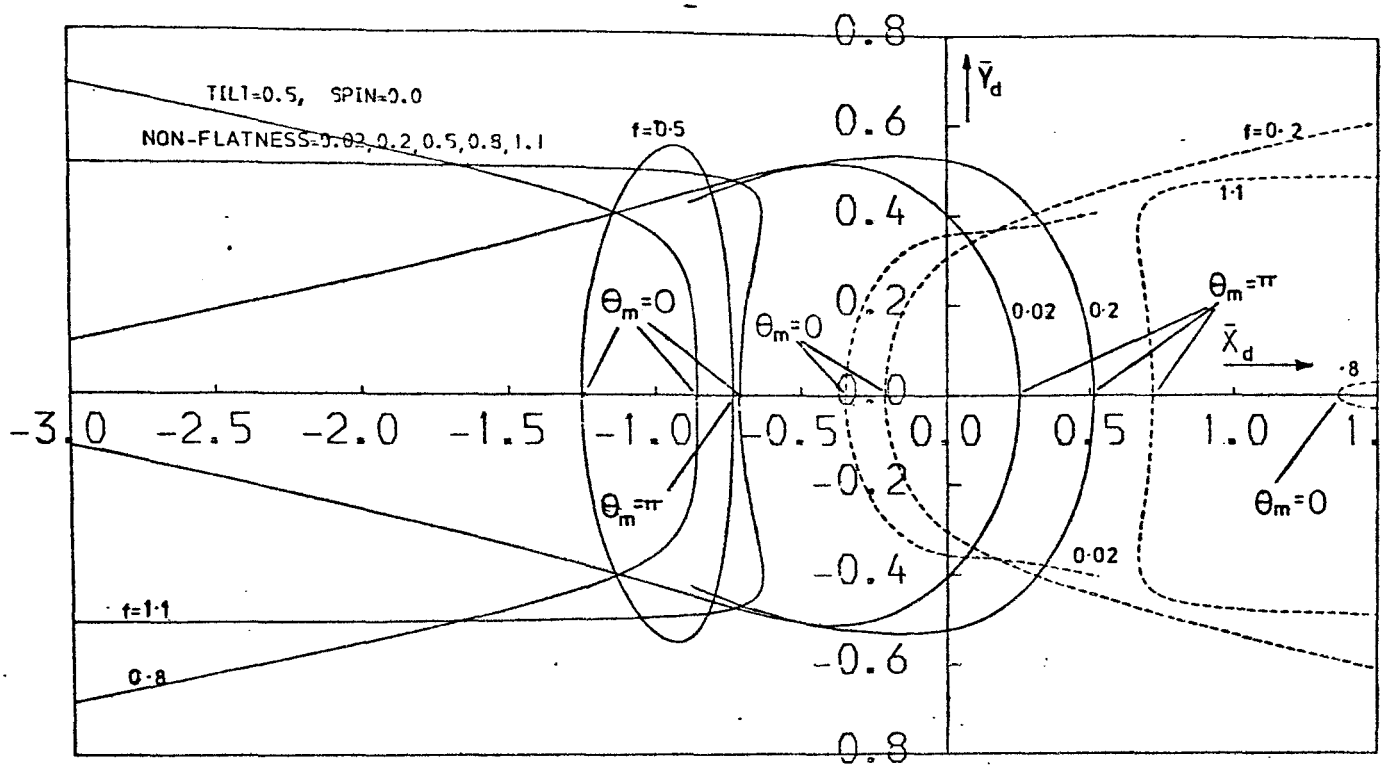

LOCUS OF HYDRODYNAMIC PRESSURE CENTRE
RELATIONSHIP WITH NON-FLATNESS
FIG. 2.15

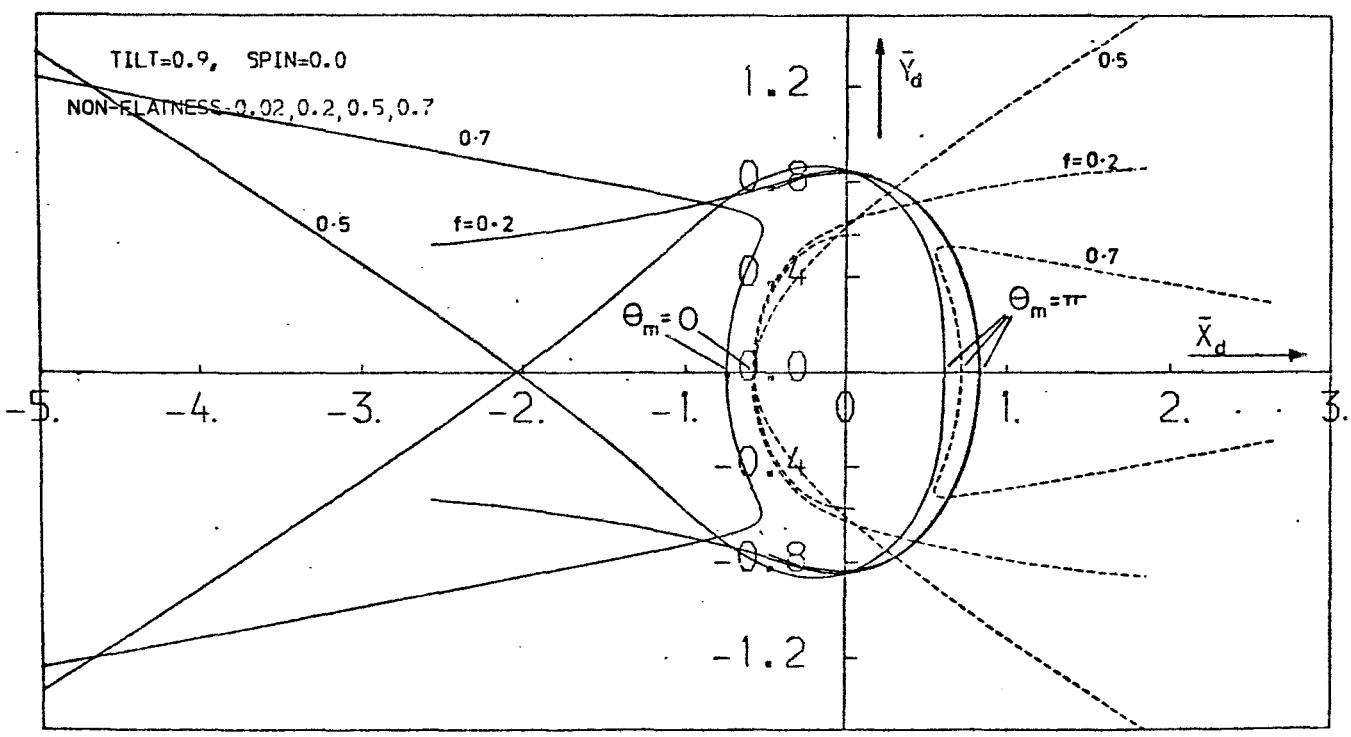

LOCUS OF HYDRODYNAMIC PRESSURE CENTRE
RELATIONSHIP WITH NON-FLATNESS
FIG. 2.16

0.02, 0.1, 0.4 and 0.7 (fig. 2.11). This was repeated with tilt equal to 0.5 and 0.9 (figures 2.12 and 2.13). For values of θ_m near 0 and π, the effect of spin is minimal and the locii describe an approximately circular path with almost the same radius as if spin was not present. However, as θ_m approaches $\pi/2$ or $3\pi/2$ the effect of spin becomes gradually more significant whilst, at the same time, departing from the circular path previously described. At $\pi/2$ and $3\pi/2$ spin terms take over completely since there is no lift due to tilt and curves corresponding to different spins intersect at the same point.

However, there is still no case where the pressure centre is at θ_m (diametrically opposite the hydrostatic pressure centre which for a flat slipper lies always at $\theta_m + \pi$) therefore a flat, spinning slipper will be still unable to function under steady state conditions and in the absence of external couples.

2.6.4.3. Effect of parabolic type non-flatness

The effect of non-flatness was similarly investigated in conjunction with tilt. With spin equal to zero and tilt equal to 0.1, θ_m was varied between 0 and 2π for non-flatness equal to 0.02, 0.2, 0.5, 0.8 and 1.5 (fig. 2.14). This was repeated with tilt equal to 0.5 and 0.9 (figures 2.15 and 2.16). The range of non-flatness was modified to avoid the possibility of negative clearances (it is theoretically possible for high values of tilt and non-flatness to have cases where parts of one or both of the slipper lands would be under the surfaces of the slipper plate. This is, of course, physically impossible and such cases were discarded).

The interaction between tilt, non-flatness and θ_m in these graphs is very complex indeed. However, a very important observation can be made. Under certain circumstances the hydrodynamic pressure centre can occur at θ_m (opposite the hydrostatic pressure centre). This means that for suitable values of $\bar{H}_c^2$ $\bar{P}_s$ the hydrostatic and hydrodynamic lift can be made to support the piston load, whilst at the same time producing zero tilting moment about any of the co-ordinate axes.

Due to the complexity of the subject any further analysis of the subject seems extremely difficult. Therefore, in trying to understand the interaction of tilt and non-flatness, it is logical to reduce initially the number of variables by assuming θ_m to be equal to π. This means that for positive tilts the leading edge of the slipper will be tilted upwards. Moreover, since the slipper is completely symmetrical about the x-z plane, the pressure centre is bound to lie on the x-axis. Under these conditions tilt is plotted against position of hydrodynamic pressure centre for a range of non-flatness between 0.0 and 0.9 (fig. 2.17). This is repeated in fig. 2.18 for non-flatness between 0.0 and -0.9. Again, solid and broken lines correspond to positive and negative overall hydrodynamic lift respectively.

For non-flatness equal to zero the distance of the pressure centre from zero decreases as tilt is reduced until it becomes zero when tilt is equal to zero. Then for negative tilts, due to the presence of diverging wedge on both lands, the outer land cavitates while the inner land produces negative pressure contribution. A similar pattern

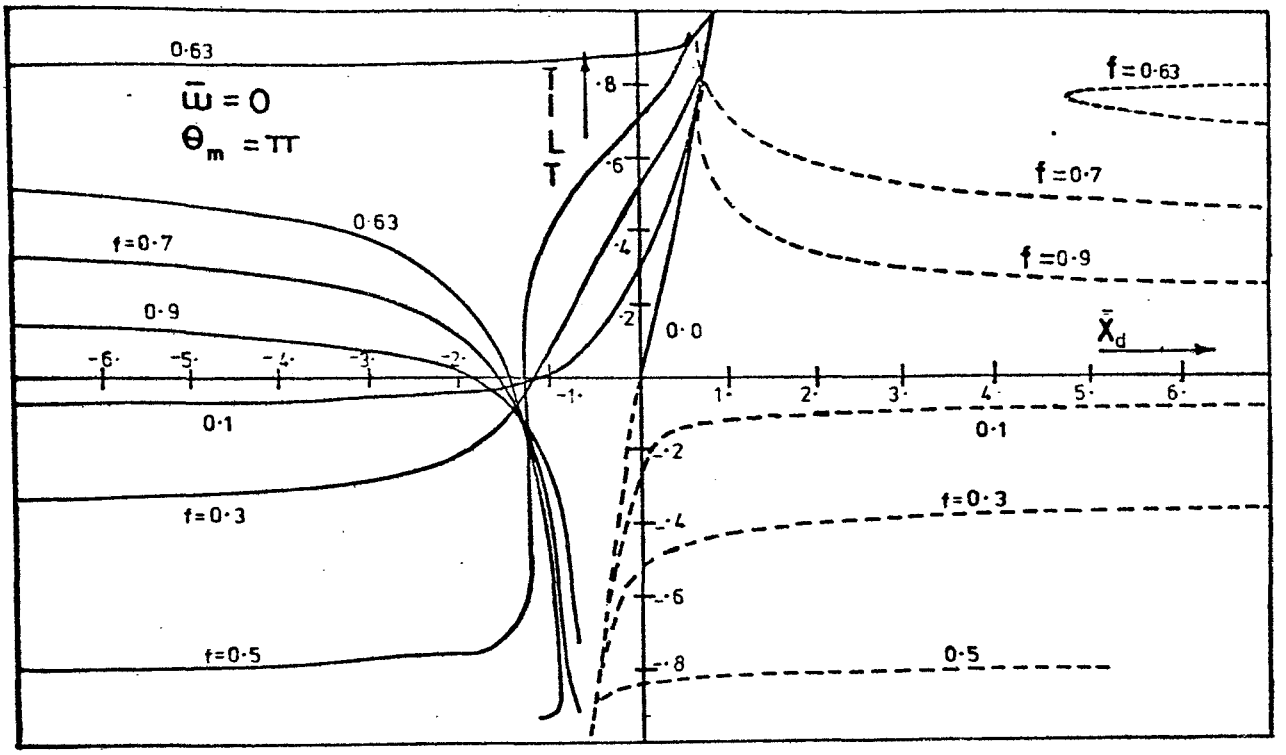

FIG. 2.17 LOCUS OF HYDRODYNAMIC PRESSURE CENTRE FOR POSITIVE NON-FLATNESS

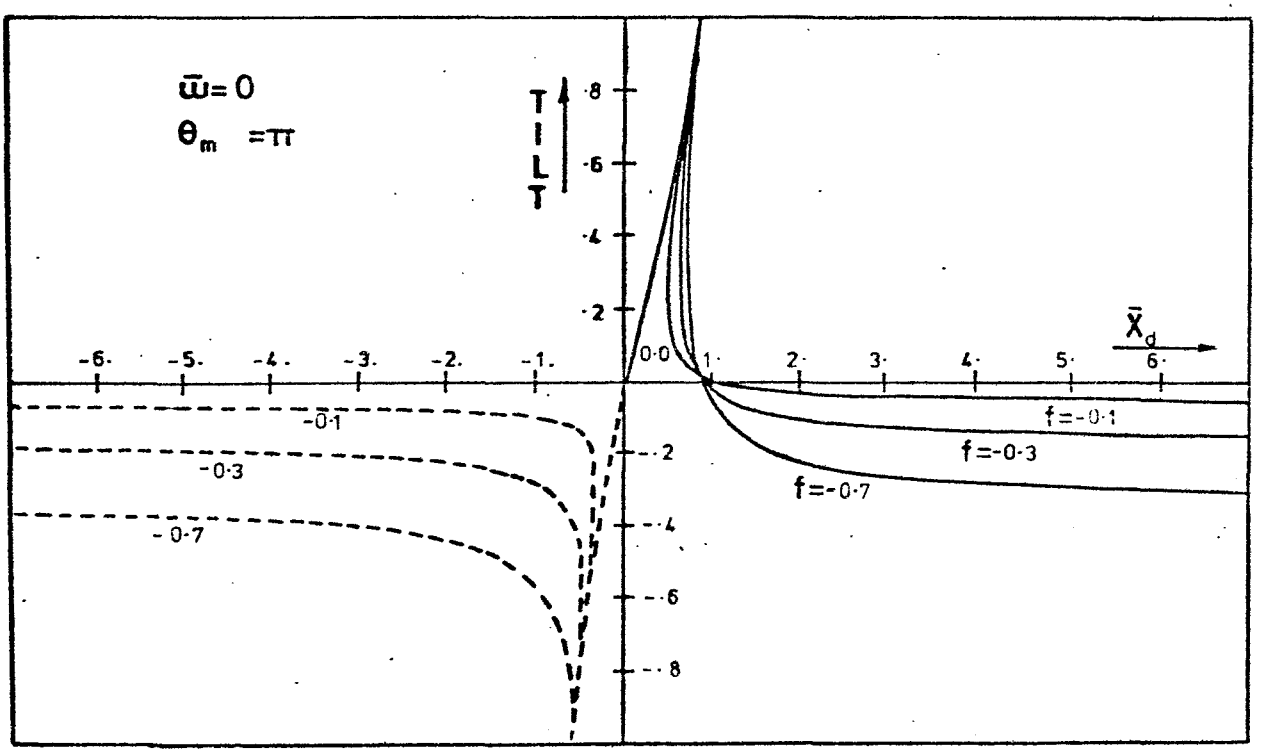

FIG. 2.18 LOCUS OF HYDRODYNAMIC PRESSURE CENTRE FOR NEGATIVE NON-FLATNESS

is obtained for non-flatness up to 0.5. However, at zero tilt the pressure centre has moved to the left. This is because non-flatness forms a converging wedge at the leading edge and a diverging wedge at the trailing edge of the slipper, thus generating positive pressure at the leading edge, negative pressure at the trailing edge of the inner land and zero pressure at the trailing edge of the outer land due to cavitation (fig. 2.19a). This distribution obviously generates a clockwise moment and a positive lift because the overall hydrodynamic lift on the inner land is zero but on the outer land it is positive due to cavitation at the trailing edge. As tilt is reduced further the 'convergence' at the leading edge is decreased whilst the suction effects at the back are increased until the latter dominate and an overall negative lift is exerted.

The opposite happens when non-flatness is 0.7 or higher. Here the suction effects dominate at high tilts due to the small clearance at the trailing edge (fig. 2.19b). However, as tilt is reduced, the clearance of the leading edge is reduced as the trailing edge lifts off. Consequently, lift at the leading edge is increased until it dominates and a positive lift appears.

Finally for negative non-flatness the pattern is similar to the one for zero non-flatness and positive tilts. At zero tilt there is suction at the leading edge and lift at the trailing edge due to converging wedge effect (fig. 2.19c). As tilt is reduced further, suction dominates and the curves join the zero non-flatness contours at the lower tilt region.

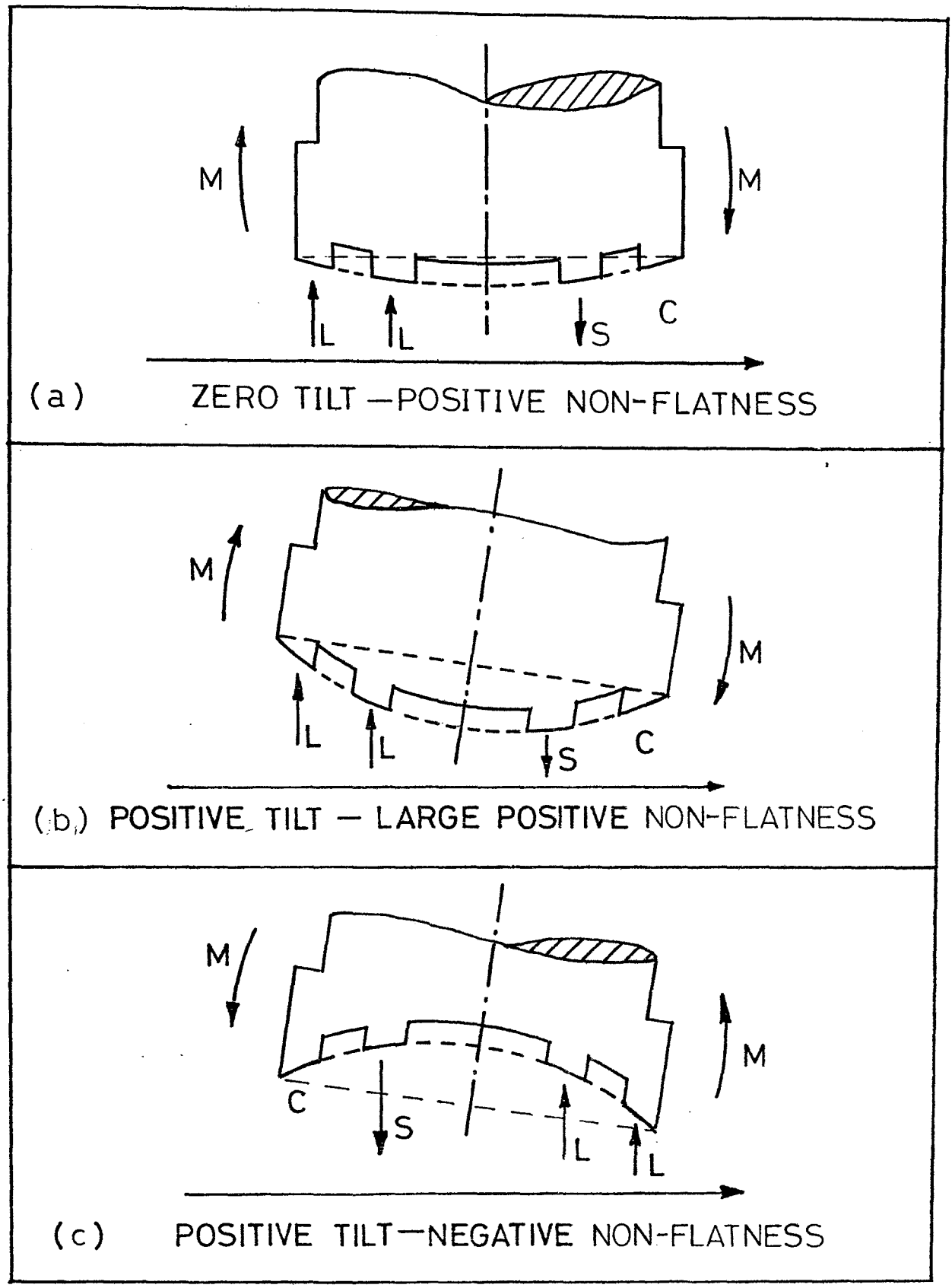

L - LIFT S - SUCTION C - CAVITATION M - MOMENT

FIG. 2.19 EFFECT OF NON-FLATNESS ON DISTRIBUTION OF LIFT

To summarize, this section has shown that non-flatness can provide a mechanism which on one hand generates hydrodynamic lift and on the other hand makes moment equilibrium possible. However, the exact amounts of tilt and non-flatness required are not yet known. This is because $\bar{H}_c$ and $\bar{P}_s$ have not yet been evaluated and all comparisons so far have been largely qualitative. The following section outlines an approach for calculating these variables by examining the equilibrium conditions in detail.

2.7. Equilibrium criteria for the slipper

A slipper operating under steady state conditions is in a state of equilibrium. To achieve this, three separate conditions must be satisfied:-

a) Load equilibrium.

b) Flow equilibrium.

c) Moment equilibrium.

In the previous section it was shown that load and moment equilibrium could be satisfied for certain combinations of tilt and non-flatness. The relationship between these two parameters whilst the slipper is at the equilibrium position is investigated more thoroughly in this section. This is done by considering the first two criteria as a system of two unknown variables. These are the ratio of slipper to piston pressure $\bar{P}_s$ and the variable $\bar{H}_c$.

Once these equations are solved and $\bar{P}_s$ and $\bar{H}_c$ found, the total lift and moments and hence the pressure centre can easily be calculated. This is then plotted against tilt as before for various values of non-flatness. In the absence of

external couples total equilibrium will occur when the pressure centre lies at the origin or when the curves cross the zero x line, (since $\theta_m = \pi$, the y co-ordinate of the pressure centre will always be zero).

2.7.1. Load equilibrium

This requires that the piston load exerted on the slipper along the z-axis is equal to the sum of the hydrostatic and hydrodynamic lift which are exerted on the undersurface of the slipper.

The piston load is equal to $P_p \pi R_p^2/\cos\alpha$. In dimensionless form this is equivalent to:-

$$\frac{\pi \bar{R}_p^2}{\bar{P}_s \cos\alpha}$$

Therefore the equation for load equilibrium can be written as:-

$$\frac{\pi \bar{R}_p^2}{\bar{P}_s \cos\alpha} = \bar{L}_s + \frac{L_{d1} + L_{d2}}{\bar{H}_c^2 \bar{P}_s} \qquad 2.59$$

Rearranging and substituting:-

$$F_p = \pi \bar{R}_p^2/\cos\alpha \qquad 2.60$$

the load equation can now be written as:-

$$F_p \bar{H}_c^2 = \bar{L}_s \bar{H}_c^2 \bar{P}_s + L_{d1} + L_{d2} \qquad 2.61$$

2.7.2. Flow equilibrium

Under steady state conditions the flow of oil entering the slipper pocket through the orifice must equal the oil flow escaping past the inner land. The latter can be divided firstly into outflow due to pressure difference between slipper pocket and pump casing and secondly due to velocity i.e. some oil will be drifted in and out of the

slipper pocket due to the sliding effect between slipper and slipper plate.

These components of flow will be considered separately.

2.7.2.1. Flow through the orifice

Experimental evidence has shown that the flow through the orifice will remain laminar for pressure differences across the orifice up to 140 bar. Since only small pressure differences are anticipated, the flow is taken to be always laminar and equal to:-

$$Q_{in} = \frac{R_o^4 (P_p - P_s)}{8\eta\, l} \qquad 2.62$$

where R_o and l are the radius and effective length of the orifice respectively.

2.7.2.2. Flow due to pressure

The flow per unit length due to pressure is given by[22]:

$$q = - \frac{h^3}{12\eta} \frac{\partial P}{\partial R}$$

For the inner land $\partial P/\partial R$ can be found by differentiating 2.30 at $R = R_{m1}$

$$\frac{\partial P}{\partial R} = - \frac{P_s}{R_2 - R_1} \qquad 2.63$$

The clearance h can be obtained from 2.16. Using substitution 2.49, the clearance h_{m1} at the middle of the inner land can be written as:-

$$h_{m1} = h_c (1 - \bar{d}_1) (1 + e_1 \cos\phi) \qquad 2.64$$

The flow due to pressure past the inner land is:-

$$Q_1 = \int_o^{2\pi} \left(q\ R_{m1}\ d\theta = \frac{R_{m1}}{12\eta} \int_o^{2\pi} - h_{m1}^3\ \frac{\partial P}{\partial R} \right) d\theta$$

Substituting 2.63 and 2.64 and integrating from o to 2π gives:-

$$Q_1 = \frac{\bar{R}_{m1}\ h_c^3\ P_s\ (1 - \bar{d}_1)^3\ \pi\ (2 + 3\ e^2)}{12\eta\ (R_2 - R_1)} \qquad 2.65$$

2.7.2.3. Flow due to velocity

The flow per unit length due to sliding is given by[22]:-

$$q = \frac{h\ U\ \cos\theta}{2}$$

In the case of the inner land the total flow will be equal to:-

$$Q_2 = \int_o^{2\pi} q_v\ \bar{R}_{m1}\ d\theta = \frac{\bar{R}_{m1}\ U}{2} \int_o^{2\pi} h_{m1}\ \cos\theta\ d\theta$$

Substituting 2.64 and integrating from o to 2π gives:-

$$Q_2 = \frac{U\ h_c\ t\ \bar{R}_{m1}^2\ R_4\ \pi\ \cos\theta_m}{2} \qquad 2.66$$

This term represents the total amount of flow leaking past the inner land as a result of sliding of the slipper plate.

2.7.3.4. Flow equation

The flow equation can be assembled as follows:-

$$Q_{in} = Q_1 + Q_2$$

Substituting 2.62, 2.65 and 2.66 for each corresponding term and rearranging gives:-

$$\frac{3\ R_o^4\ (1 - \bar{P}_s)}{2\ l\ h_c^3} = \frac{6\eta\ U\ R_4}{h_c^2\ P_p}\ t\ \bar{R}_{m1}^2\ \pi\ \cos\theta_m +$$

$$\frac{\bar{P}_s\ \bar{R}_{m1}\ (1 - \bar{d}_1)^3\ \pi\ (2 + 3\ e_1)}{(\bar{R}_2 - \bar{R}_1)}$$

Substituting for $\bar{H}_c$ (2.23) and Z (2.25) modifies the above equation to:-

$$Q_f\ (1 - \bar{P}_s) = \bar{H}_c\ Q_v + \bar{H}_c^3\ \bar{P}_s\ Q_p \qquad 2.67$$

where Q_f is the orifice term and is defined as:-

$$Q_f = \frac{3}{2}\frac{R_o^4}{l}\ Z^3 \qquad 2.68$$

also:-

$$Q_v = t\ \bar{R}_{m1}^2\ \pi\ \cos\theta_m \qquad 2.69$$

$$Q_p = \bar{R}_{m1}\pi\ (1 - \bar{d}_1)^3\ (2 + 3\ e_1)/(\bar{R}_2 - \bar{R}_1) \qquad 2.70$$

2.7.3. Combining the load and flow equations

The values of $\bar{H}_c$ and $\bar{P}_s$ which satisfy the load and flow equilibrium conditions can be found by solving 2.61 and 2.67 as a system of two equations with two unknowns. From 2.61 $\bar{P}_s$ can be expressed as:-

$$\bar{P}_s = \frac{F_p\ \bar{H}_c^2 - L_{d1} - L_{d2}}{\bar{L}_s\ \bar{H}_c^2} \qquad 2.71$$

Substituting this in 2.67 and rearranging produces a fifth order equation in $\bar{H}_c$.

$$\bar{H}_c^5\ Q_p\ F_p + \bar{H}_c^3\ (Q_v\ \bar{L}_s - Q_p\ L_{d1} - Q_p\ L_{d2}) +$$

$$\bar{H}_c^2\ Q_f\ (F_p - \bar{L}_s) - Q_f\ (L_{d1} + L_{d2}) = 0 \qquad 2.72$$

The solution of this equation can be cumbersome. However, considerable insight can be gained by examining first the cases when the orifice coefficient is set at its limiting values i.e. zero and infinity. In either case the equation is reduced to quadratic which is much easier to study. The case of a general orifice coefficient i.e. solution of the full quintic equation will be studied last.

2.7.3.1. Zero orifice coefficient

For $Q_f = 0$ equation 2.72 is reduced to:-

$$\bar{H}_c^3 \quad \bar{H}_c^2 \, Q_p \, F_p + Q_v \, \bar{L}_s - Q_p \, (L_{d1} + L_{d2}) \quad = 0$$

Obviously the solution $\bar{H}_c = 0$ would make the problem meaningless. A more appropriate solution is given by:-

$$\bar{H}_c^2 = \frac{Q_p \, (L_{d1} + L_{d2}) - Q_v \, \bar{L}_s}{Q_p \, F_p}$$

Knowing $\bar{H}_c^2$, $\bar{P}_s$ can be calculated using 2.71.

The co-ordinates of the pressure centre can be found by dividing the total moments by the total load i.e.:-

$$\bar{x}_c = \frac{\bar{M}_{sy} + \bar{M}_{dy1} + \bar{M}_{dy2}}{\bar{L}_s + \bar{L}_{d1} + \bar{L}_{d2}} \quad \text{or}$$

$$\bar{x}_c = \frac{\bar{M}_{sy} \, \bar{H}_c^2 \, \bar{P}_s + M_{yd1} + M_{yd2}}{\bar{L}_s \, \bar{H}_c^2 \, \bar{P}_s + L_{d1} + L_{d2}} \qquad 2.73$$

Similarly the y-coordinate is:-

$$\bar{y}_c = \frac{\bar{M}_{sx} \, \bar{H}_c^2 \, \bar{P}_s + M_{xd1} + M_{xd2}}{\bar{L}_s \, \bar{H}_c^2 \, \bar{P}_s + L_{d1} + L_{d2}} \qquad 2.74$$

Contours of tilt against pressure centre are shown in fig. 2.20 for various values of non-flatness. Broken lines in this case correspond to negative values of $\bar{H}_c^2$ which in turn correspond to imaginary clearances (h_c). Although physically impossible these curves have been included to show the continuity of the function.

Out of all the curves the only ones that cross the tilt axis with real clearance have non-flatness between zero and about 0.66 with tilt ranging between zero and 0.93.

2.7.3.2. Infinite orifice coefficient

With the orifice coefficient infinitely large, the orifice term Q_f becomes infinitely large too. This means that the first two terms of equation 2.72 become infinitely more significant compared to the others. Neglecting insignificant terms, 2.72 can be written as:-

$$\bar{H}_c^2 (F_p - \bar{L}_s) - L_{d1} - L_{d2} = 0 \qquad 2.75$$

Therefore, $\bar{H}_c^2$ can be expressed as:-

$$\bar{H}_c^2 = \frac{L_{d1} + L_{d2}}{F_p - \bar{L}_s} \qquad 2.76$$

As before $\bar{P}_s$ and pressure centre can be calculated using 2.71, 2.73 and 2.74.

Tilt is plotted against pressure centre for this case on fig. 2.21. Again the curves that cross the tilt axis have non-flatness between zero and 0.64 with tilt ranging between zero and 0.91.

2.7.3.3. General case for real orifice

In the last two sections, equation 2.72 was solved for the special cases when the orifice coefficient had the

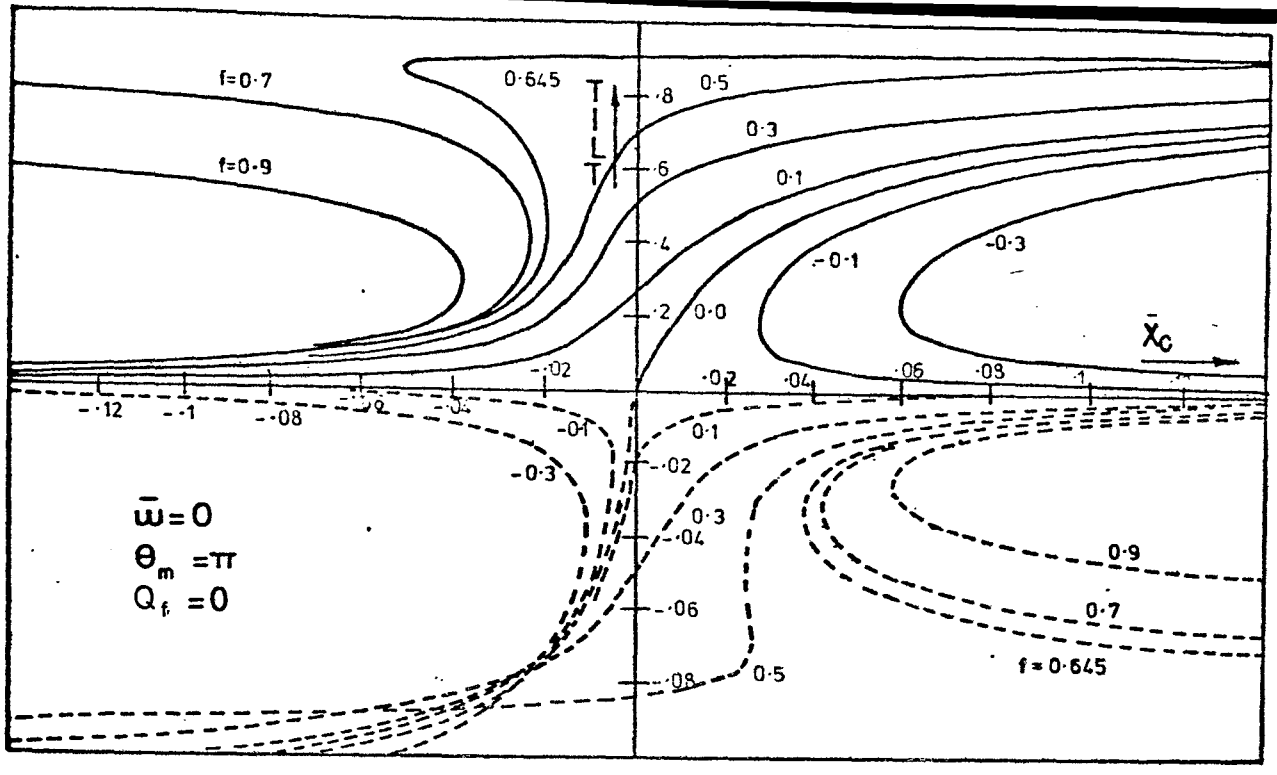

FIG. 2.20 LOCUS OF PRESSURE CENTRE FOR ZERO ORIFICE

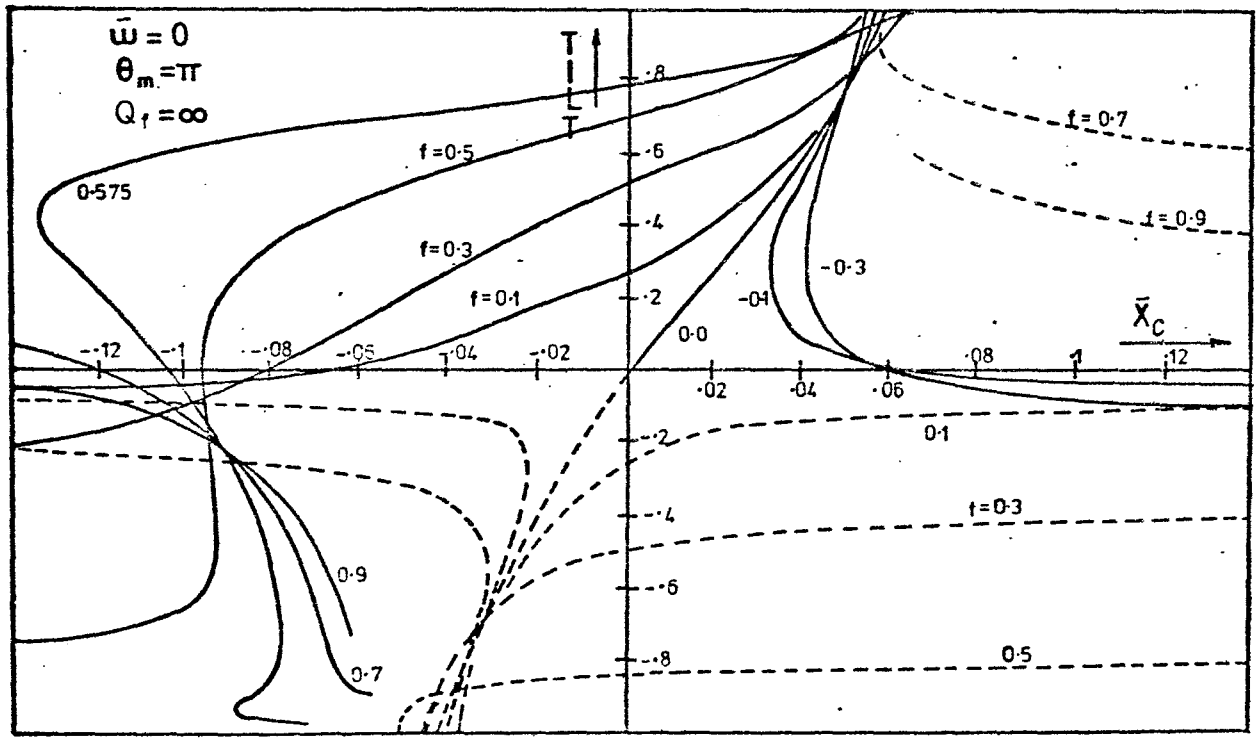

FIG. 2.21 LOCUS OF PRESSURE CENTRE FOR INFINITE ORIFICE

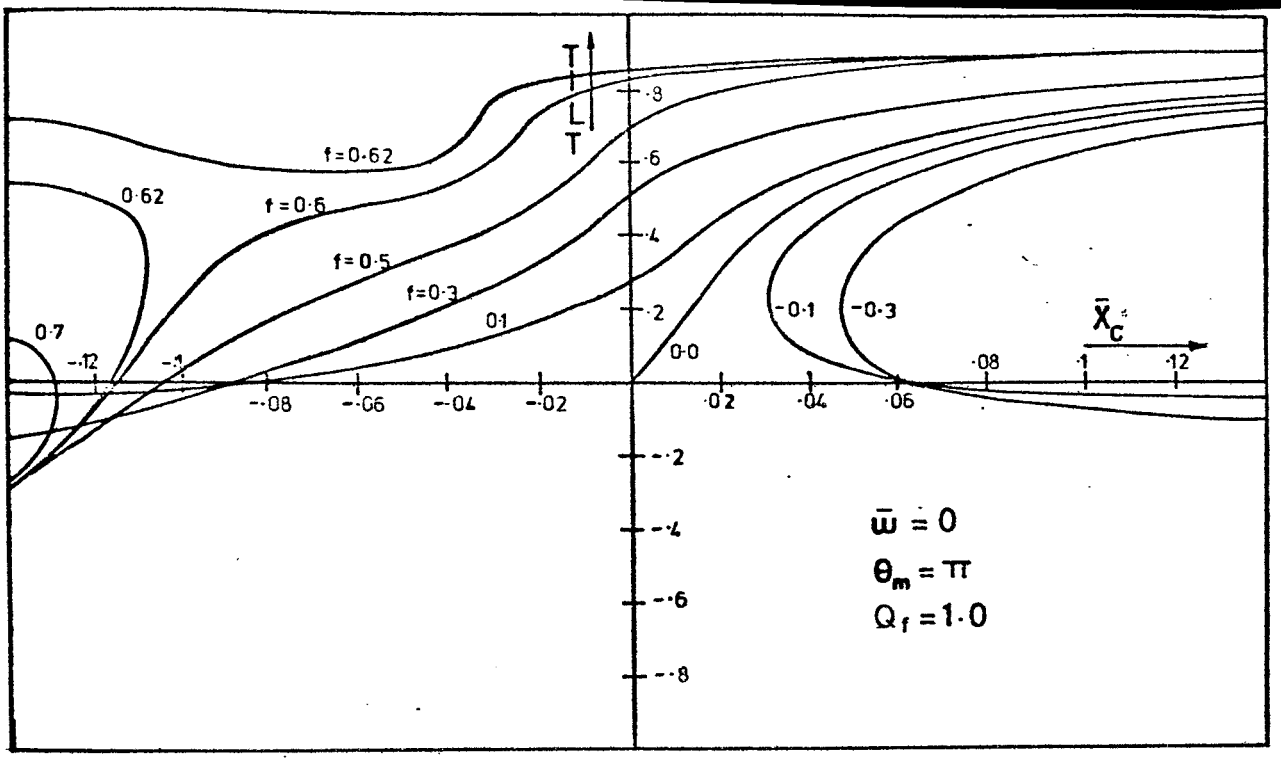

FIG. 2.22 LOCUS OF PRESSURE CENTRE
FOR ORIFICE COEF. EQUAL TO 1·0

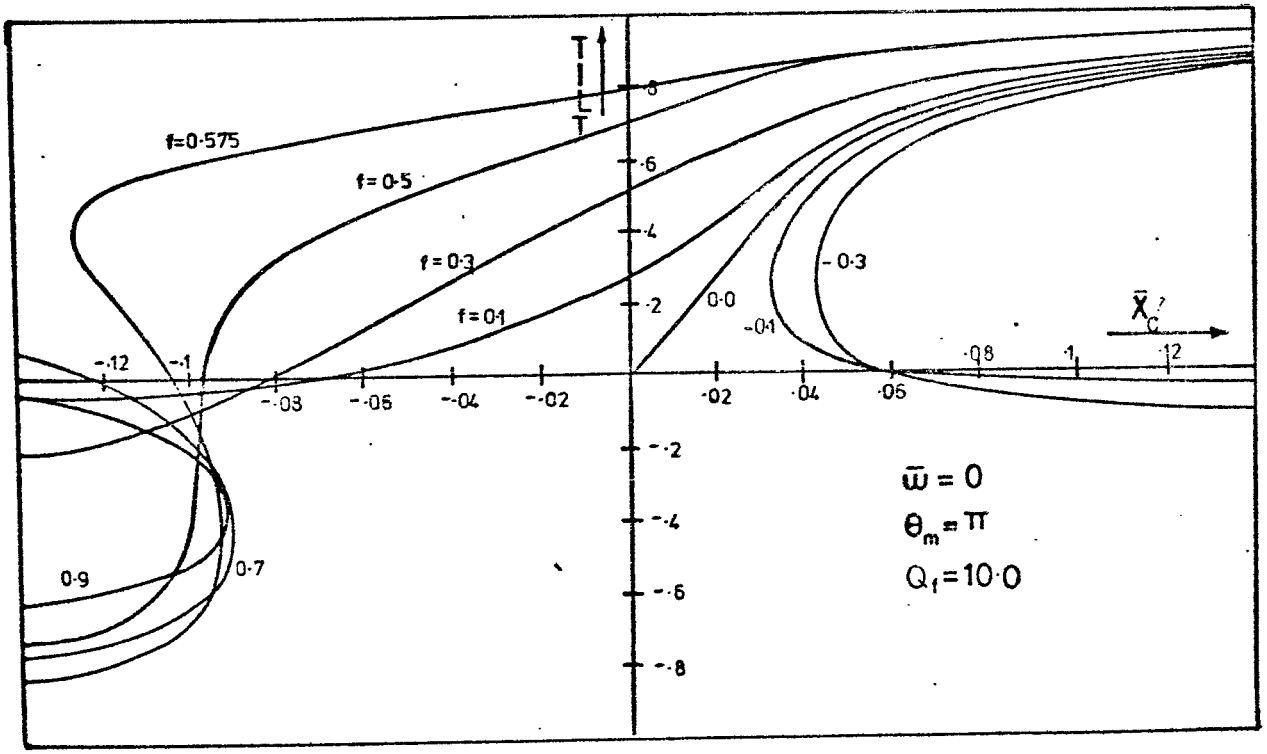

FIG. 2.23 LOCUS OF PRESSURE CENTRE
FOR ORIFICE COEF. EQUAL TO 10·0

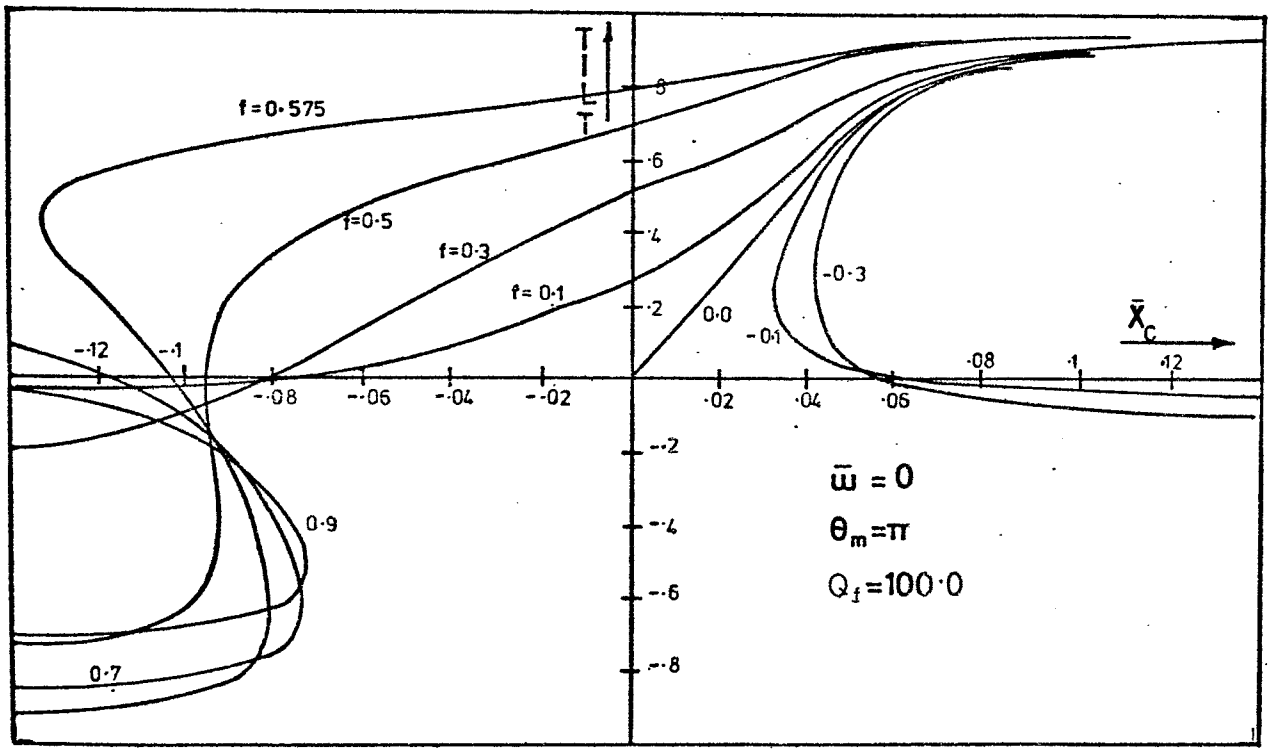

FIG. 2.24 LOCUS OF PRESSURE CENTRE
FOR ORIFICE COEF. EQUAL TO 100·0

limiting values of zero and infinity. Obviously in practice it will lie in between, but this means that the equation must be solved in its full general form. Since no analytical method is available for the solution of quintic equations, recourse must be made to numerical techniques.

In this case a computer programme was written to calculate the sturm sequence of equation 2.72. This was used to find the number of real roots between -10^6 and 10^6 and also the regions which contain one root only. In the vast majority of cases, only one real root was found between these limits. The only cases where more than one root was observed was when curvature was between 0.6 and 0.66 and orifice term (Q_f) equal to 1. The actual roots were then found using the secant technique. Having thus found the value of $\bar{H}_c$, $\bar{P}_s$ and $\bar{x}_c$ can be calculated as before using 2.71 and 2.73.

Contours of tilt against pressure centre for a range of values of parabolic non-flatness are shown on figures 2.22, 2.23 and 2.24. The orifice term Q_f is set to 1.0 in fig. 2.22, 10.0 in fig. 2.23 and 100.0 in fig. 2.24. The curves that cross the tilt axis fall in the same tilt and non-flatness region as before. However, the equilibrium position could not be investigated for non-flatness higher than 0.62 due to programming difficulties.

2.7.4. Analysis of the equilibrium position

The relationship between pressure centre and tilt for various values of parabolic non-flatness is shown in fig. 2.20 to 2.24, each corresponding to a different orifice coefficient Q_f.

The usefulness of these graphs must be extracted through the assumptions that have been made while the analysis was built up. The assumptions and definitions on geometry can be found in section 2.2. Further assumptions related to the fluid and the pressure distribution are outlined in sections 2.3 and 2.4. In addition the following assumptions have been applied to these particular graphs:-

a) The non-flat profile is of the parabolic type.

b) Slipper spin is equal to zero.

c) The angle of maximum tilt, θ_m, is equal to π. This means that for positive tilts, the leading edge of the slipper is up.

2.7.4.1. Relationship between parameters at equilibrium

The first observation which can be made from fig. 2.20 to 2.24 is that for a particular tilt, the value of the non-flatness required to produce a balanced situation (i.e. make $\bar{x}_c = 0$ is almost identical for all values of the orifice coefficient).

This similarity is better demonstrated on fig. 2.25 which shows the relationship between tilt and non-flatness at equilibrium. The curves corresponding to zero and infinite orifice coefficient are very close indeed. All curves corresponding to intermediate values of orifice coefficient lie in between. This implies that for a particular non-flatness there is only one tilt value that can produce equilibrium and the effect of orifice at equilibrium is almost negligible on these parameters. It is important to remember that both tilt and curvature are dimensionless ratios and although their relation is almost

independent of the orifice coefficient, the same does not apply to other slipper parameters as will be shown shortly. Moreover, it is impossible to have equilibrium with tilt and parabolic non-flatness outside the range zero to 0.86 and zero to 0.66 respectively.

Of a more serious nature are the curves in fig. 2.26 showing the relationship between $\bar{P}_s$ and non-flatness. Not surprisingly when the orifice coefficient is infinitely large, i.e. the restriction to flow between piston and slipper is negligible, $\bar{P}_s$ is equal to unity for all values of non-flatness. This means that slipper pocket pressure is equal to piston pressure. However, as the orifice coefficient is reduced, $\bar{P}_s$ is raised well above unity, thus making slipper pressure higher than piston pressure. For zero orifice coefficient slipper pressure needs to be between 3% to 5% higher than piston pressure in order to support the load. The difference is smaller for higher orifice coefficients. It must be stressed, however, that this apparent peculiarity is present only when there is no tilt about the x-axis. When tilt about the x-axis is introduced, $\bar{P}_s$ takes more reasonable values ranging, on average, between 0.9 to 1.0.

It is of particular interest that $\bar{P}_s$ drops sharply as parabolic non-flatness approaches 0.66. This is shown quite clearly in the case of $Q_f = 0$ and it is just beginning to show in the case of $Q_f = 1.0$.

Figure 2.27 shows the relationship between $\bar{H}_c$ and non-flatness. The main feature is that $\bar{H}_c$ increases with increasing non-flatness. On the other hand increasing the orifice decreases $\bar{H}_c$. The graph can be better seen if it

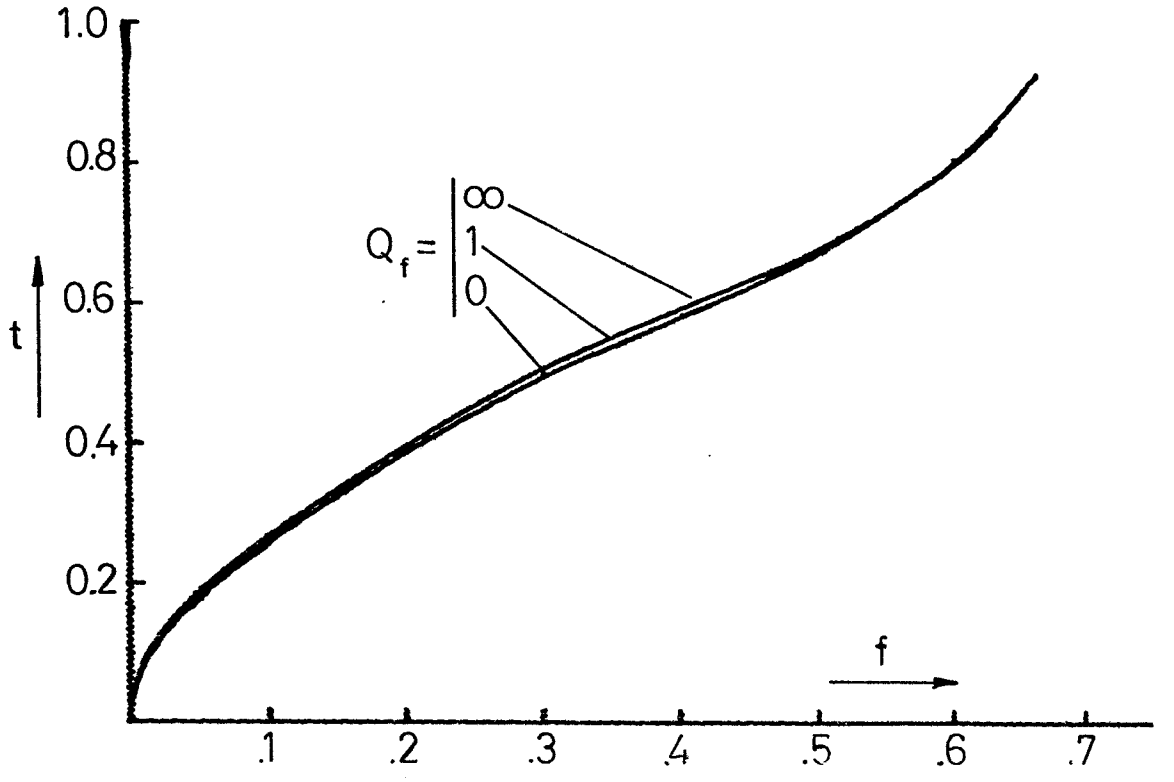

Relationship between tilt & parabolic non-flatness at equilibrium

Figure 2.25

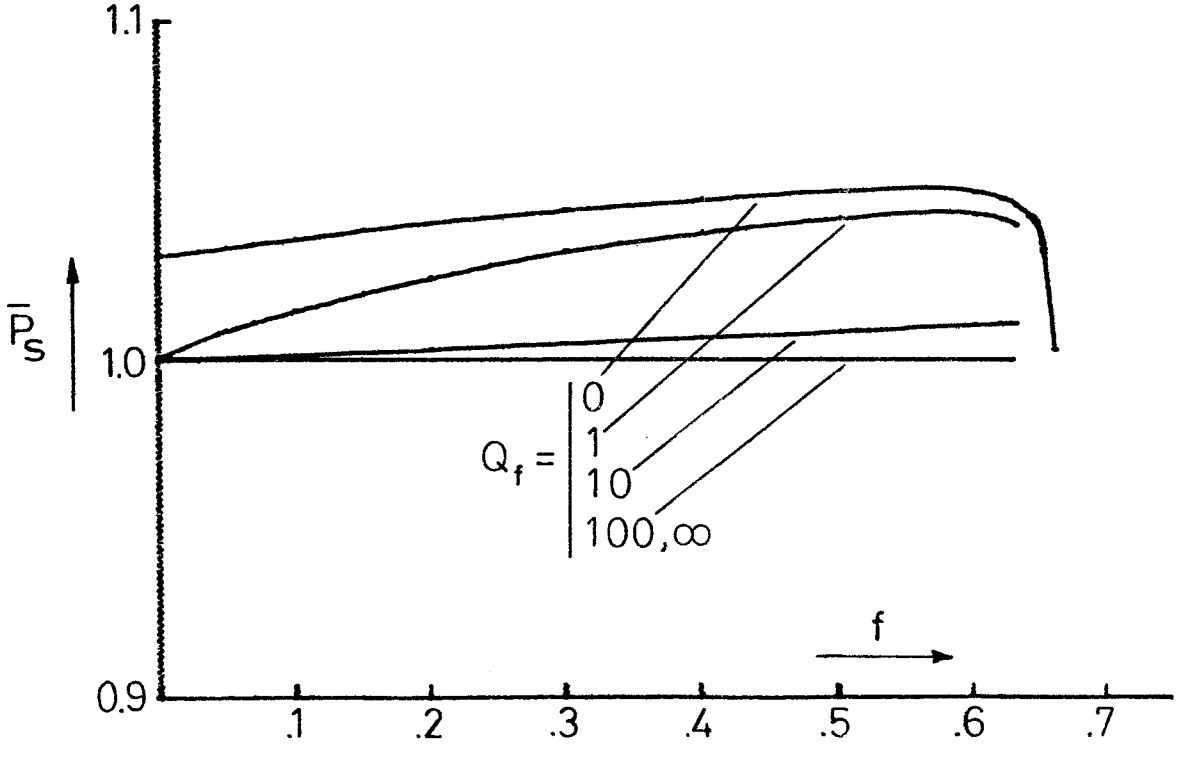

Relationship between pressure & parabolic non-flatness at equilibrium

Figure 2.26

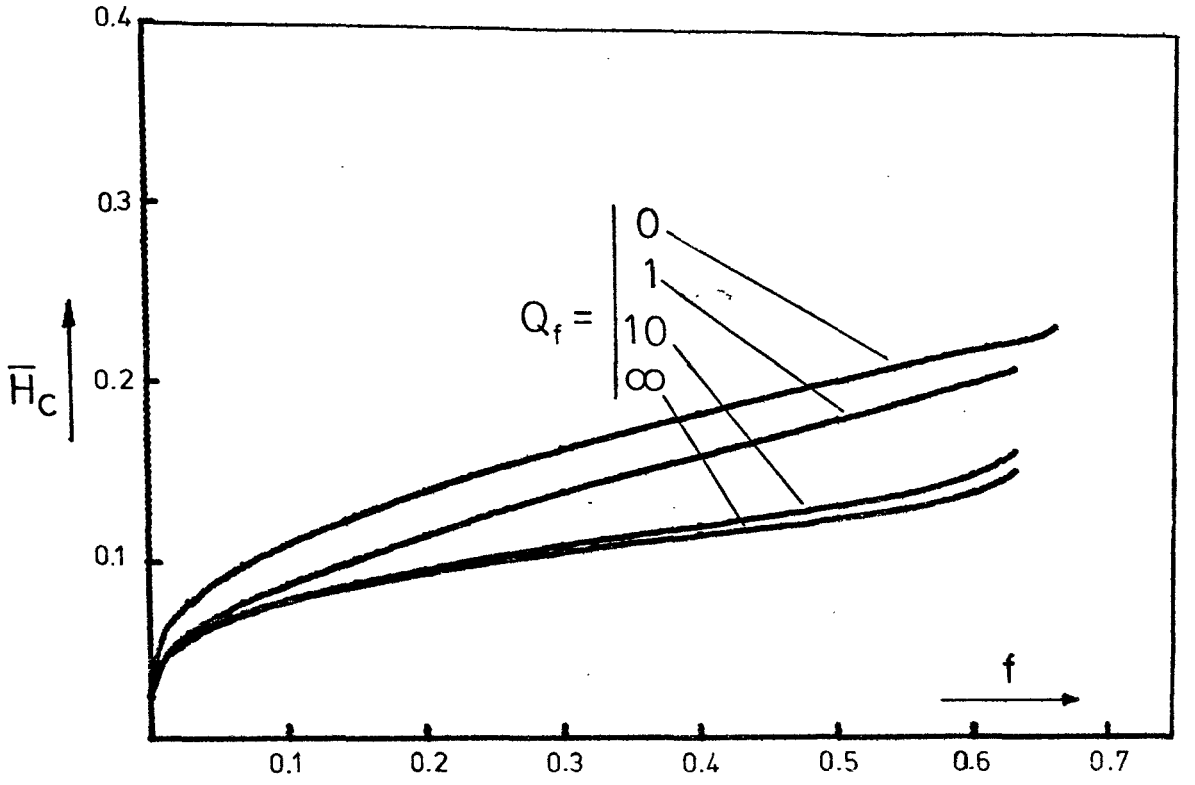

Relationship between central clearance & parabolic non-flatness at equilibrium

Figure 2.27

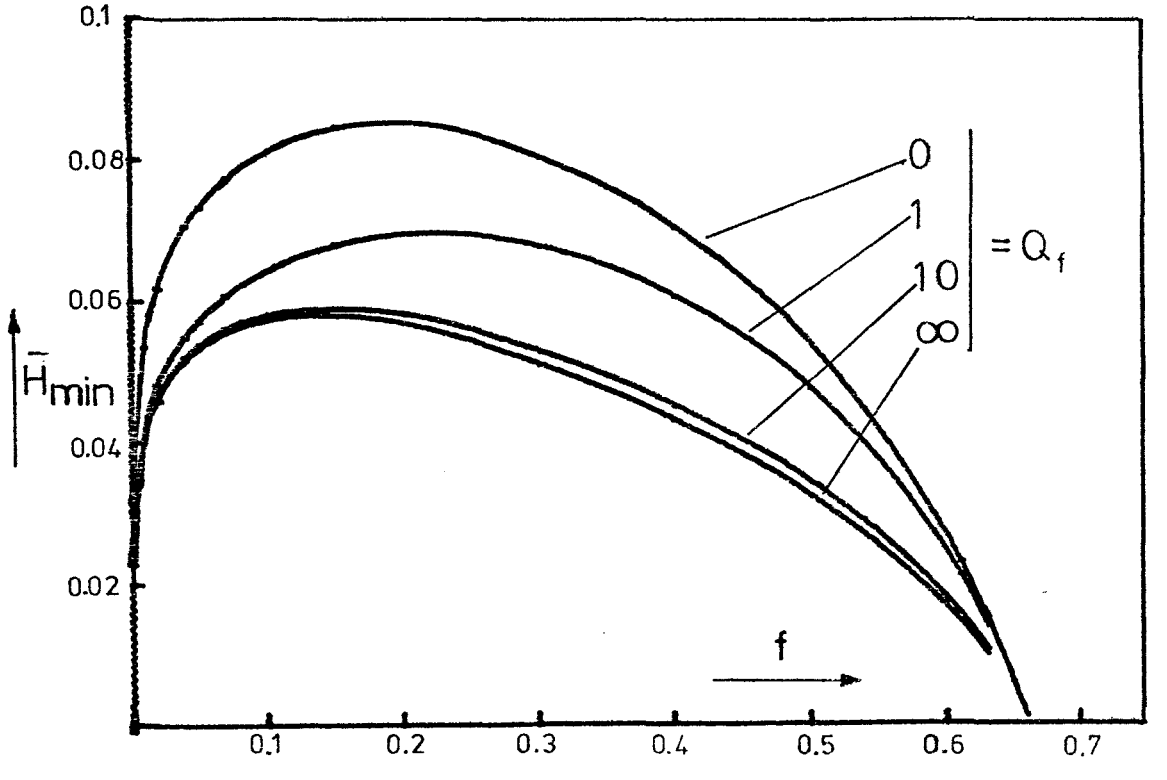

Relationship between min. clearance & parabolic non-flatness at equilibrium

Figure 2.28

is related in terms of the central clearance h_c. This can be done by dividing $\bar{H}_c$ by Z (rel. 2.26). The parameter Z is determined by the operating conditions only. The value of Z for typical conditions say speed equal to 1000 rev/min, piston pressure of 70 bar and oil temperature of 40°C will be around 23000. This means that when $\bar{H}_c$ is equal to .1 the clearance h_c will be around 4 microns which is of the right order of magnitude as the clearance measured experimentally (see section on Experiment).

The relationship between the central clearance and the operating conditions can be found by substituting 2.25 into 2.26 giving:-

$$h_c = \bar{H}_c \sqrt{\frac{6\eta \; U \; R_4}{P_p}} \qquad 2.77$$

This means that for a particular value of $\bar{H}_c$, h_c is proportional to the square root of the velocity and inversely proportional to piston pressure. It is also proportional to the square root of the viscosity which means that h_c decreases with increasing temperature. It is worth noting that these relations are in agreement with the trends established experimentally.

The dependence of h_c on orifice coefficient can be analysed in conjunction with the plots on fig. 2.26 and 2.27. Both the slipper pressure $\bar{P}_s$ and the central clearance h_c decrease as the orifice increases. These trends are in good agreement between them because as $\bar{P}_s$ decreases so does the hydrostatic lift. However, as h_c decreases the hydrodynamic lift being inversely proportional to h_c^3 increases. This

means that the total lift remains constant and equal to the piston load thus satisfying the load equilibrium condition.

So far non-flatness has been used in its non-dimensional form (rel. 2.3). It is worthwhile examining what it actually represents in dimensional form. Obviously this depends on central clearance which in turn depends on non-flatness etc. However, if one makes a rough estimate of the true non-flatness at the operating conditions quoted above using a value of f equal to 0.5 then the value of b would be equal to around 2μm. If this value is compared to the Talysurf trace of fig. 2.5 it will be seen that the theoretical and measured values of non-flatness are of the same order of magnitude.

Figure 2.28 shows the relationship between $\bar{H}_{min}$ and non-flatness at equilibrium. $\bar{H}_{min}$ can be converted to minimum clearance h_{min} using a relationship similar to 2.25.

$$\bar{H}_{min} = Z\, h_{min} \qquad 2.78$$

It must be noted that $\bar{H}_{min}$ represents true non-dimensional minimum clearance and it could occur at any land radius i.e. at R_1, R_2, R_3 or R_4.

Choosing the same conditions as before (for the central clearance) full scale on the $\bar{H}_{min}$ axis corresponds to about 4 microns. This again is of the correct order of magnitude as the minimum clearances found experimentally.

The main feature here is that $\bar{H}_{min}$ increases rapidly reaching a maximum at the low range of non-flatness and then it decreases at a slower rate reaching zero when the non-flatness is equal to 0.66. This explains why the previous graphs ended abruptly at this value of non-flatness.

2.8. Related software

All the aspects of the analysis outlined in this chapter, so far, have been simulated using a number of computer programs. All the programs have been written in FORTRAN IV and they have been implemented on a PDP11/10 computer system. Structurally they have been broken down into several modules with the object of:-

a) Following the logic of the analysis closely.

b) Being able to use them in different programs and applications.

c) Making manipulation or modification as easy as possible.

The heart of the software is a package of subroutines which can be easily linked to a number of main programmes according to the application. The subroutines are called by a controlling subroutine called "CNTRL". A flow diagram of this subroutine is shown in fig. 2.30. Input and output are as follows:-

Input:- f, t, θ_m, Q_f, $\bar{\omega}$, $\bar{R}_1$, $\bar{R}_2$, $\bar{R}_3$, $\bar{R}_4$, $\bar{R}_p$

Output:- $\bar{P}_s$, $\bar{H}_c$, $\bar{H}_{min}$, $\bar{x}_c$, $\bar{y}_c$

The input consists purely of the geometry of the slipper whereas the output provides the co-ordinates of the pressure centre as well as non-dimensional pocket pressure, central clearance, and minimum clearance.

Having developed CNTRL and its related subroutines, a variety of tasks can be done by writing simple main programs which call CNTRL. The graphs on fig. 2.20 for example were plotted using a program whose flow chart is shown in fig. 2.31.

Another slighlty more complex program was used to plot the graphs on fig. 2.25. Its flow chart is shown on fig. 2.32.

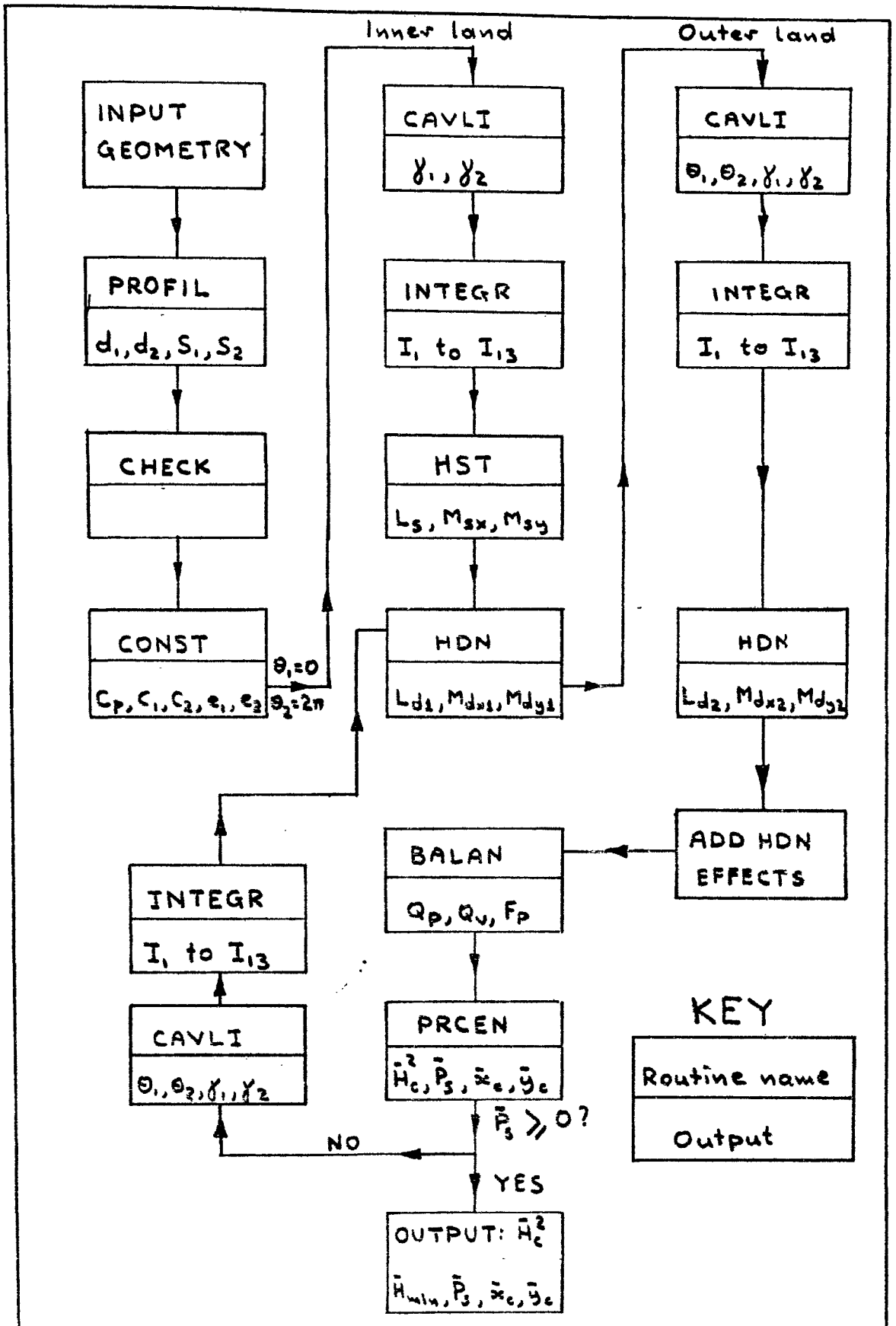

FLOWCHART OF ROUTINE "CNTRL"

FIG. 2.29

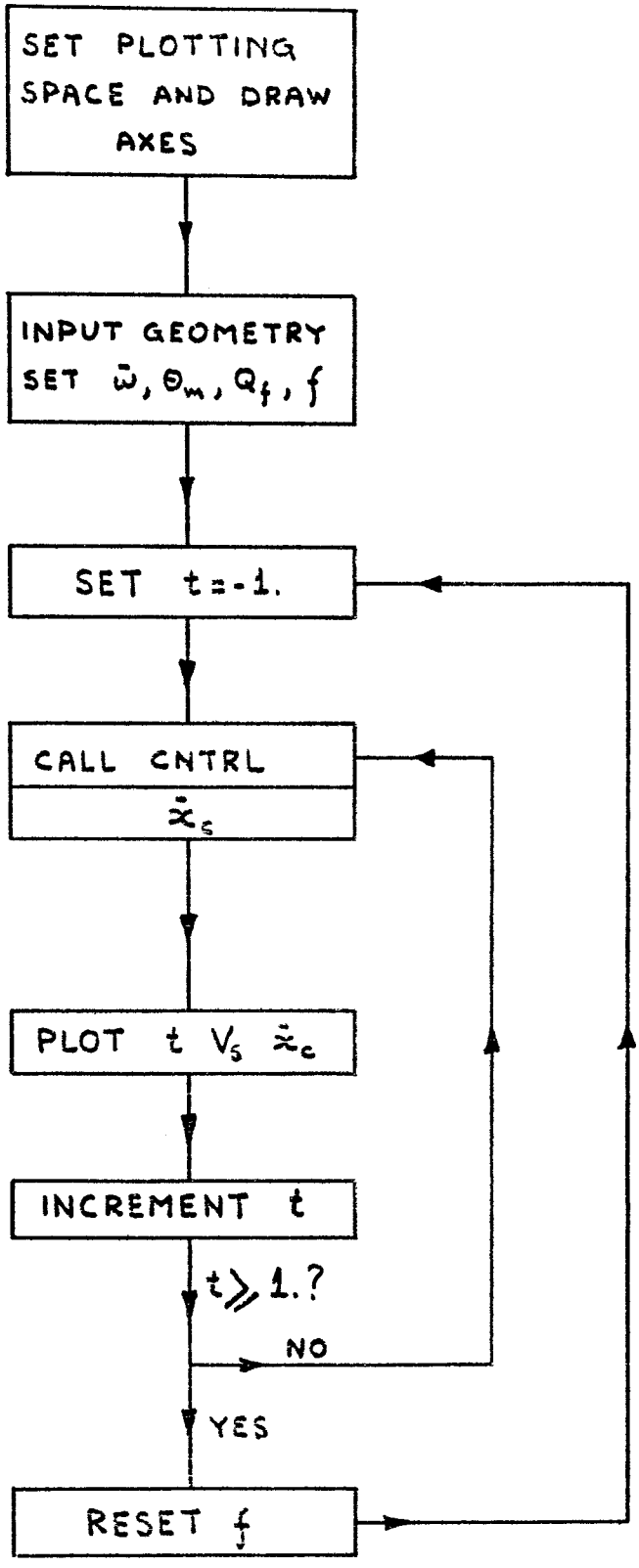

FLOWCHART FOR PLOTTING

TILT AGAINST PRESSURE CENTRE

FIG. 2.30

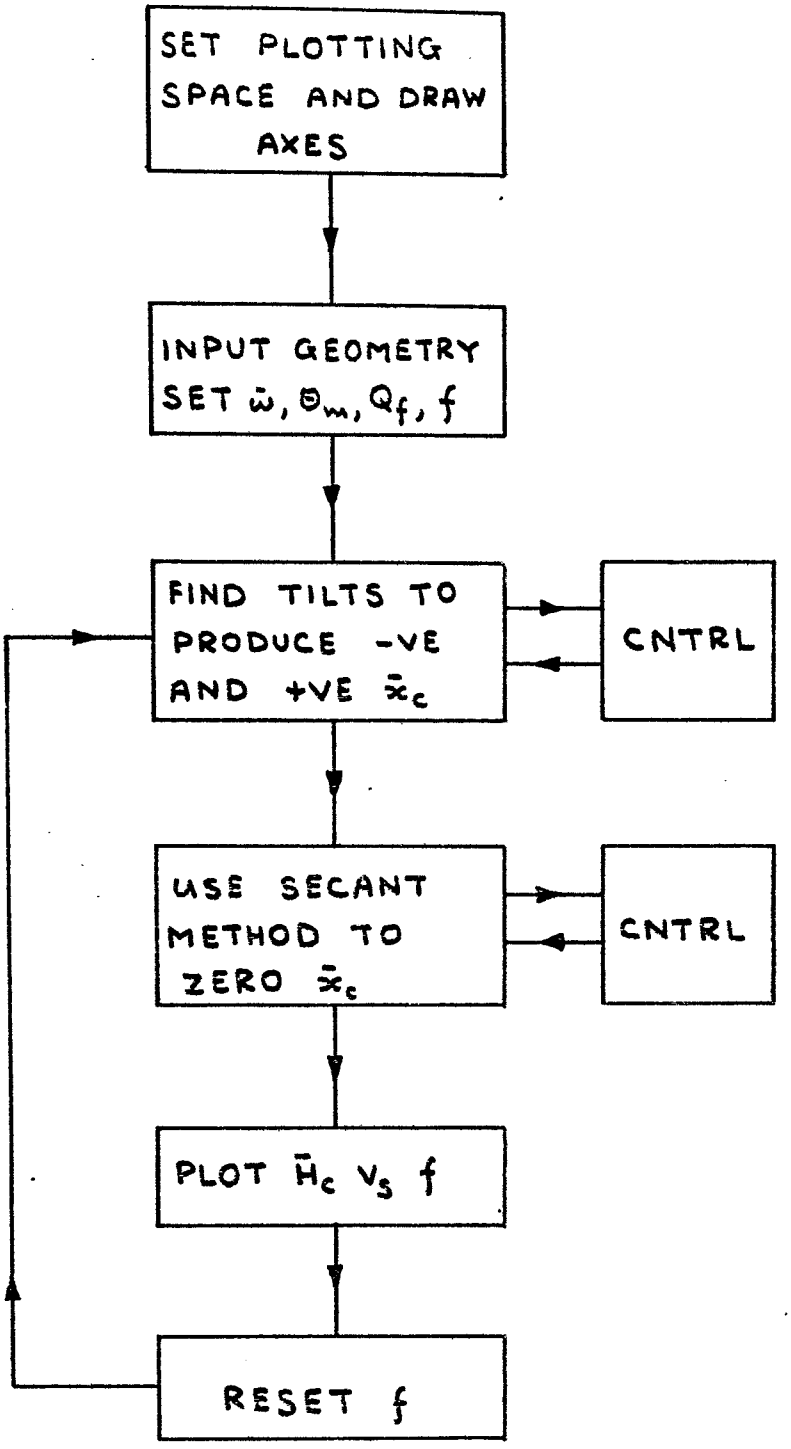

FLOWCHART FOR PLOTTING $\bar{H}_c$ AGAINST NON-FLATNESS

FIG. 2.31

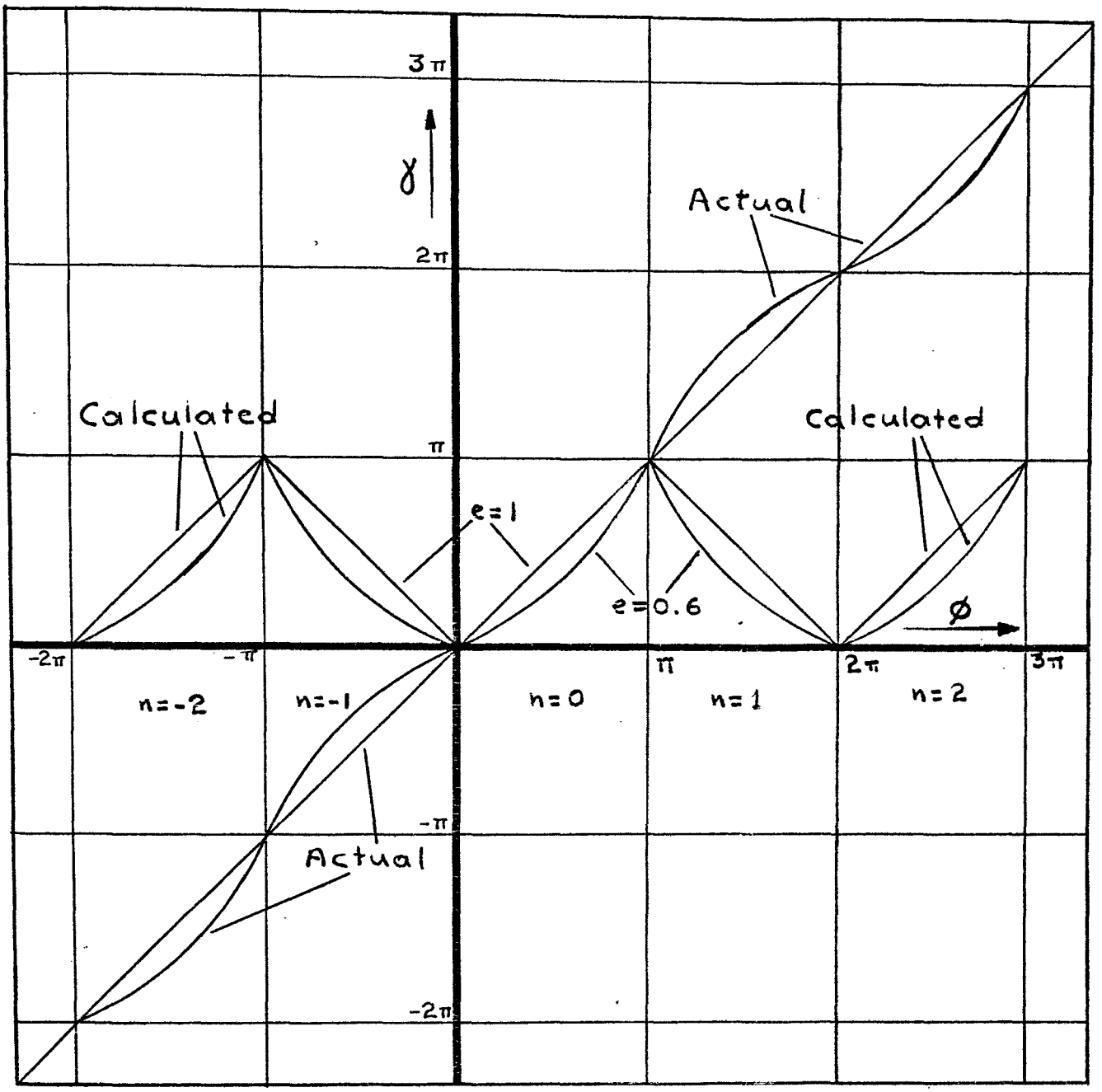

Relationship between γ and ϕ.

FIGURE 2.32

3.0. DESIGN APPLICATIONS

3.1. Introduction

In the previous chapter the investigation concentrated on the equilibrium and stability of an idealised slipper. It was shown that such a design could not operate under steady state conditions if it was completely flat. Furthermore it was shown that the non-flatness required to make load, flow and moment equilibrium possible must be of a convex type. For the type of parabolic non-flatness studied it was found that dimensionless non-flatness must lie between 0 and 0.66.

This information, however important, does not really provide much practical help from the point of view of designing. What is needed is to be able to assess a slipper design and provide guidelines as to how it can be improved. Defining and recognising a good slipper is unfortunately not a very easy task from a mathematical point of view.

Clearly a primary requirement of a satisfactory design is that the slipper does not come in contact with the slipper plate and if it does then it must not damage either surface. But being able to do that at a particular set of operating conditions is only half the solution. It must also be able to withstand sudden changes in load and a considerable amount of other forces and couples due to inertia, ball friction, viscous drag, centrifugal action, compressed springs etc. Therefore besides working well at particular conditions a good design must have a certain amount of resilience in order to withstand all these external effects some of which appear in an irregular fashion.

As far as stability is concerned the slipper must be able to accommodate external couples by shifting the position of its pressure centre thus maintaining moment equilibrium.

It appears therefore that a good slipper design must satisfy the following requirements:-

a) It must have adequate minimum clearance at the equilibrium position.

b) When acted upon by external couples, the pressure centre must move so as to balance the couple. Also the minimum clearance must remain sufficiently high over a large range of possible shifts of the pressure centre. In other words the area within which the pressure centre must remain in order to provide adequate minimum clearance must be as large as possible.

The conditions that satisfy these two requirements can be examined by analysing the relationship between pressure centre and minimum clearance of a particular design. This is done by fixing the geometry (i.e. land and piston radii as well as the type of profile and the non-flatness) and calculating the co-ordinates of the pressure centre and the related minimum clearance over a large range of possible attitudes i.e. combinations of tilt and θ_m. The unknown variables are clearly $\bar{x}_c$, $\bar{y}_c$ and $\bar{H}_{min}$ and they are calculated by satisfying flow and load equilibrium in exactly the same manner as described in section 2.7.3.

The analysis can now be used as a design tool in the following manner.

Knowing the operating conditions it is possible to represent all external effects as a single load acting at a point called the load centre. In order to satisfy moment equilibrium about the x and y-axes the pressure centre of the distribution under the slipper must coincide with the load centre. This means that the operating conditions can be used to determine the co-ordinates of the pressure centre. The next stage is to refer to the analysis and establish the minimum clearance which can be expected at this particular pressure centre. In this way the designer can have an estimate of the minimum clearance of the slipper at a particular operating condition. Clearly the accuracy of the information obtained in this way will be limited by the assumptions and idealisations which are built into the analysis. Nevertheless if the information is interpreted within the framework of the assumptions it can be a valuable aid in assessing the performance of a particular design, in establishing the trend of individual parameters or simply comparing the characteristics of different designs.

Some of these applications will be discussed in greater detail in the following sections but it must be stated that the method has not been fully explored due to lack of time. It is described here as a possible design approach with suggestions as to how it could be used and developed further. Although correlations with current information and practical experience are included wherever possible, it is believed that further experimental work can extend the scope and reliability of the method considerably.

3.2. Pseudo-dimensional non-flatness

An important requirement of a design method is that it deals with information which is easy to understand and apply. As far as the present method is concerned it would be desirable if all the relevant information could be fed into the analysis in dimensional rather than in non-dimensional form. The only geometrical parameter which has so far been used in non-dimensional form is non-flatness and it is appropriate at this stage to consider ways of modifying the analysis so that it can accept dimensional non-flatness.

The relationship between dimensional and non-dimensional non-flatness is shown in 2.3. Knowing h_c it is possible to convert f to b, thus providing non-flatness in physical units. Such an action, however, would have limited usefulness because it would be applicable only for a particular set of operating conditions; the ones which were used to convert $\bar{H}_c$ to h_c. It is advantageous to extract non-flatness in a pseudo-dimensional form where:-

$$\bar{b} = Zb \qquad 3.1$$

and

$$f = \bar{b}/\bar{H}_c \qquad 3.2$$

The advantage of using $\bar{b}$ rather than b is that f can be converted to $\bar{b}$ without introducing operating conditions at all. In this way investigating a particular $\bar{b}$ could be made to correspond to a range of values of b according to the operating conditions represented by Z.

However, the relation 3.2 solves only part of the problem because it enables $\bar{b}$ to be calculated knowing f. This, as was shown in the previous Chapter, can be done by calculating

the land slopes and offsets for a given f and then solving for $\bar{H}_c$. In the computer programme this is done by calling the routine CNTRL. Reversing the problem i.e. calculating f for a given value of $\bar{b}$ is not so straightforward because f cannot be found unless $\bar{H}_c$ is known. On the other hand $\bar{H}_c$ cannot be found unless f is known. The obvious solution in this case is an iterative approach whereby the analysis accepts a given $\bar{b}$, assumes a value of f and calculates $\bar{H}_c$. The product of fx $\bar{H}_c$ is then compared to $\bar{b}$ and if they do not match the process is repeated until they do within the limits of the required accuracy. The procedure for doing this is described in detail in the following section.

3.2.1. Conversion of $\bar{b}$ to f

In the previous section $\bar{b}$ was defined as $\bar{b} = f x \bar{H}_c$. Finding the value of f which is equivalent to a given b is not an easy problem because both f and $\bar{H}_c$ can vary simultaneously. The complexity of the problem is illustrated on fig. 3.1 which shows some typical types of relationship that can exist between $\bar{b}^2$ and f. It must be stressed that the relationship depends on orifice, tilt and angular position of tilt therefore it is not possible to follow rules which are applicable in all cases. Perhaps the only features which are common in all cases is that $\bar{b}^2$ is always zero when f is zero and also $\bar{b}^2$ tends to infinity (positive or negative) as f tends to its limiting value. The limiting value of f is the maximum value it can take without causing metal to metal contact and it is denoted by f_m. The value of f_m depends on tilt, land geometry and the type of profile in use.

In the computer simulation of the analysis, conversion of $\bar{b}$ to f and subsequent calculation of central clearance, minimum clearance, slipper pressure and co-ordinates of pressure centre is done in a routine called FIND. A flow chart of this routine is shown in fig. 3.2.

The inputs to FIND are: orifice coefficient, tilt, position of tilt and $\bar{b}^2$. The reason for using $\bar{b}^2$ rather than $\bar{b}$ is to make iteration easier in cases when $\bar{H}_c^2$ becomes negative. The first stage is to find the maximum allowable non-flatness f_m for the particular tilt. This is done in subroutine LIMC by incrementing f until metal to metal contact occurs. The accuracy of this computation is within 10^{-6}. This value of f is then used to call CNTRL in order to find $\bar{H}_c^2$ and hence $\bar{b}^2$ corresponding to maximum non-flatness. If this is positive then the relationship between $\bar{b}^2$ and f is of type 1 or 2 in fig. 3.1 and conversion from $\bar{b}$ to f can be achieved for any reasonable value of $\bar{b}$. The iteration procedure in this case is done in routine SECANT in which the initial boundaries of f are zero and f_m. Iteration will continue until the product of $\bar{H}_c^2 \times f^2$ is near the required $\bar{b}^2$ within 10^{-5}.

If $\bar{b}^2$ at maximum non-flatness is negative then it is necessary to establish whether the relationship is of type 3 or 4. Clearly if it is of type 4 there is no real solution. If it is of type 3 there could be two, one or no solutions depending on the value of $\bar{b}^2$ required. Unfortunately it is not possible to find the number of roots analytically therefore a numerical approach needs to be adopted. Starting with zero non-flatness f is incremented in ten steps up to

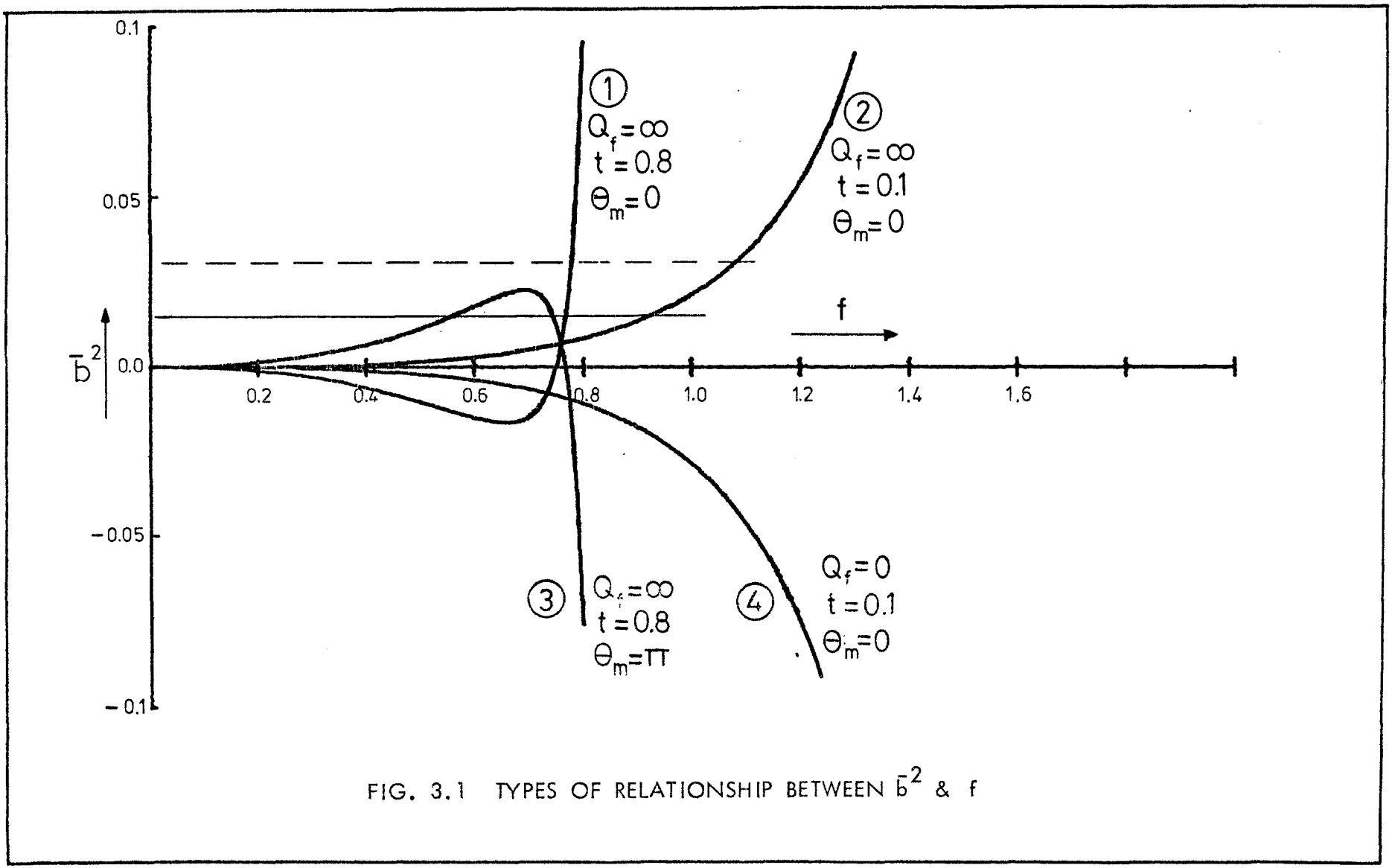

FIG. 3.1 TYPES OF RELATIONSHIP BETWEEN $\bar{b}^2$ & f

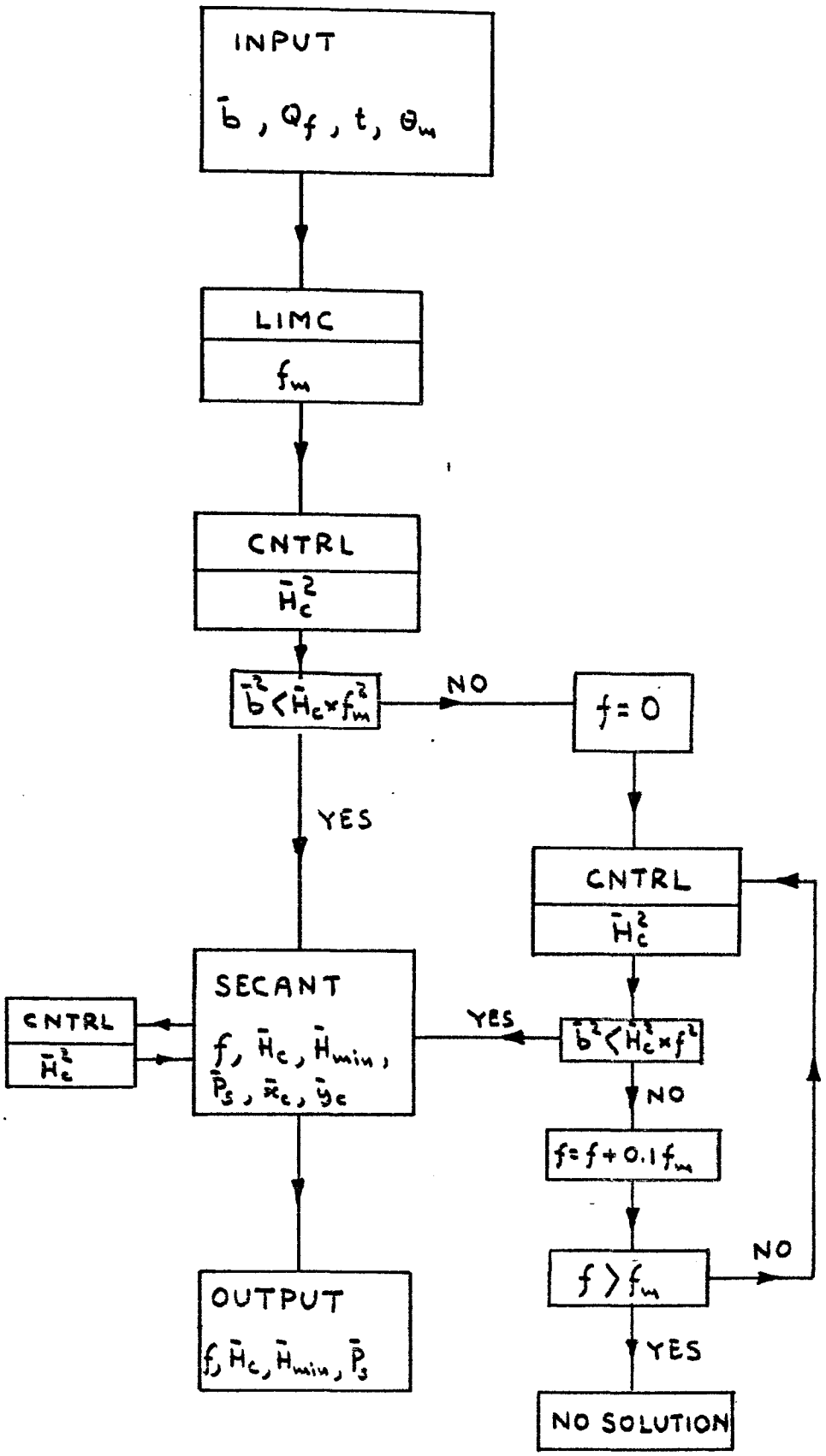

FLOWCHART OF ROUTINE "FIND"

FIG. 3.2

the value of f_m. At each step a call is made to CNTRL and the product of $f^2 \times \bar{H}_c^2$ is compared to the required $\bar{b}^2$. If it is greater than $\bar{b}^2$ that means that there is at least one solution and control is passed to the routine SECANT which iterates as before. If $\bar{b}^2$ is found to be always greater than $\bar{H}_c^2 \times f^2$ then the value of $\bar{b}^2$ is too large and consequently there is no solution.

Having found the equivalent value of f, when there is one, a final call to CNTRL is made which calculates the corresponding values of $\bar{H}_c$, $\bar{H}_{min}$, $\bar{P}_s$, $\bar{x}_c$ and $\bar{y}_c$. This procedure is wholly incorporated in the routine FIND which can now be used by a number of calling programmes to perform various functions in much the same way as CNTRL (Section 2.8).

It was stated above that when $\bar{b}^2$ is positive at $f = f_m$ then the relationship is either of type 3 or 4. Although this is true in the vast majority of cases, it is not always so. Cases where $\bar{b}^2$ increases from zero, reaches a maximum, decreases to a minimum and then increases again to infinity have also been known to occur in some extreme conditions. This means that for certain values of $\bar{b}$ there could be three solutions in f. However, it is not practical to hunt systematically for this type of relationship for two reasons:- Firstly it would severely reduce the speed of computation and secondly it occurs very rarely. The approach in this analysis has been to aim for the smallest value of f. This in turn provides the highest value of $\bar{H}_c$ which is considered to be the most stable.

3.3.1. Application of the analysis on a flat slipper

In the previous section it was shown how $\bar{b}$ can be converted to f. It is now possible to examine specific slipper designs as they may occur in practice. As far as the analysis is concerned this is done by keeping the land geometry and $\bar{b}$ constant and altering the attitude i.e. tilt and θ_m (position of max. tilt). One variable which is also kept constant is the orifice coefficient. This is based on experimental evidence which has shown that the orifice of the slipper designs under investigation behaves as if it was infinitely large and this has been adopted throughout by equating Q_f to infinity. This assumption automatically implies that $\bar{P}_s = 1$ at all times, and is likely to cause errors when the slipper is very heavily tilted. The effect in such cases however is quite clear and it will be discussed when it occurs.

The analysis is first applied to a flat slipper with infinite orifice coefficient. This means that the values of $\bar{b}$ and Q_f are set to zero and infinity respectively. Fig. 3.3 shows a plot of the pressure centre of this configuration for a range of values of tilt and θ_m. Continuous lines correspond to contours of constant tilt (iso-tilt) whereas broken lines correspond to constant θ_m values or iso-thetas for short. The main feature of these curves is that they follow a circular path round the origin with the pressure centre occurring at the same angular position as the minimum clearance i.e. at $\theta_m + \pi$. This is not surprising since both the hydrostatic and hydrodynamic pressure centres of a flat slipper always lie at an angle $\theta_m + \pi$ (see sections

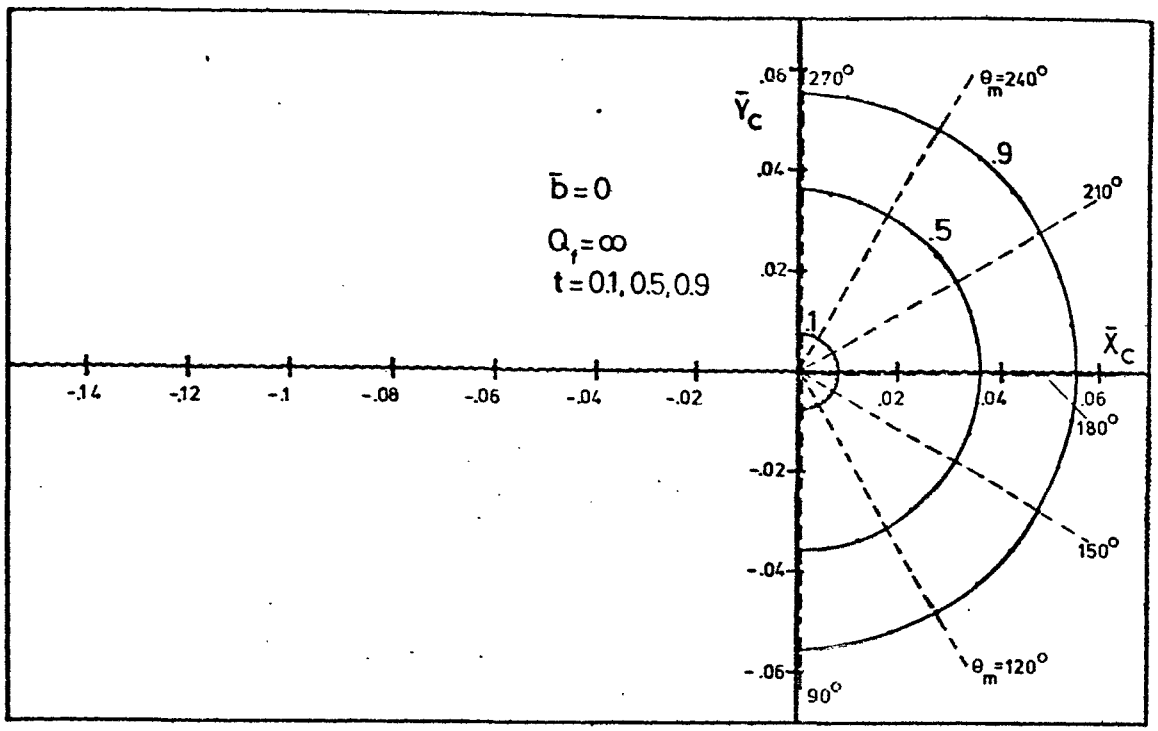

FIG. 3.3 ISO-TILT CONTOURS OF A FLAT SLIPPER

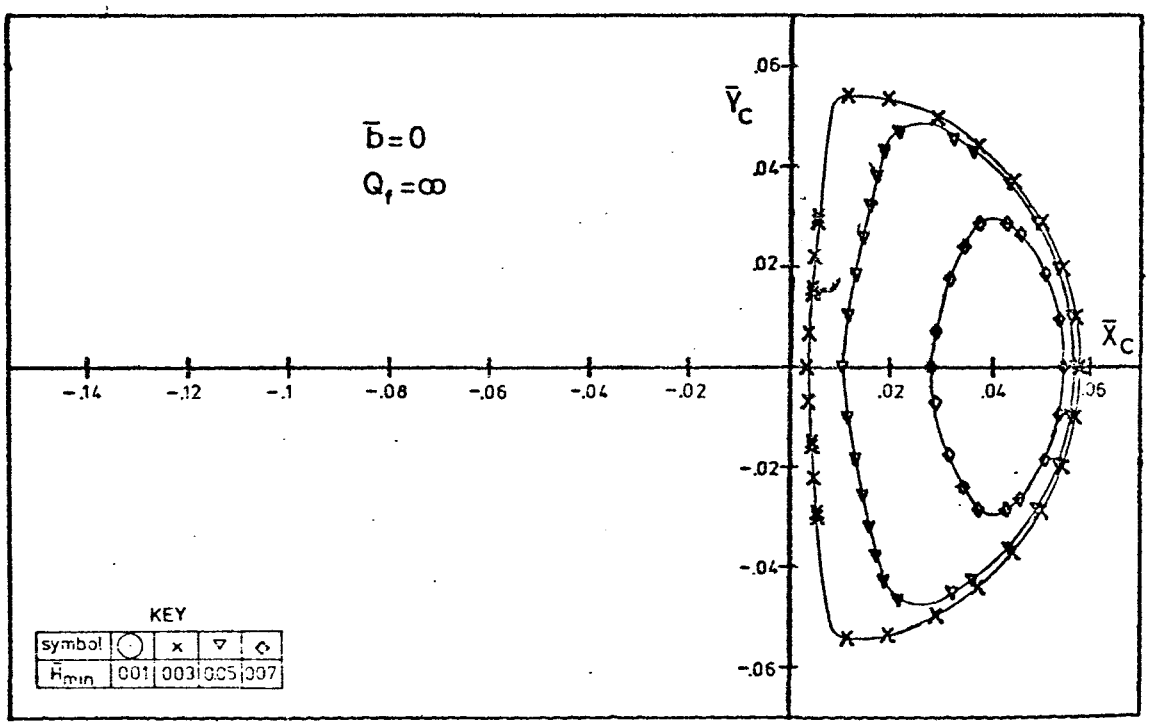

FIG. 3.4 ISO-MIN. CLEARANCE CONTOURS FOR A FLAT SLIPPER

2.6.2 and 2.6.4). In all cases there is no solution for values of θ_m between $3\pi/2$ and $\pi/2$. In practical terms this means that a flat slipper cannot function when it is tilted forward. Sufficient lift can only be generated if it is tilted backwards. In this case the pressure centre will occur at the same angle as minimum-clearance and it will thus give rise to a moment tending to restore the slipper to its zero tilt position which, as it has been shown, cannot provide adequate lift and the system collapses.

The minimum clearance of this configuration is shown in fig. 3.4. The different symbols represent a range of values of $\bar{H}_{min}$ as shown in the inset. By joining all the points corresponding to the same value of $\bar{H}_{min}$ it is possible to obtain contours of constant minimum clearance as shown. Naturally no solution is obtained when the pressure centre occurs in the negative $\bar{x}_c$ region (leading half of the slipper.

A simplified form of minimum clearance contours is shown in fig. 3.5 (for $\bar{b} = o$) where θ_m is constant and equal to π. Under these circumstances the slipper is symmetrical about the x-axis and consequently the y-coordinate of the pressure centre is always zero. The graph shows the relationship between $\bar{H}_{min}$ and the x-coordinate of the pressure centre. As can be seen $\bar{H}_{min}$ is zero when $\bar{x}_c = o$, it then increases with $\bar{x}_c$ reaching a maximum at $\bar{x}_c = 0.05$ and decreases rapidly to zero at $\bar{x}_c = 0.058$ which corresponds to a tilt value of $t = 1$ i.e. when the slipper touches down at the outside radius. The maximum value of $\bar{H}_{min}$ is just under 0.08. At a speed of

1000 rev/min and pressure of 70 bar this is equivalent to 3.5 microns.

The zero value of $\bar{H}_{min}$ at $\bar{x}_c$ = o and t = o is easily explained by the fact that at that position no hydrodynamic lift is generated at all and consequently the system is forced down and $\bar{H}_{min}$ becomes zero. Also the hydrostatic pressure distribution is symmetrical about the z-axis and this causes the pressure centre to occur at the origin.

It is more difficult to explain why the pressure centre does not occur beyond $\bar{x}_c$ = 0.058. The fact that $\bar{H}_{min}$ = o, results from t = 1 when the slipper touches down at radius R_4. At this position, the slipper is heavily tilted back and both the hydrostatic and hydrodynamic pressure centres will occur at θ = O. Due to the fact that the orifice has been assumed to be infinitely large and hence $\bar{P}_s$ = 1, the magnitude of the hydrostatic lift remains much higher than the hydrodynamic. As far as distribution is concerned, the hydrostatic centre is known to occur very close to the origin and the hydrodynamic cannot occur beyond R_4. Therefore, the combined pressure centre is bound to appear close to the hydrostatic which occurs at approximately $\bar{x}_c$ = 0.058.

Under realistic conditions of course the pocket pressure would drop well below 1 at heavily tilted positions. In order to satisfy the load equilibrium condition the magnitude of the hydrodynamic lift would increase to compensate for the reduction in hydrostatic lift. In this case the combined pressure centre would be nearer to the hydrodynamic pressure centre as indicated by the broken line

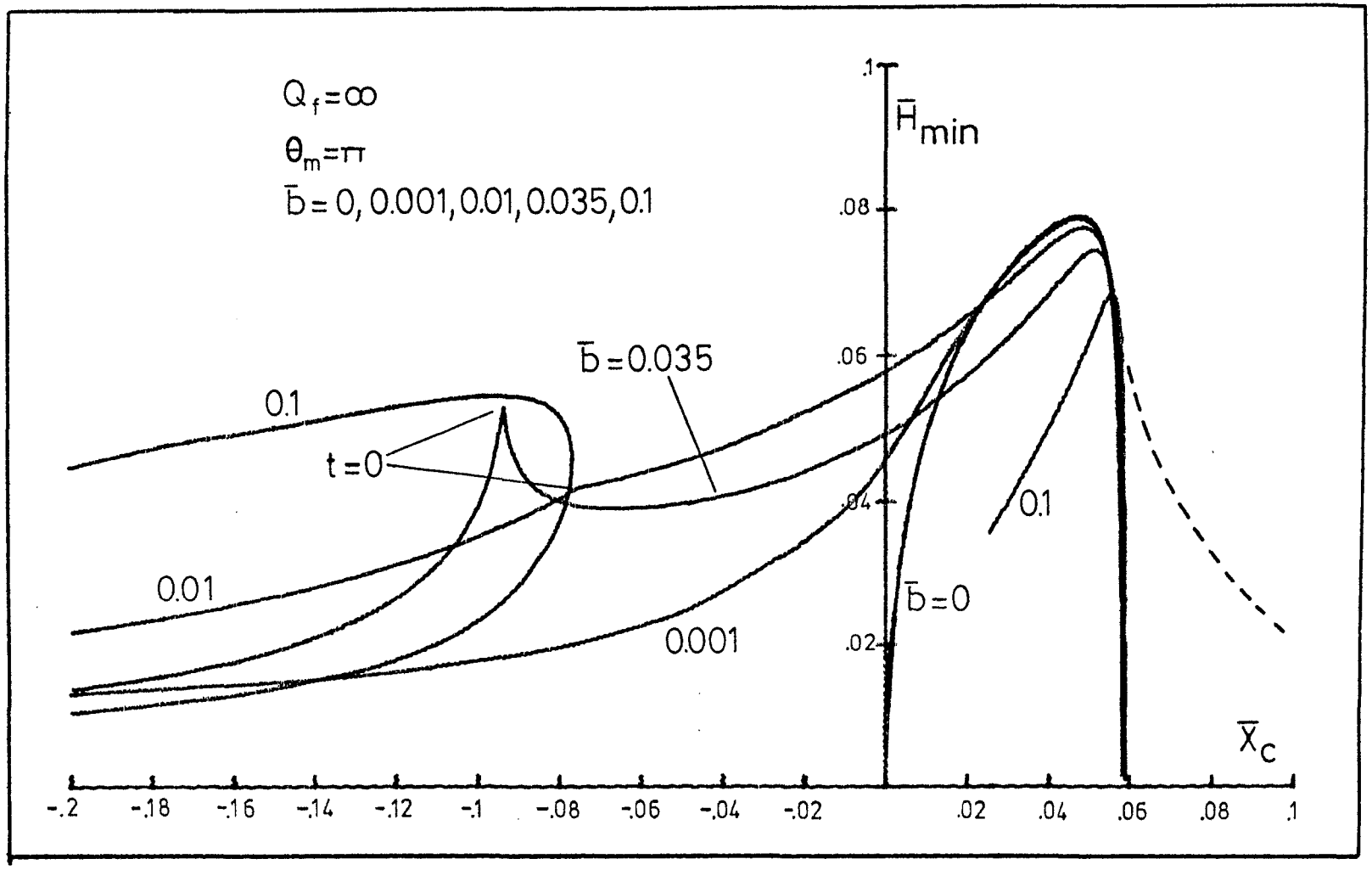

Relationship between min. clearance & pressure centre for parabolic profiles

Figure 3.5

fig. 3.5. This is acknowledged as an inaccuracy resulting from the assumption that the orifice coefficient is infinitely large. This assumption, however, is known to be valid at moderate tilts and it will continue to be adopted in this chapter as it increases the speed of calculations significantly.

3.3.2. Effect of parabolic non-flatness

Fig. 3.6 shows the iso-tilt and iso-theta contours of the pressure centre of a configuration with infinite orifice and a small amount of parabolic type non-flatness ($\bar{b} = 0.001$). The main difference from the flat slipper curves on fig. 3.3.is that the pressure centre can now occur in the negative $\bar{x}_c$ region over a considerable length. This is caused by the hydrodynamic lift generated at the leading edge of the slipper as a result of the local slope on the inner and outer land. Also the slope at the trailing edge causes cavitation and suction which with the additional lift at the leading edge produce a clockwise couple. The result of this couple is a shift of the pressure centre towards the leading edge. Another difference is that the slipper can now operate successfully with negative tilt (tilted forward) which was not possible with a flat slipper.

A plot of iso-minimum clearance for this configuration is shown in fig. 3.7. The effect of non-flatness is again a shift of the contours of constant $\bar{H}_{min}$ towards the leading edge. This effect is most pronounced at small values of $\bar{H}_{min}$ i.e. 0.01 and 0.03. The relationship between $\bar{H}_{min}$ and $\bar{x}_c$ in the simplified case of $\theta_m = \pi$ is shown in fig. 3.5. Minimum clearance can now take reasonable values

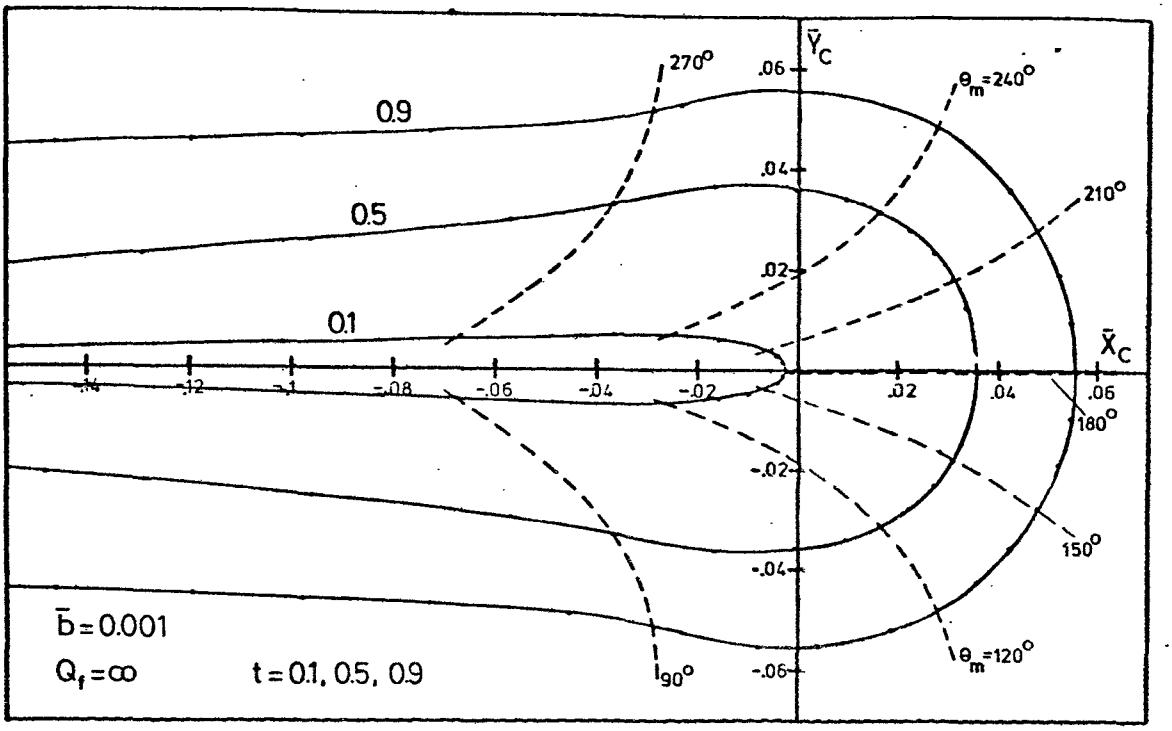

FIG. 3.6 ISO-TILT CONTOURS FOR PARABOLIC PROFILE

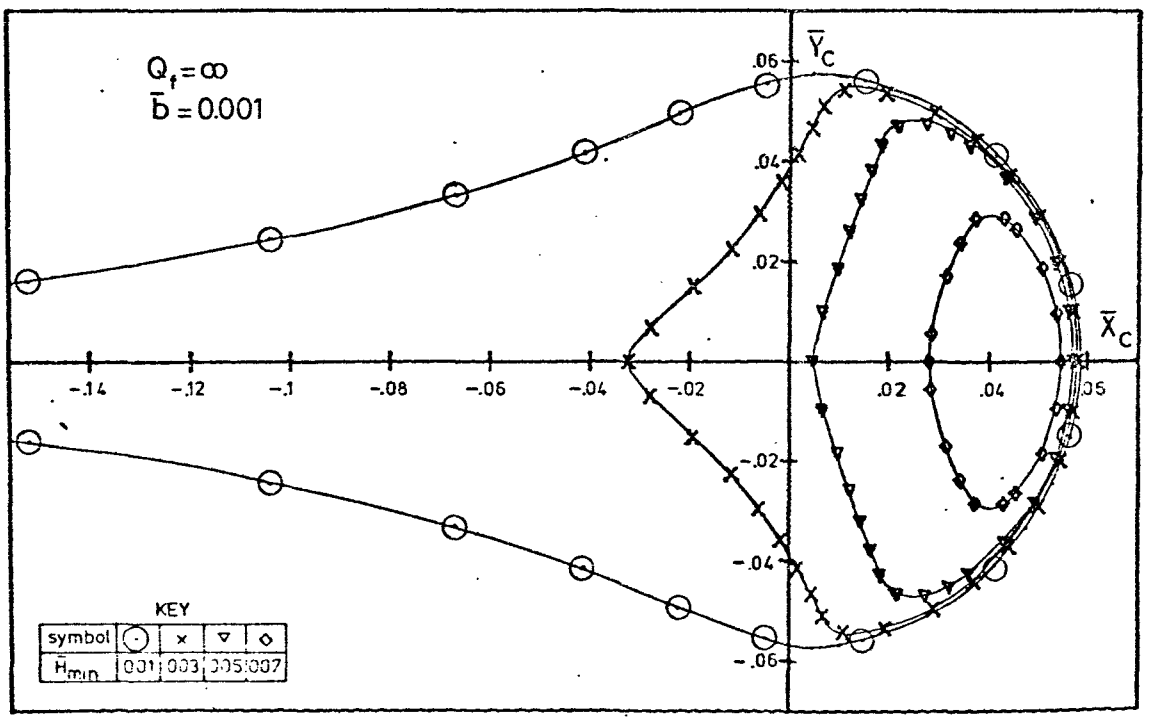

FIG. 3.7 ISO-MIN. CLEARANCE CONTOURS FOR A PARABOLIC PROFILE

in the negative $\bar{x}_c$ region as well as when $\bar{x}_c = o$. At the origin ($\bar{x}_c = o$) all three equilibrium conditions are satisfied and at that point the value of $\bar{H}_{min}$ is approximately 0.045. At the standard conditions of 70 bar and 1000 rev/min this would correspond to 2 microns.

Another iso-minimum clearance plot with larger non-flatness ($\bar{b} = 0.01$) is shown on fig. 3.8. The pattern is very similar to the one in fig. 3.7 except that it appears to have shifted towards the left even further due to the increased lift at the leading edge. In the case of $\theta_m = \pi$ shown on fig. 3.5 the pattern is much the same as before except that $\bar{H}_{min}$ is generally higher. The apparent irregularity at about $\bar{x}_c = 0.08$ is due to a change in the sign of tilt. All points to the right of the apex correspond to the minimum clearance accurring at radius $\bar{R}_1$ on the trailing edge. However, as tilt becomes negative, minimum clearance begins to occur at radius $\bar{R}_1$ on the leading edge which causes the irregularity. This effect was not clear in the previous case because of the small value of $\bar{b}$.

A big change in pattern occurs when $\bar{b}$ is increased further to 0.1 (fig. 3.9). The iso-minimum contours in this case are rather complex and the problem can be better analysed with $\theta_m = \pi$ on fig. 3.5. The discontinuity of the curve is due to the excessive amount of non-flatness which produces cavitation and suction at the trailing edge to such an extent that the system cannot generate adequate lift to support the piston load. A solution can be found only when the slipper is heavily tilted backwards or heavily tilted

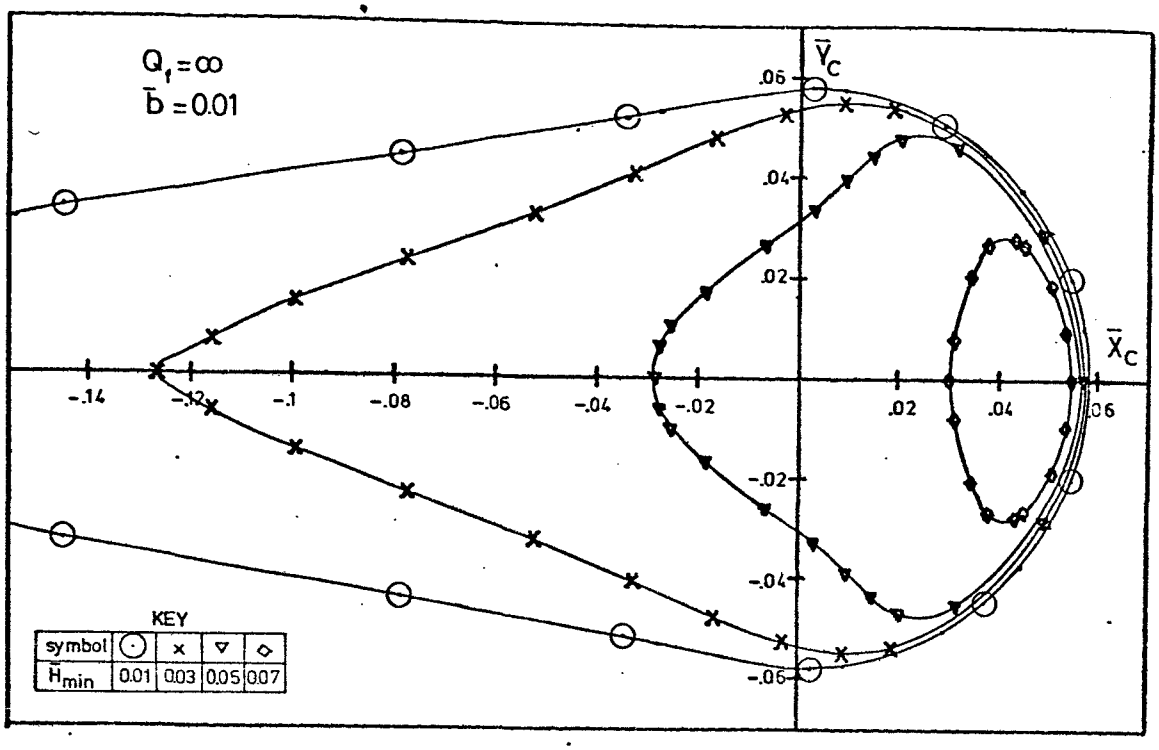

FIG. 3.8 ISO-MIN. CLEARANCE CONTOURS FOR A PARABOLIC PROFILE

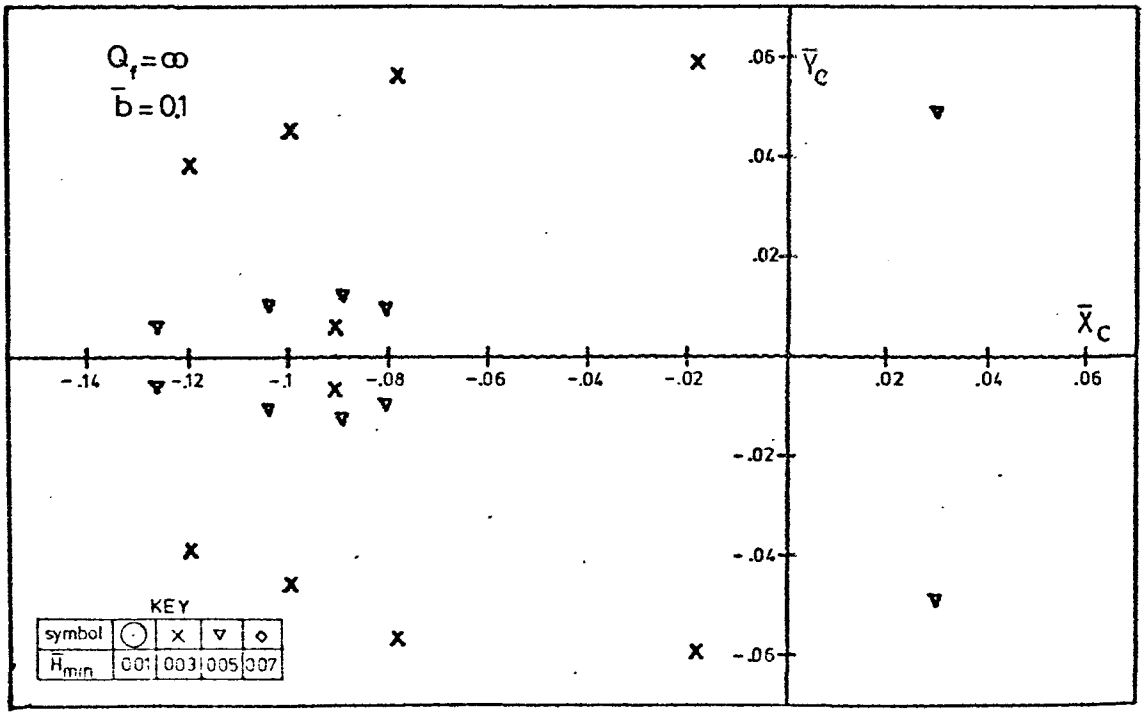

FIG. 3.9 ISO-MIN. CLEARANCE FOR A PARABOLIC PROFILE
(EXCESSIVE NON-FLATNESS)

forward. In the first case the tilt backwards is so large that it overrides the effect of non-flatness which results in a converging wedge and the generation of hydrodynamic lift. However, this disappears as the tilt is reduced in which case a diverging wedge is formed at the trailing edge and the suction effects there, reduce considerably the overall lift. When the slipper is tilted forward very heavily (negative tilt) the suction effects at the trailing edge diminish in view of the large clearance there. Adequate lift, however, appears to come from the leading edge where the local slope is converging and the clearance is small.

This situation of an excessive $\bar{b}$ appears to indicate an unstable situation since the slipper cannot provide adequate lift in the region around the origin and hence it can never satisfy all three equilibrium conditions. A configuration of this type could only work if it was always heavily tilted either backward or forward and was balanced in that position by an external couple such as friction. However, the slipper is well known to rotate when in normal operation. If this configuration was to continue functioning in this fashion there ought to be an additional mechanism forcing the slipper to swash about its axis thus maintaining the heavily tilted position. At the same time the direction of the frictional couple must remain constant so that it can balance the couple due to the offset of the pressure centre. Such a mechanism is not known to exist and is most unlikely to occur in practice therefore this pattern of discontinued $\bar{H}_{min}$ at large values of $\bar{b}$ is considered unstable.

The maximum value of $\bar{b}$ which can provide this type of stability for a parabolic profile is approximately 0.035. At 1000 rev/min and 70 bar this would correspond to a real non-flatness of 1.5 micron.

A common feature of all the curves on fig. 3.5 is that $\bar{H}_{min}$ decreases sharply at $\bar{x}_c = 0.058$. This is a result of the orifice coefficient which has been assumed to be infinitely large. In a realistic situation the orifice would cease to behave as if it was infinite at heavily tilted positions. Instead $\bar{H}_{min}$ would decrease in a fashion shown by the dotted lines which correspond to an orifice coefficient of finite size. This means that the slipper can also operate successfully when the pressure centre extends beyond 0.058.

3.3.3. Other types of non-flatness

In the previous section it was shown that for a parabolic profile the range of suitable non-flatness is typically zero to 1.5 micron. Clearly this range is small by any standards and certainly not easy to manufacture. One possible explanation for the range being so limited is the fact that with this type of profile metal to metal contact can occur at radius $\bar{R}_1$ at moderate values of $\bar{b}$. In practice this part of the slipper is known to polish quickly thus producing a flatter inner land. With the analysis as it stands, however, the proximity of the edge of the inner land to the slipper plate inevitably gives rise to severe suction effects and eventual metal to metal contact thus distorting slipper behaviour as it occurs in practice.

In an attempt to extend the range of acceptable values of $\bar{b}$ a number of other profiles were also investigated.

One such profile is a conical one as described in Section 2.2.6. It is not possible to include the full results of this investigation here due to lack of space except for fig. 3.10 which shows the relationship between $\bar{H}_{min}$ and pressure centre in the simplified case of $\theta_m = \pi$. These results are very similar indeed to the results obtained with a parabolic profile. A marginal increase in the maximum value of $\bar{b}$ was found in the case of the conical profile. In this case non-flat profiles up to a value of $\bar{b} = 0.05$ could be tolerated. The similarity between the results obtained with the parabolic and conical profiles appeared to underline that the cause for such a limited range of acceptable $\bar{b}$ were the suction effects at the trailing end of the inner land.

It seemed therefore logical to simulate a profile which would minimize these undesirable effects. A profile most likely to do so is the chamferred profile as defined in section 2.2.6. Low values of $\bar{b}$ showed a behaviour very similar to low values of parabolic non-flatness. An iso-minimum clearance plot of a chamferred profile for $\bar{b} = 0.1$ is shown on fig. 3.11. It is significant that at this value of $\bar{b}$ both the parabolic and conical profiles were unstable. A plot of $\bar{H}_{min}$ against pressure centre at $\theta_m = \pi$ is shown on fig. 3.12. This shows that stable configurations can be obtained for $\bar{b}$ up to 0.2. At 1000 rev/min and 70 bar this corresponds to nearly 9 microns. This range of non-flatness is 6 times larger than the acceptable range obtained with a parabolic profile. It also means that a slipper design with a given non-flatness can operate successfully over a much

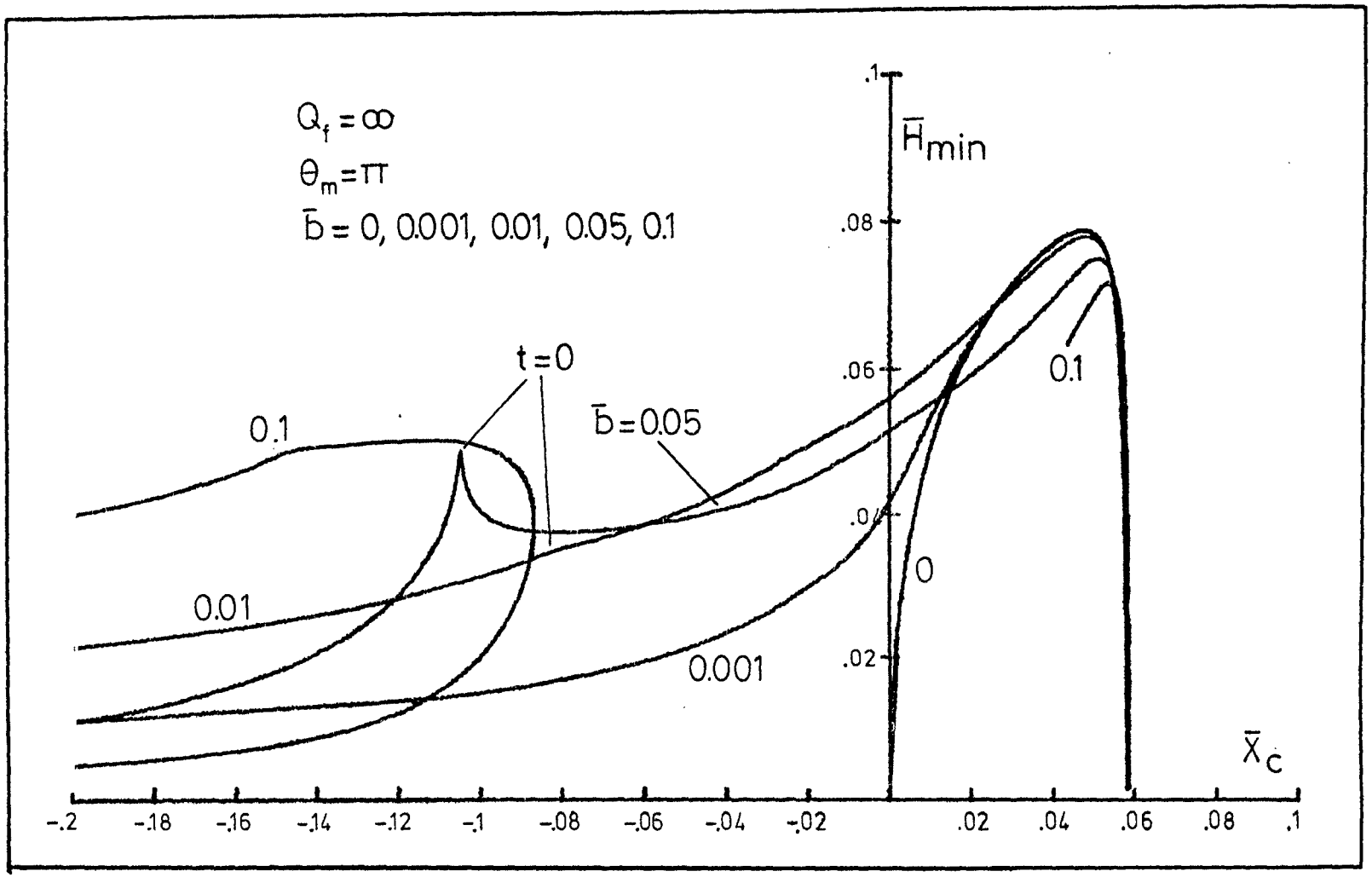

Relationship between min. clearance & pressure centre for conical profiles

Figure 3.10

wider range of operating conditions with a chamferred profile rather than a parabolic one.

As shown on fig. 3.12 the behaviour of a chamferred profile at low $\bar{b}$ values is very similar to a parabolic one. Differences begin to arise at higher $\bar{b}$ values. In this case the apex corresponding to zero tilt is more pronounced. As before the reason for the irregularity is due to the switching of the minimum clearance from the trailing end to the leading end as tilt goes through zero. At higher values of $\bar{b}$ (1.0) the apex occurs at a higher $\bar{H}_{min}$ but it drops sharply and it then follows the $\bar{x}_c$ axis asymptotically. The reason for the sharp decrease is due to the fact that at negative tilts, the inner land does not contribute hydrodynamically because it diverges the oil flow at all points. Adequate hydrodynamic lift appears to be generated, however, at the leading edge of the outer land which due to the relatively large non-flatness continues to converge even at negative tilts. This situation ceases to exist when the forward tilt is so large that the front of the outer land is parallel to the slipper plate. In this case no hydrodynamic lift is generated and the system ceases to function.

The behaviour of this profile when $\bar{b}$ has exceeded its maximum limit is shown on fig. 3.12 (for $\bar{b}$ = 10.). In this case non-flatness is so large that the effect of the outer land is negligible compared to the inner land and the system behaves like a flat slipper with only one land. Indeed if this curve is compared to the flat slipper curve on fig. 3.5 ($\bar{b}$ = 0) it is found that the two curves are very similar. One difference is that the curve for the

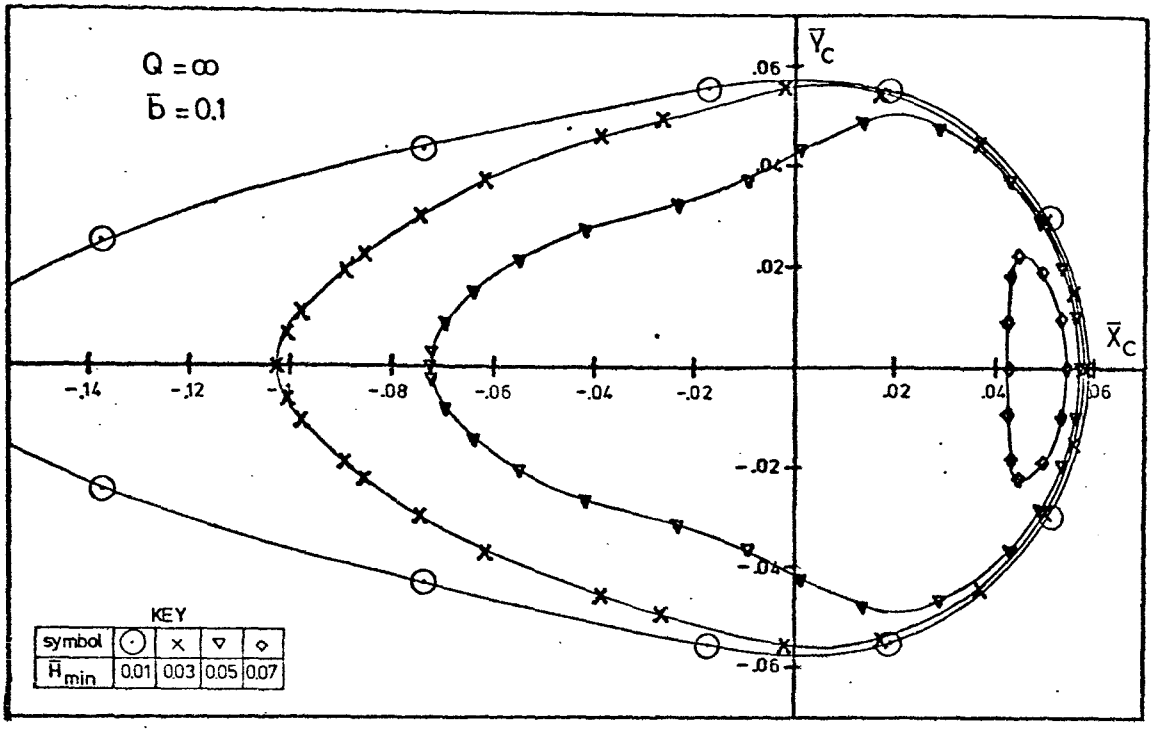

FIG. 3.11 ISO- MIN. CLEARANCE CONTOURS FOR A CHAMFERRED PROFILE

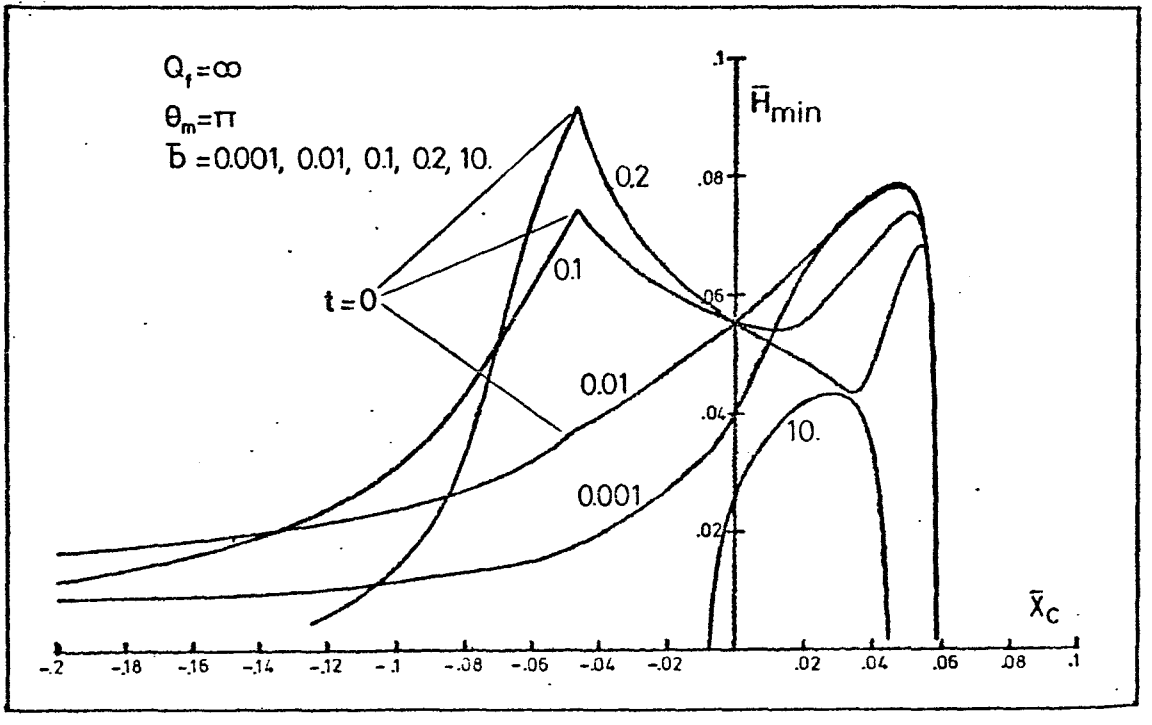

Relationship between min. clearance & pressure centre for chamferred profiles

Figure 3.12

chamferred profile crosses into the negative $\bar{x}_c$ region as a result of very small amounts of hydrodynamic lift generated at the leading edge when the slipper is at the zero tilt position. Another difference is that the start of the curve at large positive tilt occurs at a smaller value of $\bar{x}_c$. Again this is due to the excessive non-flatness which makes the outer land almost redundant. When heavily tilted the outer land is parallel to the slipper plate or cavitating therefore most of the hydrodynamic lift comes from the trailing edge of the inner land which presents a converging wedge to the oil flow.

3.4. Design Applications

In previous sections of this Chapter it was shown how different profiles could affect the minimum clearance of the slipper. Various ways of examining and presenting slipper performance were also outlined. It is now possible to apply these methods as a design aid.

There are two areas in which the analysis can provide information with practical applications:-

1. Finding the optimum amount of non-flatness which is necessary to make the slipper work over a range of operating conditions.
2. Estimating the minimum clearance which can be expected in operation.

The application of the analysis into these areas is examined in this section. One important fact which must be borne in mind is that the results obtained with this method must be interpreted within the framework of the assumptions which support the method. Admittedly it is

not possible for every designer to be familiar with the body of the theory; however, familiarity with the basic mechanisms and limitations of the method is considered to be a necessity.

3.4.1. Determination of the maximum non-flatness

Before attempting to quantify non-flatness it is necessary to decide on the type of profile. This will depend on a multitude of factors such as cost of manufacture, operating conditions, type of oil, space restrictions, material to be used and last but not least practical experience related to failures and their causes, wear on the slipper lands, polishing marks etc. This is clearly a complex problem which can vary enormously from case to case and it is advisable that the advantages and disadvantages of each profile are examined individually. The simulation of slipper behaviour in the analysis is done under idealised conditions therefore any information must be extracted in the form of guidelines rather than absolute values. This inadequacy of the method can be overcome by the interaction between theory and experimentation.

As far as maximising the non-flatness is concerned this can be done by referring to a plot such as the one shown in fig. 3.5. Obviously it is desirable to have the largest possible non-flatness without causing instability. The maximum value of $\bar{b}$ can thus be found by plotting $\bar{H}_{min}$ against $\bar{x}_c$ until the curves begin to be discontinuous near the origin. It is not necessary to consider minimum clearance at any angle other than $\theta_m = \pi$ at this stage because the relationship between $\bar{H}_{min}$ and $\bar{x}_c$ is very similar

at all other angles; except that it is scaled down. The object of this exercise is to maximise $\bar{b}$ without encoutering any discontinuities if the relationship between $\bar{H}_{min}$ and $\bar{x}_c$. In the case of the parabolic profile the maximum allowable value of $\bar{b}$ has already been found to be around 0.035 (section 3.3.2). This means that the slipper can operate satisfactorily under steady state conditions provided that $\bar{b}$ is within the range 0 to 0.035. The reason for aiming for the largest $\bar{b}$ value is because that would generally provide the largest minimum clearance (see fig. 3.5).

This value of $\bar{b}$ must now be converted to physical units by dividing it by Z so that it can be manufactured; this is done by referring to the specification regarding the range of operating conditions that the slipper is designed for. As an example assume the slipper is required to operate within a pressure range of 10 to 350 bar and a speed range of 2 to 8 m/s. Temperature must also be taken into consideration since it can alter the viscosity of the fluid; however, it is assumed to be constant in this example for the sake of simplicity. It is not necessary to consider every combination of speed and pressure because the only values of Z which are needed are the maximum and minimum. Assuming that the oil has the same viscosity as Shell Tellus 27 at 40°C, the limiting values of Z will be as follows:-

$\bar{b}$	P_p (bar)	U (m/s)	Z	b (μm)
0.035	10	8	6147	5.7
0.035	350	2	72732	0.5

The values of b quoted in the above table are the optimum values for the particular conditions they are related to. What is required, however, is a single value of b which can cope with both conditions as well as the ones between them. If b = 5.7 micron is adopted, that would be satisfactory at low pressures and high speeds. However, when the conditions are reversed i.e. at high pressures and low speeds the equivalent value of $\bar{b}$ would be 0.41 which is much larger than 0.035 and therefore unacceptable. A more reasonable design would be obtained with b = 0.5 micron. The limiting values of $\bar{b}$ in this case are 0.035 and 0.003 which are both acceptable. Also the value of $\bar{b}$ at all intermediate conditions will lie between 0.003 and 0.035. Therefore for this particular design and operating conditions the non-flatness should not exceed 0.5 micron.

3.4.2. Determination of Minimum Clearance

Having adopted a particular profile and non-flatness it is now possible to estimate the minimum clearance at a particular operating condition. In order to do that it is necessary to know the co-ordinates of the load centre and hence the pressure centre. The minimum clearance can then be found by referring to a minimum clearance plot such as the one shown in fig. 3.8.

The co-ordinates of the load centre can be found by calculating the total load on the slipper F and the moments M_x and M_y about the x and y-axes respectively. Their magnitude depends largely on operating conditions such as speed and pressure but also on external effects such as spring loads, friction etc. Having established F, M_x and

$\bar{M}_y$ the co-ordinates of the load centre are given by:-

$x_1 = M_y/F$ and

$y_1 = M_x/F$

Loading conditions can thus be represented by a force F acting at the point (x_1, y_1) as shown in fig. 3.13. In order to satisfy equilibrium about the x and y-axes the pressure centre of the slipper must have the same x and y co-ordinates as the load centre i.e.:-

$\bar{x}_c = x_1/R_4$

$\bar{y}_c = y_1/R_4$

Flow or load equilibrium are not considered here because they are already incorporated in the analysis. It is worth noting that the above expressions which relate pressure centre to load centre imply two important assumptions:-

1. The angle of tilt is small. Although tilt values between -1 to 1 are quoted in the analysis, these values are non-dimensional and the actual angle of tilt is very small indeed. Typical tilts as they have been encountered in practice are 10 micron clearance in 30 mm. When converted to degrees this corresponds to 0.02^{o}. This is clearly very small and it can be safely ignored.
2. The consideration that the slipper is in equilibrium automatically excludes the possibility of it moving along the z-axis or rotating about the x or y-axes. This limitation of the analysis is a direct consequence of its confinement to steady state. The justification

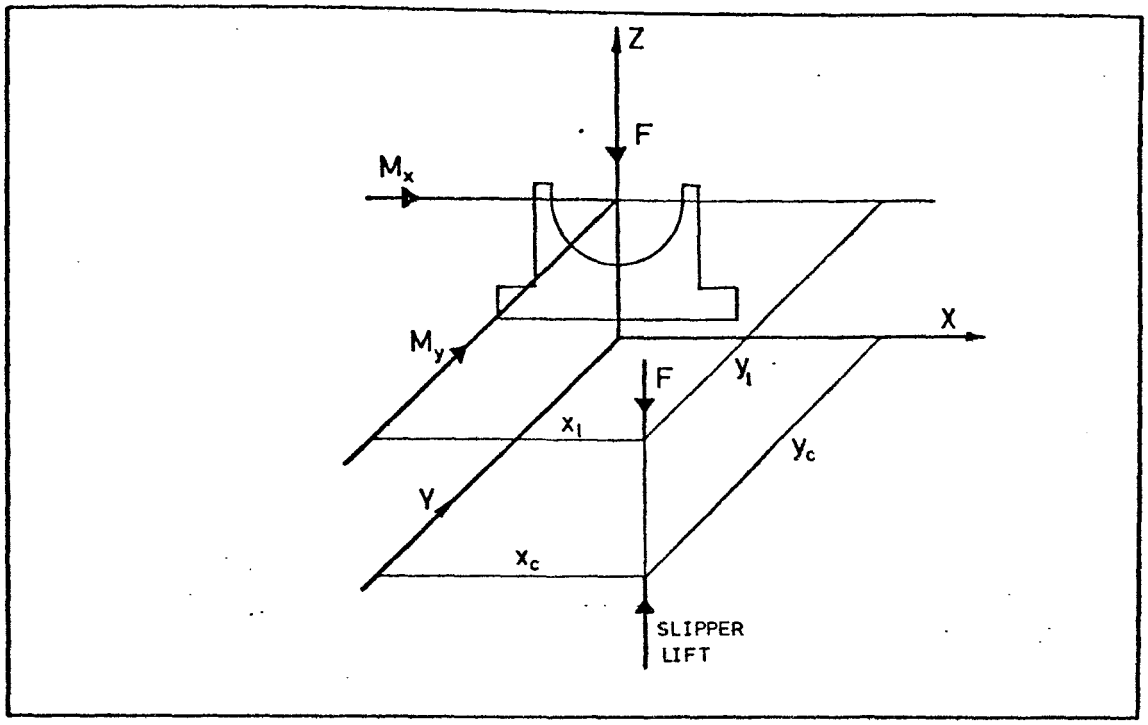

FIG. 3.13 LOADING CONDITIONS AT EQUILIBRIUM

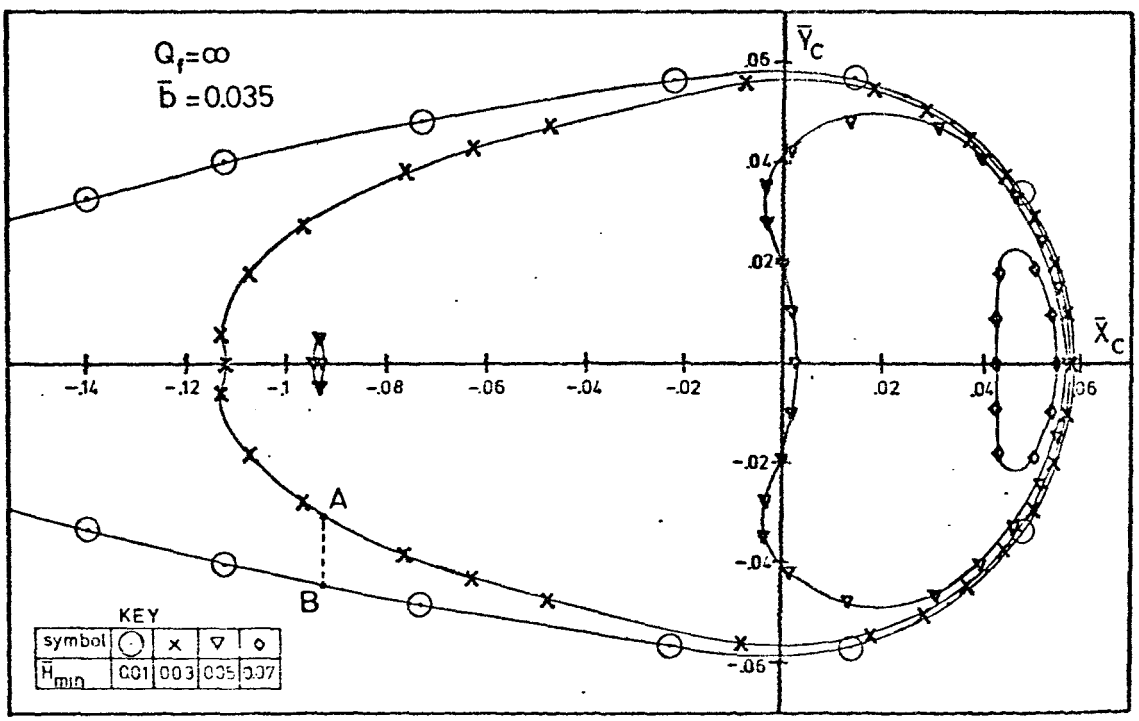

FIG. 3.14 CONTOURS OF ISO-MIN. CLEARANCE OF PARABOLIC PROFILE AT OPTIMUM NON-FLATNESS

for this assumption is outlined in section 2.1.

Reference can now be made to the iso-minimum clearance plot on fig. 3.14 which corresponds to $\bar{b} = 0.035$ and an infinitely large orifice coefficient. In this example Q_f is set to infinity. It is recommended, however, that in a design study Q_f is set to its proper value which can be found using expression 2.68. This was not necessary in the calculation of $\bar{b}$ since the effect of orifice was very small. It can, however, affect the layout of minimum clearance contours and as such it should be taken into consideration. In this example an arbitrary position has been chosen for the pressure centre as shown by point A in fig. 3.14. The value of $\bar{H}_{min}$ at that point is 0.03. The physical minimum clearance h_{min} can be found by applying $h_{min} = \bar{H}_{min}/Z$. For the range of conditions used in the previous section (10 to 350 bar and 2 to 8 m/s) the limits of h_{min} will depend on the maximum and minimum values of Z. i.e.:-

$\bar{H}_{min}$	P_p (bar)	U (m/s)	Z	h_{min} (μm)
0.03	10	8	6147	4.9
0.03	350	2	72732	0.4

This information, despite its limitations, should provide a good indication of the slipper performance in a pump. If problems are still found to be present, the designer has the option of altering the original geometry i.e. the type of profile, $\bar{b}$ or land geometry and repeat the procedure until minimum clearance is adequately large. If the problems appear to occur at a particular position

of the slipper path the designer must try and simulate the conditions at that point as closely as possible.

The method can also be extended to investigate the possible effects of a factor when its magnitude or direction are uncertain or variable. A typical such factor is friction and it can be dealt best in the form of an example.

Suppose that the pressure centre of a particular configuration is normally at point A on fig. 3.14 and it is required to find the effect of friction on the minimum clearance. The effect of friction is not known accurately but it is likely to increase M_x by up to 15%. In this case $\bar{x}_c$ will remain unaffected but $\bar{y}_c$ is likely to decrease from its present value by up to 15%. Transferred to the iso-minimum clearance plot on fig. 3.14 such an increase will shift the pressure centre to point B where $\bar{H}_{min}$ is 0.01. This means that the pressure centre could occur anywhere between A and B depending on the effect of friction on M_x and the value of $\bar{H}_{min}$ will range between 0.01 and 0.03. At a pressure of 10 bar and a speed of 8 m/s the effect of friction could be a reduction in minimum clearance from 4.9 microns to 1.6 microns.

The above example is clearly a simplified one and the values used were arbitrary. It does indicate, however, the ease with which one can examine the effect of individual parameters. Naturally in the course of a design study it is necessary to incorporate the proper value of the orifice coefficient and include more contours of constant minimum clearance in order to improve the accuracy.

4. EXPERIMENT. INSTRUMENTATION AND APPARATUS

4.1. Introduction

The aim of the experimental study is to provide further insight into the slipper problem which is hoped to assist and improve the design of slippers and axial piston pumps in general. This was also one of the aims of the theoretical study described in chapters 2 and 3 but unlike that, the approach is now from a practical point of view. The results obtained from this experimental study are expected to provide valuable information about the mechanism and general behaviour of the slipper and also to correlate, where possible, with theoretical results. Like many other investigations the relation between theory and experiment has been one of continuous interaction where one provides support or guidelines to the development and interpretation of the other.

The experimental study concentrates on the measurement of slipper clearance (oil film thickness between the slipper lands and the slipper plate) and slipper pocket pressure. Another investigation, the measurement of piston spin, is described and discussed separately in chapter 6. All the measurements were taken on-line from typical units running under typical operating conditions.

Some tests were carried out at the National Engineering Laboratory in East Kilbride using a 330 ml/rev (20 in^3/rev) variable displacement pump. In the remainder of the tests a Commercial Hydraulics 92 ml/rev (5.6 in^3/rev) fixed displacement pump was used; these tests were carried out at the University of Birmingham.

However, the method of data logging, storage, data processing and presentation of the results was the same in all the tests and it was done with a data logging system based on a PDP11/10 processor.

The instrumentation used in all the tests was also practically identical. Slipper clearance measurements were taken using a cluster of 4 capacitance displacement transducers which were installed in the slipper plate. In order to measure the small clearances (down to one micron) which are normally encountered as well as meeting the space restrictions, these transducers were specially developed at the University of Birmingham and they were very similar to the ones used by Madera[23] in the measurement of portplate clearances. The rest of the electronic instrumentation included a Wayne Kerr displacement measuring unit which was modified to accommodate the intermittent films which occur between the slipper lands and the slipper plate.

Slipper pocket pressure was measured with a purpose built strain gauge type pressure transducer which was also installed in the slipper plate and was conveniently placed in the centre of the cluster.

4.2. Test rig and hydraulic circuit

A standard circuit was used in almost all the tests. Fig. 4.1 shows the test rig used at the National Engineering Laboratory and fig. 4.2 shows the hydraulic circuit layout, as it was used in the tests, in schematic form.

A D.C. electric motor (1) drives the pump under investigation (2). The pump output is passed through a

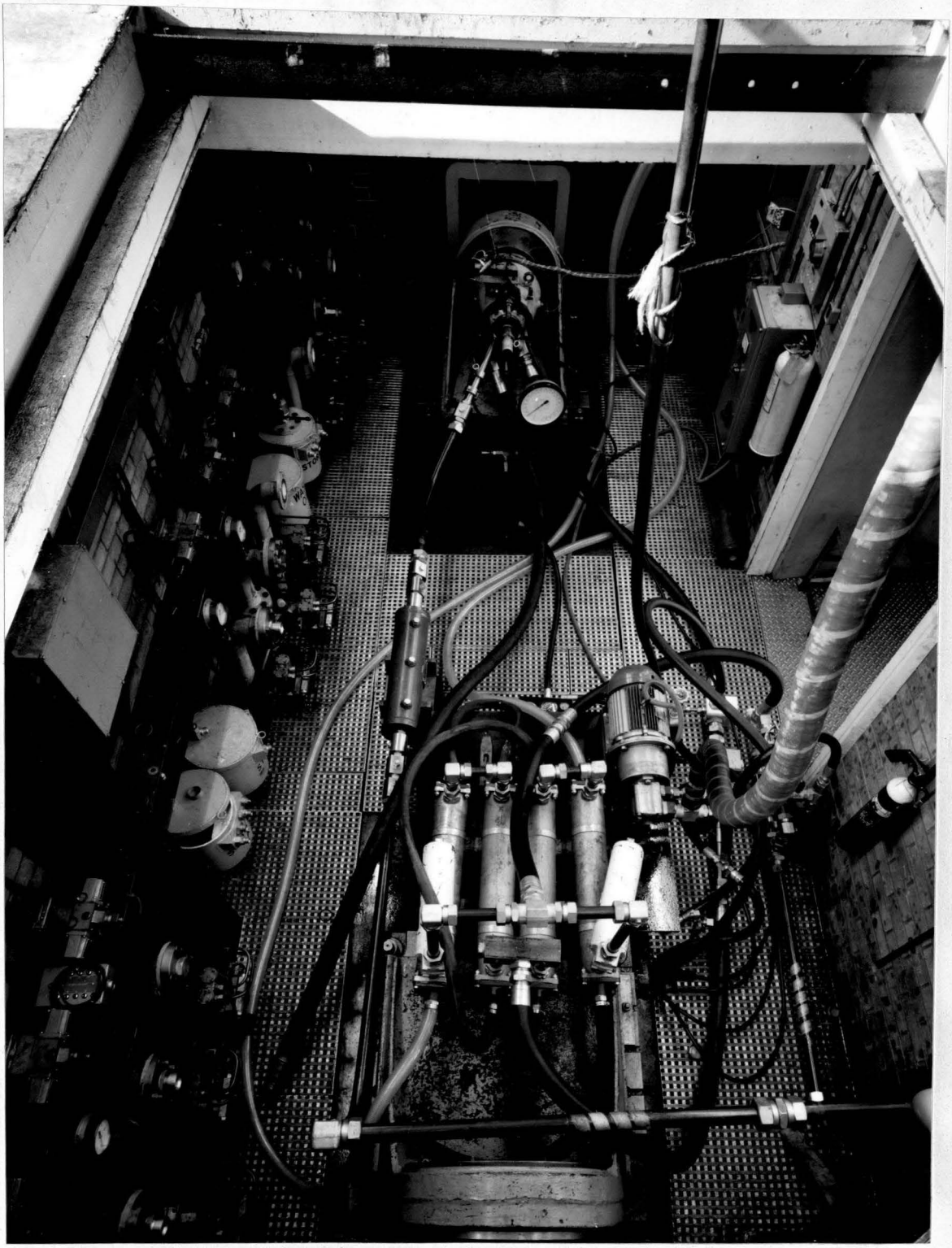

TEST RIG AT N.E.L.

FIGURE 4.1

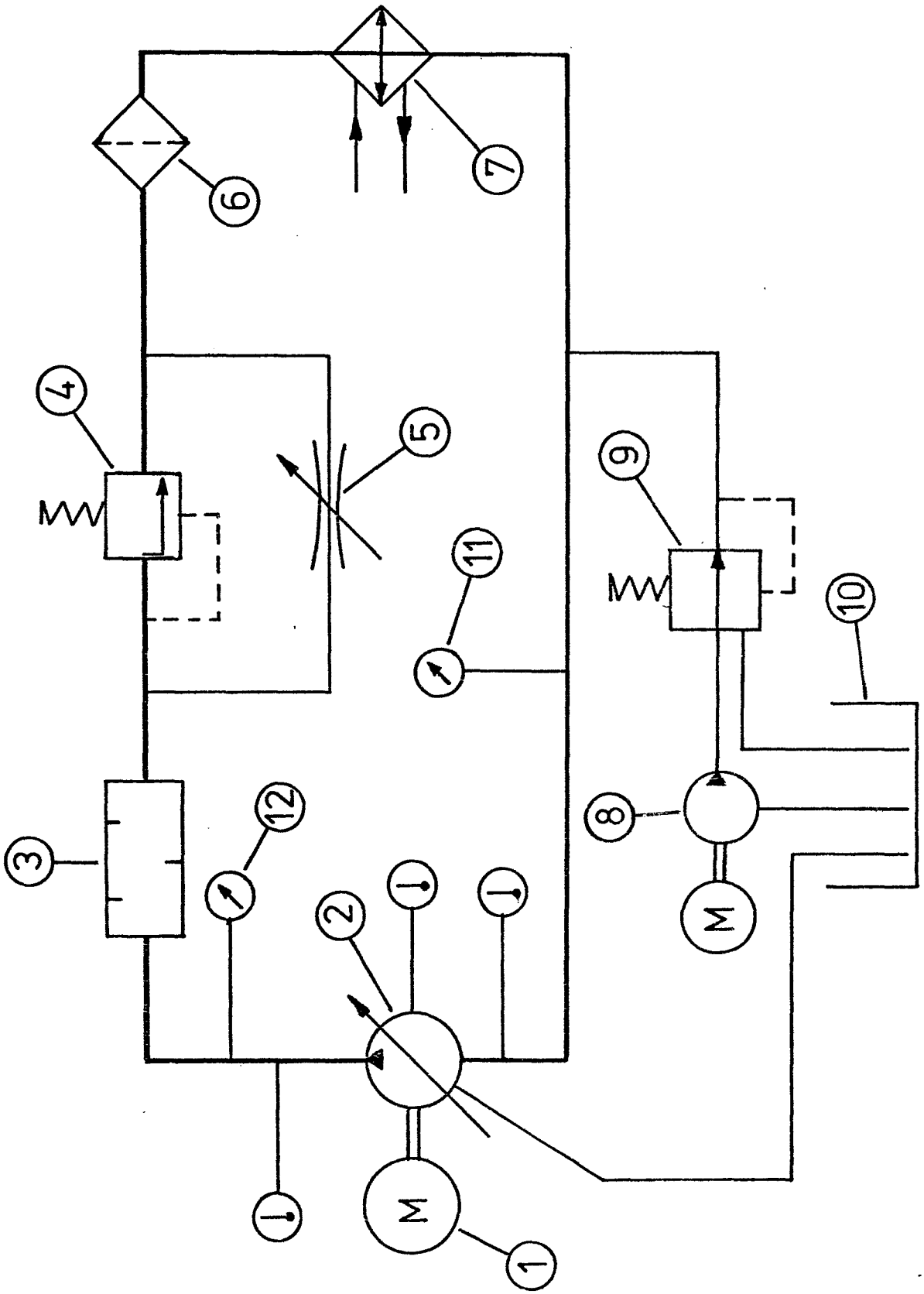

TEST RIG CIRCUIT DIAGRAM

FIGURE 4.2

silencer (3) and connected to a load valve (4) in parallel with a by pass needle valve (5). Before being fed back to the input stage of the pump, the oil flow is passed through oil filters (6) and coolers (7). The boost pack (8) provides back-up pressure to the system and compensates for leakages while the pressure relief valve (9) maintains the pressure of the input stream at a steady level. All excess oil is returned to tank (10). The pressure gauges (11) and (12) give approximate values for the inlet and outlet pressure respectively. Temperature was measured at the inlet, outlet and casing of the pump.

The hydraulic circuit used for the tests at the University of Birmingham was very similar but did not have a silencer in the output circuit. The temperature of the inlet stream was automatically controlled by a Taylor temperature control system.

4.3. Displacement measuring equipment

The film thickness between the slipper lands and the slipper plate was measured using a Wayne Kerr Dimeq TE600B Transducer Equipment in conjunction with capacitive type displacement transducers which had been developed at the University of Birmingham. Although displacement transducers are commercially available, they are not suitable for applications such as this because they are too large (the smallest one is approximately 30 mm long by 10 mm in diameter). Due to their large size these transducers are almost impossible to install on slipper plates, which can be less than 15 mm thick, and also they are not accurate enough for clearances of the order of a

few microns. In order to obtain satisfactory measurements the transducer must be considerably smaller than the width of the slipper lands so that it remains covered by them for a reasonable period of time when in operation. The transducers which were developed for this application are based on the same principles as the commercial ones but they are considerably reduced in size (3 x 12 mm).

A cross section of a typical displacement transducer in situ is shown in fig. 4.3. The main parts are:-

1. The central probe.
2. The guard ring.
3. The mounting ring.

The three parts are concentric and electrically insulated from each other. They are held together by a thin film of high strength adhesive not normally thicker than 50 μm. The diameter of the central probe is determined by the range of clearances it is designed for. In this case (for a 50 μm range) it is typically around 0.75 mm. The transducer is connected to the rest of the electronic equipment by a screened lead whose core and screen are attached to the central probe and guard ring respectively. The complete transducer assembly is securely fixed in the slipper plate so that it is very close to the working surface but not protruding above it.

The other end of the screened lead is connected to a Wayne Kerr displacement measuring unit which is shown in schematic form in fig. 4.4.

An oscillator (1) feeds an operational amplifier (2) with a carrier waveform through an isolating transformer (3).

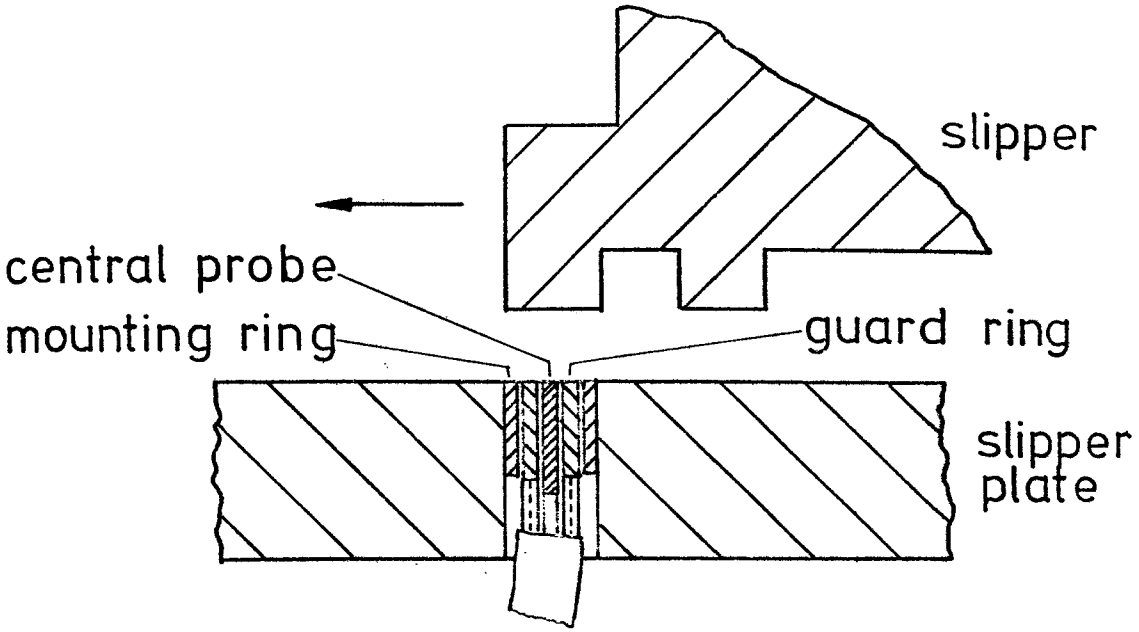

Installation of displacement transducer

Fig. 4.3

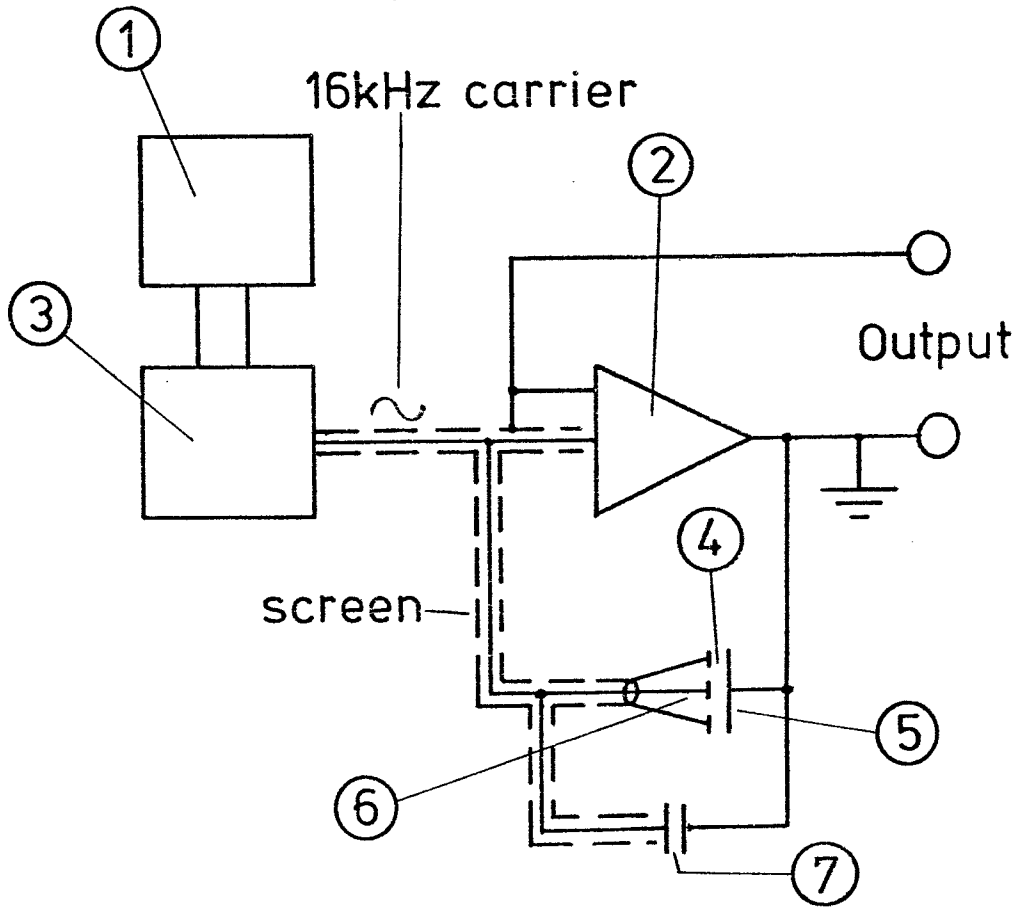

Displacement Measuring circuit

Fig. 4.4

The carrier is sinusoidal, of constant amplitude (approx. 3.5 V r.m.s.) and frequency equal to 16 kHz. The theory of operational amplifiers shows that the output V_o is equal to:-

$$V_o = \frac{K_1}{C_t} \qquad 4.1$$

where C_t is the capacitance of the feedback circuit (4). This is normally formed by the central probe of the transducer (6) and the test surface (5), in this case it is the slipper which is earthed through the body of the pump. The feedback capacitance can thus be expressed in terms of the distance $d + d_o$ between the central probe and the test surface and the relation 4.1 can be modified to:-

$$V_o = K_2 (d + d_o) \qquad 4.2$$

The output is taken between the floating earth and ground. It consists of a 16 kHz sine wave whose amplitude is directly proportional to the effective reactance of the feedback capacitor and hence the distance between the central probe and the slipper. In normal operation therefore, the output consists of a 16 kHz carrier modulated according to the distance of the slippers as they pass over the transducer. (Fig. 4.5a).

A demodulating circuit is provided with the equipment which demodulates the output of the amplifier. However, it was soon realised that due to its limited frequency response (3 kHz maximum) all vital information was overshadowed by the characteristics of the demodulating circuit. One attempt to avoid this problem was the modification of a separate

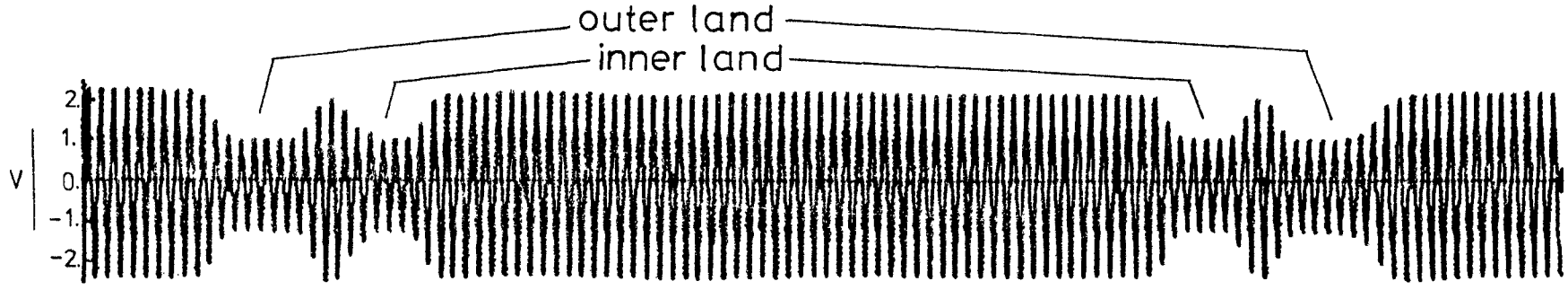

a. MODULATED TRACE

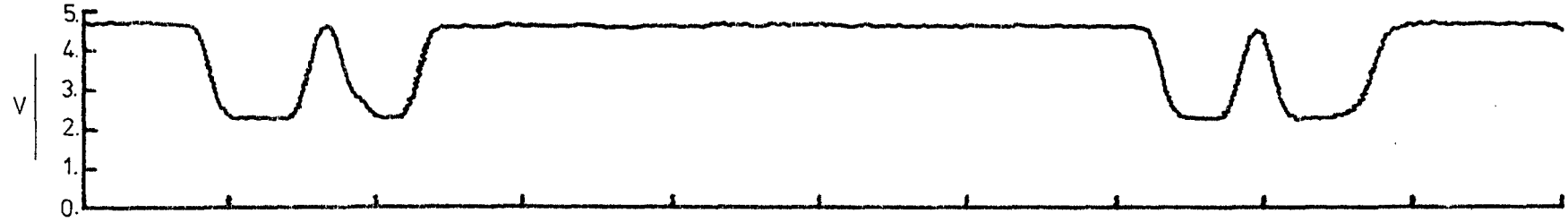

b. DEMODULATED TRACE

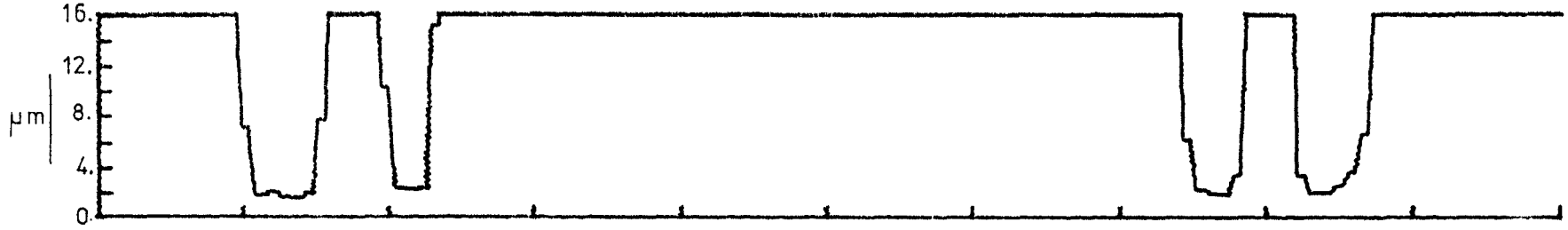

c. CALIBRATED TRACE

FIG. 4.5 DATA PROCESSING OF CLEARANCE SIGNALS

displacement measuring unit to operate at the much higher frequency of 125 kHz. It is expected that this will improve significantly the frequency response of the system and that in this way it will be possible to demodulate the signals electronically. This project has already been initiated and at the moment it is at the testing stage. Unfortunately it was not available when the tests described in this thesis were carried out, therefore all the results presented here were obtained by processing the output of the conventional displacement measuring unit (operating at 16 kHz) before it was fed to the demodulating circuit.

The first problem that was encountered with this set up was overloading. Whenever the distance between the test surface and the transducer exceeded a certain limit the amplifier overloaded and chopped off the peaks of the modulated carrier. This situation arose while the slipper pocket was above the transducer thus making the feedback reactance excessively high. When the feedback reactance came down to a reasonable level due to the passage of a slipper land over the transducer, the amplifier took some time to revert to its normal operating state thus introducing an unacceptable level of distortion to the output wave form.

This problem can be avoided by connecting a fixed capacitor ((7) in fig. 4.4) in parallel with the transducer so that the feedback reactance does not exceed the maximum allowable level at any time. Under such conditions relation 4.1 is modified to:-

$$V_o = \frac{K_1}{C_t + C_f} \qquad 4.3$$

where C_f is the capacitance of the fixed capacitor. By expressing C_t in terms of clearance, as before, and rearranging, relation 4.3 becomes:-

$$\frac{1}{V_o} = \frac{1}{V_m} + \frac{1}{K_2 (d + d_o)} \qquad 4.4$$

V_m is equal to the maximum output voltage which occurs when d tends to infinity (i.e. when there is no earthed surface within the range of the transducer). With this arrangement it is possible to select the fixed capacitor so that the amplifier does not overload even when the test surface is removed. The only disadvantage is that V_o is no longer linearly related to d.

4.3.1. Calibration of displacement transducers

Typical slipper clearances in axial piston pumps appear to be of the order of 1 μm. To measure film thickness of this magnitude requires not only a reliable measuring process but also an accurate calibration procedure.

Early attempts to calibrate included rectangular steel blocks about 30 mm long and 10 mm square as shown in the upper part of fig. 4.6. One of the long sides was ground within very close limits of flatness and surface finish. A grinding wheel 10 mm wide was then used to machine a recess across the block. A number of blocks were made in this way with the recess depth ranging from 5 μm to 50 μm. Each block was then placed in turn on the surface of the slipper plate with the recess directly above the transducer and the gap filled with oil. The output was measured on a digital volt meter connected to the output of the operational amplifier. The results obtained using this

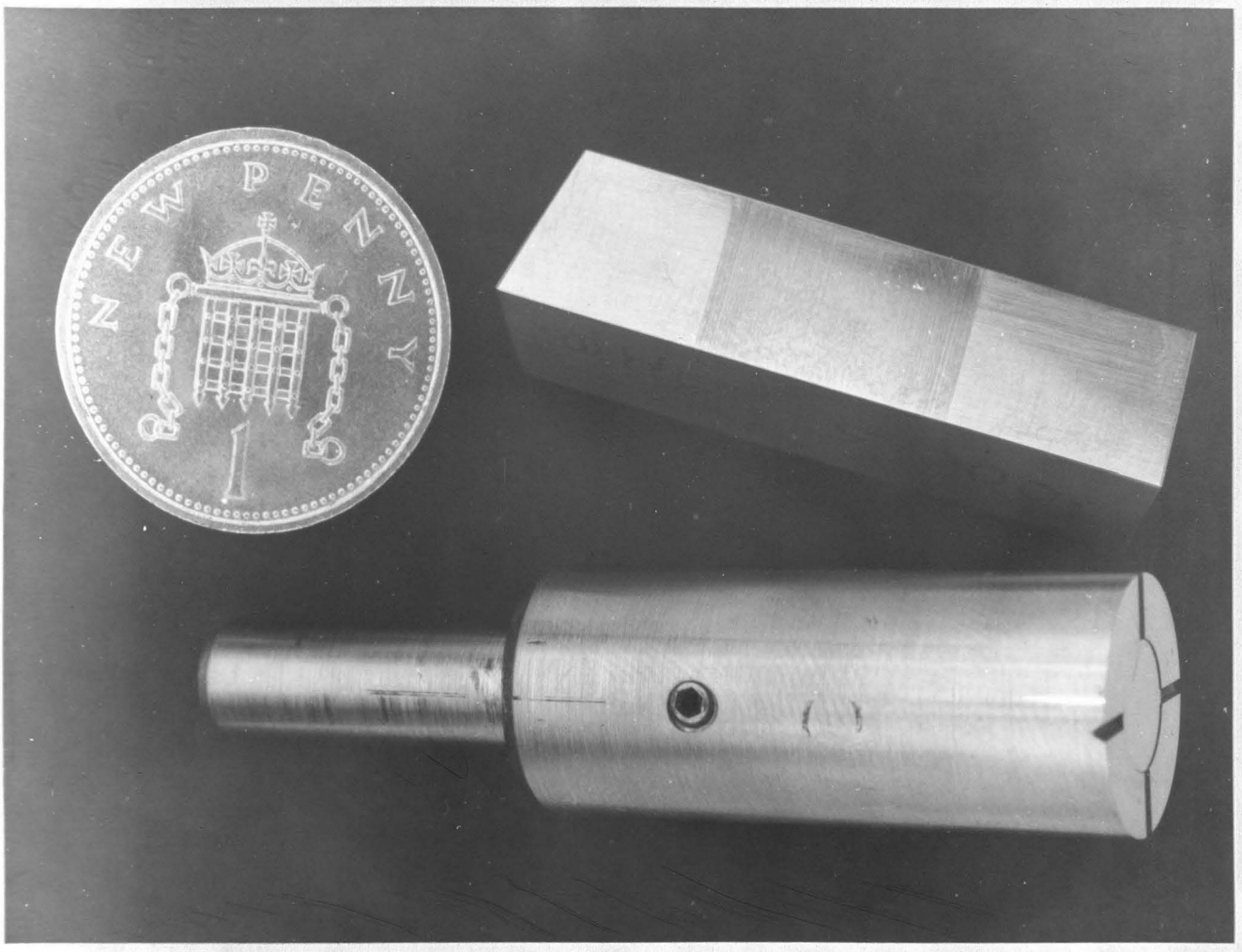

CALIBRATION BLOCKS FOR DISPLACEMENT TRANSDUCERS

FIGURE 4.6

method were unsatisfactory for a number of reasons:-

Firstly, due to their long span the blocks tended to rest on 'hills' of the surface of the slipper plate thus increasing considerably the gap between the transducer and the recess of the block. Moreover, the apparent gap changed with a slight shift of the block as a result of the plate's unevenness.

Secondly, it was difficult to exclude all the oil out of the contact area between the two surfaces. Thus, there was always an error due to the blocks' floating on trapped oil.

Thirdly, the recess showed all the imperfections of the profile of the grinding wheel during manufacture. This made the apparent gap over the transducer vary with the position of the block.

A number of modifications to this technique were investigated and the method described below was adopted.

A new set of calibration blocks such as the one shown in the lower part of fig. 4.6 were made. These blocks consisted of a hollow cylinder 30 mm long, 13 mm outside diameter and 6 mm inside diameter. A tight fitting pin was then pushed inside and the two parts were hardened and lapped at one end to a flatness of well below 0.5 micron CLA. The pin was then recessed slightly, without being turned, and then slowly pushed up by a screw adjustment while its depth below the outer cylinder was continually monitored by a Talylin. When the required depth was reached the pin was clamped in position by a grub screw. A final Talylin trace was then taken and was used to calculate the

recess depth at the centre of the pin. In this way any slight tilting effects (rarely more than 0.5 micron) of the pin in relation to the outer cylinder were accounted for and eliminated. Talylin traces of a typical block before and after it was calibrated are shown in fig. 4.7. Ten calibration blocks were made in this way with the pin depth ranging from one to fifty micron.

Due to the relatively small outside diameter of these blocks, calibration is now considerably less affected by the surface roughness of the slipper plate. Also the problem of trapped oil is overcome by machining four small slots on the outer part of the block. During the calibration process, a small perspex plate with a 14 mm hole is secured on the slipper plate with the hole concentric with the transducer. This is then filled with oil and a calibration block is placed in the hole and pressed against the slipper plate. Any trapped oil between the outer part of the block and the slipper plate can be easily expelled by rotating the block until metal to metal contact is positively achieved. It was found helpful in this calibration process to use a lower viscosity oil with the same dielectric constant where one was available.

With the area of interest being in the region around 1 μm it is important that this area is reliably calibrated. This proved to be particularly difficult due to instability in the operational amplifier caused by excessively small feedback reactance. The simplest way to overcome this was to recess the transducers slighlty below the surface of the slipper plate (typically 2-5 μm) thus increasing d_o. This

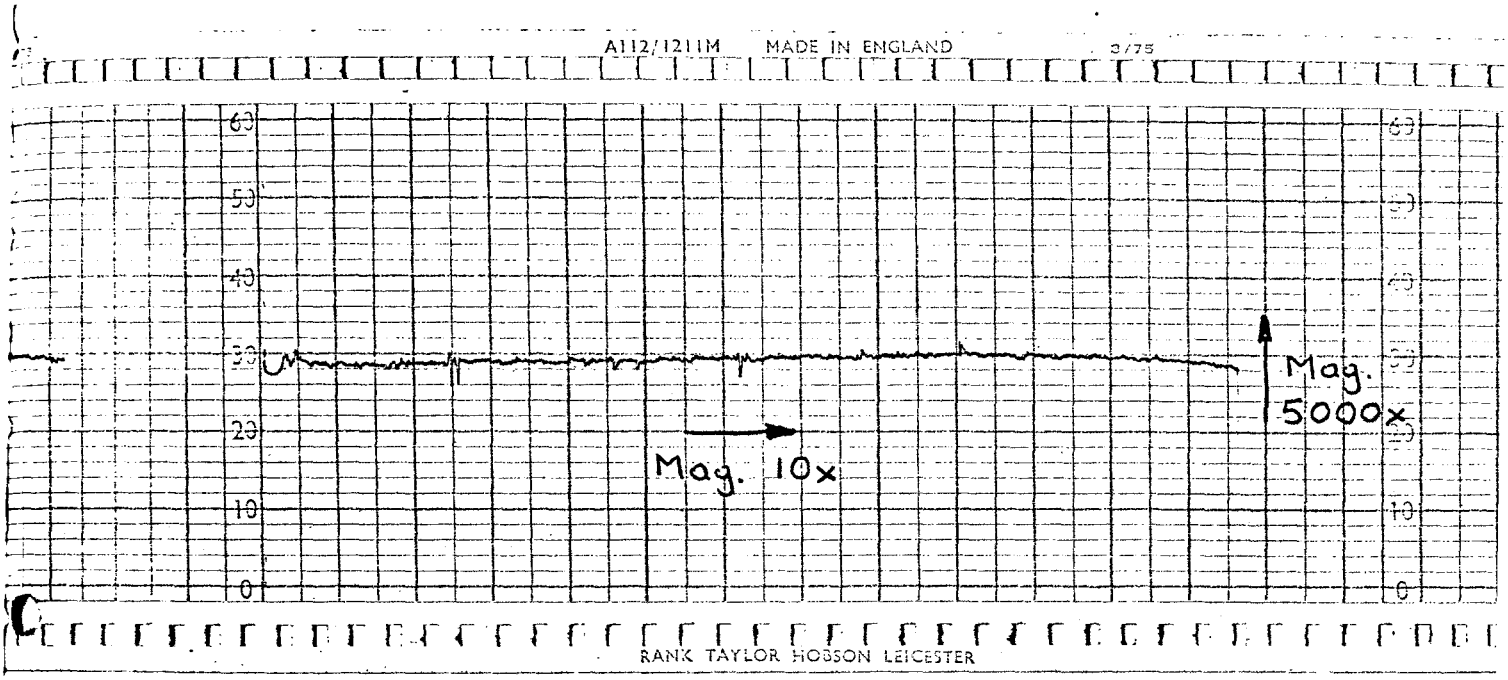

(a) Before Setting

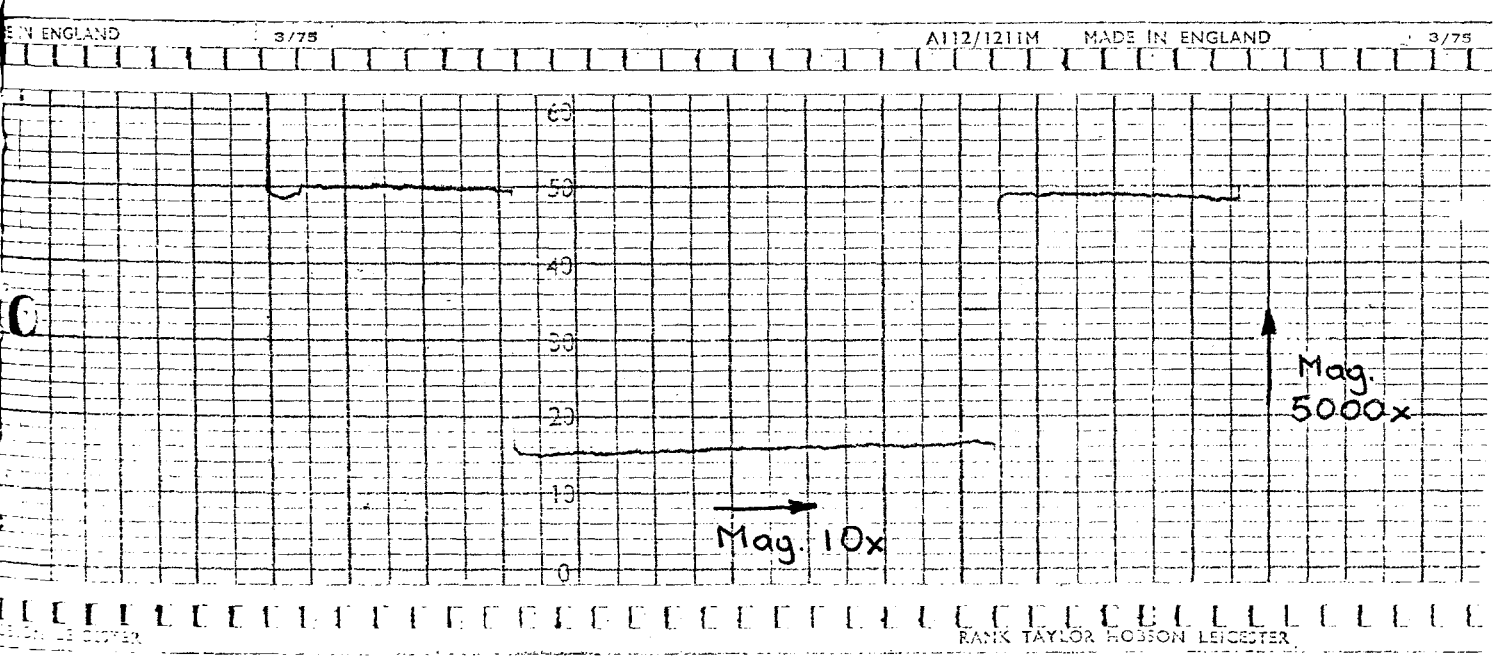

(b) After Setting

TALYLIN TRACES OF A CALIBRATION BLOCK FOR DISPLACEMENT TRANSDUCERS.

FIG. 4.7

was done by turning a thin, flat ended rod with diamond paste at one end against the transducer for a few minutes.

A further problem is presented by the fixed capacitor which alters the relationship between V_o and d to non-linear. It is possible, however, to linearise the relationship by modifying relation 4.4 and thus to obtain the best straight line fit through the calibration points. By rearranging equation 4.4 and introducing Z which is defined as:-

$$Z = \frac{V_m V_o}{V_m - V_o} \qquad 4.5$$

the relationship can be rewritten as:-

$$Z = K_2 (d + d_o) \qquad 4.6$$

A typical calibration plot of Z against d is shown in fig. 4.8. The standard deviation of the points from the best straight line is typically of the order of 0.5 μm.

Fig. 4.8 also shows the relationship between V_o and d. The curve illustrates the tendency of V_o to V_m as d tends to infinity.

The advantages of using the linearised curve (Z against d) rather than V_o against d are:-

1. It is much easier and accurate to fit a straight line through a set of points rather than a curved one.
2. Conversion of recorded signals from the pump from voltage to clearance is considerably easier. The transducer can be completely described by the slope of the straight line (K_2) and the intercept on the d-axis (d_o).

3. An estimate of the offset of the transducer from the surface of the slipper plate can be obtained by referring to the intercept of the straight line with the d-axis.
4. The slope K_2 and offset d_o are independent of V_m. This means that V_m does not have to be set to the same value when calibrating and when taking results.

4.3.2. Data logging of slipper clearance signals

With the transducers calibrated and installed in the slipper plate as described in the previous two sections, it is possible to measure the clearance of the slipper lands while the pump is running. This information is obtained from the output of the operational amplifier and it consists of the 16 kHz carrier waveform which is modulated according to the clearance of the slipper lands. A typical such signal is shown in fig. 4.5a.

Madera[23] recorded portplate clearance using a storage oscilloscope in conjunction with a camera. The accuracy of the results, however, was low and an alternative procedure was sought. Some preliminary results were obtained by recording the output signal on an S.E. Labs tape recorder and then playing it back to the ADC (Analogue to Digital Converter) of an IBM1130 computer system. Due to limitations in the sampling rate, the speed of the tape recorder was reduced to 1/16th of the recording speed; the signal was then sampled at the rate of 20 kHz and the peak to peak amplitude of the carrier was found using numerical techniques. This procedure was also found to be unsatisfactory mainly due to inaccuracies caused by the tape recorder.

More reliable and accurate results were obtained with a data logging system which is shown in schematic form in fig. 4.9. This enabled the results to be recorded on-line thus increasing considerably the accuracy of the recording process. The output signal from the displacement measuring equipment was fed to a 10 bit, 16 channel ADC which was controlled by a PDP11/10 processor. All the digitised data collected through the ADC was checked by displaying it on an oscilloscope and the operation could be repeated if it was found necessary. The relevant information was eventually transferred to a dual floppy disc system for storage and further processing. The instructions to the processor were issued from a visual display unit (VDU).

Due to limitations in the sampling speed of the ADC (35 kHz maximum) and computer memory (12K words) it was necessary to use an efficient data logging method. For this reason the carrier was sampled at the peaks (maxima and minima) thus automatically providing the peak to peak voltage in every period. This was done by tapping the input of the operational amplifier, which consisted of a steady 16 kHz waveform, and feeding it into a purpose built pulse generator; this produced a pulse whenever it detected zero slope at the input. The timing of the pulse could be adjusted so that its trailing edge coincided with the next peak of the signal as shown in fig. 4.10. This was fed to the 'external clock input' of the ADC so that sampling was taking place at the rate of 32 kHz (twice in every period of the carrier) and only the peaks were measured. Thus in a sampling operation involving 4000 points, two complete

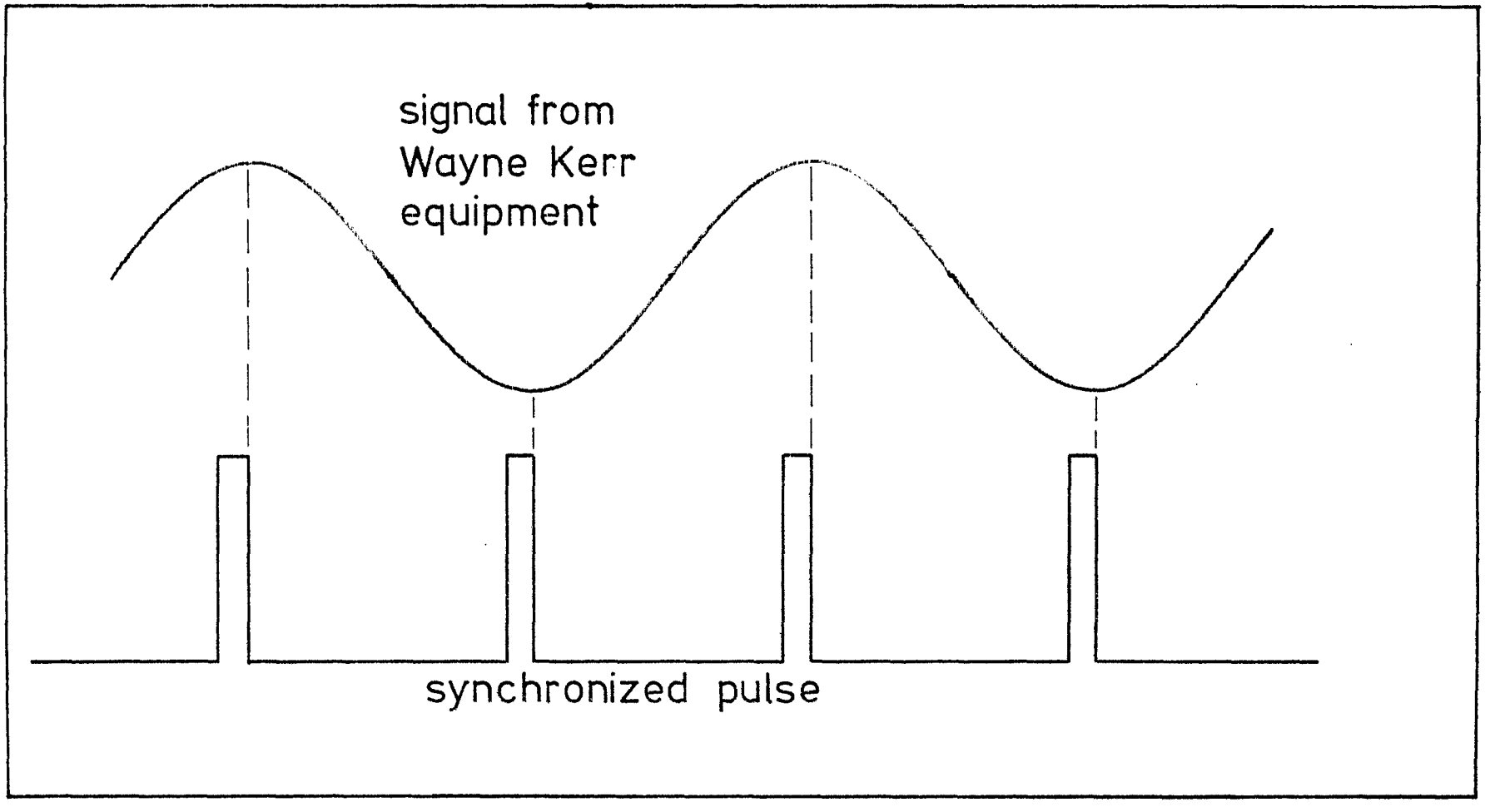

FIG. 4.10 TRIGGERING OF CLEARANCE SIGNALS

revolutions could be recorded at a pump speed of 1000 rev/min.

Finally, in order to be able to identify individual slippers it was necessary to start the sampling operation always at the same point with reference to shaft position. This was achieved by placing a magnetic pick-up close to the pump shaft which produced one pulse in every revolution of the pump. This pulse was connected to another channel of the ADC and was used to initiate the sampling of the signals from the displacement measuring unit.

4.3.3. Processing of slipper clearance signals

Data processing involves calibration of the stored signals and plotting the clearance d against time. In order to do this it is necessary to follow the reverse procedure to the one described in section 3.

Firstly the signal is read from the discs and stored in an array in the memory of the processor. This signal consists of alternate maxima and minima and it must be converted to a demodulated form. This is done by subtracting each successive pair of values, in the appropriate order, and overwriting the original stored value with the result. A demodulated trace of the signal in fig. 4.5a is shown below in fig. 4.5b. The next stage is to convert all points to R.M.S. voltage by multiplying them with the appropriate factor. This factor is obtained immediately before each test by comparing the R.M.S. voltage of a steady signal as measured by the digital voltmeter, with the peak to peak voltage as measured by the data logging system. This eliminates any errors that might be introduced by:-

1. Possible phase shifts between the trigger pulses, which are produced by the pulse generator, and the carrier.
2. Possible discrepancies between the digital volt meter, which was used during calibration, and the ADC.

Knowing V_m which is the maximum amplitude of the carrier and can be found by referring to any section of the signal which is not modulated it is possible to calibrate the trace in terms of clearance d using:-

$$d = \frac{Z}{K_2} - d_o \qquad 4.7$$

which is the same as relation 4.6 but rearranged.

The trace in fig. 4.5a is shown fully calibrated in fig. 4.5c. The passage of each land is represented by a peak pointing downwards and the clearance is equal to the distance of the relevant peak from the time axis.

4.4. Pressure measuring equipment

For the measurement of slipper pool pressure a miniature pressure transducer was purpose developed and installed as shown in fig. 4.11. Two 120 Ohm strain gauges were attached to the cylindrical stem which had a 0.6 mm hole drilled halfway down its axis. The active gauge (1) measured the hoop strain and thus pressure inside the hole while the dummy gauge (2) was used for temperature compensation. One end of the active gauge was connected to one end of the dummy gauge. In this way there were only three electrical connections to be made to the transducer: The active, common and dummy.

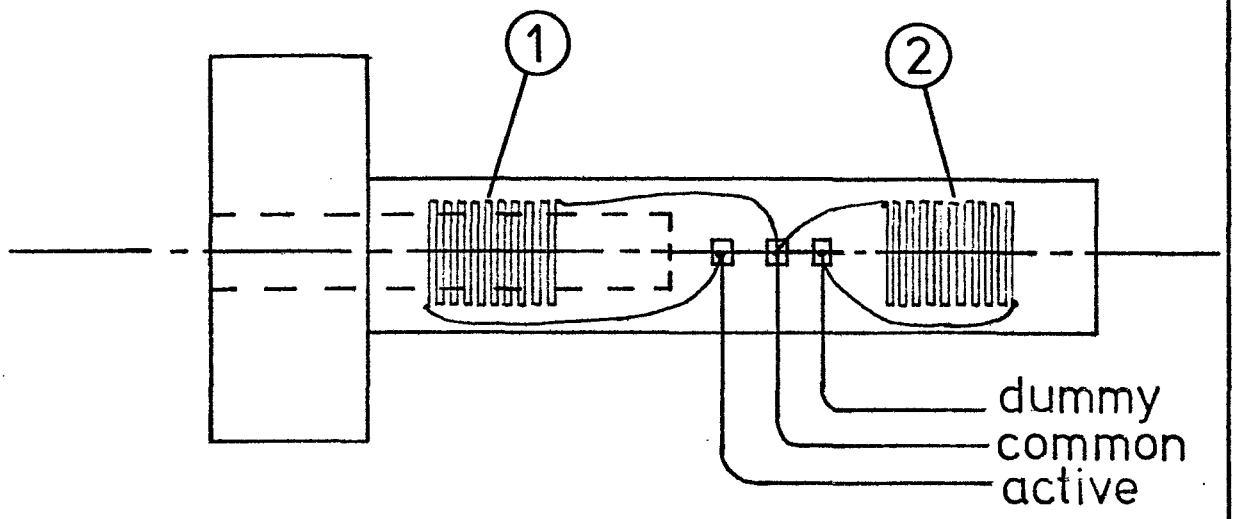

ARRANGEMENT OF STRAIN GAUGES ON
PRESSURE TRANSDUCER

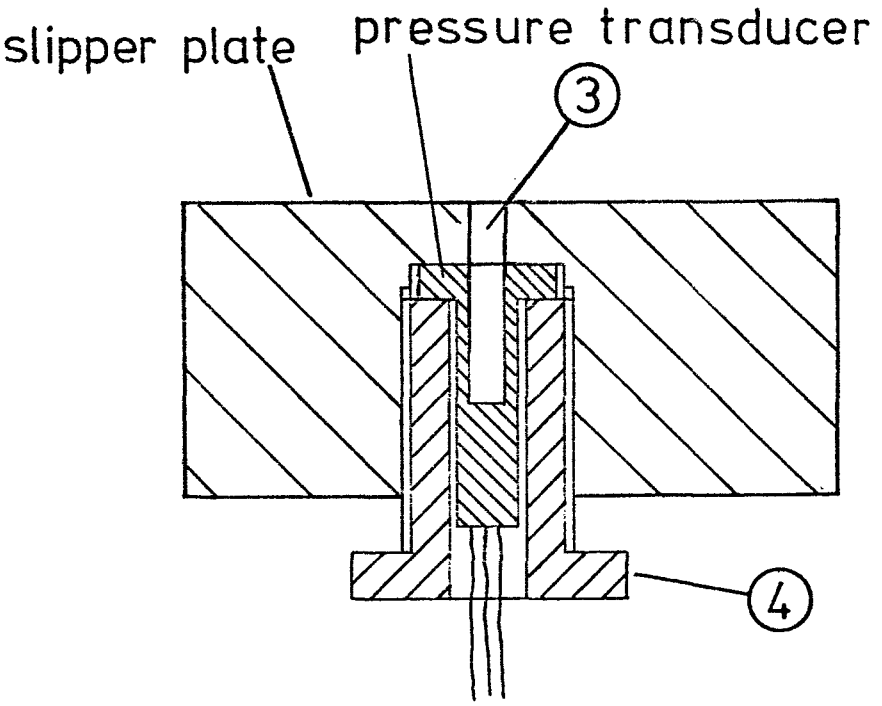

INSTALLATION OF PRESSURE TRANSDUCER

FIGURE 4.11

A 0.6 mm hole (3) was then drilled in the slipper plate and the transducer was inserted in a recess at the back face. It was held there by a retaining nut (4) so that the hydraulic oil could penetrate into the transducer cavity but it could not escape through to the back face of the slipper plate.

The wires from the transducer were then connected to a simple Wheatstone bridge circuit the output of which was fed to a Fylde D.C. Amplifier with the gain set at 5000.

As far as calibration is concerned, the transducer was connected to a dead weight tester. The voltage output of the Fylde amplifier was measured before and after the transducer was pressurised to allow for drift. The difference was then plotted against pressure and a linear relationship was obtained as shown in fig. 4.12. The standard deviation in calibrating was typically of the order of 0.84 bar. Despite the temperature compensation it was found that the output increases by approximately 0.02% per ^{o}C.

Results were obtained by feeding the output signal to the A.D.C. of the PDP11/10 computer system. The incoming signal was sampled every 60 micro seconds (approximately 17 kHz) and stored. Subsequently, the digitised signals were calibrated and plotted on the X-Y plotter.

A number of attempts were also made to record piston pressure and compare it to the slipper pool pressure as measured by the strain gauge transducer. In some of the early tests a Kulite semiconductor type pressure transducer was attached to one of the piston bores. All connecting wires were taken along the centre of the cylinder block and

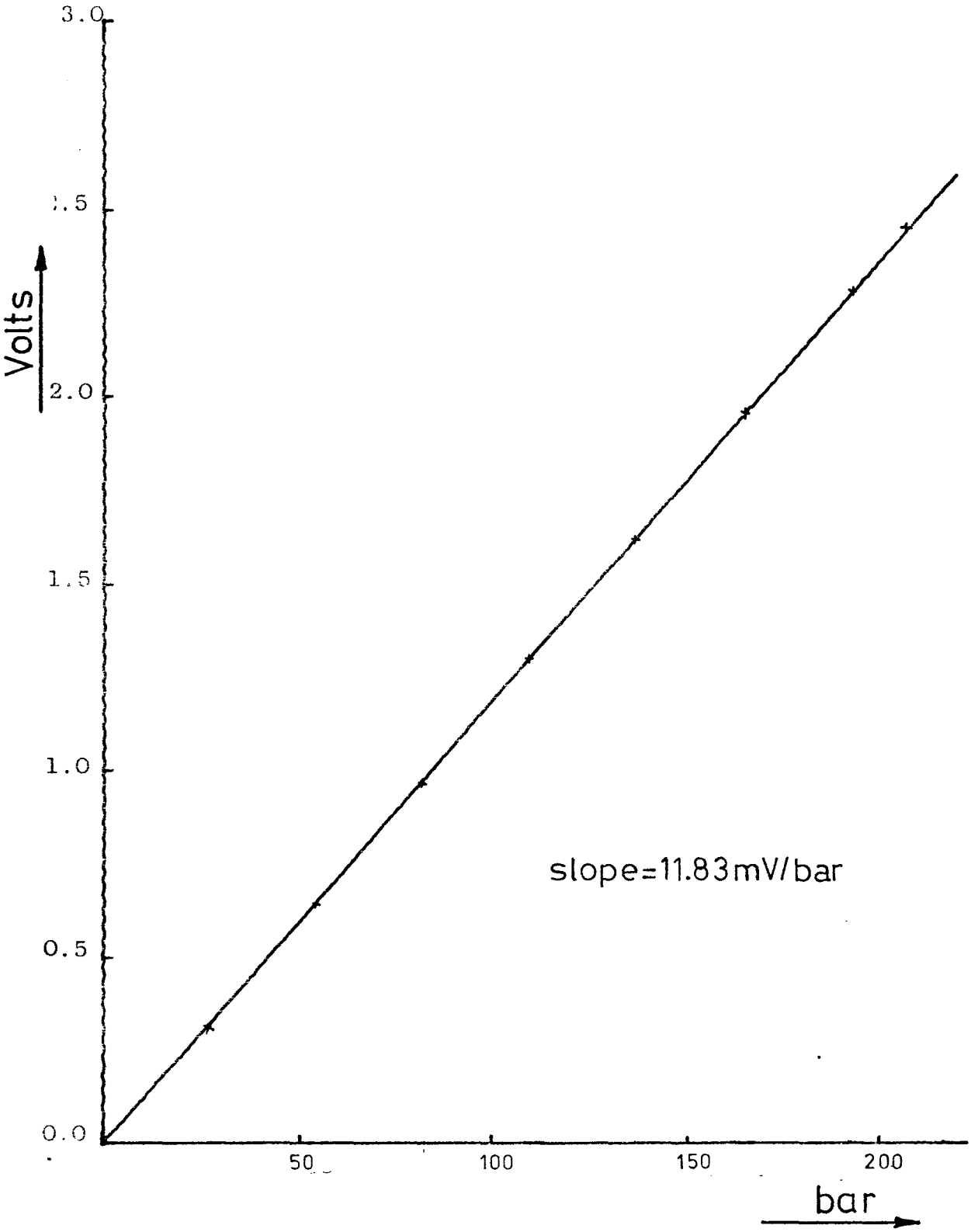

CALIBRATION CURVE FOR PRESSURE TRANSDUCER

FIGURE 4.12

from there to the rest of the instrumentation. The signal was then sampled by the ADC, as for slipper pocket pressure, every 60 micro seconds, stored and later calibrated and plotted. One aspect which was not satisfactory with this measuring method was the difficulty of accounting and eliminating any possible drift of the output level. This inadequacy of the instrumentation meant that it was not possible to measure the pressure difference across the orifice of the piston.

5. EXPERIMENTAL RESULTS

5.1. Introduction

The results described and discussed in this chapter consist of measurements of slipper clearance and slipper pocket pressure. These results were obtained on line from two typical axial piston pumps running under typical operating conditions. The two units used in the tests were a Hastie 330 ml/rev (20 in^3/rev) variable displacement pump which was supplied by the National Engineering Laboratory and a 92 ml/rev (5.6 in^3/rev) fixed displacement pump which was supplied by Commercial Hydraulics Ltd. All the tests with the Hastie pump were carried out at the Special Projects Division of the N.E.L. at East Kilbride whereas the tests with the C.H.L. pump were carried out at the Department of Mechanical Engineering of the University of Birmingham.

The slippers of the two pumps are designed to operate on the same principles, however, there are four notable differences between them:-

1. The piston and slipper (and radii of the Hastie unit are 1½ times bigger than the corresponding C.H.L. ones. Also the pitch circle diameter is twice as big in the Hastie pump.
2. The overclamp ratio of the C.H.L. piston/slipper is larger by 1.8%.
3. The spring load in the C.H.L. pump is exerted through the swivel plate as shown in fig. 1.2 whereas the Hastie pistons are subjected to the load of individual springs in the bores.

4. The ball joint of the C.H.L. pistons is as shown in fig. 1.2 whereas in the Hastie pump it is the other way round with the ball end on the slipper.

As far as operating conditions are concerned the following range was examined:-

a) Speed was varied between 500 and 1750 rev/min. Although both pumps can run at higher speeds the above range was not exceeded during the tests due to limitations in the maximum speed of the driving motors.

b) The swashplate angle was fixed in the C.H.L. pump at approximately 15^{o}. However, some results at different swashplate angles were obtained with the Hastie pump.

c) Delivery pressure was varied between 7 bar and 210 bar. The reason for limiting pressure to this relatively small range was purely practical. It was found that when the pumps were run at pressures exceeding the above range, the adhesive holding the displacement transducers on the slipper plate began to yield as a result of which the transducers extruded out of the plate. This invariably produced a considerable amount of damage to the running gear and therefore high pressures were carefully avoided.

d) Temperature was generally kept at $50^{o}C$ at the inlet of the pump although in some tests the inlet temperature was varied between $30^{o}C$ and $70^{o}C$. Higher temperatures were not attempted because it

was found that the yielding point of the adhesive is lowered considerably at temperatures above 70°C.

e) Boost pressure was also kept constant during the majority of the tests (7 bar and 14 bar for the C.H.L. and Hastie pumps respectively). In some tests, however, the effect of pressure at the inlet was investigated by varying the boost pressure up to 35 bar.

The first successful set of results was obtained from the Hastie pump and the object was to investigate the repeatability of slipper behaviour as well as the effect of speed, pressure and swashplate angle. The results from each test were stored in individual files on floppy discs bearing the code name "NEL" and the number of the test (files NEL1 to NEL32).

The same set of tests was repeated on the C.H.L. pump. In addition to the above parameters these tests included investigation of the effect of boost pressure in the L.P. region and the effect of temperature in general (files COM1 to COM66).

The effect of the position of the centre of gravity was investigated in another series of tests using 3 different versions of Hastie slippers. The results were stored in files CG1 to CG86.

A final set of tests was carried out on the C.H.L. pump with the object of examining the effect of orifice size on slipper behaviour. Results were obtained with three different orifice sizes and they were stored in files OR1 to OR41.

It is not possible to include the results of all the above 225 tests due to shortage of space. Enough results are included, however, in order to demonstrate the trends which have been observed.

5.2. Slipper clearance measurements

The arrangement of the instrumentation was practically the same in all the tests.

In the measurement of slipper clearance the instrumentation consisted of a cluster of 4 displacement transducers, of the type described in section 4.3, which were inserted in the slipper plate as shown in fig. 5.1. The cluster was installed in the middle of the high pressure region because it was thought that conditions at that point were nearest to steady state thus maximising the possibility of correlating theory and experiment. Measurements of slipper clearance under low (inlet) pressure conditions could easily be obtained with the same instrumentation by reversing the rotation and connections to the pump.

The arrangement of the individual transducers on the slipper plate is shown in fig. 5.2. This arrangement was chosen in order to be able to measure the clearance of the inner land of the slippers as they pass through the middle of the H.P. (high pressure) or L.P. (low pressure) region. In this manner, it is also possible to measure clearance as well as radial and tangential tilt. Unfortunately, it was not possible to have a consistent direction of rotation in all the tests for practical reasons and both directions (clockwise and anticlockwise) were freely used according to

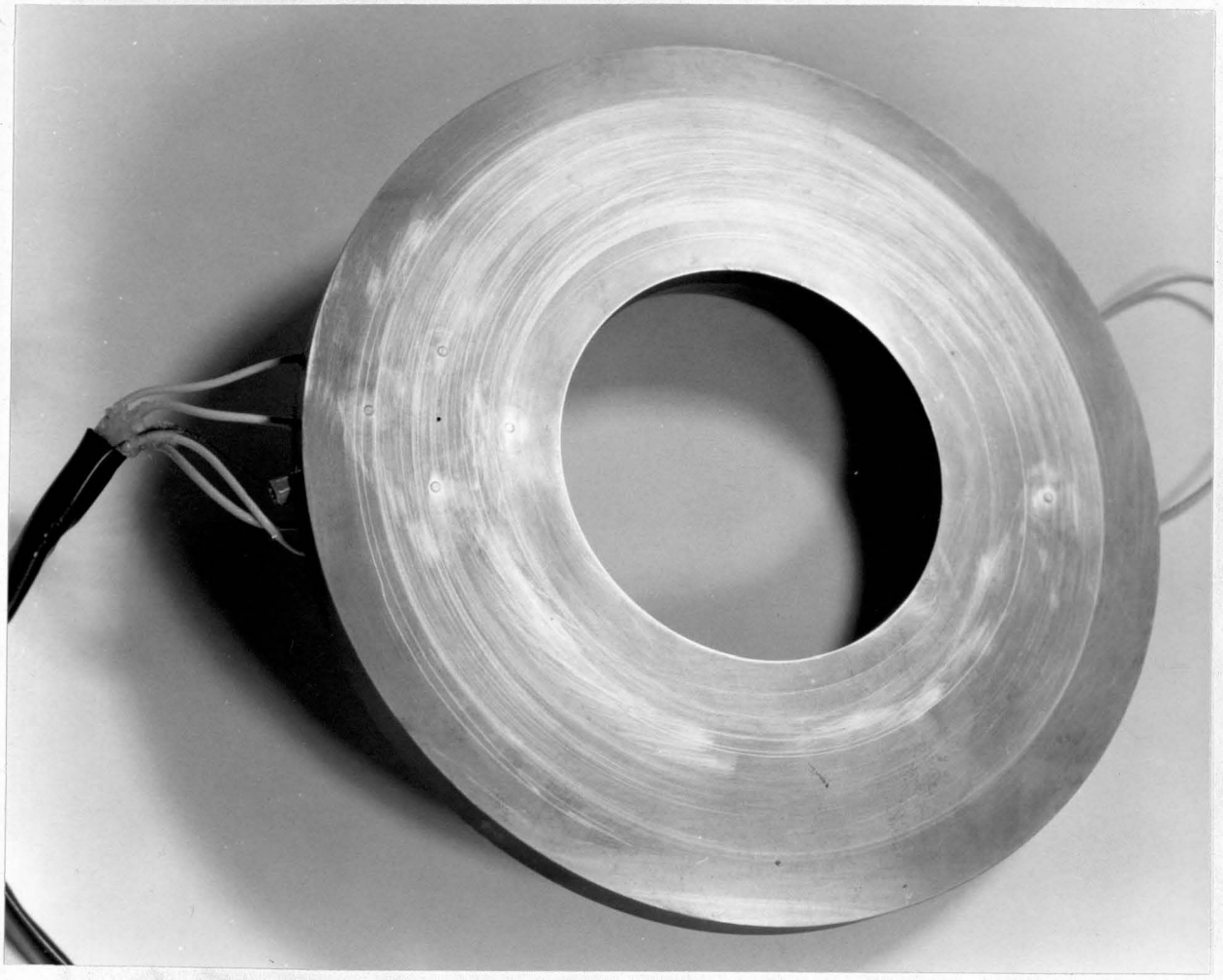

SLIPPER PLATE FOR HASTIE PUMP

FIGURE 5.1

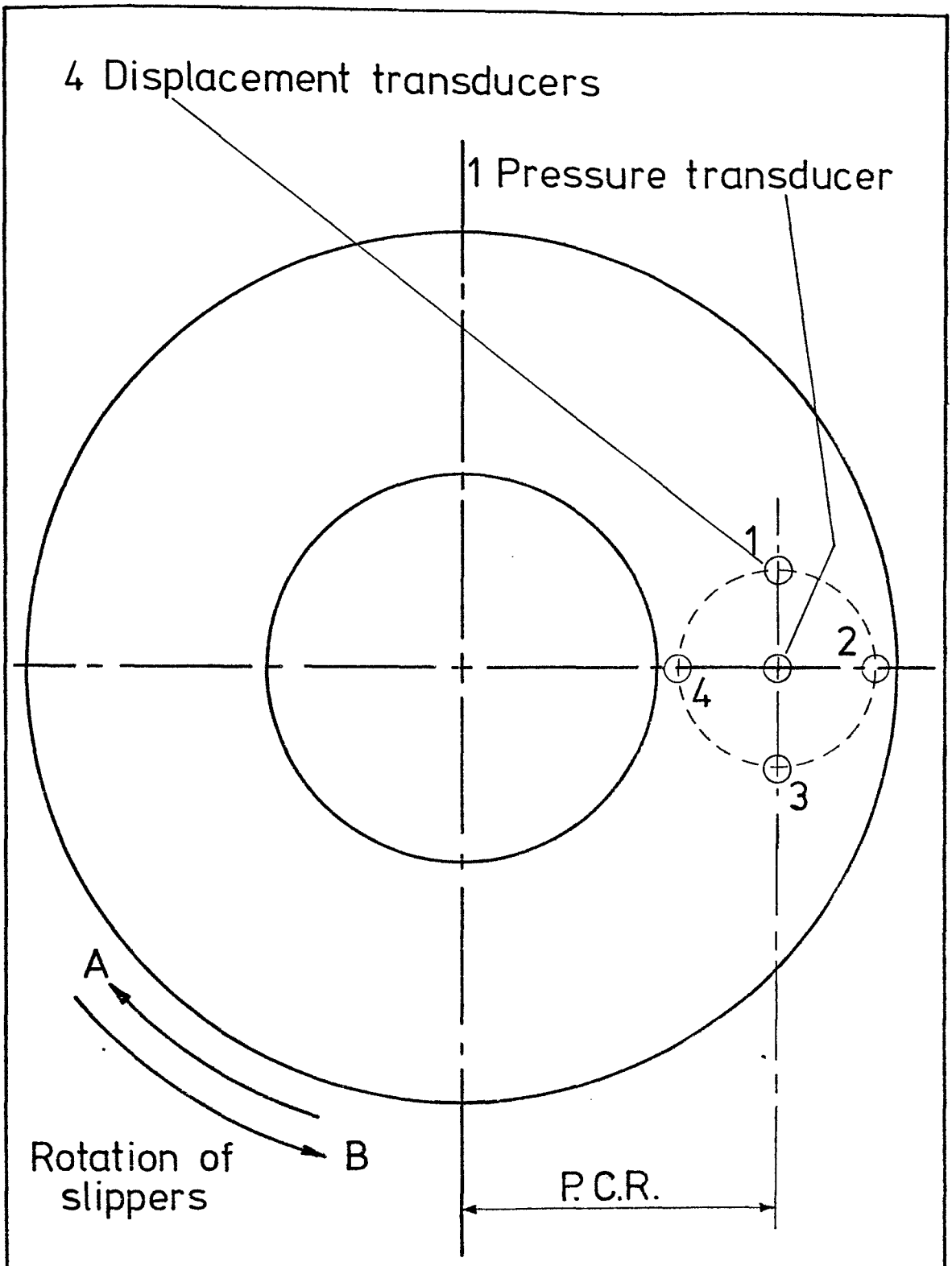

Instrumented Slipper Plate

FIGURE 5.2

the circumstances. However, all the results displayed in this chapter indicate the rotation of the slippers, viewed from the piston end, as A for clockwise and B for anti-clockwise. The two directions are also clearly shown in fig. 5.2.

Slipper clearance results are shown in figures 5.4 to 5.35. Each figure corresponds to one test and includes 4 traces corresponding to the 4 displacement transducers. Where no plot is given, the relevant transducer gave no usable result due to electrical contact with at least one slipper. This may be interpreted as corresponding to film thicknesses below 1 micron. Unless otherwise stated the scale used in all the plots is 0 to 16 microns in graduations of 2 microns.

In these plots, slipper lands are represented by peaks pointing downwards. Hence the clearance of each land is the distance of the peak from the x-axis. With transducers 1 and 3 the large gaps between peaks correspond to slipper pocket. On the other hand transducers 2 and 4 sense the passage of the inner and outer land only (see figure 5.3). The absence of an outer land suggests that the transducer sensed the groove on the outer land or that the film thickness was larger than 16 μm.

5.2.1. Triggering

The sampling of the signals from all the transducers was initiated by a pulse from a magnetic pick-up which was produced once in every pump revolution. With the exception of some of the early tests this mechanism appears to have worked satisfactorily.

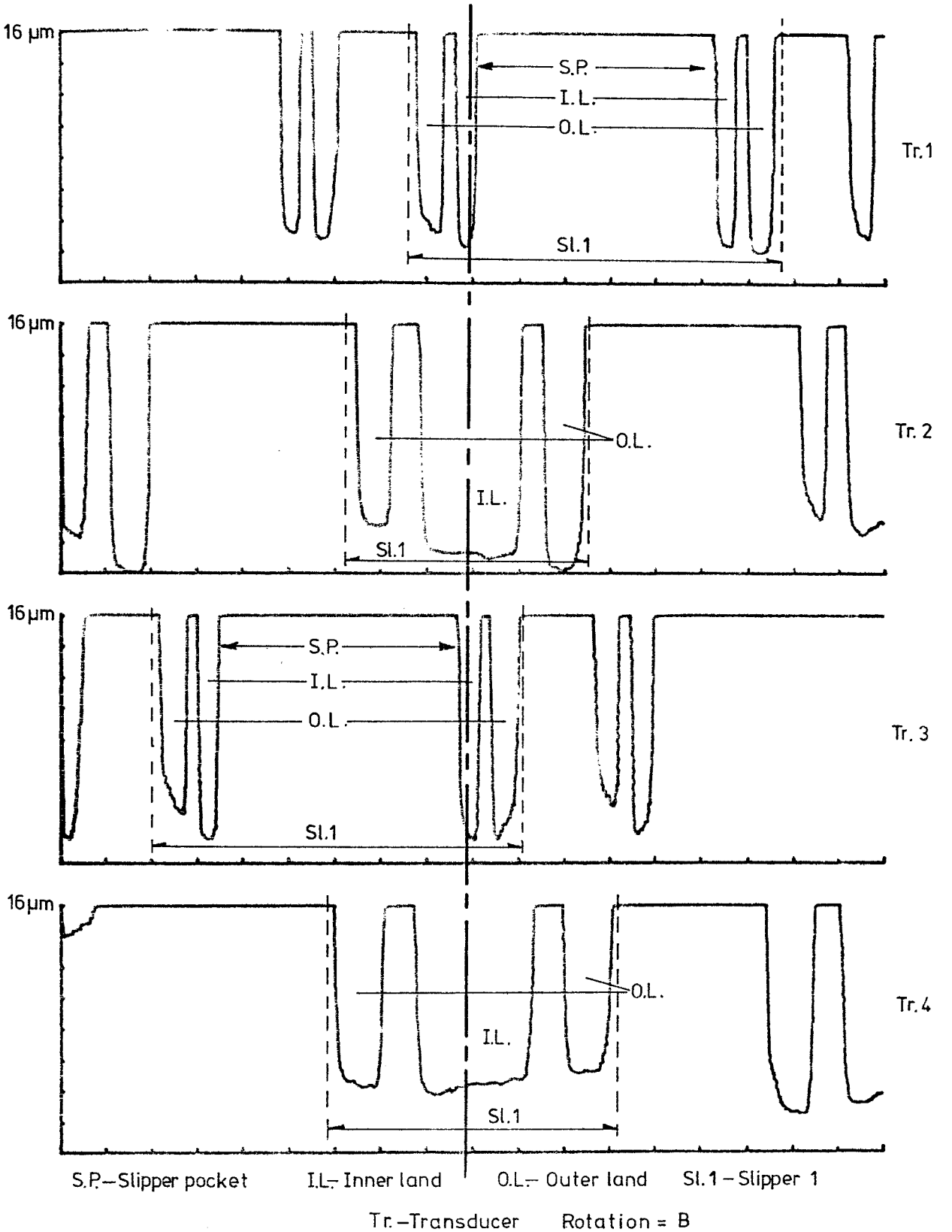

TIMING OF CLEARANCE RESULTS

FIGURE 5.3

The arrangement of the cluster was such that when a slipper was in the middle of the high pressure side, all four displacement transducers would be under the inner land (fig. 5.2).

Examination of most tests reveals that the leading end of an inner land recorded with transducer 1 ties well with the trailing end of the inner land on transducer 3. These also tie with the inner land recorded with transducers 2 and 4. This is demonstrated in fig. 5.3 where the dotted line through the inner land sensed by transducers 2 and 4 also passes through the inner land sensed by transducers 1 and 3. This pattern would be reversed if the rotation was in the "A" direction. In this case the trailing end on transducer 1 would tie with the leading end of the inner land on transducer 3. The timing of transducers 2 and 4 should not be affected.

Where the triggering is successful it is possible to identify individual slippers and correlate their clearance as it was measured by different transducers.

5.2.2. Repeatability and consistency of results

One of the first observations that may be made concerns the considerable variation in the behaviour of different slippers even within the same revolution and this is a common feature of almost all the clearance results. One parameter which usually exhibits considerable variability is the radial tilt. For example, in fig. 5.4 slipper 9 is heavily tilted outwards whereas slipper 2 appears to be running flat. Also in fig. 5.6 slipper 3 is tilted outwards whereas slipper 8 is tilted inwards.

Circumferential tilt can also vary from slipper to slipper, within the same revolution, but certainly not as much as radial tilt. Most slippers in fig. 5.4, 5.5 and 5.6 appear to be running fairly flat (i.e. the tilt in circumferential direction as measured by transducers 1 and 3 is relatively small). There are, nonetheless, some notable exceptions. Slipper 7, for instance, on transducer 3, fig. 5.4 appears to be tilted backwards whereas slipper 5, in the same trace, is tilted forward. This tilt, however, is of the order of 2 micron across the slipper pocket.

More important, however, is the repeatability of the behaviour of individual slippers not only from revolution to revolution but also from day to day. Figures 5.4, 5.5 and 5.6 include the results of two consecutive revolutions and they were taken with the same set of slippers under identical operating conditions. The timing of these tests was as follows: Test NEL7 was taken a few hours after NEL1, and NEL20 was taken 2 days after NEL7.

The repeatability of the results obtained with transducers 2 and 4 in successive revolutions was excellent and it was typically within 1 micron. The repeatability of these transducers was also very good from test to test as shown by slipper 7 on transducer 4 in fig. 5.4, 5.5 and 5.6. There are, however, some exceptions for instance slipper 9 is heavily tilted inwards in figures 5.4 and 5.5 but the radial tilt is reduced in fig. 5.6. Clearly the repeatability appears to deteriorate with time.

As far as circumferential tilt is concerned, good repeatability was observed from revolution to revolution

(as shown by slipper 7 in fig. 5.4, transducer 1) but it was generally not as good as the repeatability of the radial tilt. The repeatability of the circumferential tilt from test to test was also generally inferior to radial tilt (compare slipper 6, transducer 3 on fig. 5.4 and 5.5; also slipper 9, transducer 1 on fig. 5.5 and 5.6).

One important fact is that repeatability is very good within the short period (approximately 2 minutes) that it normally takes to collect the data from all 4 displacement transducers. If this was not so, i.e. if behaviour was changing considerably with time, correlating traces obtained from different transducers would be meaningless.

The consistency of the results also provides some evidence to support the reliability of the measuring method.

The reliability of the results is further supported by the fact that the clearance of any slipper as measured by different transducers is compatible with the flatness specification of the slippers. For example slipper 7 on fig. 5.4 has a small clearance on the inside and a large one on the outside of its path. On the contrary slipper 5 appears to touch down on the outside and has a relatively large clearance on the inside. The flatness test can be applied to any slipper by taking the average of the clearances on transducers 2 and 4 and comparing it to the average of the clearances measured by transducers 1 and 3. The difference between the two averages rarely exceeds 2 microns.

One important aspect of the circumferential tilt comes from correlating the clearance of particular slippers as it was measured by transducers 1 and 3. Considerable

differences can be observed with most slippers. For example in fig. 5.4 slipper 4 appears to be tilted forward in transducer 1 whereas in transducer 3 it is tilted backwards. Also slipper 9 in transducer 1 of the same fig. has a much larger clearance than in transducer 3. This suggests that dynamic effects must alter the attitude of the slippers while they travel from one transducer to the other. One reason for this could be the inertia force of the piston which is in opposite directions at the two transducers.

A more reliable estimate of circumferential tilt can be obtained by referring to the clearance of the leading edge of the inner land measured by transducer 1 and the clearance of the trailing edge of the same land on transducer 3. One way of doing this is by drawing a straight line through the middle of the inner land of a particular slipper on the traces obtained from transducers 2 and 4 (as in fig. 5.3). Careful examination of the slippers in fig. 5.4 reveals that with the exception of slipper 2 all the others are running flat or tilted backwards (trailing end down). The same trend is also present in fig. 5.6. The magnitude of this tilt is between 0-2 micron across the slipper pocket. Although this attitude appears to be consistent at this operating condition, it is dangerous to consider it as a genuine trend simply because its magnitude is so small. (The accuracy of each measurement is of the order of ± 1 micron and the repeatability of clearance on these transducers is also of the same order of magnitude).

On the other hand, radial tilts tend to be much larger and therefore the trends related to them much clearer.

For this reason, the following sections which deal with the effect of various operating parameters, tend to concentrate a lot more or radial rather than circumferential tilt.

The above observations can be summarised as follows:-

1. Repeatability: The behaviour of particular slippers is largely repeatable under the same conditions.
2. Variability: There can be large differences between slippers even under the same conditions.
3. Tilt: Circumferential tilts are generally small. Radial tilts can be much larger and they are more repeatable.

So far this section has concentrated on analysing the results and little has been said about possible explanations.

As far as repeatability is concerned there is no reason why slipper behaviour should not be so if the operating conditions remain the same and slipper geometry does not change from run to run. One parameter which is found to be very repeatable is the radial tilt. As will be shown in the following sections this is largely dictated by the operating conditions and in particular speed and the combined effect of viscous drag, friction in the ball joint and pressure. The radial tilt will, therefore be repeatable, if these conditions are kept constant.

The same argument can also be applied in explaining the variability of behaviour between slippers. If pressure, speed, viscous drag and ball friction dictate radial tilt it is logical that variation in these parameters would result in variation of the radial tilt. The fact that slippers can

be subjected to the same running conditions, i.e. speed and pressure and still behave differently indicates that ball friction and viscous drag play an important role in determining radial tilt. Practical experience also shows that markings on slipper plates are much more random when a unit is first run. This is clearly related to ball friction which is initially high and slipper behaviour is likely to be erratic while the two surfaces grind themselves to a smoother finish. It has also been shown that more uniform behaviour is obtained if all the working surfaces are stoned before assembly or if the unit has been running for some time.

The variation in circumferential tilt and clearances on transducers 1 and 3 which was found to occur even on successive revolutions can be explained by the rotation of the slippers. The fact that slippers turn about their axis can be seen by following the groove on the outer land of certain slippers. For example on fig. 5.4 transducer 1 senses all four lands of slipper 4 in the first revolution but only three in the second indicating that the groove had shifted. Further evidence about piston rotation is outlined in chapter 6. Having accepted that slippers turn about their axes, it is reasonable to expect slightly different clearances at each revolution as a result of variations in the non-flatness in the circumferential direction. Typical type of such variation is the saddle-shape profile shown in fig. 2.6. One interesting feature is that although the slippers can rotate and thus present varying types of non-flatness to the oil flow, this does

not seem to affect radial tilt.

5.2.3. Effect of Speed

The effect of speed was investigated on both the H.P. and L.P. regions in the Hastie pump at 500, 1000, 1500 and 1750 rev/min and in the C.H.L. pump at 500, 1000, 1500 rev/min over a range of pressures and temperatures.

The most obvious effect of speed appears to be on the radial tilt. Figs. 5.7, 5.8 and 5.9 show the clearance of the Hastie slippers at no-load conditions and speeds of 1750, 1000 and 500 rev/min respectively. At 1750 rev/min (fig. 5.7) all the slippers appear to be heavily tilted outwards with very small clearance at transducer 4. The radial tilt is reduced considerably at 1000 rev/min (fig. 5.8) and at 500 rev/min it is reduced even further to the extent that all slippers are tilted inwards. The tendency to tilt outwards with increasing speed is also present in the L.P. region. At 500 rev/min (fig. 5.11) all slippers are tilted outwards. However, at 1500 rev/min (fig. 5.10) the radial tilt is so large that transducer 4 shorts due to extremely small clearances and transducer 2 produces clearances in excess of 50 microns. One important difference between the L.P. and H.P. region is that the radial tilts in the L.P. are generally much higher. This is partly due to the effect of pressure and it is discussed in the following section.

This pattern clearly indicates that speed tends to tilt the slippers outwards by reducing the clearance at the inside of the slipper path. This is believed to be a direct result of the centrifugal force which acts at the

centre of gravity of the slipper thus producing a couple about the ball joint which tends to rotate the slipper outwards.

The same pattern was noted on the L.P. side of the C.H.L. pump (figs. 5.12 and 5.13) but it was not so clear on the H.P. side (figs. 5.14 and 5.15) where an increase of speed from 500 to 1500 rev/min did not seem to make much difference. This apparent peculiarity is believed to be a result of the small P.C.R. and also the reduced size of the C.H.L. slippers. The effect of speed in the H.P. region of the C.H.L. pump, although present, it is believed to be overshadowed by the effect of pressure as discussed in the following section.

The mechanism on a complete slipper track is demonstrated on fig. 5.24a. The direction of the couple due to speed coincides with the direction of motion of the slipper. Under the influence of this couple the slipper tends to tilt so as to produce minimum clearance on the inside of the slipper path as indicated by the solid line.

Correlation between results obtained with transducers 1 and 3 shows a small backward tilt of about 2 micron across the slipper pocket in the H.P. region. Results from the L.P. region showed that the majority of slippers were running very flat. These trends were found in both the Hastie and C.H.L. pumps.

5.2.4. Effect of pressure

The effect of pressure was also investigated on both the H.P. and L.P. regions of the Hastie and C.H.L. pumps at pressures up to 210 bar. The units were not tested at

higher pressures, because that resulted in serious damage to the instrumentation.

One effect of pressure appears to be the tendency to decrease clearance generally. But even more pronounced is its effect on radial tilt. Comparing figs. 5.14 and 5.16 which were obtained at the same speed (1500 rev/min) but different pressures (no load and 105 bar respectively) it can be seen that increasing the pressure tends to tilt the slipper inwards in the H.P. region. The negative clearances on fig. 5.16 are a result of noise in the instrumentation and they are within the limits of accuracy (± 1 micron). The same pattern was also observed at other speeds (fig. 5.15 and 5.17). In this case some of the slippers appear to lift slightly at transducer 4 as the pressure is increased from no-load to 70 bar (fig. 5.17). Results from the Hastie pump confirm this trend as shown on fig. 5.18 and 5.19. At no-load conditions (fig. 5.18) all the slippers appear to be running fairly flat. When the pressure is increased to 140 bar (fig. 5.19), however, very small clearances occur at transducer 2, and transducer 4 produces considerably increased clearances indicating that the slippers are tilted inwards.

As far as the L.P. region is concerned, a similar but opposite pattern appears to be present. For example an increase in boost pressure from 21 to 35 bar (fig. 5.20 and 5.21) appears to increase the radial tilt outwards (increased clearance at transducer 2). This trend was also confirmed with results from the Hastie pump as shown in figs. 5.22 and 5.23.

The above evidence together with a substantial amount of practical evidence from polishing marks on slipper plates indicates that pressure acts in conjunction with friction in the ball joint and it gives rise to a couple of fixed direction with regards to the pump casing. In the case of a pump rotating clockwise, as shown in fig. 5.24b, the direction of this couple, is in the direction of B.D.C. to T.D.C. as shown. Under these circumstances, pressure tends to produce minimum clearance at the points on the solid line.

The generation of this couple can be explained in conjunction with ball friction. Although the slipper is quite free to move about the piston ball when outside the pump, it is likely that the piston/slipper assembly is converted to a more rigid configuration when loaded in view of the increased friction within the ball. When in normal operation, therefore, the piston is forced to rotate within the bore thus giving rise to a viscous drag tending to rotate the piston in the opposite direction i.e. the direction of rotation of the cylinder block. This drag can be represented by a vector pointing towards the slipper plate (fig. 5.25).

This vector can be resolved into components along and perpendicular to the slipper plate and it is believed that it is the vector along the plate (represented by C) which affects the radial tilt. The two diagrams in fig. 5.25 show how the direction of 'C' can be the same or opposite to the direction of motion depending on whether the slipper is in the L.P. or H.P. region. Another interesting

fact is that the direction of 'C' will be reversed when the unit is run as a motor instead of a pump.

Although C is not directly related to pressure, the influence of the latter on the radial tilt is explained by the fact that pressure is related to friction in the ball joint thus providing the means of transmitting the effect of 'C' to the slipper. If there was no friction in the joint, the radial tilt would be unaffected by pressure through this mechanism. In conclusion the radial tilt of the slipper is affected by speed and pressure as well as the friction coefficient of the ball joint and the viscous drag on the piston. The latter is examined individually in chapter 6.

A more realistic picture of slipper behaviour emerges when the effects of speed and pressure are considered together by superimposing fig. 5.24a and 5.24b.

Firstly in the middle of the L.P. region the two couples are additive and this generally results in high radial tilts outwards. On the other hand in the middle of H.P. the two couples oppose each other. Radial tilt at this point can occur in either direction depending on which couple is dominant. Further areas of interest are the transition regions. At T.D.C. the pressure couple acts so as to tilt the slippers forward. Obviously other effects particular to this area are also present but the effects of the pressure couple appear to dominate and the slippers are well known to enter H.P. 'nose down', sometimes with undesirable consequences.

The opposite happens at B.D.C. where the pressure couple tends to tilt slippers backwards. This usually results in rapid loss of pressure out of the slipper pocket and the slippers are forced down onto the slipper plate as soon as they enter the L.P. region. Evidence of this behaviour can be found on some slipper plates with crescent-type markings just after B.D.C.

5.2.5. Effect of Temperature

This was investigated by testing the C.H.L. pump at 30, 50 and 70°C inlet temperature over a range of speeds and pressures. The unit could run at higher temperatures; however, these were avoided because it was found that at temperatures above 70°C the yielding point of the adhesive was lowered and the transducers were likely to be extruded out of the slipper plate.

As far as its effect on clearance is concerned it was found that increasing temperature tends to reduce clearance at all four transducers. This is shown on fig. 5.26 and 5.27 where an increase of 20°C resulted in a considerable reduction of running clearances. The same pattern but not as clear is shown on fig. 5.28 and 5.29 which were taken with the pump loaded at 70 bar.

5.2.6. Effect of orifice size

The effect of enlarging the size of the orifice which connects the piston pressure to the slipper pocket was investigated using the C.H.L. pump. Results were obtained from both the L.P. and H.P. sides over a range of speeds and pressures with an orifice of 0.75 mm in diameter. The tests were then repeated twice more with the same set of

slippers but with the orifice diameter increased first to 1 mm and later to 1.5 mm. Throughout the tests, the temperature of the inlet stream was kept constant at 50°C.

Results obtained from the H.P. side of the pump indicate that increasing the orifice size makes negligible difference to the clearance of the slippers, at least in the middle of the H.P. region. This is shown on fig. 5.30 and 5.31 which were obtained with the diameter of the orifice equal to 0.75 mm and 1.5 mm respectively. The results obtained from the remainder of the tests confirmed that increasing the orifice did not change appreciably the behaviour of the slippers in the H.P. region. This led to the conclusion that the pressure difference across the orifice was very small in the region where the measurements were taken and the standard orifice of 0.75 mm did not present any significant obstruction to the oil flow, i.e. it was behaving as if it was effectively infinitely large. Under these circumstances a further increase in orifice size was bound to make no noticeable difference.

This evidence was applied in chapter 3 on Design Applications by assuming that the orifice coefficient Q_f was infinitely large. (Section 3.4).

Some small changes in behaviour were observed, however, in the L.P. region as shown in fig. 5.32 and 5.33. The changes are related to radial tilt which appeared to increase as the orifice was increased from 0.75 mm to 1.5 mm. This increase was also noted at other operating conditions.

This effect of the orifice size in the L.P. region has been attributed to the high radial tilts which are normally encountered in that area. As a result of the large tilt the leakage out of the slipper pocket is significant; this results in a pressure drop across the orifice and consequently the latter ceases to operate as if it was infinitely large. Clearly when the orifice diameter is increased, more oil is allowed to flow through it thus producing an increased pressure in the pocket which, in turn, results in an increased clearance.

This also illustrates the limitations of the assumption in chapter 3 and it indicates that the assumption that the orifice coefficient is infinitely large, is in error when the angle of tilt is large.

5.2.7. Effect of the position of the centre of gravity

This was investigated using the Hastie pump. The unit was first tested over a range of speeds and pressures using a standard set of slippers. The tests were then repeated with the slippers replaced by a set of more compact slippers in which the centre of gravity was nearer to the centre of the ball joint than in the standard set. Finally an even more compact set was used which was designed so that the centre of gravity of the slippers coincided with the centre of the ball joint. In this way there should be no centrifugal couple acting on the slippers while they were running.

The results have shown that the modified slippers tend to run flatter, on both the H.P. and L.P. sides. Fig. 5.34 and 5.35 show that the slippers with zero

centrifugal force run closer and flatter to the slipper plate than the standard ones which, at these conditions are normally tilted outwards. This is a result of the reduction of the centrifugal force and it confirms the interpretation given in section 5.2.3 that speed tends to tilt the slippers outwards by means of a centrifugal couple about the ball joint.

As far as the effects of pressure are concerned, they were found to be present in the same way as before. All three sets of slippers tended to tilt inwards at the H.P. region and outwards in the L.P. region as the pressure was increased.

5.2.8. Effect of running-in

The effect of the running-in procedure on the slippers was investigated using the C.H.L. pump and an unused set of slippers.

The standard running-in procedure was followed and results were obtained every hour. The only consistent trend found in these tests was that transducers 2 and 4 gave no meaningful results at all due to shorting with the slippers despite the fact that they had been recessed before the experiments. During these tests transducers 1 and 3 were functioning normally. When the running-in procedure was completed the slippers were tested again using the same instrumentation. Full results were then obtained at typical conditions from all four transducers and the trends described in the previous sections were detected.

The fact that transducers 2 and 4 were shorting during the running-in period suggests that the slippers were running in an irregular fashion as far as radial tilt is concerned. Instead of uniform trends normally observed with used slippers, these tests showed that some slippers were heavily tilted inwards whereas others were tilted outwards.

This behaviour is also interpreted as a result of ball friction. Despite the effort that goes into producing good surface finish of the spherical surfaces, ball friction is believed to be high with new slippers. The random radial tilts which occur during the running-in period are believed to be caused by slip-stick effects while the two surfaces settle to a smoother finish.

5.3. Measurement of Slipper Pressure

The pressure in the slipper pocket of the Hastie pump was measured using a strain gauge pressure transducer which was installed in the slipper plate as shown in fig. 5.2. The pressure in a piston was also measured using a Kulite semiconductor type transducer. The latter was connected to the rest of the instrumentation through a set of slip rings (see section 4.4). The output of both pressure transducers was recorded by the A.D.C. and the results were stored on floppy discs as for clearance measurements. The sampling of these signals was initiated by the pulse from the magnetic pick-up. In every sampling operation 2000 points were taken at the rate of 16667 kHz. Two full revolutions could thus be recorded at a pump speed of 1000 rev/min. Data processing was considerably simpler

than clearance measurements because the relationship between voltage and pressure of both transducers was linear.

Plots of slipper pocket pressure and piston pressure are shown on figures 5.36 to 5.40. In all the plots, piston pressure ripple was plotted above slipper pressure to enable comparison between the two. Although the scale is the same in both types of plot, the zero pressure level of both traces is arbitrary due to the presence of considerable drift in the instrumentation.

A substantial amount of decaying pressure ripple appears at the onset of each slipper pocket. This is interpreted as a result of resonance occurring within the transducer cavity. More interesting is the pressure ripple which appears once resonance has died down. This follows very closely the pressure ripple within the piston in all the tests. As far as pressure differences between piston and slipper pocket are concerned it is not possible to assess with the present set up of the instrumentation. This is due to the fact that both transducers are subject to drift over a period of time. With pocket pressure the problem can be overcome by using the pressure between slippers as a reference point (case pressure). This, however, cannot be applied to the transducer in the piston because it is constantly under pressure and its level is not precisely known.

One conclusion that can be derived out of these results is that slipper pocket pressure follows very closely the pressure ripple in the pocket. Moreover, any variations in line pressure induced by external components of the

hydraulic circuit are likely to be transmitted to the slipper pocket.

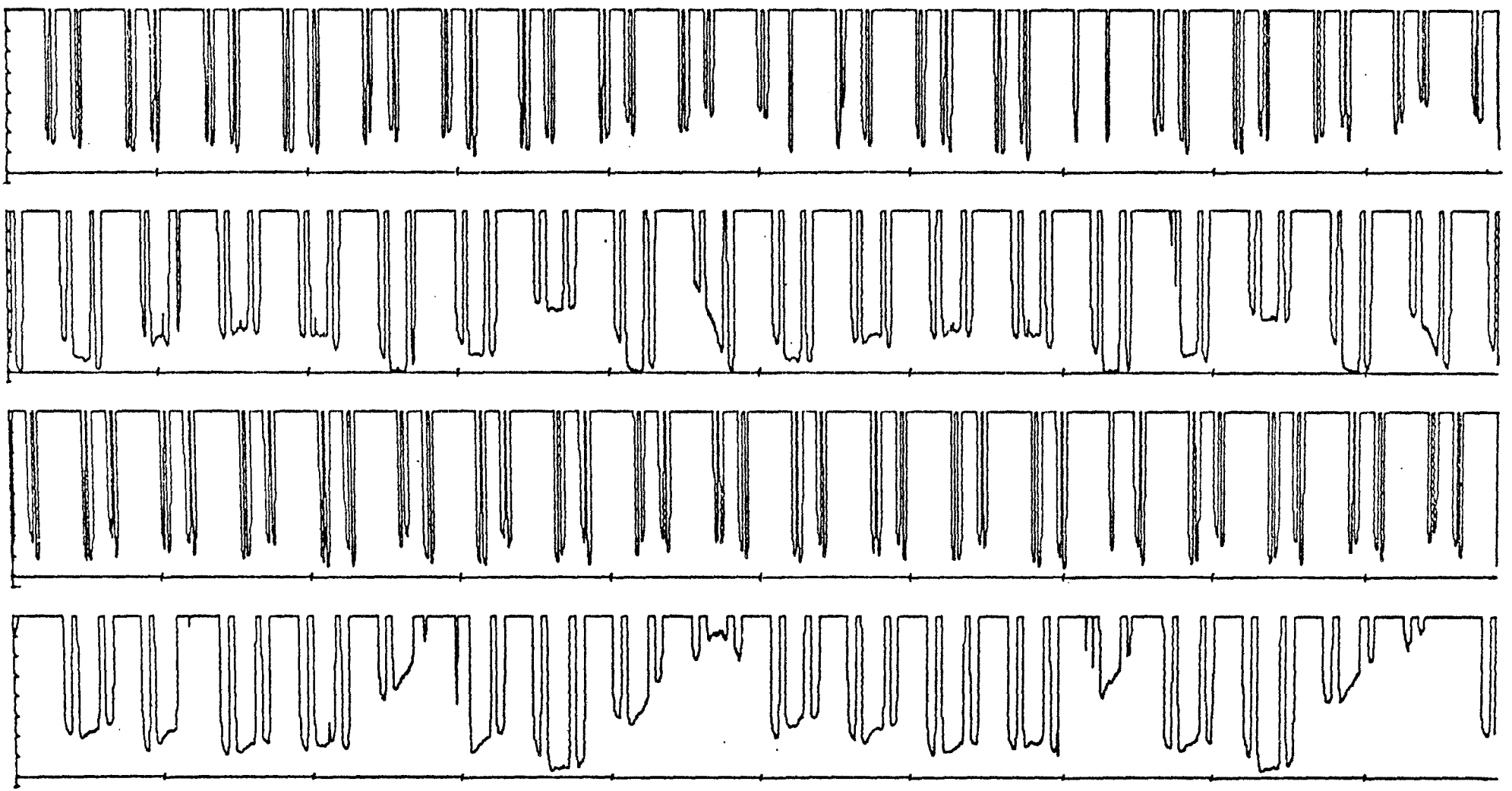

FIGURE 5.4 FILE-NEL1 70 BAR 1000 REV/MIN CLUSTER ON H.P. ROTATION-B

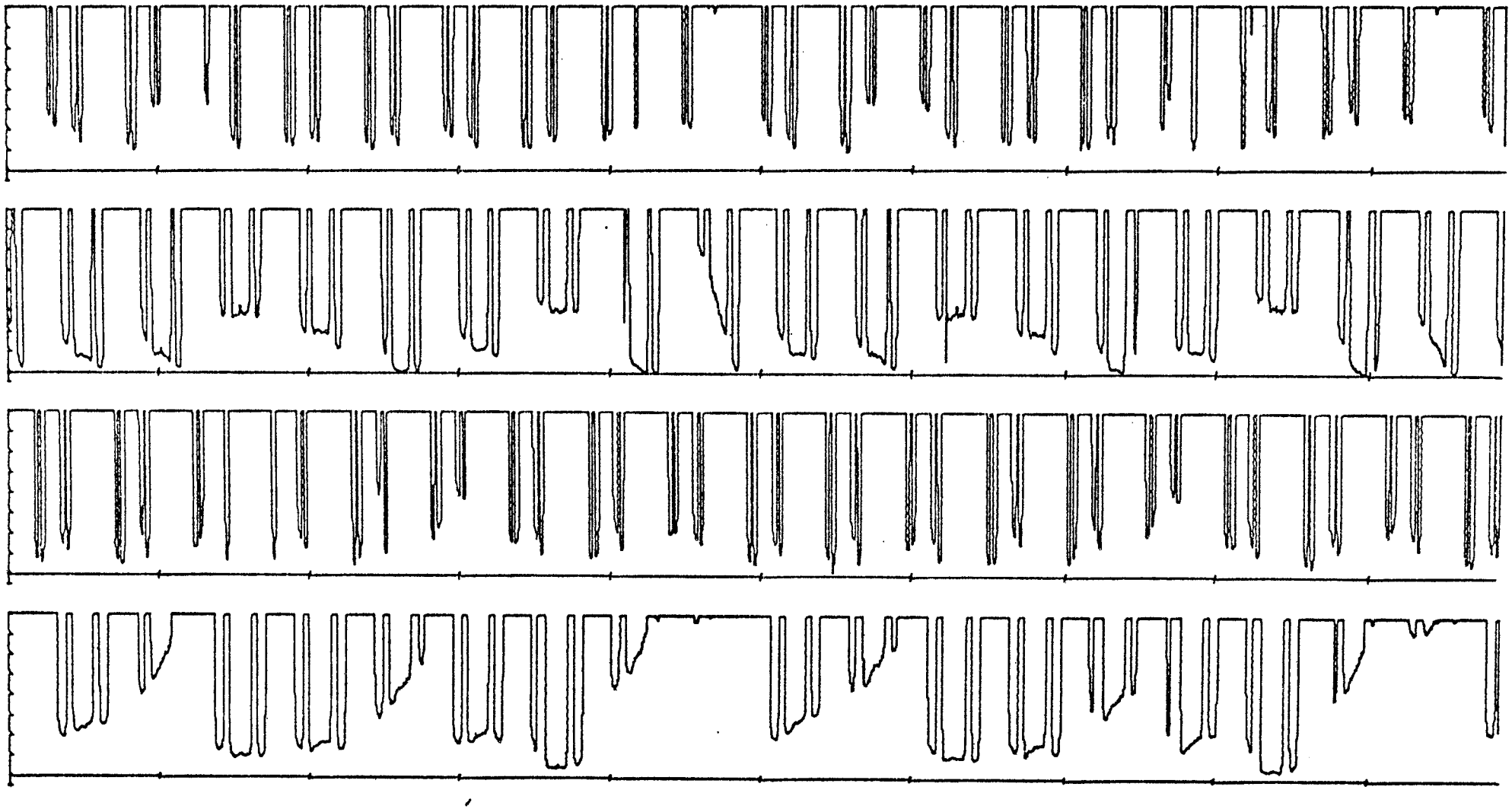

FIGURE 5.5 FILE-NEL7 70 BAR 1000 REV/MIN CLUSTER ON H.P. ROTATION-B

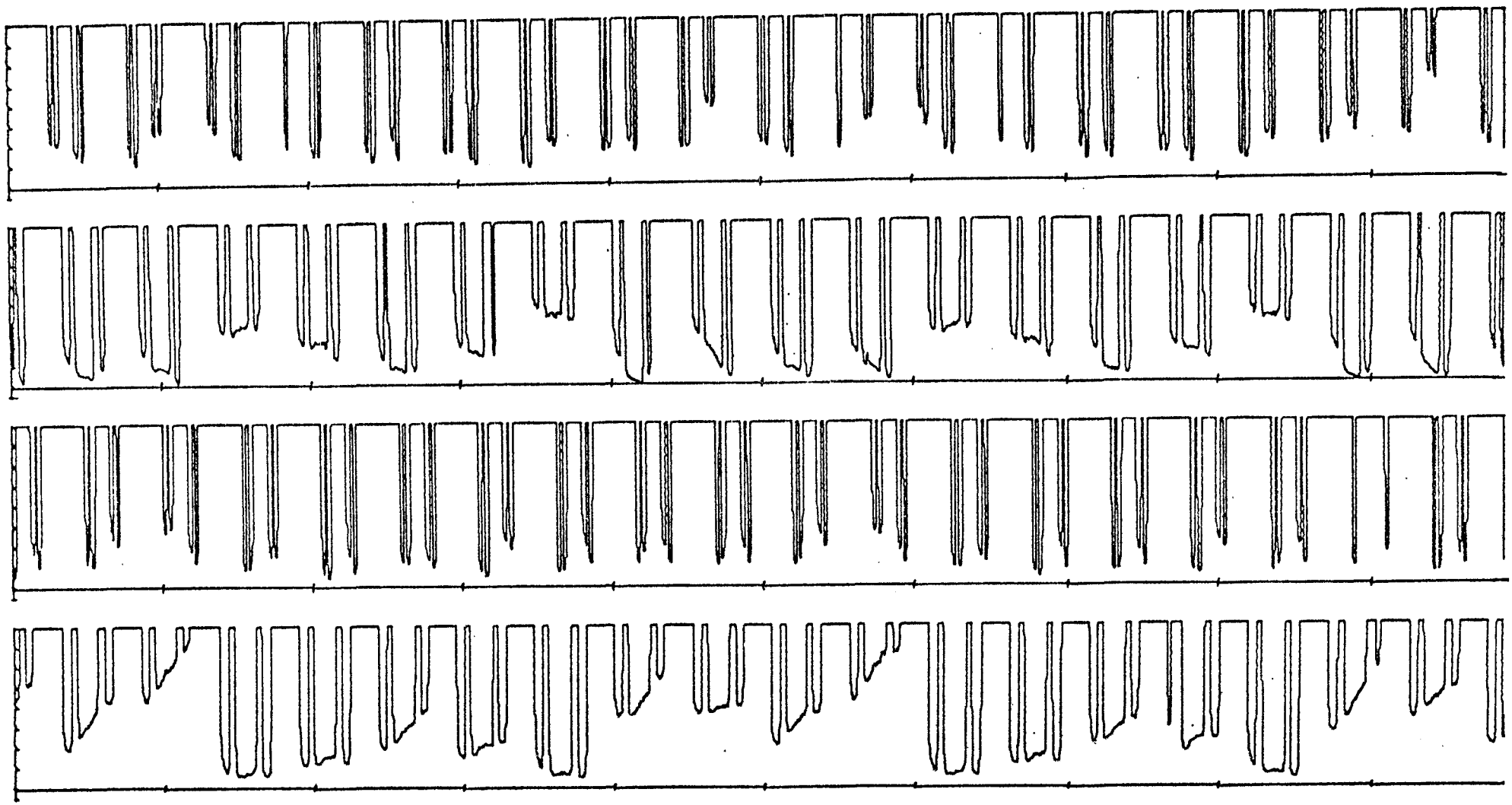

FIGURE 5.6 FILE-NEL20 70 BAR 1000 REV/MIN CLUSTER ON H.P. ROTATION-B

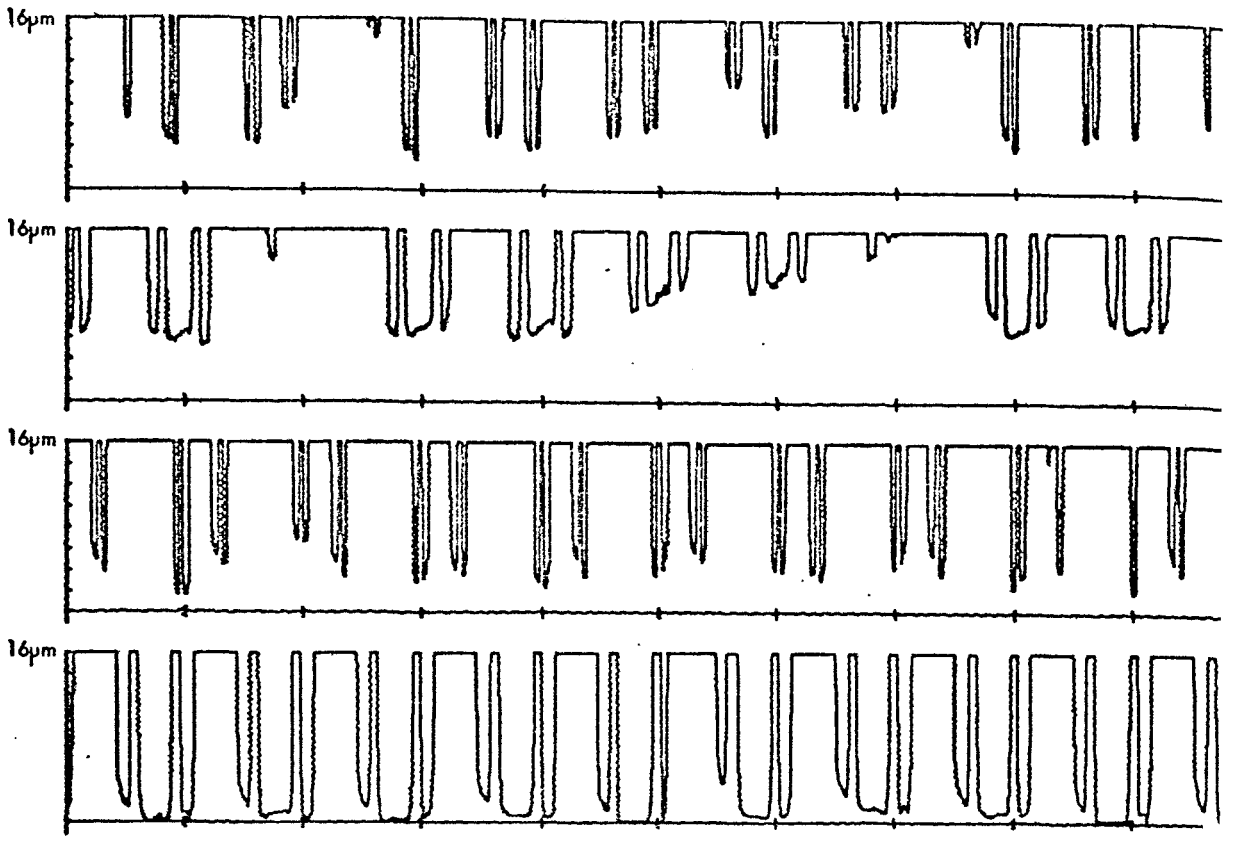

File-NEL13 No-load 1750 rev/min Cluster on H.P. Rotation-B

Figure 5.7

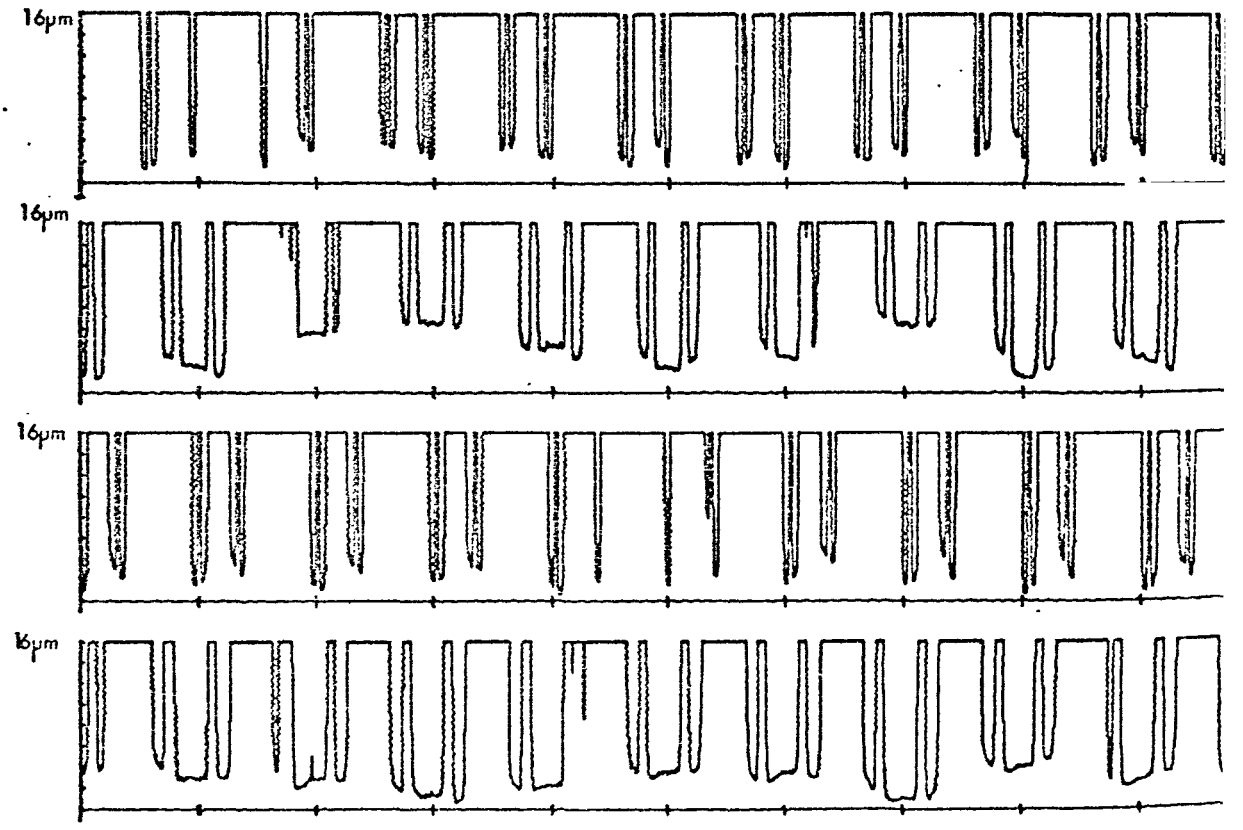

File-NEL15 No-load 1000 rev/min Cluster on H.P. Rotation-B

Figure 5.8

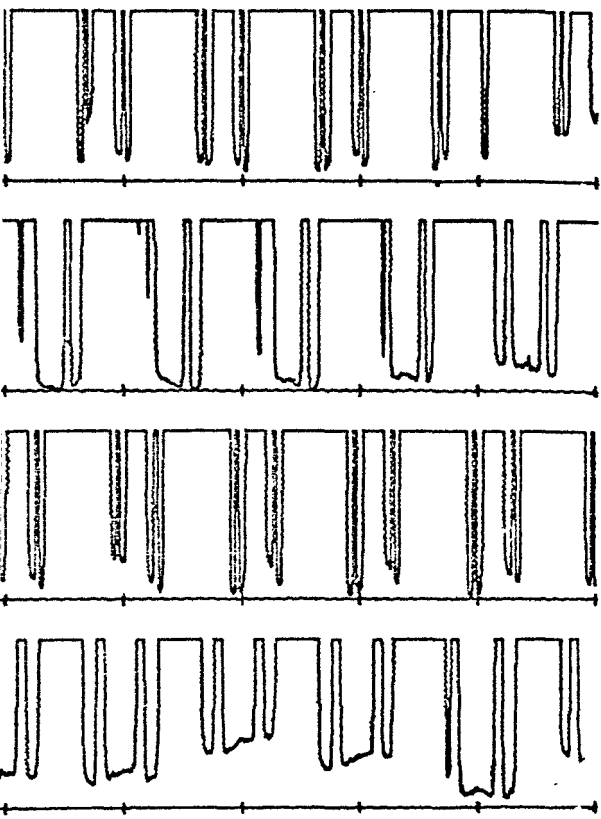

n Cluster on H.P. Rotation-B

e 5.9

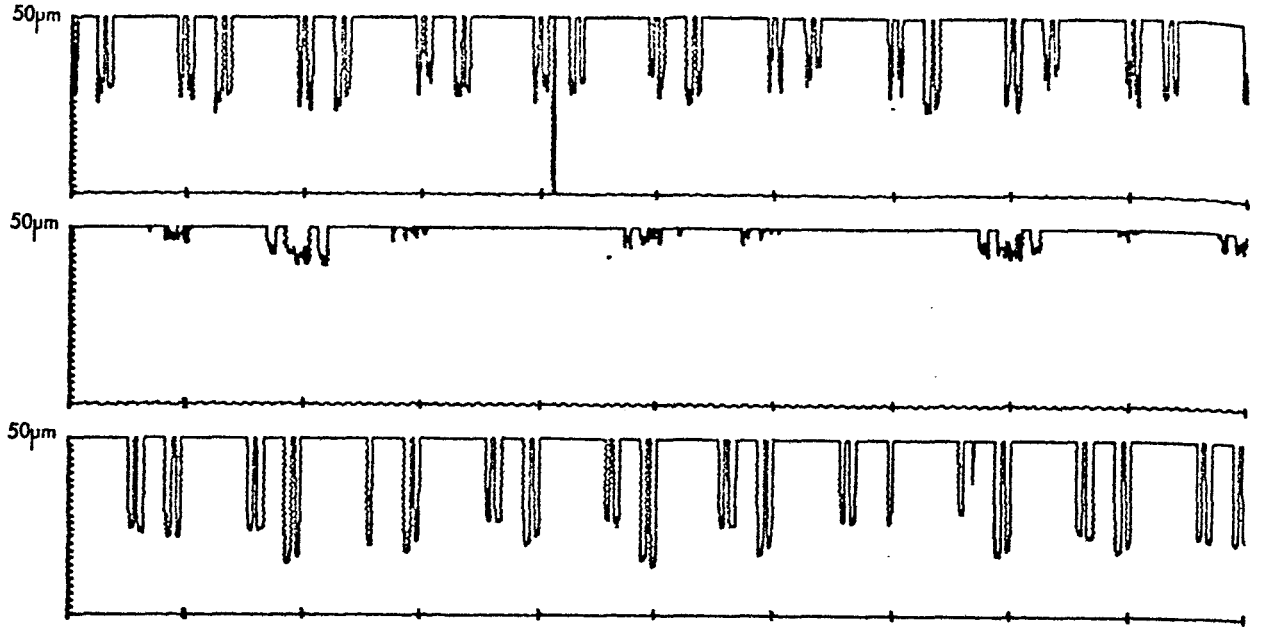

File-NEL27 14 bar 1500 rev/min Cluster on L.P. Rotation-A

Figure 5.10

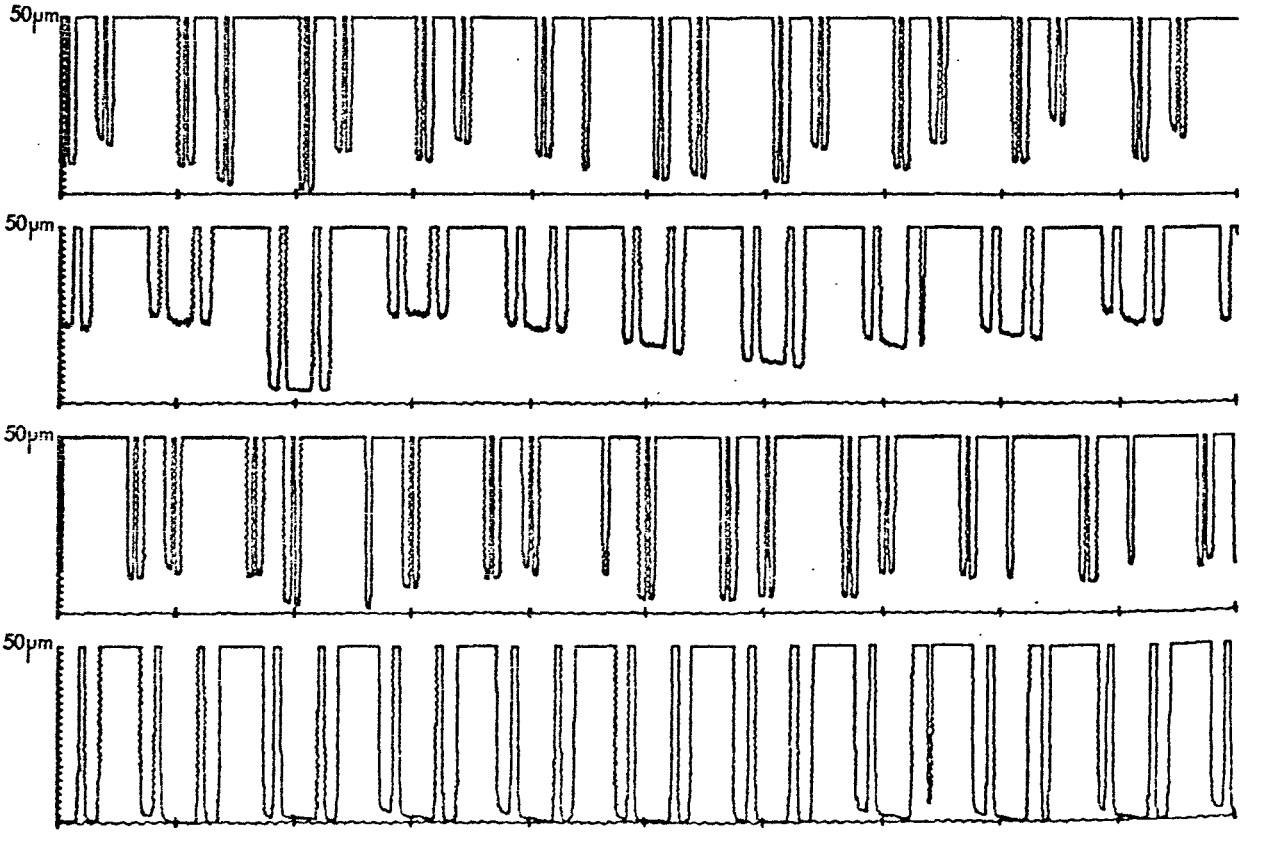

File-NEL25 14 bar 500 rev/min Cluster on L.P. Rotation-A

Figure 5.11

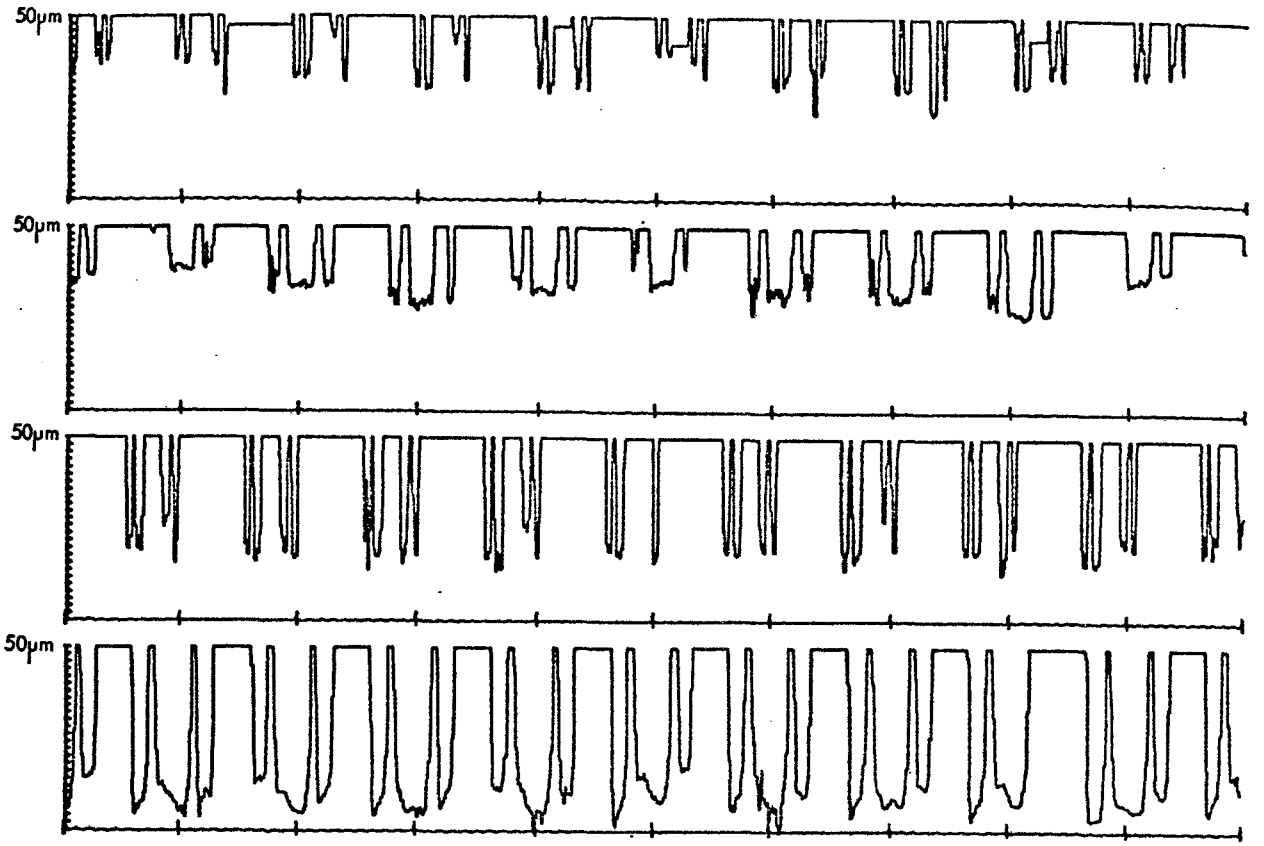

File-COM34 7 bar 1500 rev/min Cluster on L.P. Rotation-A

Figure 5.12

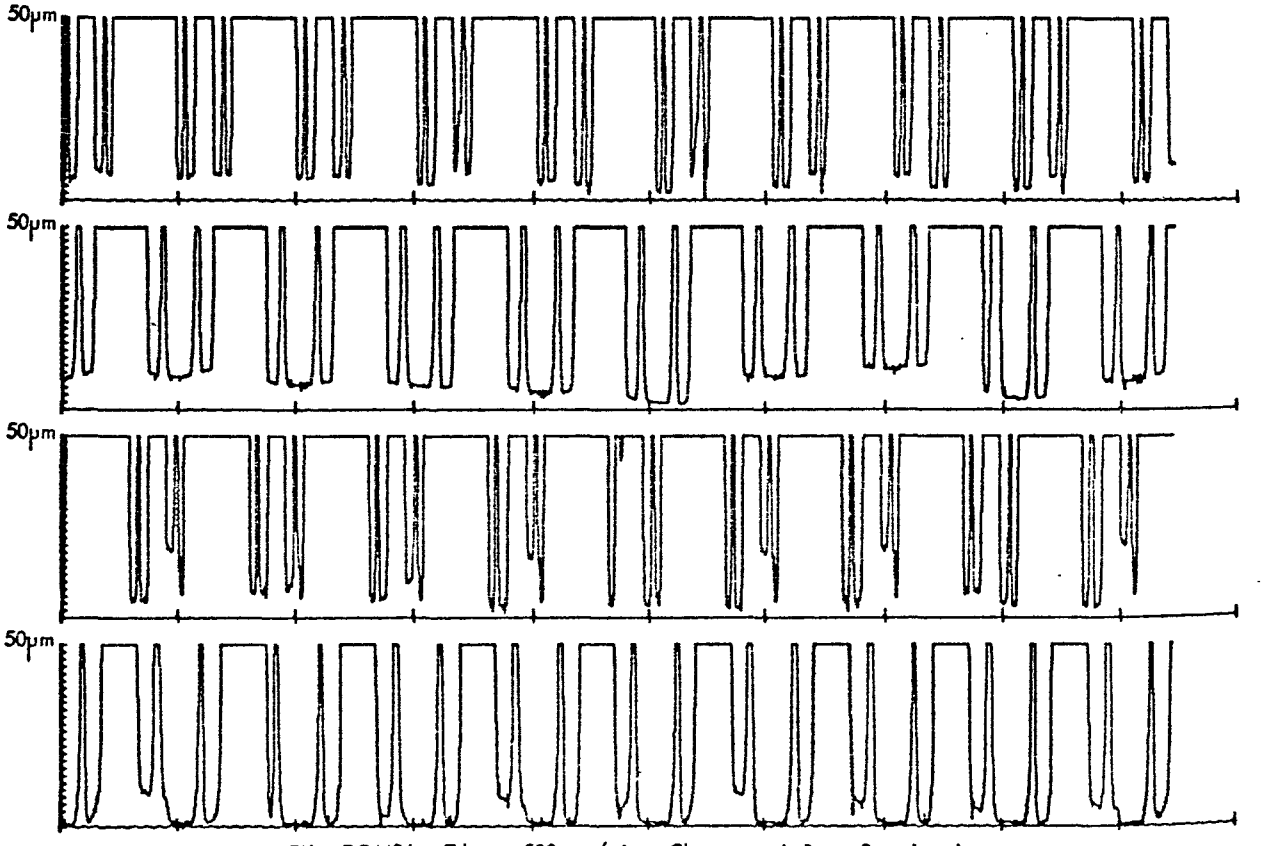

File-COM24 7 bar 500 rev/min Cluster on L.P. Rotation-A

Figure 5.13

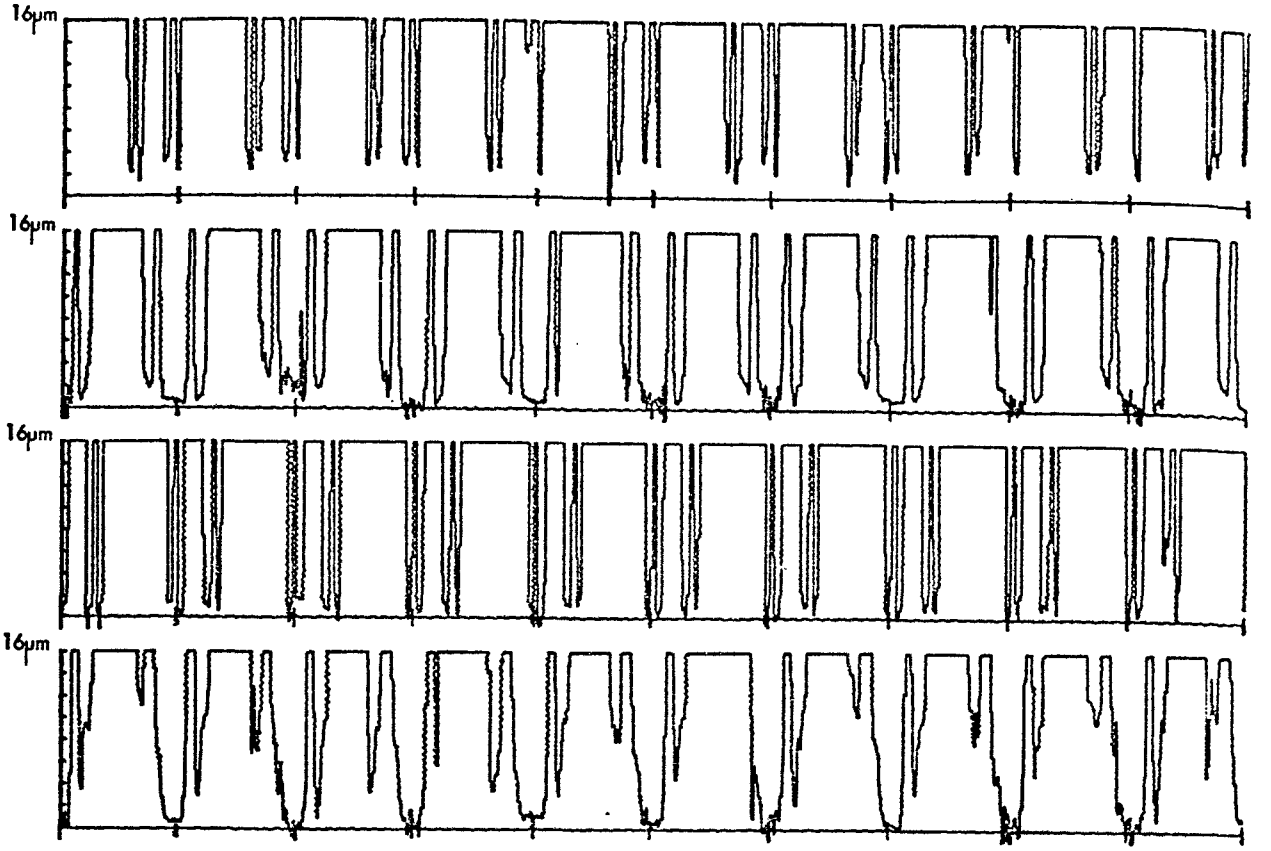

File-COM13 35 bar 1500 rev/min Cluster on H.P. Rotation-B

Figure 5.14

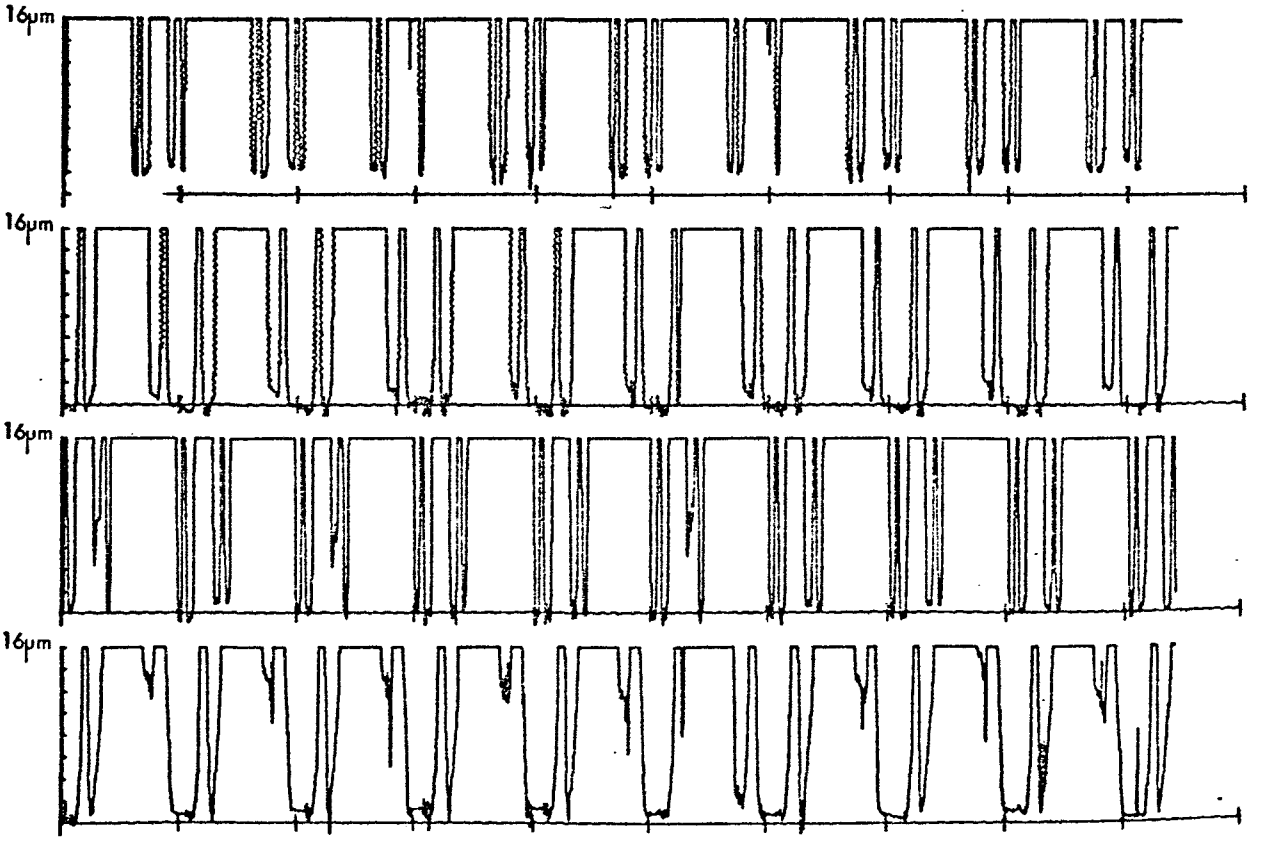

File-COM19 35 bar 500 rev/min Cluster on H.P. Rotation-B

Figure 5.15

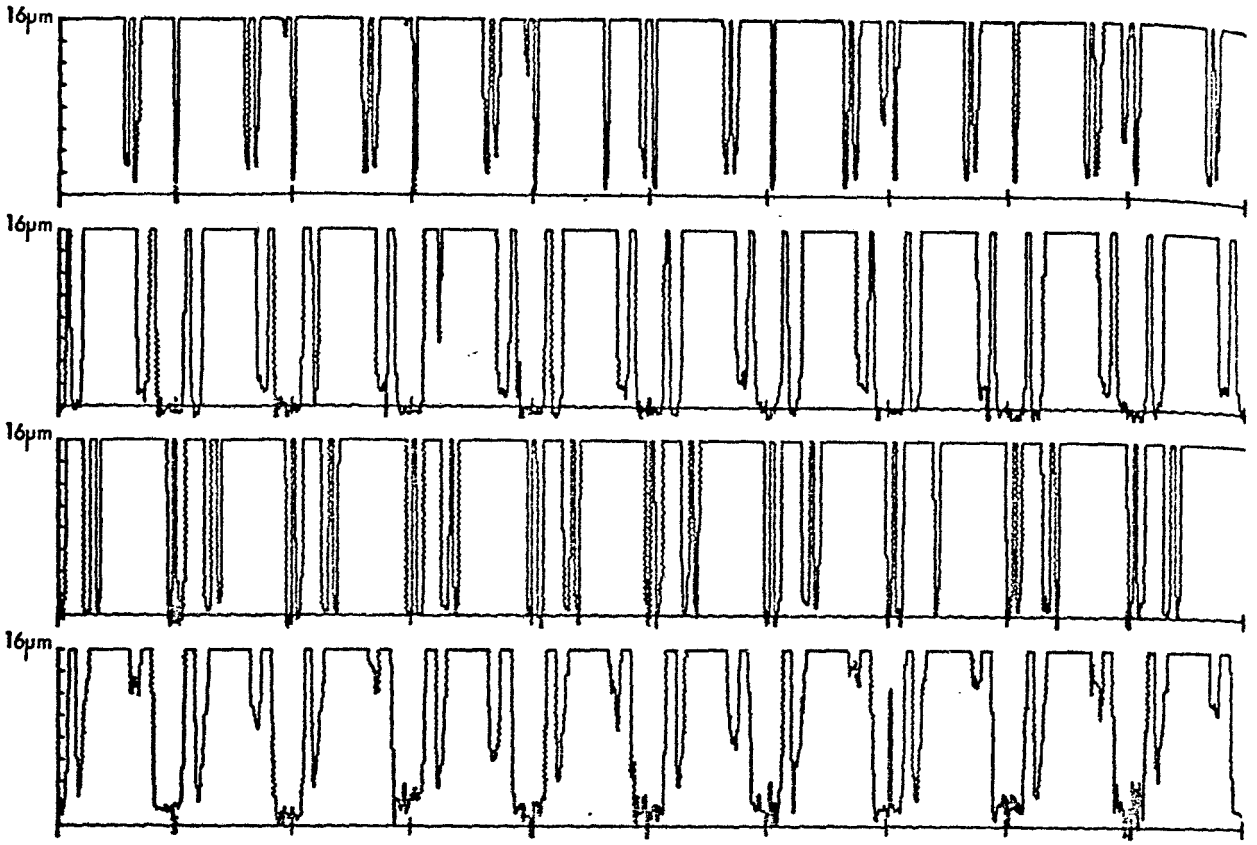

File-COM15 105 bar 1500 rev/min Cluster on H.P. Rotation-B

Figure 5.16

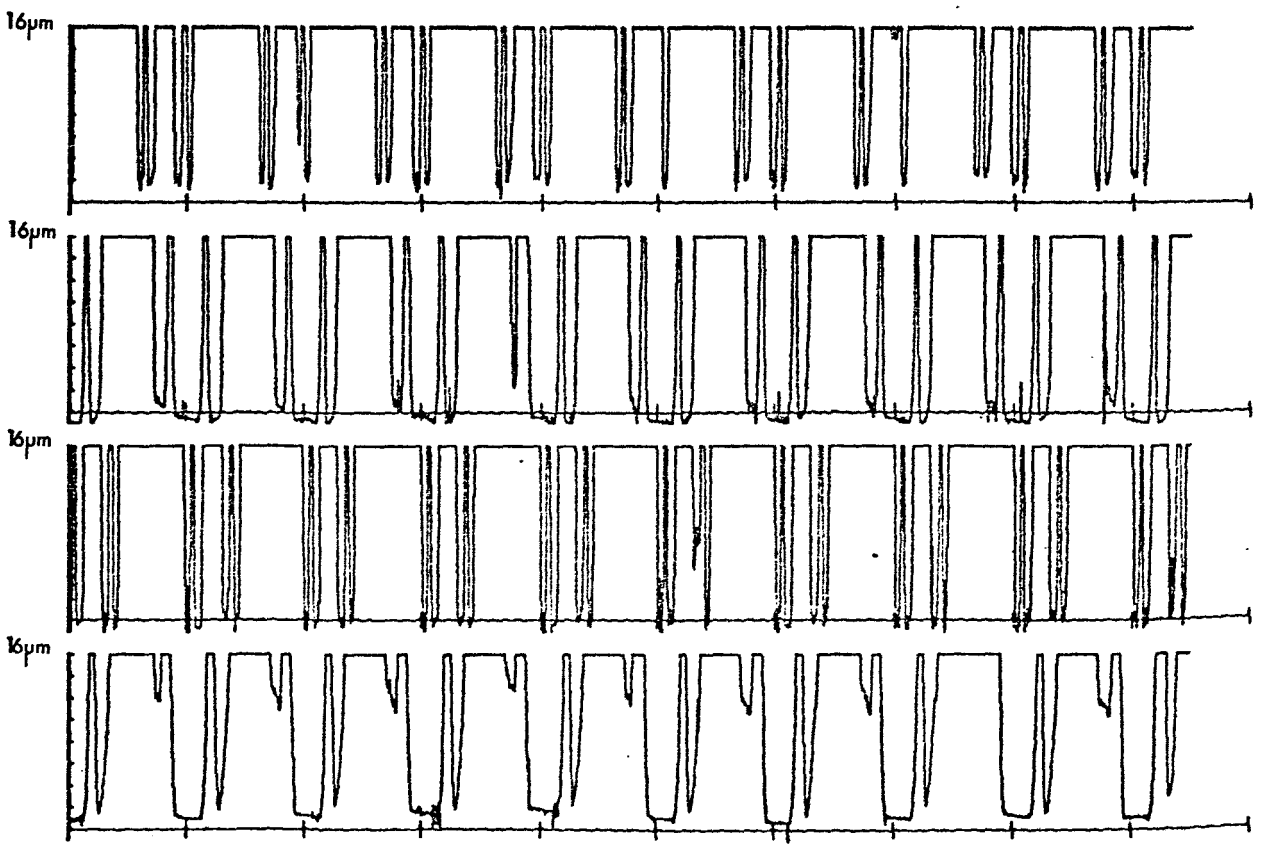

File-COM20 70 bar 500 rev/min Cluster on H.P. Rotation-B

Figure 5.17

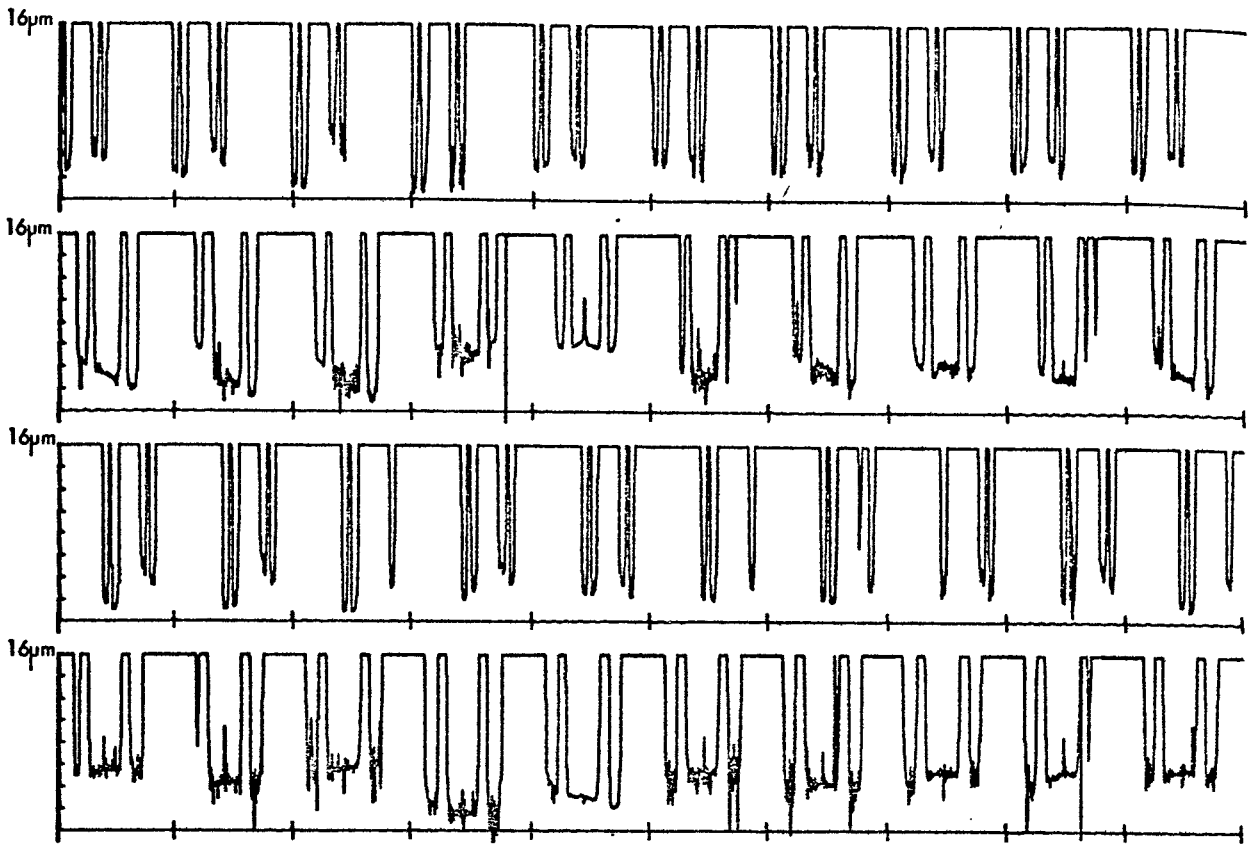

File-CG6 No-load 1000 rev/min Cluster on H.P. Rotation-B

Figure 5.18

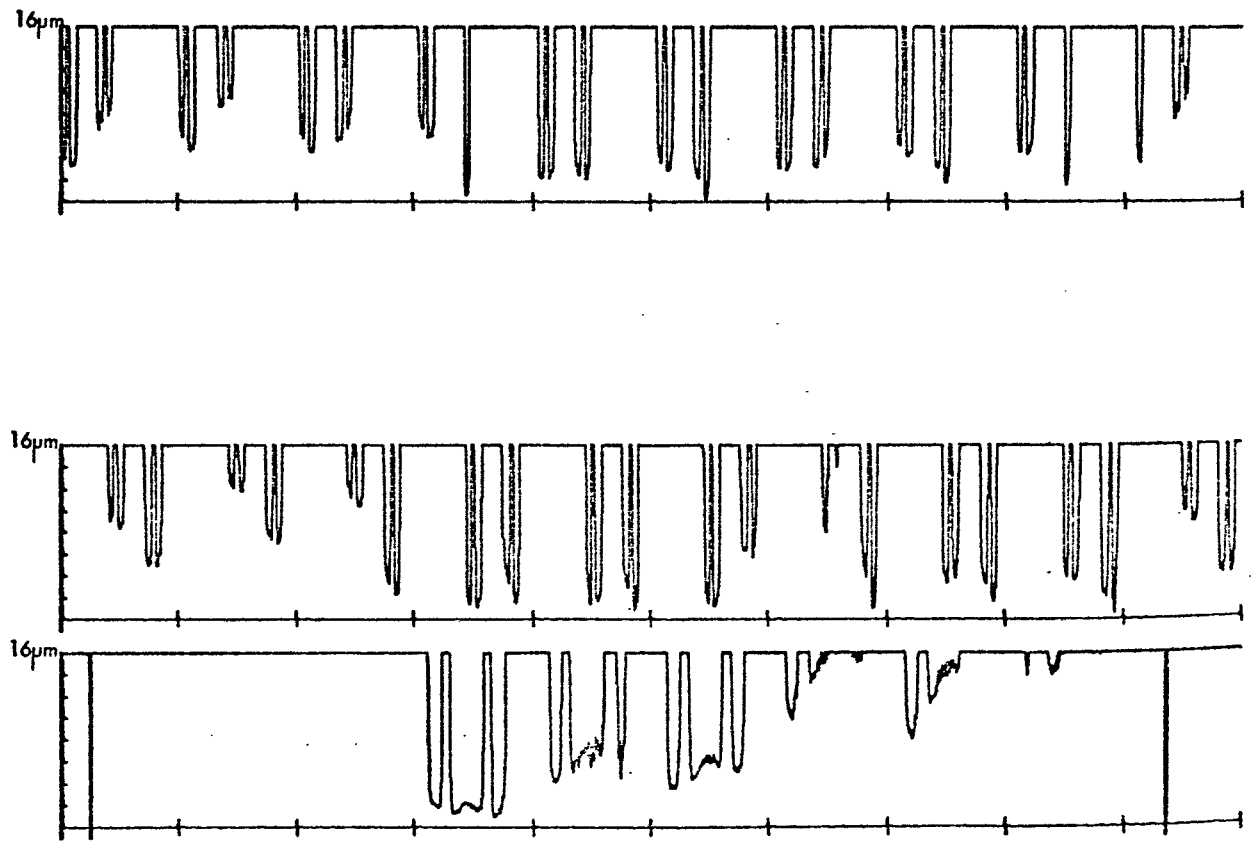

File-CG4 14 bar 1000 rev/min Cluster on H.P. Rotation-B

Figure 5.19

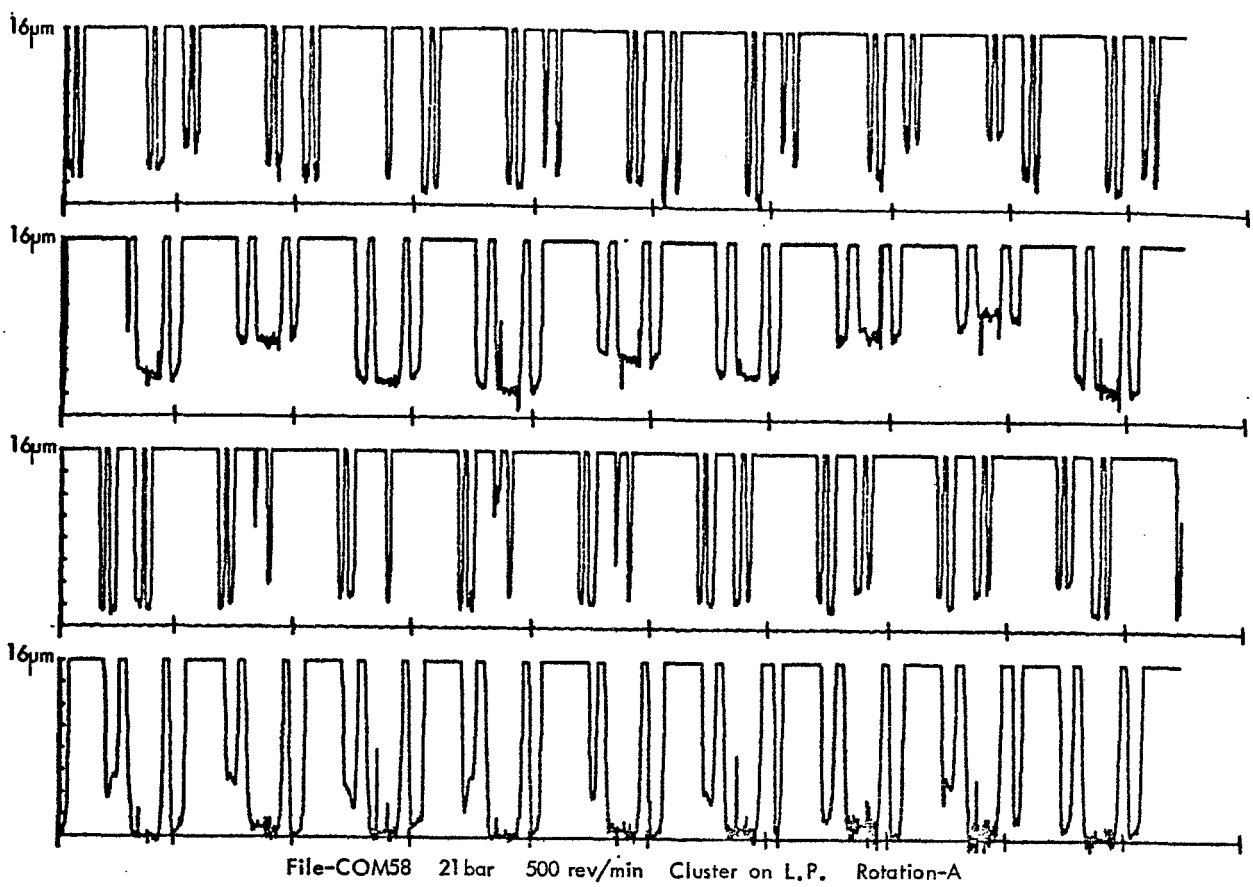

File-COM58 21 bar 500 rev/min Cluster on L.P. Rotation-A

Figure 5.20

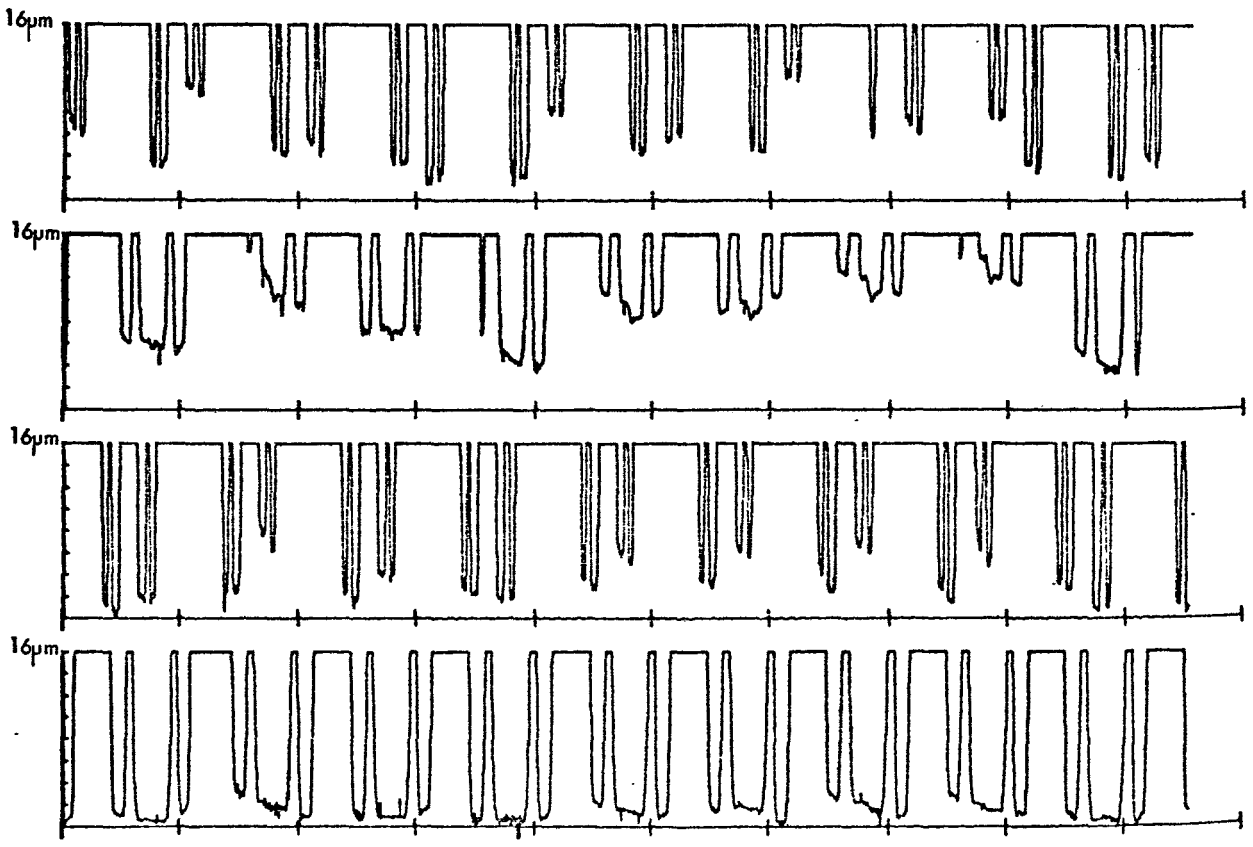

File-COM61 35 bar 500 rev/min Cluster on L.P. Rotation-A

Figure 5.21

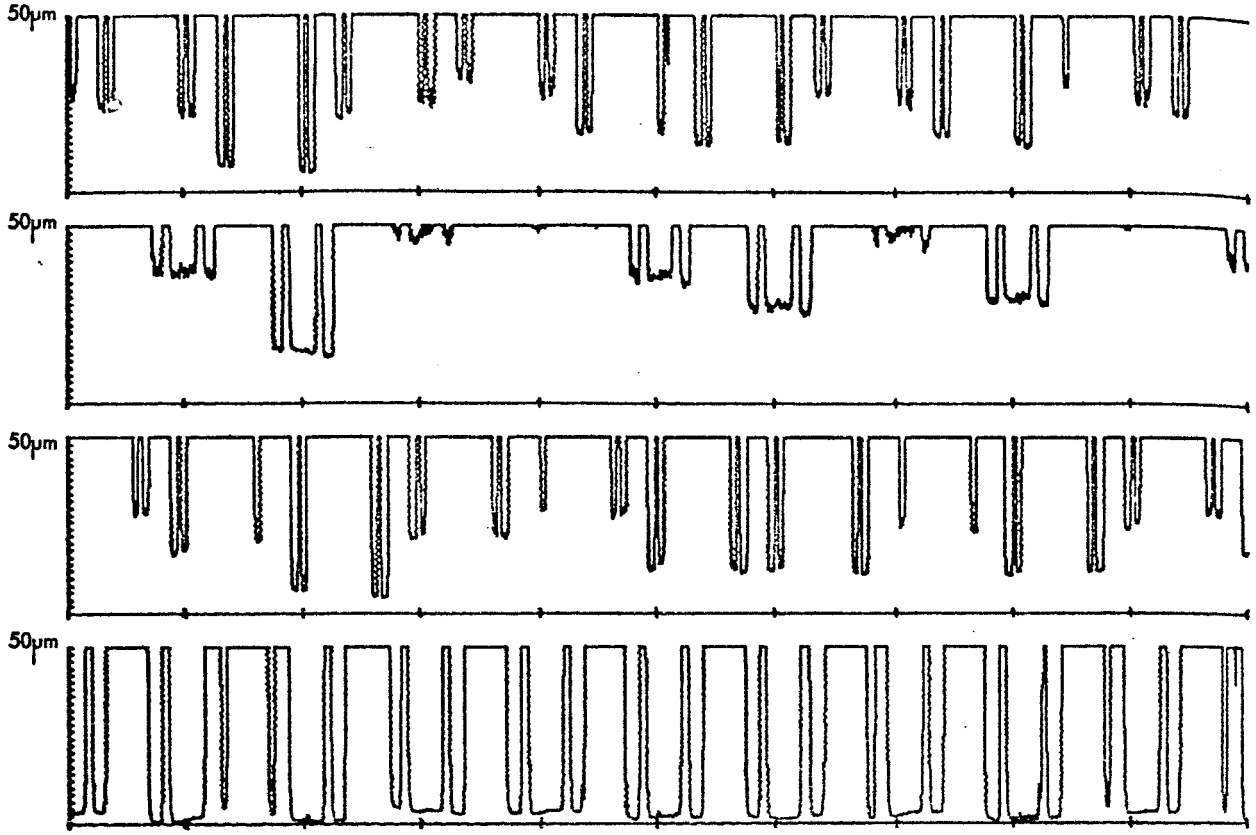

File-NEL29 10.5 bar 1000rev/min Cluster on L.P. Rotation-A

Figure 5.22

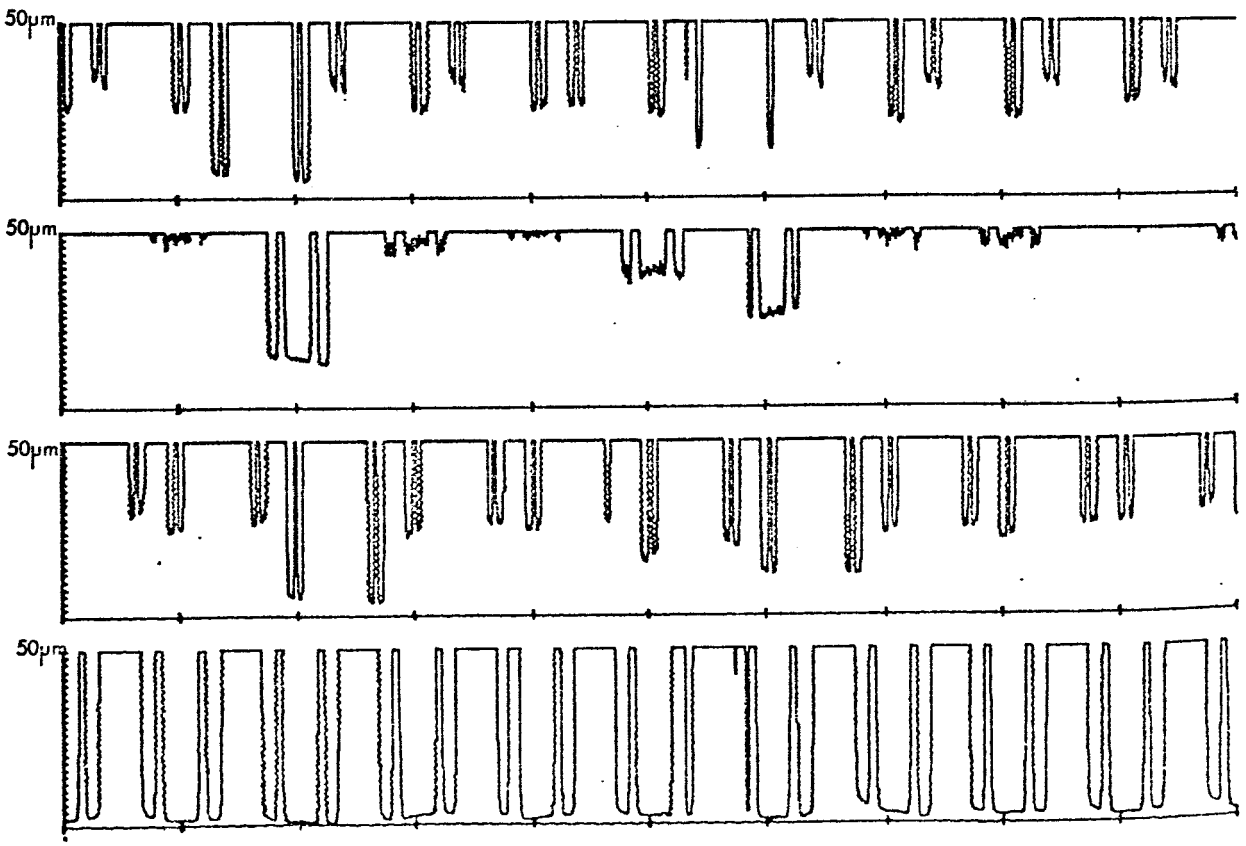

File-NEL30 17.5 bar 1000rev/min Cluster on L.P. Rotation-A

Figure 5.23

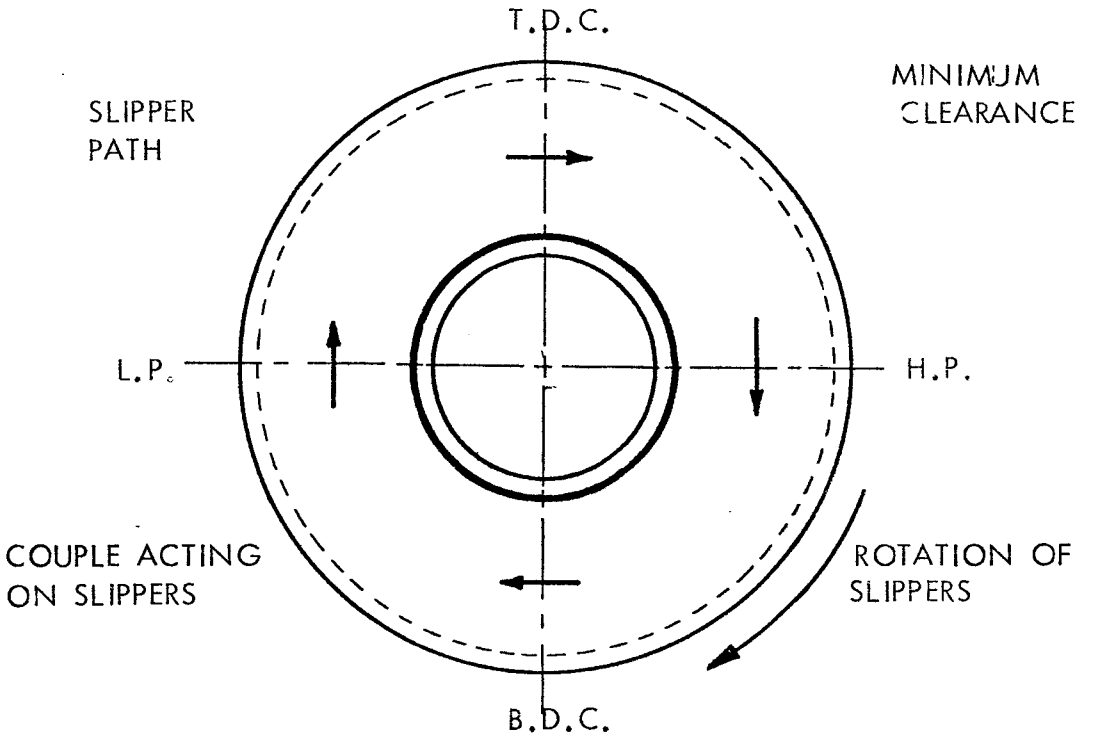

a. EFFECT OF SPEED

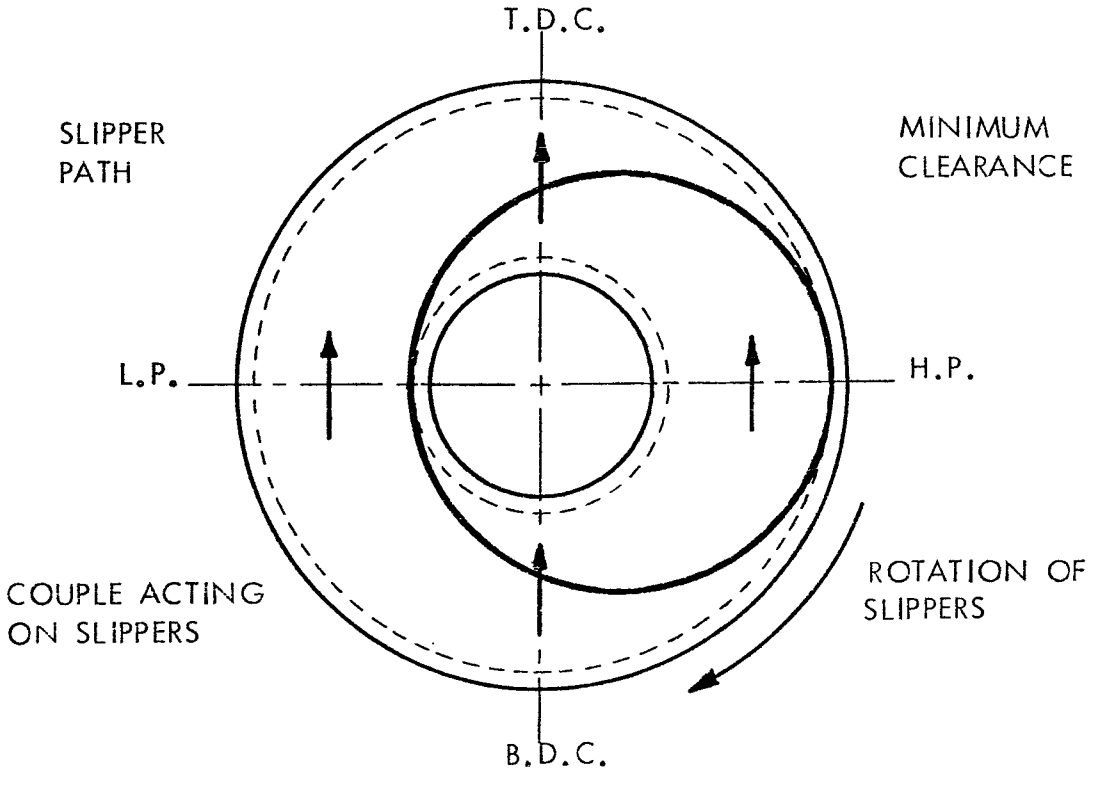

b. EFFECT OF PRESSURE

FIG. 5.24 COUPLES ON THE SLIPPERS DUE TO SPEED & PRESSURE

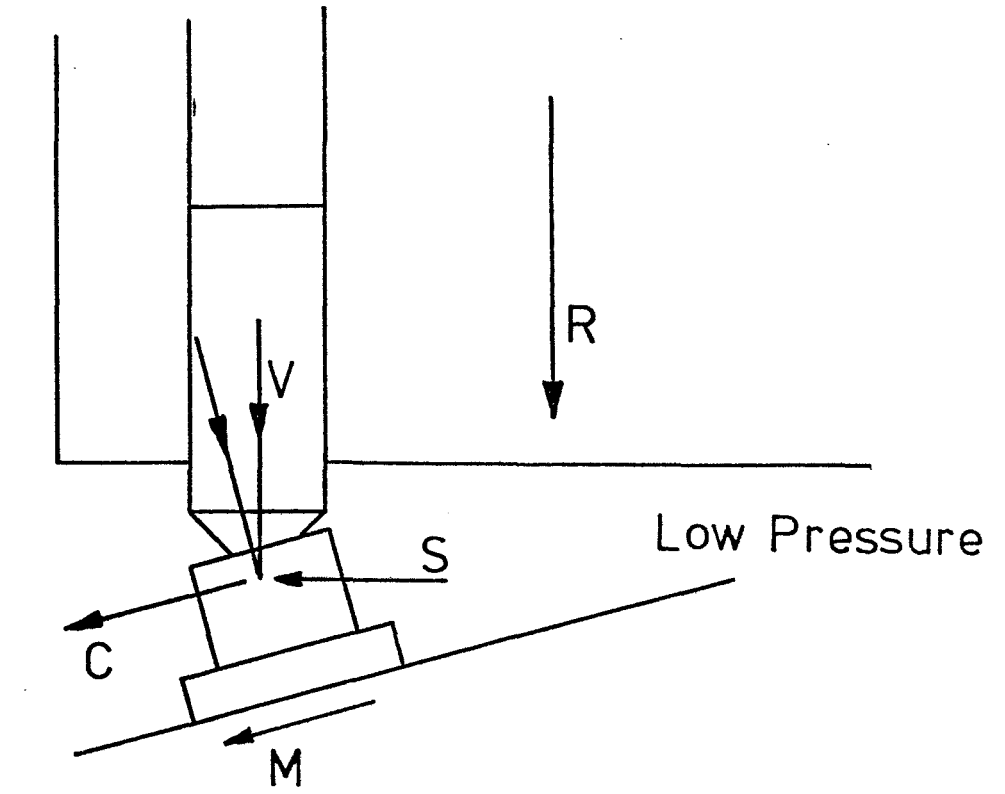

R - Rotation of Cylinder Block
v - Couple due to Viscous drag
S - Couple due to speed
C - Component of Viscous drag along slipper plate
M - Direction of Motion of slipper

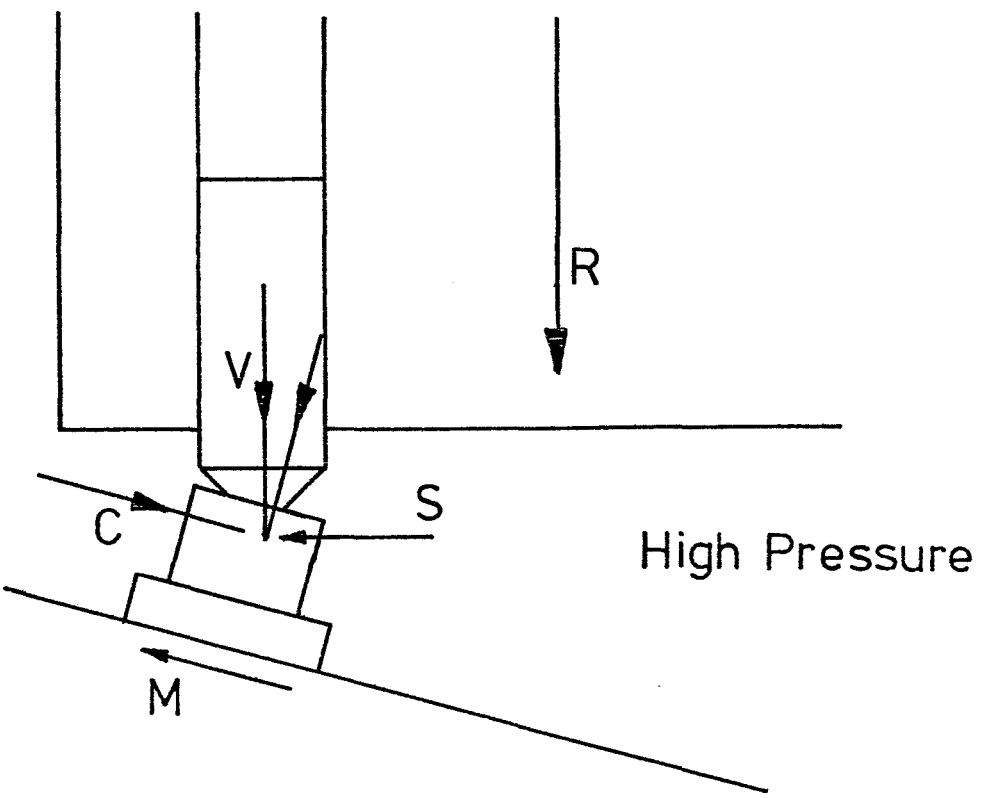

Couples on slipper due to speed and viscous drag in piston bore

Figure 5.25

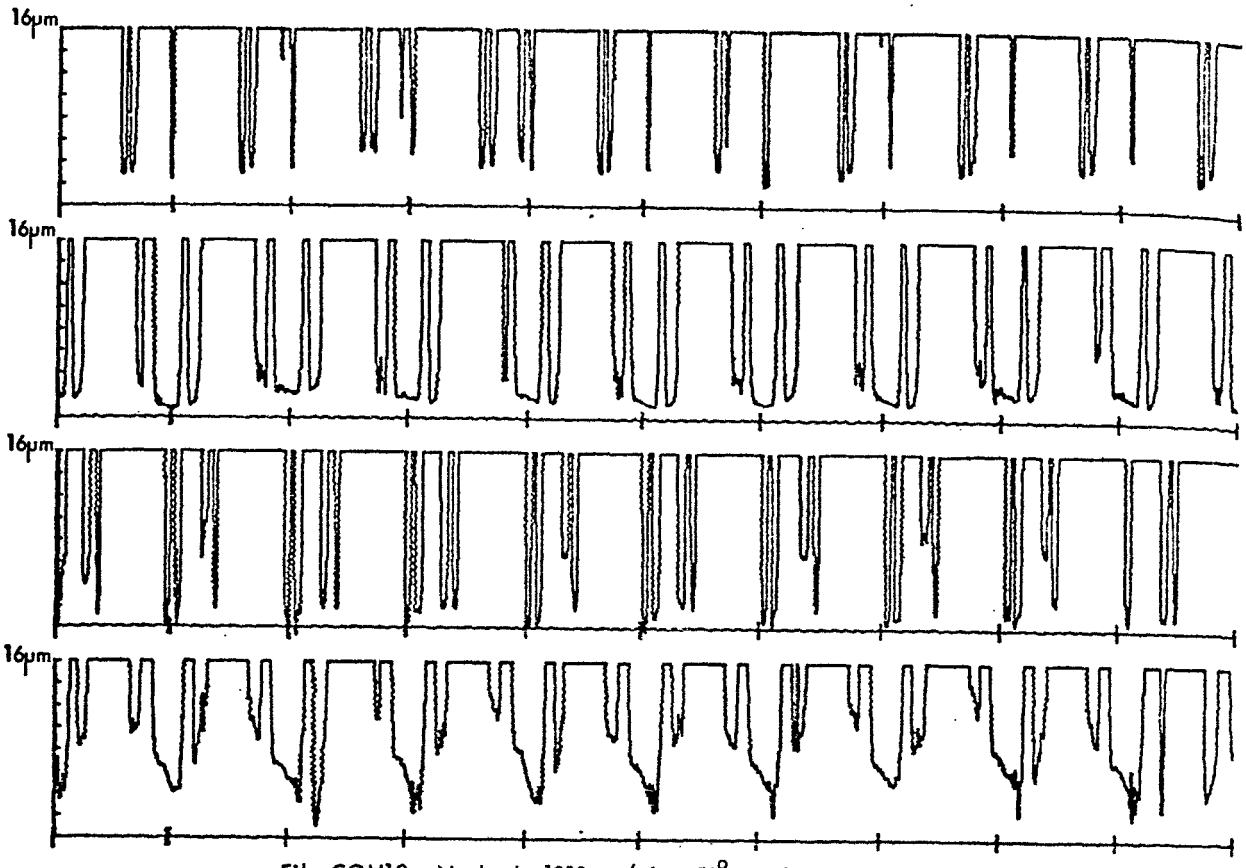

File-COM12 No-load 1000 rev/min 50°C Cluster on H.P. Rotation-B

Figure 5.26

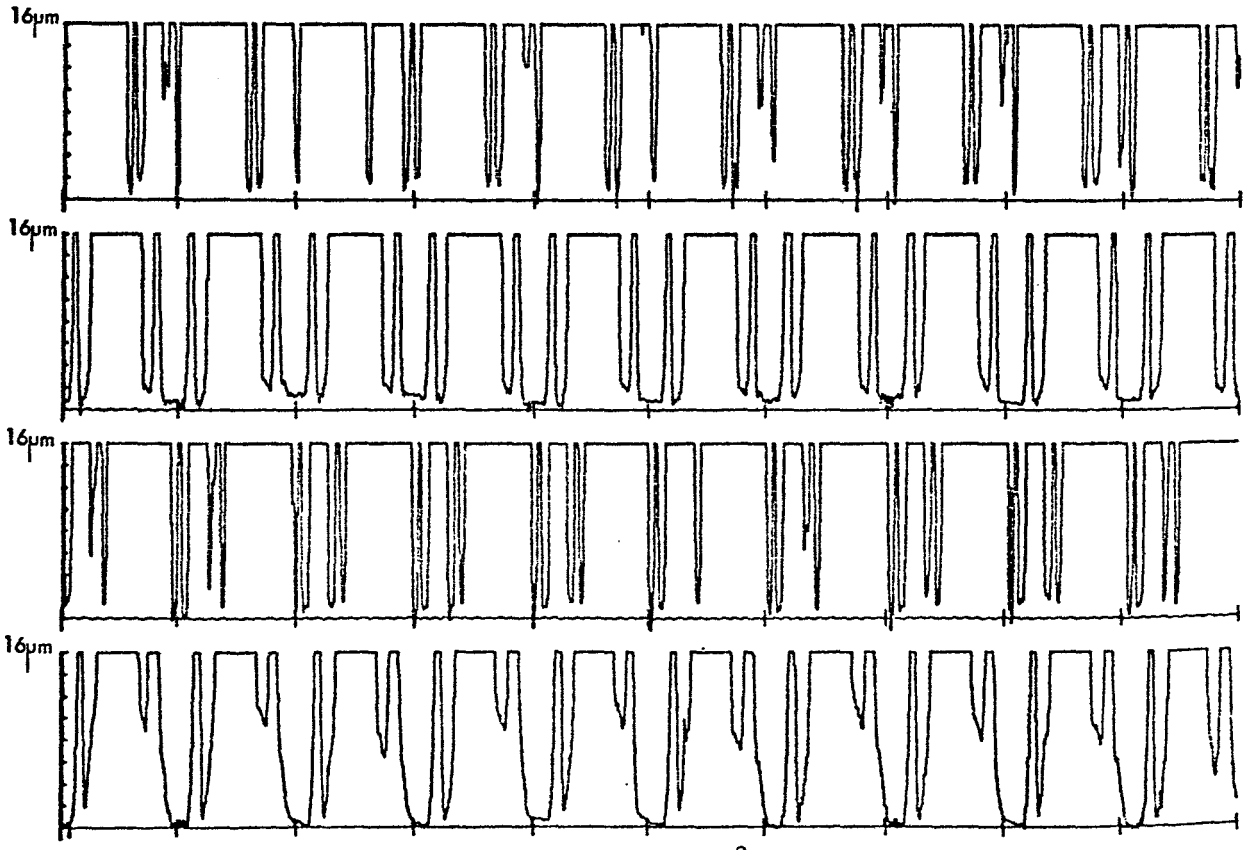

File-COM46 No-load 1000 rev/min 70°C Cluster on H.P. Rotation-B

Figure 5.27

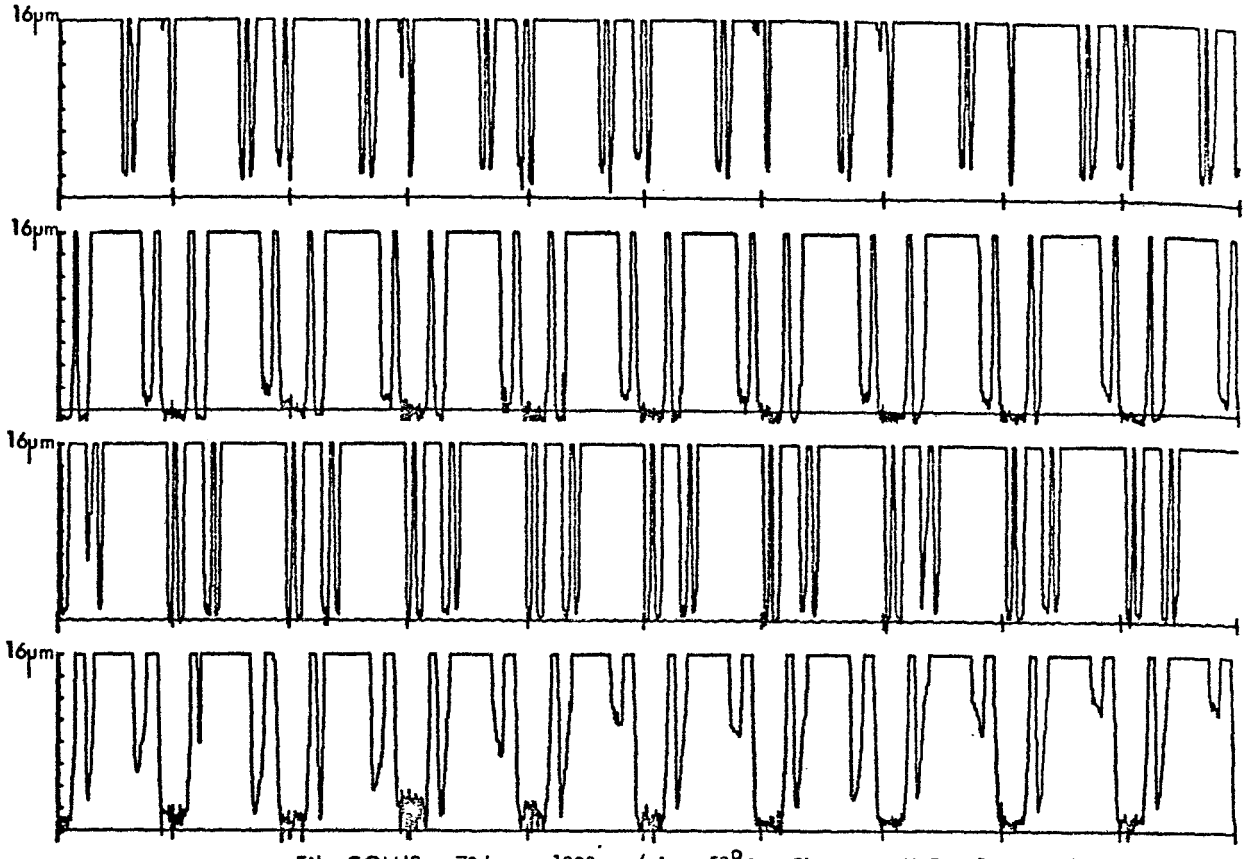

File-COM43 70 bar 1000 rev/min 50°C Cluster on H.P. Rotation-B

Figure 5.28

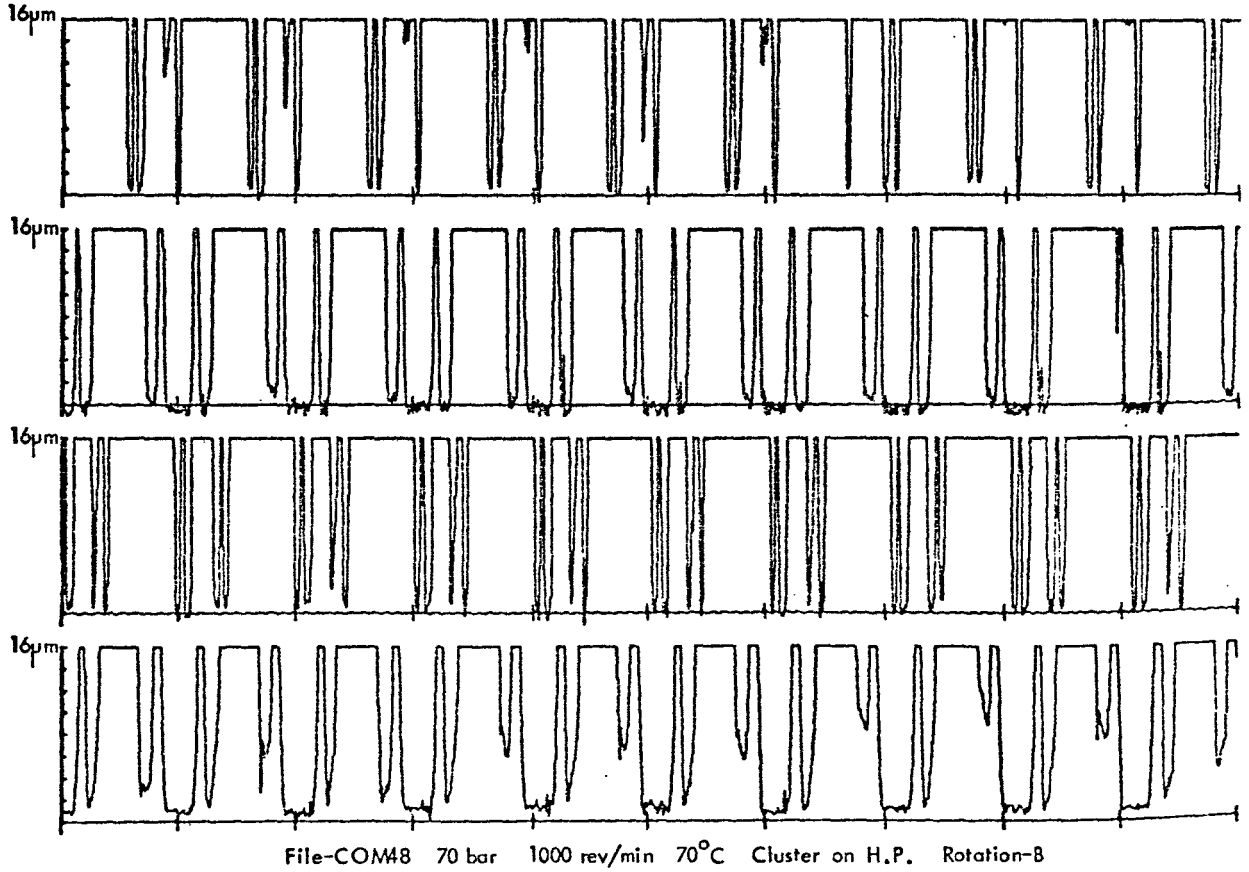

File-COM48 70 bar 1000 rev/min 70°C Cluster on H.P. Rotation-B

Figure 5.29

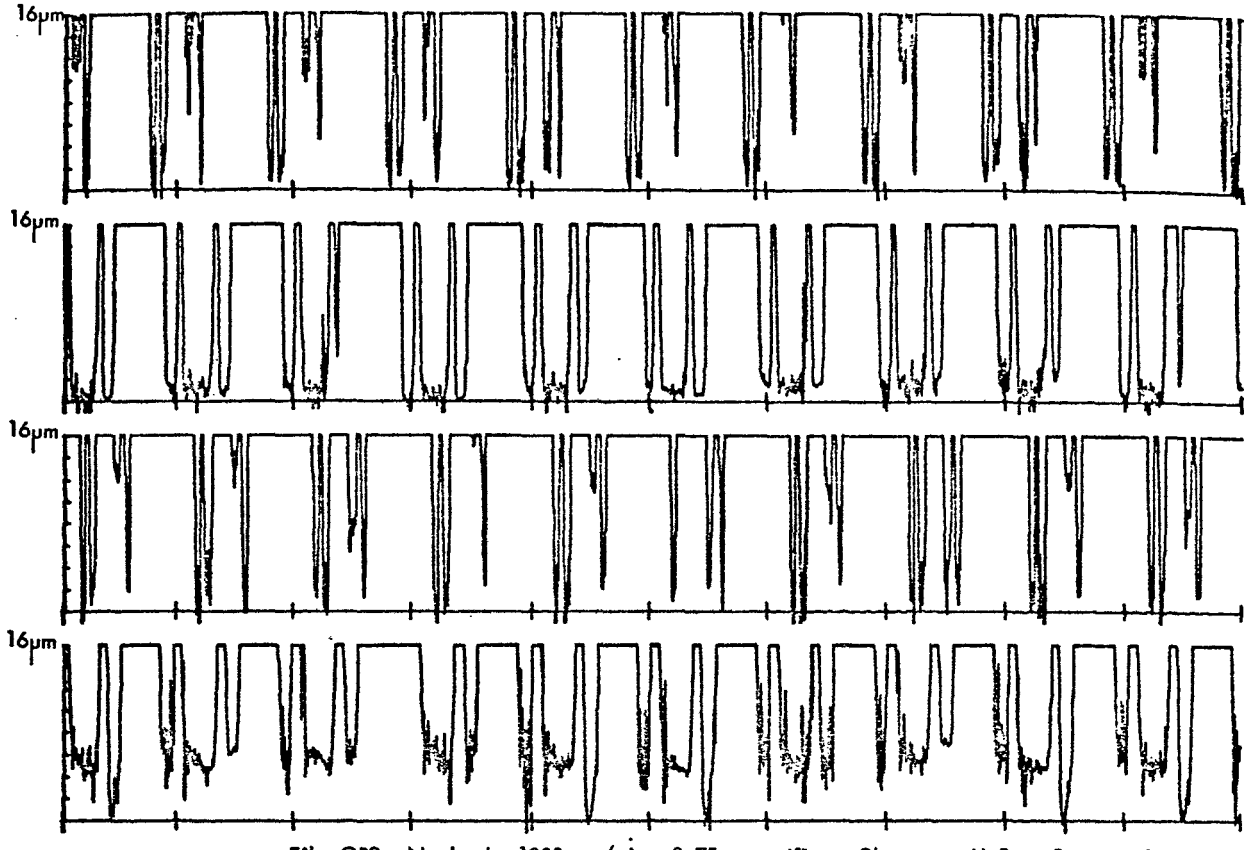

File-OR3 No-load 1000 rev/min 0.75 mm orifice Cluster on H.P. Rotation-B

Figure 5.30

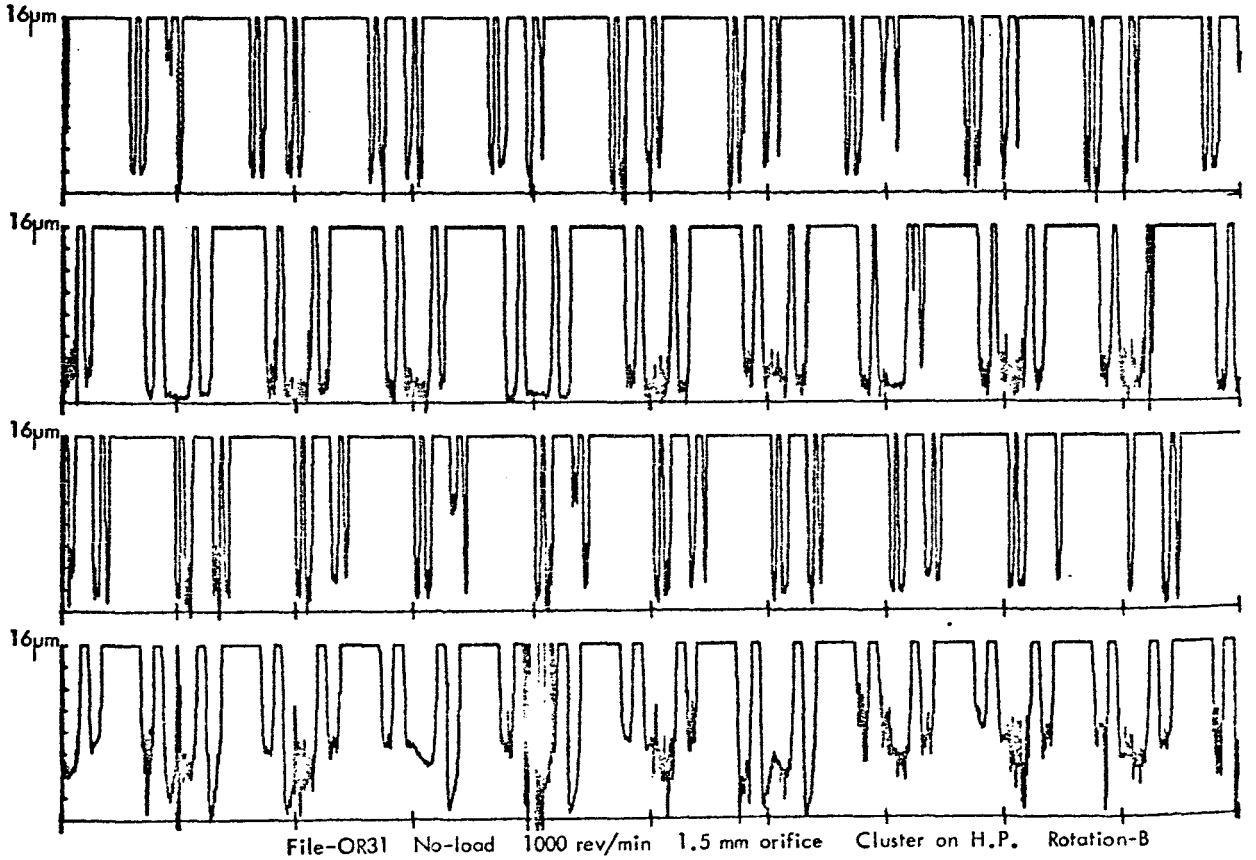

File-OR31 No-load 1000 rev/min 1.5 mm orifice Cluster on H.P. Rotation-B

Figure 5.31

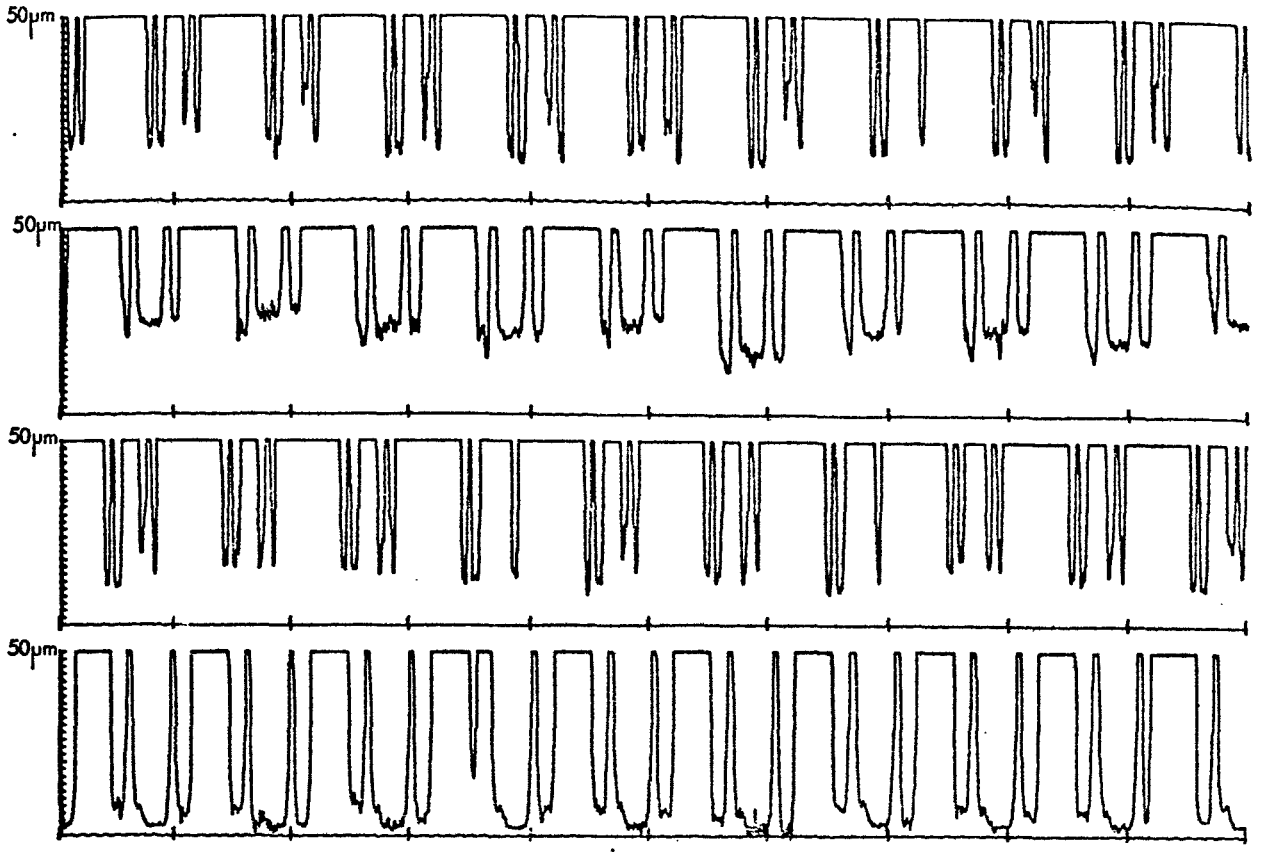

File-OR12 7 bar 1500 rev/min 1.5 mm orifice Cluster on L.P. Rotation-A

Figure 5.32

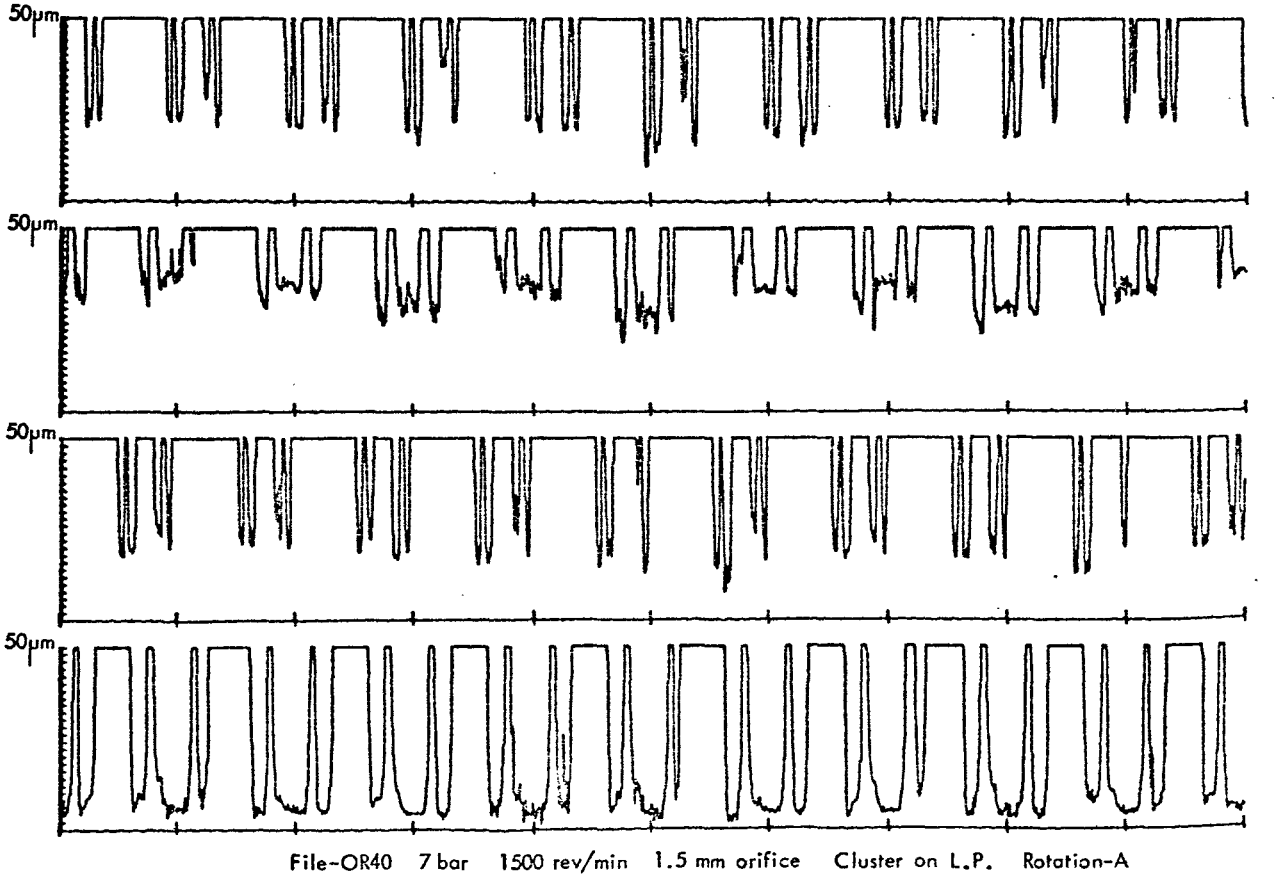

File-OR40 7 bar 1500 rev/min 1.5 mm orifice Cluster on L.P. Rotation-A

Figure 5.33

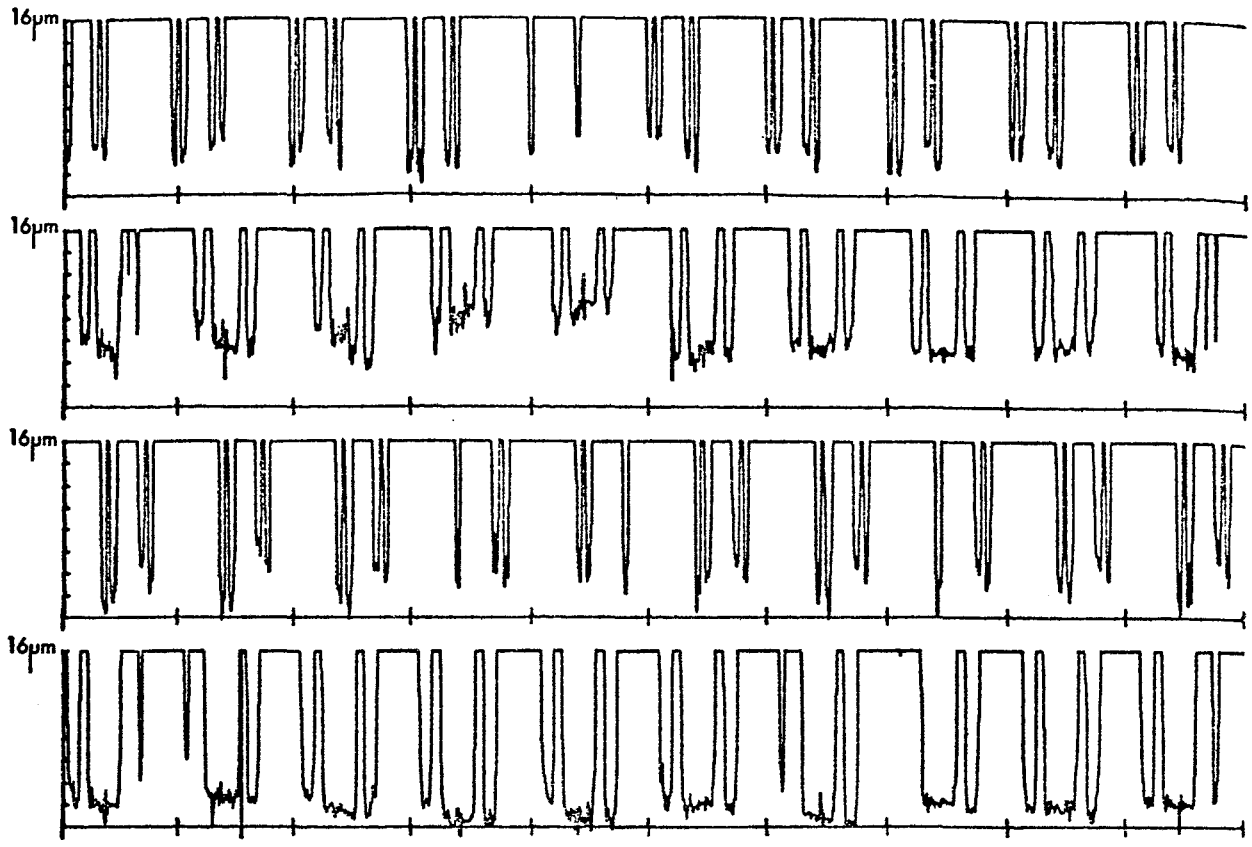

File-CG3 No-load 1500 rev/min Cluster on H.P. Rotation-B

Figure 5.34 Standard set of slippers

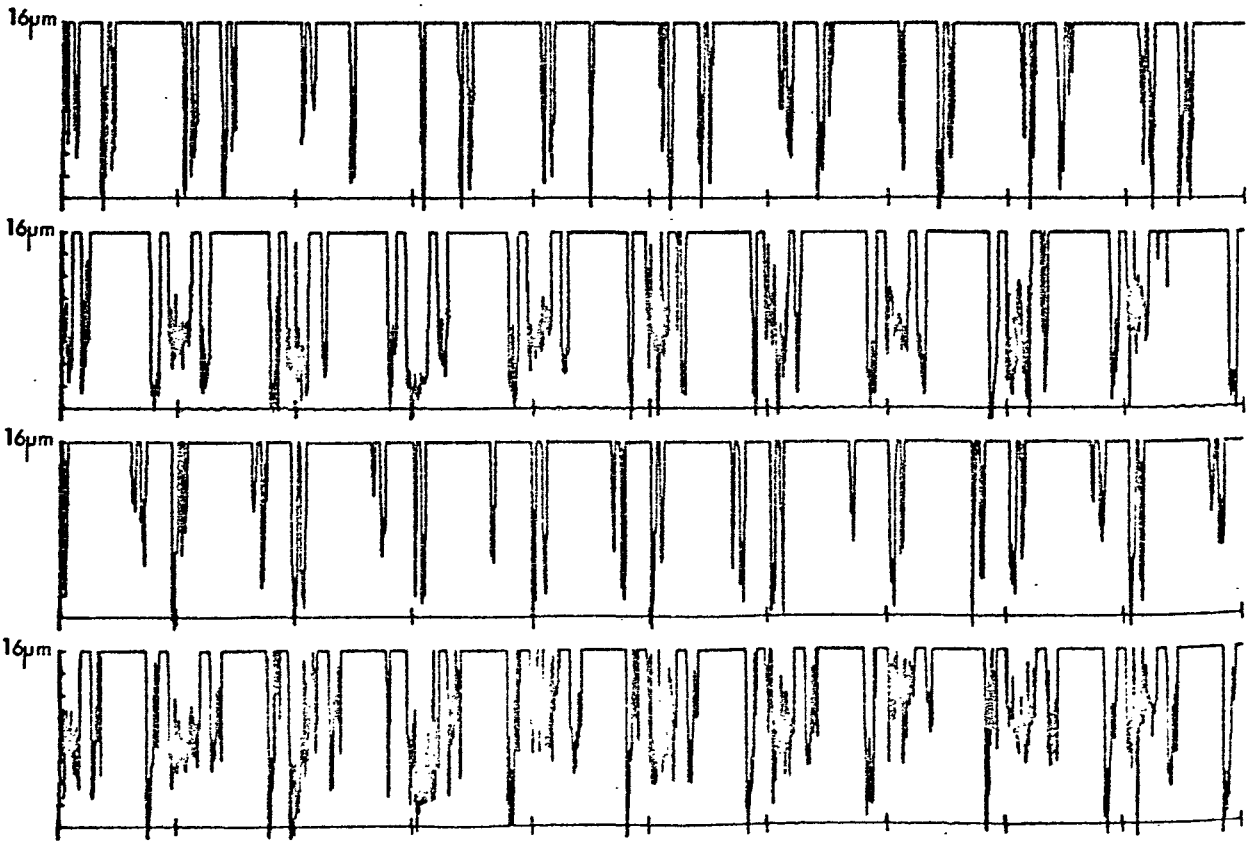

File-CG64 No-load 1500 rev/min Cluster on H.P. Rotation-A

Figure 5.35 Slippers with zero centrifugal force

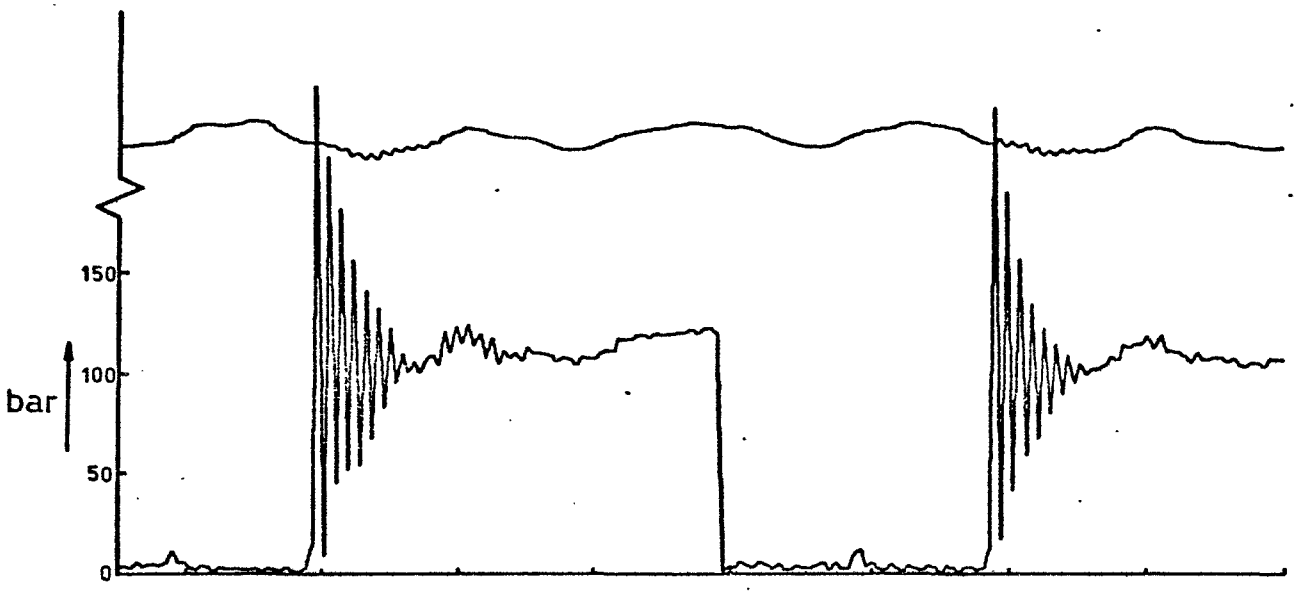

File-NEL9 105 bar 1000 rev/min

Figure 5.36

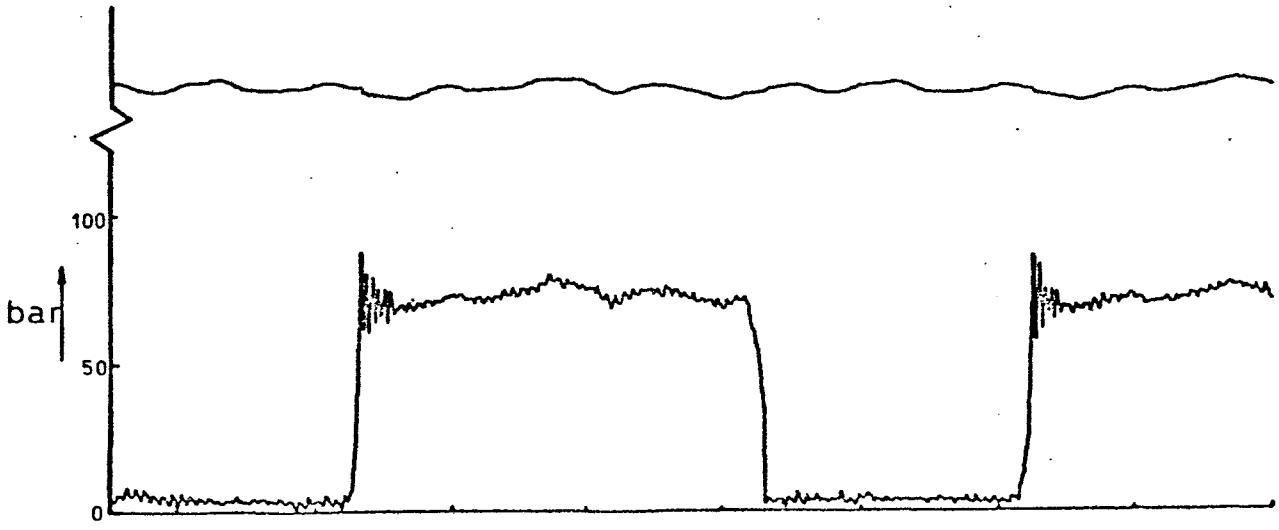

File-NEL10 70 bar 500 rev/min

Figure 5.37

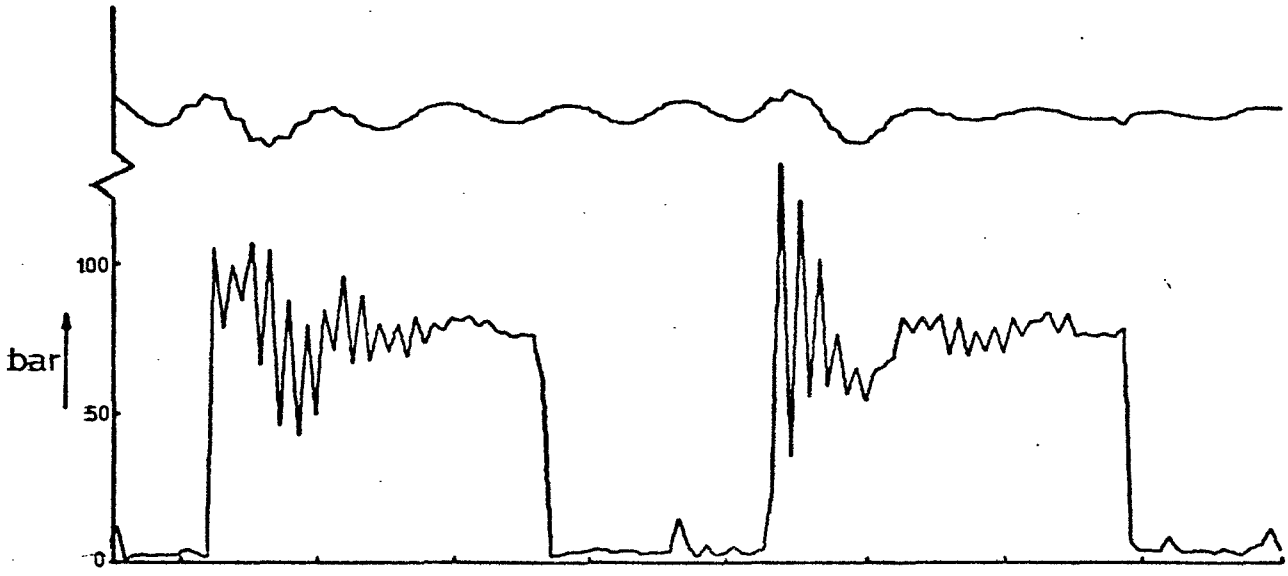

File-NEL1 2 70 bar 1750 rev/min

Figure 5.38

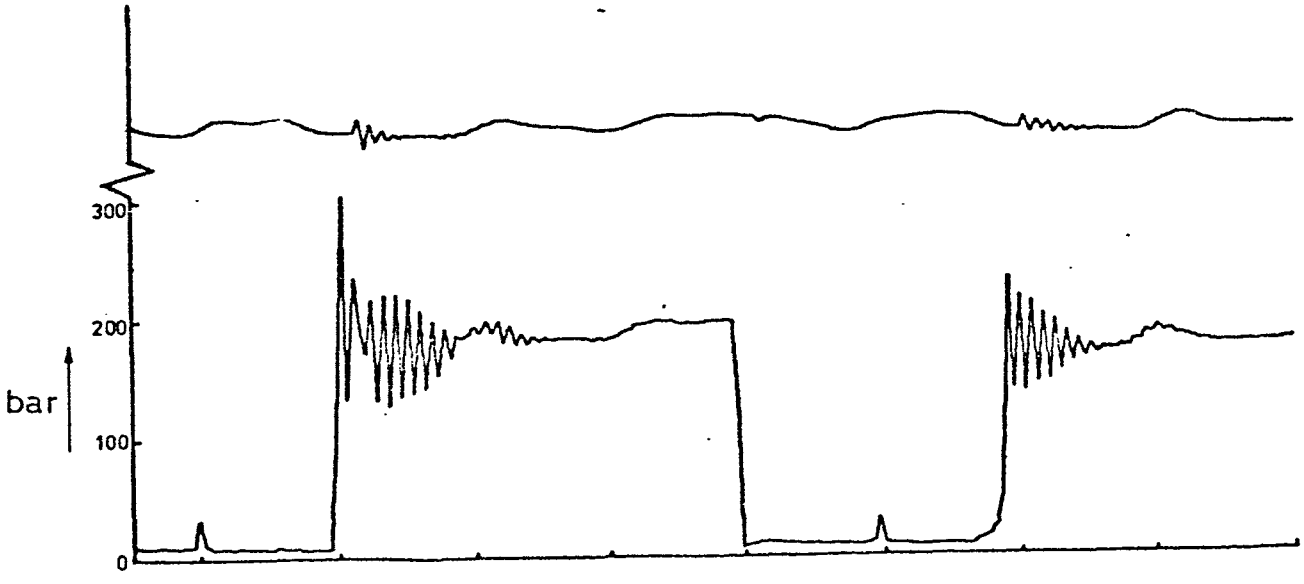

File-NEL1 8 175 bar 1000 rev/min

Figure 5.39

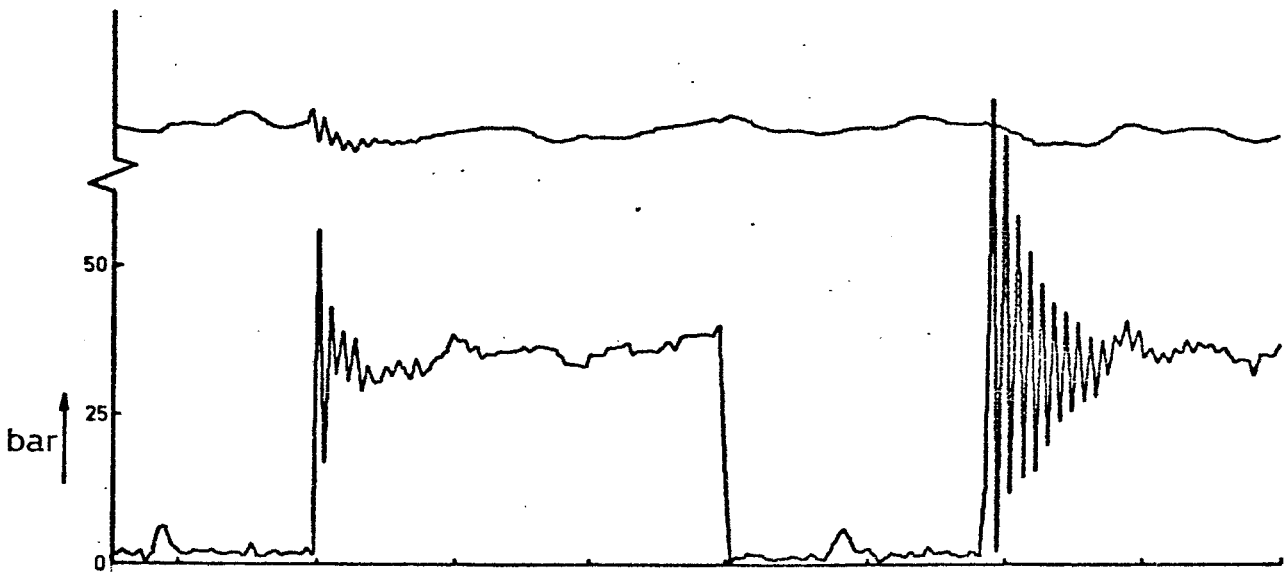

File-NEL21 35 bar - 1000 rev/min

Figure 5.40

6.0. MEASUREMENT OF PISTON SPIN

6.1. Introduction

In section 5.2.4 of the previous Chapter it was shown that pressure can affect the radial tilt of slippers in conjunction with friction in the ball joint and viscous drag in the piston/bore interface. Very little appears to be known about either of the latter two parameters either from the experimental or theoretical point of view. This Chapter describes and discusses a series of tests which were carried out with the object of gathering information related to the rotation of pistons in axial pistons machines. The reason for selecting this parameter is because piston rotation within the bore is the result of two couples The first is due to viscous drag on the piston and the second comes from the friction in the ball joint. The rate of piston spin, therefore, is a vital piece of information in the understanding of these two parameters.

6.2. Instrumentation

The investigation is wholly experimental. Results were obtained on line from a C.H.L. 92 ml/rev variable displacement pump at typical operating conditions. The instrumentaion used consisted of a powerful bar magnet which was securely fixed inside a piston sc that the axis of the magnet was at right angles to the axis of the piston. The motion of the piston in relation to the cylinder block was monited by a purpose built coil transducer (Fig. 6.1) which was inserted in one of the 9 holes normally used to hold the springs supporting the swivel bush. The piston carrying the magnet was placed in the bore nearest to the coil. The principle of operation of the transducer relies on the fact that as the piston, and hence the magnet, moves in relation to the coil, an emf is generated in the coil. This emf is proportional

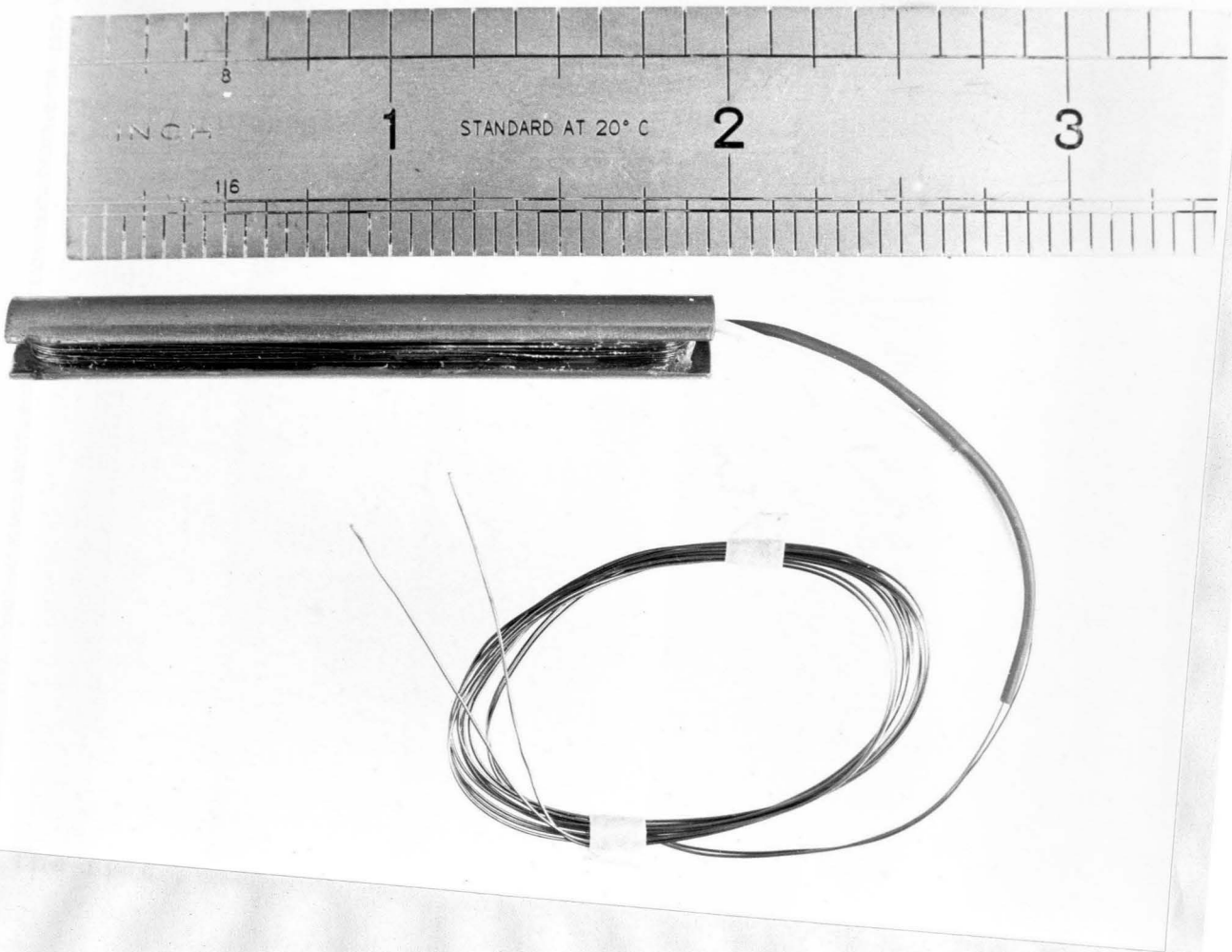

COIL TRANSDUCER

FIGURE 6.1

to the rate of change of the number of lines of magnetic flux crossing the coil and therefore it is related to the motion of the piston.

Two signals were recorded in every test. The first was the output of the coil transducer amplified by a D.C. amplifier 5000 times. The second was a pulse marker which was obtained once in every pump revolution from a magnetic pick-up which was positioned close to the pump shaft. Both signals were recorded by the data logging system (the same one which was used to record slipper clearances and pressures; for a fuller description of the system see section 4.3.2.) at the rate of 2000 Hz. In each test the number of readings taken from each signal was 8000. This means that at a shaft speed of 1500 rev/min the total number of consecutive pump rotations recorded was 100.

6.3. Principle of Spin Measurement

The emf induced in the coil is, by Faraday's law, proportional to the number of turns of the coil and the rate of change of the flux linkage.

$$E = - N \frac{dF}{dt}$$

The flux linkage through the coil depends on the position and orientation of the magnet relative to the coil. The position of the magnet (along the bore) depends on the angular position of the rotor ϕ. The orientation of the magnet can be represented by Θ (the angular position of the magnet within the bore). The flux linkage through the coil at any instant, therefore, can be expressed as

$$F = f(\Theta, \phi) \qquad 6.2$$

but the precise nature of the relationship f is unknown. Hence the emf can be expressed as

$$E = - N \frac{df}{dt} \qquad 6.3$$

The time element of the relationship can be eliminated by integrating both sides with respect to time thus obtaining a relationship which is a pure function of Θ and ϕ.

$$\int_{t_1}^{t_2} E \, dt = - N f(\Theta, \phi) + \text{constant} \qquad 6.4$$

The above relationship indicates that it is possible by integrating the output of the coil transducer to obtain a plot which is independent of rotor speed ($d\phi/dt$) and piston spin ($d\Theta/dt$). The integrated trace as shown in 6.4 is dependent on the position and orientation of the magnet within the bore In order to minimise the effect of reciprocation the shape of the coil was elongated so that the rate of flux linkage through the loops is much greater by rotating rather than by transposing the piston. For example an increase of Θ by 2π (i.e. a full revolution of the piston about itself) causes a much greater change of flux through the coil than a full cycle of the piston in and out of the bore. Moreover, the effect of ϕ can usually be isolated since it is synchronous to pump speed.

6.4. Signal Processing

Two types of signal were obtained from every test, and each signal consisted of 8000 points. Altogether, 50 tests were carried out and the data from each test was stored in individual files on floppy discs bearing the code 'SP'.

Some typical traces are shown in Figures 6.2 to 6.5. Each figure corresponds to a particular test and consists of two traces. The top trace shows the signal obtained from the magnetic pick-up in which every vertical line corresponds to one revolution of the pump. The lower trace corresponds to the integrated version of the spin signal and it was plotted in the following way.

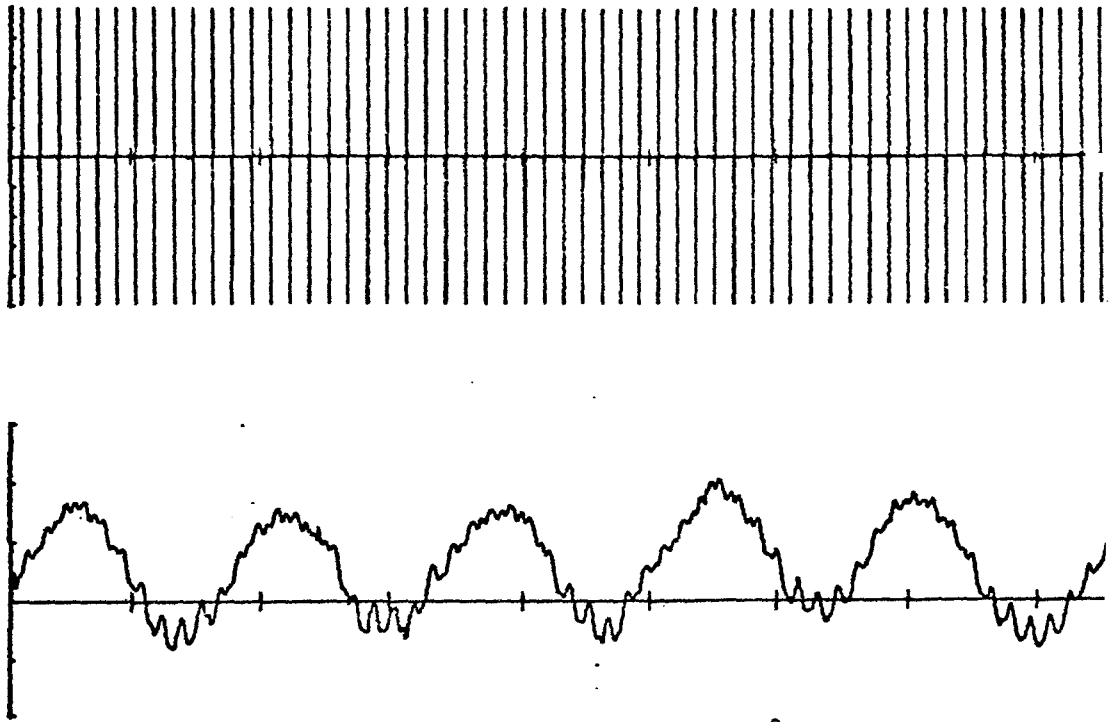

File-SP2 35 bar 1000 rev/min Full swash 50°C

Figure 6.2

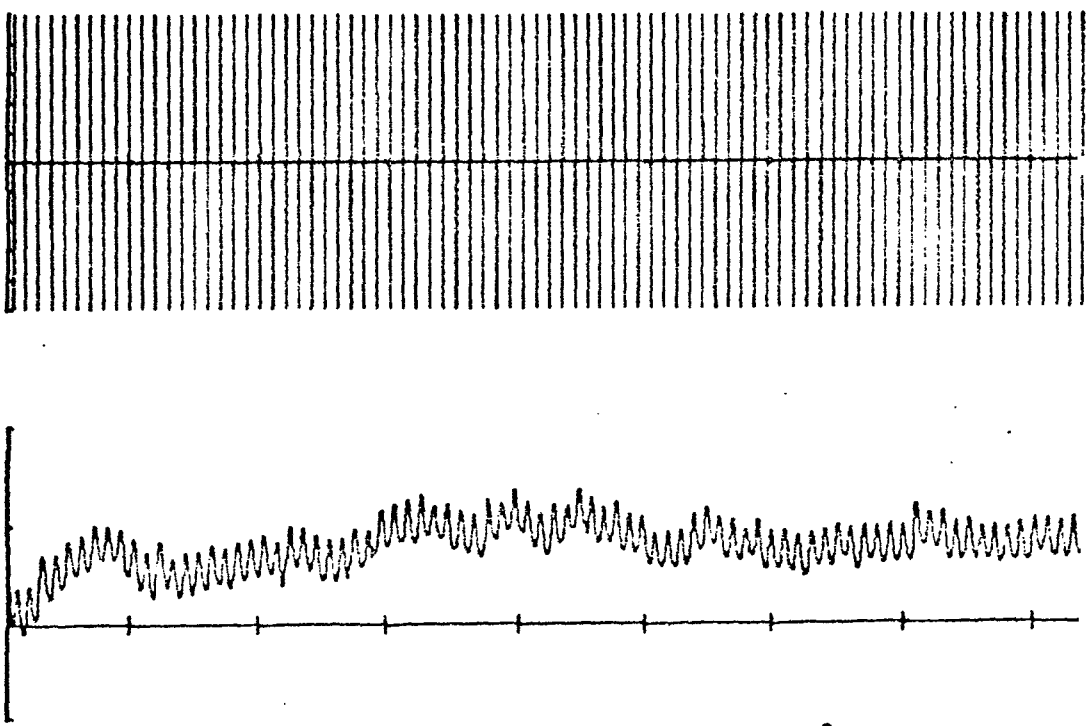

File-SP13 No-load 1500 rev/min Full swash 50°C

Figure 6.3

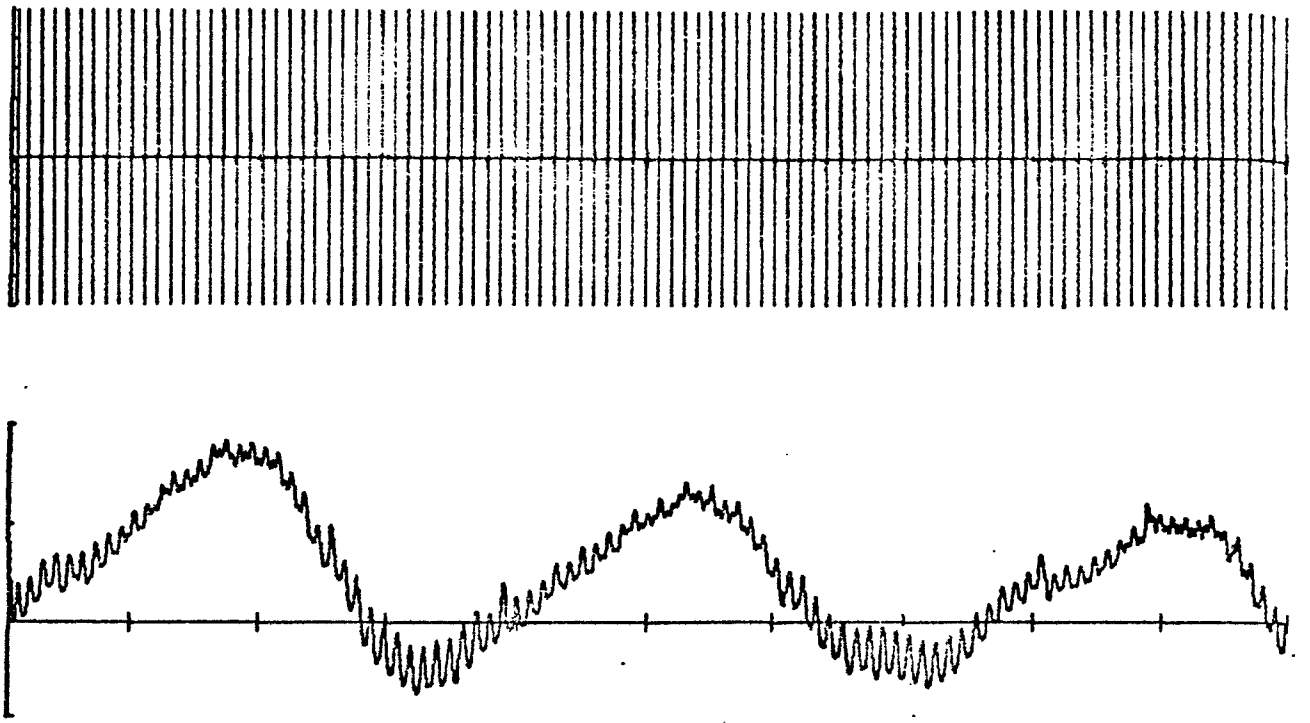

File-SP14 35 bar 1500 rev/min Full swash 50°C

Figure 6.4

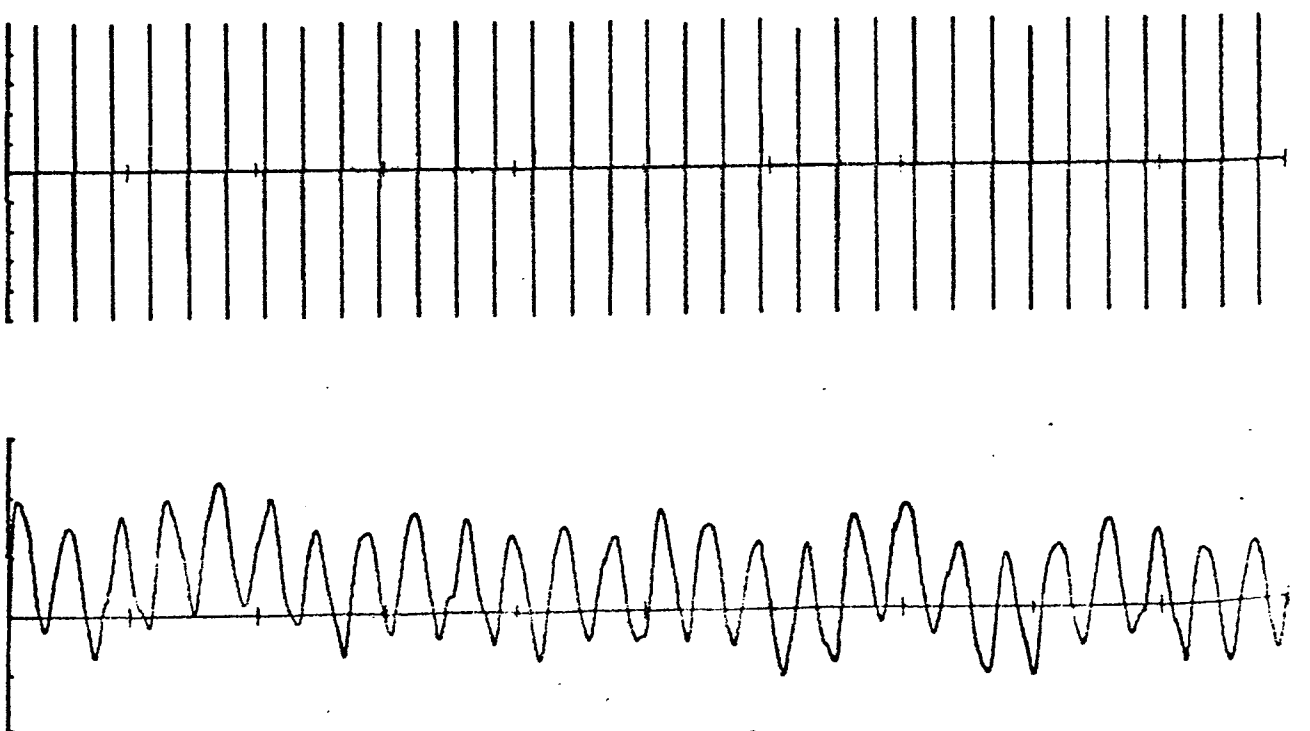

File-SP31 70 bar 500 rev/min ¼ swash 50°C

Figure 6.5

Firstly, the sum of all the readings was found. This was multiplied by the time interval between each reading and then divided by the number of readings thus producing the offset of the trace. Each point on the plot was then found by adding all the previous points, multiplying them by the time interval between each reading and subtracting the product of the offset times the number of previous readings. This procedure is necessary in order to avoid integration of any D.C. level in the signal.

6.5. Interpretation of Results

Some typical results are shown in Fig. 6.2 to 6.5. In all cases the lower trace corresponds to the integrated spin signal. Careful examination of a large number of such traces has indicated that they consist of two superimposed waveforms.

(1) One that repeats with every pump revolution. This has been attributed to the reciprocating motion of the piston within the piston bore. Its amplitude ranges from ¼ to ½ unit on the y-axis (one unit equals approximately 1 μ V sec).

(2) The second waveform is the result of piston rotation and it is generally independent of pump frequency. The peak amplitude for a full piston rotation is approximately 2 units (2 μ V sec).

There is also some lower frequency noise superimposed on the signal. This is due to slip ring and general electrical noise.

The three superimposed waveforms of piston rotation, piston reciprocation and noise can be separated by referring to their individual amplitudes. Figure 6.4 for example shows a waveform which repeats itself approximately every 34 shaft revolutions. The amplitude of this is around 2 units and cannot be related

to anything but piston rotation. Superimposed on it is a secondary waveform which is synchronous with shaft revolutions. The amplitude in this case varies depending on the angular position of the piston within the bore but does not exceed ½ unit. A similar but perhaps not as clear case is shown in Figure 6.2. Again the primary waveform has an amplitude of 2 units whilst the amplitude of the secondary is below ½ unit.

In Figure 6.3 the piston appears to be absolutely still. The reason for making this interpretation is twofold. Firstly, no waveform with amplitude equal to 2 units can be observed. Secondly the waveform related to piston reciprocation which is also synchronous to pump speed, maintains a constant amplitude throughout. This can only happen when the magnet is not rotating. Any other variations are random and can be attributed only to noise.

Figure 6.5 is a case of high piston spin. The main waveform cannot be related to piston reciprocation firstly because the peak amplitude is too high and secondly because it is not synchronous with shaft speed. Piston reciprocation is just noticeable and modifies the main waveform slightly.

In interpreting these results it should be borne in mind that piston spin is the result of couples of frictional nature and therefore some deviation from uniform behaviour is to be expected.

A useful parameter is the spin ratio which is defined as the ratio of piston spin to shaft speed.

We can examine two possible limiting cases. These are:

(a) When the friction in the ball-joint is negligibly small. Under these circumstances the piston will not rotate inside the bore at all and the spin ratio will be zero.

(b) When the friction in the ball-joint is infinitely large the piston and slipper will be interlocked in a rigid configuration. In this case the piston will maintain its orientation with respect to the pump casing all the time and it will complete one full revolution within the bore for every pump revolution; the spin ratio will thus be equal to one.

The limiting values of spin ratio are therefore zero and one.

From the results of this investigation, case (b) has not been identified under any of the conditions examined. The maximum recorded value of spin ratio was 0.82. This leads to the first general conclusion that full locking of the piston/slipper joint does not occur under normal operating conditions. This inherently implies that there must be relative movement of some kind between pistons and slippers.

The second conclusion can be derived from the fact that piston spin is negligibly low when the pump is operating on no-load, whatever the other conditions. This implies that pressure is a primary factor in creating piston spin. Since boost pressure appears to be unable to do so, it can be argued that the largest part (if not all) of the rotation of the piston takes place while the latter is in the high pressure or transition regions.

The couples that can affect the rotational state of the piston come from its interaction with the cylinder block and with the slipper. Of these the cylinder block can generate a viscous drag in the gap between the piston and the bore. This is of purely resistive nature and can only retard piston rotation. The only remaining factor that can actively induce rotation of the piston relative to the cylinder block is the slipper. This can happen

only when the following two pre-requisites are fulfilled:

a) The slipper must have a component of rotation about the axis of the piston bore.

b) There must be adequate friction in the ball-joint otherwise no couple can be transmitted to the piston from the slipper end.

As far as the behaviour of the slipper about the cylinder block is concerned, little is known. The problem is further complicated by the fact that the piston can influence the slipper in much the same way as the slipper influences the piston. One significant fact that is known to be true from above is that the piston and slipper are not locked together because the ball friction is finite. Obviously as ball friction increases the orientation of the slipper with respect to pump casing will tend to remain unchanged. At the same time the spin ratio will be increasing tending to approach unity. Therefore, the most significant single factor for creating piston spin must be the ball friction.

6.6. Effect of Operating Conditions

It was established above that the main factors that influence piston spin are the friction in the ball joint and the resistance in the cylinder/piston interface. The effect of operating conditions can now be analysed by examining their influence on these two factors.

6.6.1. Delivery pressure

The effect of pressure on piston spin was investigated at pressures of up to 210 bar and speeds of 500, 1000 and 1500 rev/min. Other operating conditions were full swashplate angle, boost pressure equal to 7 bar and inlet temperature equal to 50^{o}C.

Pressure (bar)	500	1000	1500
210		0.29	0.33
175	0.39	0.36	
140	0.46	0.36	0.20
105		0.32	
70	0.43	0.14	0.09
35	0.31	0.09	0.03
No-load	0.09	0	0

Speed (rev/min)

TABLE 6.1

The results are shown in tabulated form in Table 6.1. As mentioned above the piston appears to rotate very slowly or not at all at no-load conditions. However, any increase in pressure is followed by a marked increase in the spin ratio. This ties well with the mechanism described above since ball friction is understood to increase with the load. The increased friction, therefore, is believed to reduce the relative motion between pistons and slippers and the pistons are forced to follow the motion of the slippers more closely, thus increasing the spin ratio.

This trend is also in agreement with the effects of pressure on the radial tilt described in section 5.2.4. As piston spin increases so does the couple due to the viscous drag. This couple tends to rotate the piston/slipper assembly about the piston axis. The direction of this couple, in the case of a pump, coincides with the direction of rotation of the cylinder block. In the H.P. region this couple tends to turn the trailing end of

the slipper towards the outer part of the slipper track. However, the slippers are already tilted relative to the pistons in view of the inclination of the slipper plate. The effect of the viscous couple in the middle of H.P., therefore, appears as a tendency to tilt the slippers inwards. The opposite effect is present in the middle to the L.P. region. The direction of the couple due to the viscous drag is still the same but due to the reversed inclination of the slipper plate relative to the motion of the cylinder block,any tendency to rotate the piston/slipper assembly in that direction appears as an increase of radial tilt outwards.

A peculiar reversal of this trend was found at the top of the pressure range (175 and 210 bar). This could not be dismissed as spurious because the tests were repeated at those conditions and the same results were obtained. Although it is not clear why this is happening, one explanation is that at high pressures the side loads on the piston increase more rapidly than ball friction thus tending to reverse the trend.

6.6.2. Temperature

The effect of temperature was investigated at 30, 50 and 70^{o}C, under no-load and 70 bar delivery pressure. Other conditions were 7 bar inlet pressure and full swashplate angle.

The results are shown on Tables 6.2 and 6.3 corresponding to 70 bar and no-load respectively. In all the cases increasing the temperature appears to increase piston spin. It is thought that the lubrication of the ball joint becomes less effective as temperature increases and this results in increased ball friction and higher spin rate.

Temperature (°C)	500	1000	1500
70	0.46	0.35	0.15
50	0.43	0.14	0.09
30	0.25	0.11	0.06

Speed (rev/min)

Pressure = 70 bar

TABLE 6.2

Temperature (°C)	500	1000	1500
70	0.03	0.03	0
50	0.09	0	0
30	0.09	0.03	0

Speed (rev/min)

No-load

TABLE 6.3

6.6.3. Swashplate angle

Piston spin was measured at near zero, ¼, ½, ¾ and full swash at no-load and 70 bar delivery pressure. The other condition were as before i.e. 50°C inlet temperature and 7 bar inlet pressure.

The results are tabulated against speed on Tables 6.4 and 6.5 corresponding to 70 bar and no-load respectively. The trend in this case is decrease of piston spin as the swashplate angle is increased. The cause of this behaviour is not clear but the following possible explanations have been advanced:

(1) As the swash is reduced so are the side loads on the piston. With reduced resistance to rotation the piston is forced to rotate faster.

(2) At low swashplate angles the relative movement between piston and slipper is reduced. This can increase ball friction and in particular slip-stick effects thus resulting in increased piston spin.

Swash	500	1000	1500
Full	0.43	0.14	0.09
$\frac{3}{4}$	0.62	0.50	0.06
$\frac{1}{2}$	0.64	0.76	0.60
$\frac{1}{4}$	0.82	0.79	0.63

Speed (rev/min)

Pressure = 70 bar

TABLE 6.4

	500	1000	1500
Full	0.09	0	0
$\frac{3}{4}$	0.2	0	0
$\frac{1}{2}$	0	0	0
$\frac{1}{4}$	0	0	0
0	0	0	0

Speed (rev/min)

No-load

TABLE 6.5

6.6.4. Speed

The effect of speed on spin rate can be seen on Tables 6.1 to 6.5 since all other conditions were tabulated against it. With only one exception spin ratio appears to decrease with shaft speed under all conditions. The only possible explanation of this trend is that increased speed results in improved lubrication of the ball joint thus reducing ball friction and hence piston spin.

7.0. CONCLUSIONS

Despite the idealisations which were introduced in the theoretical study broad agreement was detected between theory and experiment in vital areas of the operation of slippers. As a result of this the following conclusions were drawn.

1. The hydrostatic lift of a slipper design such as the one used in the C.H.L. and Hastie pump is insufficient to support the piston load under most of the conditions encountered in normal operation. When the pump is stationary the slippers are in direct contact with the slipper plate irrespective of the pressure in the pistons. The hydrostatic lift can be increased by enlarging the radii of the inner load. Practical experience, however, indicates that this action can lead to instability.

2. In the case of a slipper with flat bearing surface, additional hydrodynamic lift can be generated if the slipper is tilted backwards. In this mode, adequate combined lift can be produced to support normal loads. The pressure distribution, however, is such that it produces a couple tending to restore the slipper to the zero tilt position. This behaviour indicates that a flat slipper which is free from external couples cannot be tilted and stable; this view is also shared by Fisher[14].

3. One mechanism which can explain the satisfactory operation of slippers is the presence of small amounts of non-flatness on the bearing surface. With appropriate combinations of tilt and non-flatness it is possible to modify the pressure

distribution so that all three equilibrium conditions (load, flow and moment equilibrium) can be satisfied. This possibility was also acknowledged by Fisher[14] but it does not appear to have been studied systematically by other workers.

The presence of non-flatness was confirmed from Talysurf measurements of slipper profiles which indicated that most slippers were convex. In some cases non-flatness can take the form of rounded land edges but the overall effect appears to be the same as global convexity. Simulation of parabolic type of non-flatness has shown that the above equilibrium conditions can only be satisfied if dimensionless non-flatness remains in the range 0 to 0.66. As far as the limits of physical non-flatness are concerned they depend on the range of operating conditions and the type of non-flatness. However, as long as non-flatness remains within these limits, it does not appear to have a significant effect on minimum clearance.

Best performance is believed to be obtained with a slipper profile in which the inner load is flat and the outer is sloping (chamferred).

4. The clearance of slippers lands was measured to an estimated accuracy of ± 1 μm. Clearances varied widely (from less than 1 μm up to 50 μm or more) depending on operating conditions and the point of measurement on the slipper plate. The behaviour of individual slippers was found to be repeatable from revolution to revolution and also from day to day (at the same conditions). Most repeatable parameter was the radial tilt. The repeatability was not

as good with circumferential tilt and this has been attributed to the combined effect of variations in non-flatness along the lands and the rotation of slippers. Considerable differences in behaviour were noted between different slippers especially in radial tilt. This has been attributed to variations in ball friction which is a key factor in determining the radial tilt.

5. Speed was found to produce a couple tending to tilt the slippers outwards. This is the result of centrifugal couples arising from the rotation of the slippers about the pump shaft. The direction of this couple was consistent on both the low and high pressure regions.

6. Piston pressure was also found to affect primarily the radial tilt. It is believed to act on the slippers in conjunction with the friction in the ball joint and the viscou drag on the piston. The combined effect is a couple of constant direction with regards to the pump casing. At the middle of the L.P. region this couple tends to tilt the slippers outwards. Its effect is thus superimposed on the effect of speed and high tilts are normally encountered there. The opposite is true at the middle of the H.P. region. In this case the tendency of this couple is to tilt the slippers inwards thus opposing the effect of speed. At this point the slippers can be tilted either way depending on which of the two couples dominates.
At the low to high pressure transition the pressure couple tends to tilt the slippers forward (leading edge down). This behaviour, in conjunction with the suddenly increased

loads accounts for the markings usually found at the beginning of the H.P. region.
Conversely at the high to low pressure transition the tendency of this couple is to tilt the slippers backwards. This often results in a rapid discharge of pocket pressure and the slippers are forced onto the slipper plate thus producing crescent type markings on the plate's surface. Another effect of pressure was the tendency to reduce mean clearance. This is in agreement with theory which predicts that central clearance is inversely proportional to the square root of piston pressure.

7. Temperature was found to tend to reduce clearances in general. This is in agreement with theory which predicts that the central clearance is proportional to the square root of the viscosity of the fluid (as a general rule viscosity decreases with temperature).

8. Tests with slippers and pistons of enlarged orifice have shown no difference in behaviour in the middle of the H.P. region and a very small increase in radial tilt (outwards) in the middle of the L.P. region. This, together with evidence from measurments of pocket pressure has led to the conclusion that the standard orifice size of 0.75 mm in the C.H.L. pump behaves as if it was infinitely large in the middle of the H.P. and large in the middle of the L.P. region.

9. Tests with sets of slippers differing in the postion

of the centre of gravity show that increasing the centrifugal force tends to tilt the slippers outwards.. Slippers with no centrifugal force run flatter and closer to the slipper plate.

10. Rotation of the piston within the piston bore was detected under certain operating conditions. It is believed to be the result of viscous drag on the piston, friction in the ball joint and to a lesser extent side loads exerted on the piston by the sides of the bore. The viscous drag and side loads are of purely resistive nature; the driving couple is believed to come from the slipper and it is transmitted to the piston by the friction in the ball joint.

Although of frictional nature piston rotation follows a consistent and repeatable pattern over a large number of pump revolutions. Synchronous motion (i.e. one piston revolution in every pump revolution) was not detected under any of the conditions investigated. This implies that interlocking between pistons and slippers does not occur and therefore relative motion between the two must be the norm.

Piston rotation was very small or zero at all the tests with no load on the output. The fact that pistons do rotate when the pump is loaded implies that most of the rotation must take place inthe H.P. or transition regions.

11. Operating conditions affect piston spin in the following way:

a) As a general rule, increasing the delivery pressure

results in increased piston spin. This is due to ball friction which increases with pressure. However, this trend was reversed at pressures above 140 bar and speeds of 500 and 1000 rev/min. This is thought to be caused by increased side loads which oppose the rotation of the piston.

b) Increasing temperature increases the piston spin. This is attributed to reduced oil viscosity and hence increased ball friction as the oil temperature is increased.

c) Increasing the speed reduces the piston spin. It is thought that at higher speeds ball lubrication is improved and therefore the couple due to friction in the ball joint is reduced.

d) Piston spin increases considerably at low swashplate angles. One explanation for this behaviour is the reduced side load on the pistons.

APPENDIX A

Solution of Standard Integrals

1. Integral $I_1 = \int \frac{d\phi}{(1 + e\cos\phi)^3}$ A.1

use the substitution

$$\cos\gamma = \frac{e + \cos\phi}{1 + e\cos\phi} \quad \text{A.2}$$

hence the relations

$$\sin\gamma = \frac{\sin\phi\sqrt{1 - e^2}}{1 + e\cos\phi} \quad \text{A.3}$$

from A.2

$$\cos\phi = \frac{\cos\gamma - e}{1 - e\cos\gamma} \quad \text{A.4}$$

$$1 + e\cos\phi = \frac{1 - e^2}{1 - e\cos\gamma} \quad \text{A.5}$$

Combining A.3 and A.5 produces

$$\sin\phi = \frac{\sin\gamma\sqrt{1 - e^2}}{1 - e\cos\gamma} \quad \text{A.6}$$

Also differentiating A.5

$$\sin\phi\, d\phi = \frac{(1 - e^2)\sin\gamma\, d\gamma}{(1 - e\cos\gamma)^2} \quad \text{A.7}$$

$$d\phi = \frac{\sqrt{1 - e^2}\, d\gamma}{(1 - e\cos\gamma)} \quad \text{A.8}$$

Substituting A.5 and A.8 into A.1 transforms the integral into

$$I_1 = \frac{1}{(1 - e^2)^{2.5}} \int \left[1 - 2\,e\cos\gamma + \frac{e^2}{2}(\cos 2\gamma + 1)\right] d\gamma$$

and hence

$$I_1 = \frac{1}{(1 - e^2)^{2.5}} \left(\gamma - 2\,e\sin\gamma + \frac{e^2\gamma}{2} + \frac{e^2}{4}\sin 2\gamma\right) \qquad A.9$$

for limits of ϕ between 0 and 2π, γ will also range from 0 to 2π (Appendix B). In this case the integral will simplify to

$$I_1 = \frac{\pi\,(2 + e^2)}{(1 - e^2)^{2.5}} \qquad A.10$$

2. Integral $I_2 = \int \frac{\sin\phi\, d\phi}{(1 + e\cos\phi)^3}$ A.11

let $t = 1 + e\cos\phi$ hence $d\phi = -\frac{dt}{e\sin\phi}$

A.11 can be transformed into

$$I_2 = \int -\frac{dt}{et^3} = \left[\frac{1}{2\,et^2}\right] = \left[\frac{1}{2\,e(1 + e\cos\phi)^2}\right]$$

transforming into γ gives

$$I_2 = \frac{1}{2\,e(1 - e^2)^2}\left[(1 - e\cos\gamma)^2\right] \qquad A.12$$

for ϕ between 0 to 2π

$$I_2 = 0 \qquad A.13$$

3. Integral $I_3 = \int \frac{\cos\phi\, d\phi}{(1 + e\cos\phi)^3}$ A.14

using A.4, A.5 and A.8 transforms A.14 into

$$I_3 = \frac{1}{(1 - e^2)^{2.5}} \int \left((1 + e^2) \cos\gamma - e - e\cos^2\gamma \right) d\gamma$$

$$I_3 = \frac{1}{(1 - e^2)^{2.5}} \left((1 + e^2) \sin\gamma - \frac{3\, e\gamma}{2} - \frac{e \sin 2\gamma}{4} \right) \quad \text{A.15}$$

for ϕ between 0 to 2π

$$I_3 = - \frac{3\, e\pi}{(1 - e^2)^{2.5}} \quad \text{A.16}$$

4. Integral $I_4 = \int \frac{\sin\phi \cos\phi \, d\phi}{(1 + e\cos\phi)^3}$ A.17

using A.4, A.5 and A.7, A.17 becomes

$$I_4 = \frac{1}{(1 - e^2)^2} \int \left(\sin\gamma \cos\gamma - e\sin\gamma \right) d\gamma$$

$$I_4 = \frac{1}{(1 - e^2)^2} \left(e\cos\gamma - \frac{\cos 2\gamma}{4} \right) \quad \text{A.18}$$

for ϕ between 0 to 2π

$$I_4 = 0 \quad \text{A.19}$$

5. Integral $I_5 = \int \frac{\sin^2\phi \, d\phi}{(1 + e\cos\phi)^3}$ A.20

using substitutions A.6, A.7 and A.5, A.20 becomes

$$I_5 = \frac{1}{(1 - e^2)^{1.5}} \int \sin^2\gamma \, d\gamma$$

$$I_5 = \frac{1}{(1 - e^2)^{1.5}} \left(\frac{\gamma}{2} - \frac{\sin 2\gamma}{4} \right) \quad \text{A.21}$$

for ϕ between 0 to 2π

$$I_5 = \frac{\pi}{(1 - e^2)^{1.5}} \qquad \text{A.22}$$

6. Integral $I_6 = \int \frac{\cos^2\phi \, d\phi}{(1 + e\cos\phi)^3}$ A.23

This can be related to I_1 and I_5 by splitting $\cos^2\phi$

$$I_6 = \int \frac{1 - \sin^2\phi \, d\phi}{(1 + e\cos\phi)^3} = I_1 - I_5$$

Substituting A.9 and A.21

$$I_6 = \frac{1}{(1 - e^2)^{2.5}} \left(\frac{\gamma}{2} + e^2\gamma - 2\, e\sin\gamma + \frac{\sin 2\gamma}{4} \right) \qquad \text{A.24}$$

for ϕ between 0 to 2π the relations A.10 and A.22 are used

$$I_6 = \frac{\pi\,(1 + 2\,e^3)}{(1 - e^2)^{1.5}} \qquad \text{A.25}$$

7. Integral $I_7 = \int \frac{\cos 2\,\phi}{(1 + e\cos\phi)^3} \, d\phi$ A.26

writing $\cos 2\,\phi = 2\cos^2\phi - 1$, I_7 can be related

$$I_7 = 2\, I_6 - I_1$$

however since $I_6 = I_1 - I_5$

$$I_7 = I_1 - 2\, I_5$$

substituting A.9 and A.21

$$I_7 = \frac{1}{4\,(1 - e^2)^{2.5}} \left[6\, e^2\gamma - e^2 \sin 2\gamma + 2 \sin 2\gamma - 8\, e\sin\gamma \right] \qquad \text{A.27}$$

for ϕ between 0 to 2π

$$I_7 = \frac{3\, e^2\pi}{(1 - e^2)^{2.5}} \qquad \text{A.28}$$

8. Integral $I_8 = \int_0^{2\pi} \frac{d\phi}{1 + e\cos\phi}$ A.29

Substituting A.5 and A.8

$$I_8 = \frac{1}{\sqrt{1 - e^2}} \int_0^{2\pi} d\gamma = \frac{2\pi}{\sqrt{1 - e^2}} \quad \text{A.30}$$

9. Integral $I_9 = \int_0^{2\pi} \frac{\sin\phi\, d\phi}{1 + e\cos\phi}$ A.31

using the substitution $t = 1 + e\cos\phi$

$$I_9 = -\frac{1}{e}\left[\ln (1 + e\cos\phi)\right]_0^{2\pi} = 0 \quad \text{A.32}$$

10. Integral $I_{10} = \int_0^{2\pi} \frac{\cos\phi\, d\phi}{1 + e\cos\phi}$ A.33

Rearranging and using the integral I_8

$$I_{10} = \frac{1}{e} \int_0^{2\pi} \left(1 - \frac{1}{1 + e\cos\phi}\right) d\phi = \frac{1}{e}\left(2\pi - \frac{2\pi}{\sqrt{1 - e^2}}\right)$$

$$I_{10} = \frac{2\pi}{e}\left(1 - \frac{1}{\sqrt{1 - e^2}}\right) \quad \text{A.34}$$

11. Integral $I_{11} = \int_0^{2\pi} \frac{\cos^2\phi}{1 + e\cos\phi}\, d\phi$ A.35

Rearranging as before and using integral I_{10}

$$I_{11} = \frac{1}{e}\int_0^{2\pi}\left(\cos\phi - \frac{\cos\phi}{1 + e\cos\phi}\right)d\phi = -\frac{1}{e} I_{10}$$

$$I_{11} = \frac{2\pi}{e^2}\left(1 - \frac{1}{\sqrt{1 - e^2}}\right) \qquad \text{A.36}$$

12. Integral $I_{12} = \int_0^{2\pi} \frac{\sin^2\phi}{1 + e\cos\phi}\, d\phi$ A.37

$$I_{12} = \int_0^{2\pi} \frac{1 - \cos^2\phi}{1 + e\cos\phi}\, d\phi = I_8 - I_{11}$$

$$I_{12} = \frac{2\pi}{e^2\sqrt{1 - e^2}}\left(e^2 + \sqrt{1 - e^2} - 1\right) \qquad \text{A.38}$$

13. Integral $I_{13} = \int_0^{2\pi} \frac{\sin\phi\cos\phi\, d\phi}{1 + e\cos\phi}$ A.39

Rearranging

$$I_{13} = \frac{1}{e}\int_C^{2\pi}\left(\sin\phi - \frac{\sin\phi}{1 + e\cos\phi}\right) d\phi = -\frac{1}{e} I_9$$

since $I_9 = 0$

$$I_{13} = 0 \qquad \text{A.40}$$

APPENDIX B

Relationship between γ and ϕ

The relationship between γ and ϕ used to facilitate integration of frequently used integrals in Appendix A (A.2) was

$$\cos\gamma = \frac{e + \cos\phi}{1 + e\cos\phi} \qquad \text{B.1}$$

and in explicit form

$$\gamma = \cos^{-1}\frac{e + \cos\phi}{1 + e\cos\phi} \qquad \text{B.2}$$

It is often necessary to obtain values of γ for corresponding values of ϕ. The difficulty is that direct application of B.2 on a computer or calculator will produce a discontinuous relation as shown in figure 2.32. The two curves coincide only in the region 0 to π. This is clearly due to the fact that inverse trigonometric functions produce angles that always lie between certain limits (0 to π in the case of inverse cosine). This discrepancy can be rectified by making use of n, which is an indicator of the position of ϕ as shown in figure 62 and of the following convention

For n odd

$$\gamma_{actual} = (n + 1)\pi - \gamma_{calc} \qquad \text{B.3}$$

For n even

$$\gamma_{actual} = n\pi + \gamma_{calc} \qquad \text{B.4}$$

where n can be defined as the integer part of the ratio $\frac{\phi}{\pi}$. Additionally in the event of this ratio being negative, n needs to be decremented by 1.

REFERENCES

1. Holzbock W.G. — "Hydraulic Power and Equipment". Industrial Press Inc. 1968.

2. Ernst W. — "Oil Hydraulic Power and its Industrial Applications". McGraw Hill Book Co. Inc. 1960.

3. — "Vickers Dynapad Piston Pump". Hydraulic & Air Engineering August/September 1974.

4. Helgestad B.O., Foster K. and Bannister F.K. — "Pressure Transients in an Axial Piston Pump". Proc. of the Inst. of Mech. Eng. 1974 Vol. 188 17/74.

5. Lord Rayleigh — "A Simple Problem in Forced Lubrication' Engineering. December 14th and 28th 1917.

6. Cunningham S.V. and McGillivray D. — "The Design and Operation of Hydrostatic Slipper-Pad Bearings in Hydrostatic Motors". Proc. Instn. Mech. Engrs. Vol. 180 Pt 3L.

7. Boinghoff O. — "The Friction Characteristics of the Pistons and of the Slide Shoes in the Swash Plate Axial Piston Machine". Braunschweig Technical. University.

8. Howarth R.B. — "Effects of Tilt on the Performance of Hydrostatic Thrust Pads". Proc. Instn. Mech. Engrs. Vol. 185 51/71.

9. Turnbull D.E. and Shute N.A. — "A Preliminary Investigation of the Characteristics of Hydrostatic Slipper Bearings". B.H.R.A. Rep. RR610 December 58.

10. Shute N.A. and Turnbull D.E. — "An Experimental Study of the Lift of a Simple Hydrostatic Bearing". B.H.R.A. Rep. RR659 April 60.

11. Turnbull D.E. and Shute N.A. — "A review of Hydrostatic Thrust Bearings". B.H.R.A. Rep. SP666 October 60.

12. Nau B.S. — "A Reconsideration of Pressure Generation in Radial Face seals". B.H.R.A. Rep. RR699 September 61.

13. Bennett T.P. — "The Resistance to Tilt of Hydrostatic Slipper Pads". B.H.R.A. Rep. 713 December 61.

14. Fisher M.J. — "A Theoretical Determination of some Characteristics of a Tilted Hydrostatic Slipper Bearing". B.H.R.A. Rep. RR728 April 62.

15. Shute N.A. and Turnbull D.E. "The Minimum Power Loss of Hydrostatic Slipper Bearings". B.H.R.A. Rep. SP 721 April 62.

16. Shute N.A. and "The Losses of Hydrostatic Slipper Bearings Under Various Operating Conditions". B.H.R.A. Rep. RR 743 October 62.

17. Shute N.A. and Turnbull D.E. "The Axial and Tilting Stiffness of Hydrostatic Slipper Bearings". B.H.R.A. Rep. RR 759 March 63.

18. Fisher M.J., Shute N.A. and Turnbull D.E. "A Preliminary Investigation into the Behaviour of Hydrostatic Slipper Pads Using a 5% Oil in Water Emulsion". B.H.R.A. Rep. RR 817 August 64.

19. Crook A. and Fisher M.J. "The Lift of a Hydrostatic Slipper Pad Operating with Dilute Oil-Water Emulsion". B.H.R.A. Rep. RR 890 April 67.

20. Crook A. and Fisher M.J. "An Investigation into the Dynamic Behaviour of Hydrostatic Slipper Bearings". B.H.R.A. Rep. RR 1023 October 69.

21. Royle J.K. and Raizada R.S. "Numerical Analysis of Effects of Tilt Sliding and Squeeze Action on Externally Pressurised Oil Film Bearings". Proc. Instn. Mech. Engrs. Vol. 180 Pt. 3K.

22. Cameron A. "The Principles of Lubrication". Longmans Green and Co. Ltd., 1966.

23. Madera G. "Valve Plate Performance of an Axial Piston Swash Plate Pump" Ph.D. Thesis. University of Birmingham, 1975.